



NTNU – Trondheim
Norwegian University of
Science and Technology

Modeling of Transient CO₂ Flow in Pipelines and Wells

Eirik Soland Thu

Master of Energy and Environmental Engineering

Submission date: Januar 2013

Supervisor: Petter Nekså, EPT

Co-supervisor: Gelein de Koeijer, Statoil ASA
Morten Hammer, SINTEF Energi AS

Norwegian University of Science and Technology
Department of Energy and Process Engineering

MODELING OF TRANSIENT CO₂ FLOW IN PIPELINES AND WELLS

EPT-M-2012-139

MASTER THESIS

for

Eirik Thu

Autumn 2012

Modelling of transient CO₂ flow in pipelines and reservoir wells*Modellering av transient strømning av CO₂ i rørsystemer og reservoar brønner***Background and objective**

Transport of CO₂ in pipeline systems has become increasingly important due to CO₂ handling resulting from the interest in decreasing CO₂ emissions to the atmosphere and for use of captured CO₂ for enhanced oil recovery purposes. CO₂ is typically transported at supercritical pressures, e.g. 110 bar, in pipelines from a CO₂ processing plant to an injection point into a geological structure, off- or onshore. Especially for subsea pipeline transport, it is crucial to understand the dynamics the fluid transport and the interaction with the surrounding environment. Normal operation will involve transients occurring in pipeline systems typically several km long and in the reservoir wells, but equally important are behaviour at service intervals, e.g. service of the down hole safety valve, and possible non-intentional incidents, such as a pipe rupture. Transient CO₂ flow may be more demanding than natural gas or oil flow due to CO₂'s critical and triple point properties.

The aim of this Master's project is to develop and test methods for modelling of transient flow in CO₂ pipelines and wells. Transient flow in wells and pipes consist mainly of shut-ins and depressurizations. This project consists of interdisciplinary tasks requiring thermodynamics, fluid flow, process engineering and reservoir engineering. New tools are under development and some are already on the market. These tools are similar to the tools routinely in normal oil and gas industry. But the novelty is the application to CO₂ and its specific thermodynamic behaviour, with both the triple and critical point within the pressure-temperature range of operations. It is expected that the known tools need adaption and even own adaptation of methods. OLGA is currently the leading tool for CO₂, and will primarily be used in this project. Of importance is to map its capabilities and limitations through case studies.

The following tasks are to be considered:

1. Perform a general literature review with respect to shut-ins in oil, gas and CO₂ wells
2. Review of information on shut-ins in the CO₂ wells at Snøhvit, Sleipner, In Salah and Ketzin
3. Compare different simplified reservoir descriptions for implementation in OLGA with knowledge of the different reservoir wells in cooperation with reservoir expertise

4. History matching with:
 - a. Shut-ins at Snøhvit's CO₂ well and derive storage reservoir properties
 - b. CO₂-N₂ depressurisation experiments at Rotvoll
5. Modelling and simulation of different scenarios for depressurisation and blow-outs
6. Investigate and benchmark "new" OLGA capabilities and the robustness thereof, e.g. with respect to grid size, presence of impurities in the CO₂ mixtures, available EOSs

-- ” --

Within 14 days of receiving the written text on the master thesis, the candidate shall submit a research plan for his project to the department.

When the thesis is evaluated, emphasis is put on processing of the results, and that they are presented in tabular and/or graphic form in a clear manner, and that they are analyzed carefully.

The thesis should be formulated as a research report with summary both in English and Norwegian, conclusion, literature references, table of contents etc. During the preparation of the text, the candidate should make an effort to produce a well-structured and easily readable report. In order to ease the evaluation of the thesis, it is important that the cross-references are correct. In the making of the report, strong emphasis should be placed on both a thorough discussion of the results and an orderly presentation.

The candidate is requested to initiate and keep close contact with his/her academic supervisor(s) throughout the working period. The candidate must follow the rules and regulations of NTNU as well as passive directions given by the Department of Energy and Process Engineering.

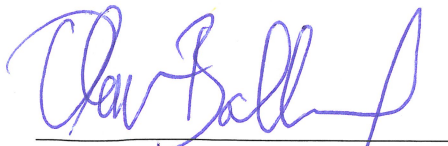
Risk assessment of the candidate's work shall be carried out according to the department's procedures. The risk assessment must be documented and included as part of the final report. Events related to the candidate's work adversely affecting the health, safety or security, must be documented and included as part of the final report. If the documentation on risk assessment represents a large number of pages, the full version is to be submitted electronically to the supervisor and an excerpt is included in the report.

Pursuant to “Regulations concerning the supplementary provisions to the technology study program/Master of Science” at NTNU §20, the Department reserves the permission to utilize all the results and data for teaching and research purposes as well as in future publications.

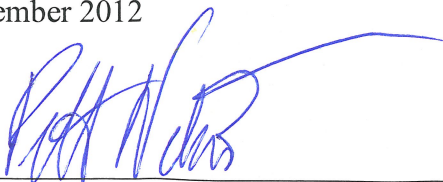
The final report is to be submitted digitally in DAIM. An executive summary of the thesis including title, student's name, supervisor's name, year, department name, and NTNU's logo and name, shall be submitted to the department as a separate pdf file. Based on an agreement with the supervisor, the final report and other material and documents may be given to the supervisor in digital format.

- Work to be done in lab (Water power lab, Fluids engineering lab, Thermal engineering lab)
- Field work

Department of Energy and Process Engineering, 1. September 2012



Olav Bolland
Department Head



Adjunct Professor Petter Neksa
Academic Supervisor

Research Advisors:

Principal Researcher Gelein De Koeijer, Statoil ASA

Research Manager Morten Hammer, SINTEF Energi AS

ABSTRACT

CO₂ capture and storage (CCS) may play a significant role in reducing carbon dioxide emissions in the near future, but to achieve this, there are some key challenges that need to be addressed further. This work will focus mainly on the injection part and is largely based on simulations of the Sleipner, Snøhvit, In Salah and Ketzin injection wells.

The aim of this work is to model transient flow in the CO₂ injection wells at Sleipner, Snøhvit, In Salah and Ketzin with OLGA, in order to identify the current capabilities and limitations. This in turn will form the basis for discussing some of the challenges related to injecting CO₂ under various operating and ambient conditions. Large scale implementation of CCS would naturally involve a wide range of operational conditions, both in terms of pressure, temperature, composition, flow regimes and fluid properties, to mention some. The geological spread will naturally also define the boundary conditions at the specific location, and will together with the operational conditions determine how the well behave and respond under various conditions. Varying boundary conditions involve amongst others changes in surface pressure and temperature, temperature and pressure gradients, heat transfer and reservoir conditions, and will depend on factors such as the geographical location, reservoir depth and the properties of the surrounding formations.

Four existing injection wells, Sleipner, Snøhvit, In Salah and Ketzin, were modeled in order to show how various operating and boundary conditions may change how the wells respond to different scenarios. For all the models, a steady state solution was obtained assuming normal operating conditions. Then, using this as the initial conditions, typical transient scenarios such as blowout and shut-in were simulated for all the wells. This should intentionally illustrate how dynamic simulations can be used to increase the general understanding of the behavior of CO₂ under various conditions. All simulations were performed using the dynamic multiphase flow simulator OLGA v7.2 and the single component module. When viewing the results however, it is important to acknowledge the limitations of the module and the assumptions made in the design of the models. Due to license issues, it was not possible to run all the simulations with the CO₂ VIP module as initially intended. This would likely have given a more stable results, as the governing equations has been rewritten to better handle pure components and fluids with narrow phase envelopes.

The simulations did to a large extent confirm the known limitations of the applied single component module. Accordingly, numerical instabilities were encountered in a varying extent, near the critical point. The reason for the numerical instabilities is that the fluid properties in this region may change drastically for small changes in pressure and temperature. The CO₂ VIP module, did on the other hand show promising results, and nearly eliminated the numerical instabilities related to operation in the critical region. Some fluctuations were still present within the two-phase region, but without operational data, it was not possible to validate the model or estimate the accuracy of the results.

It was a general trend that all the simulations operating near the critical point did experience numerical instabilities. For the blowout simulations with reservoir backflow, the results were particularly unstable. This seemed to be caused by the elevated pressure which caused the conditions to remain in the critical region for a large part of the simulation. The blowout simulations without reservoir backflow gave better

result, but instabilities were still encountered for those simulations entering the critical region. Sleipner was the only well subject to numerical instabilities of significance during the shut-in. This seemed to be caused by the specified boundary conditions, which also here lead the solution to remain in the critical region for a large part of the simulation. Operation below the triple point seemingly gave rise to more unphysical results, and was experienced for both the blowout scenarios, depending on whether the wellhead left the phase envelope before the triple point pressure was reached or not. This was also expected to some degree, as pressures and temperatures below the triple point are outside the validity range of OLGA. The initial and boundary conditions also proved to have a major impact on the results. Although the Snøhvit well was specified with a higher backpressure due to the subsea wellhead, the lower initial temperature did seem to give a more isenthalpic depressurization when compared to In Salah for instance. This in turn, seemed to be the reason why the discharge temperature did not decrease as much as the In Salah case, as large parts of the depressurization was done in the liquid region where the isotherms are more vertical. The Ketzin well did not encounter any numerical issues of significance and can largely be explained by the initial state, well within the superheated region.

The main difference that distinguishes the behavior of CO₂ from common substances such as oil, natural gas and water, is the location of the critical and triple point. As shown by the simulations, the critical region was within the operational range for Sleipner at constant injection and during the shut-in, and all Sleipner, Snøhvit and In Salah blowout simulations. The Ketzin well barely touched the saturation line towards the end of the shut-in, but did not enter the two-phase region during the blowout simulations. The low wellhead pressure also led the solution outside the critical region. None of the shut-in simulation did show excessive drop in temperature, and was largely explained by the gradual shut-in procedure obtained from the operational data at Snøhvit. The blowout simulations on the other hand, did indicate temperatures well below -20°C for all the wells except Snøhvit. The low temperature is mainly explained by the large drop in pressure and the subsequent evaporation of the liquid content. CO₂ also has a high Joule-Thomson coefficient, which causes additional cooling as the fluid expands up the well. It is therefore the rate of change in pressure which gives rise to the low temperature in the wells, as the heat transfer with the surroundings at this rate becomes too low to maintain the temperature.

Operational data were also made available by Statoil, and used to match the simulation results from the Snøhvit shut-in. The results did close in on the measured data at the wellhead, but the final result seemed to be at the expense of accuracy of the respective parameters. As the iteration cycle is determined to find the solution with the lowest deviation from the measured data, it does not necessarily have to be the most likely combination of parameters. It is therefore very important to be aware of what to expect, and how the parameters are likely to vary.

In general, all simulations operating in the critical region did show signs of numerical instability, but the extent varied according to the operating and bounding conditions. Operation below the triple point gave more unphysical results. The CO₂ VIP module showed promising results and nearly eliminated the numerical instabilities in the critical region, but needs to be verified. Critically low temperatures were experienced during blowout, but the extent was largely dependent on the operating and bonding conditions. During shut-in on the other hand, all wells remained above 0°C.

ACKNOWLEDGEMENTS

I would like to thank Statoil and Geleijn de Koeijer for great help and support during the project, and for letting me publish the results. Supervisors Petter Nekså and Morten Hammer from NTNU/SINTEF for valuable feedback during my work and SPT group and Monica Håvelsrud for assistance with OLGA and the CO₂ VIP simulations. Your time and effort has been very much appreciated. Finally I would also like to thank NTNU for an exceptional time in Trondheim.

TABLE of CONTENTS

<i>Abbreviations</i>	<i>vii</i>
<i>List of Figures</i>	<i>ix</i>
<i>List of Tables</i>	<i>xv</i>
1 INTRODUCTION	1
2 THEORY	5
2.1 Carbon Dioxide Properties	7
2.1.1 Basic Properties	7
2.1.2 CO ₂ With Impurities	8
2.1.3 Equation of State For Pure CO ₂	8
2.1.4 Equation of State For CO ₂ Mixtures	9
2.1.5 Joule-Thomson Effect	9
2.2 OLGA	10
2.2.1 History	10
2.2.2 Conservation Equations	10
2.2.3 Thermal Calculations	13
2.2.4 Single Component and CO ₂ -VIP	13
2.2.5 Reservoir Modeling	16
2.3 Geological Storage	18
2.4 Transient Scenarios	19
3 METHOD	21
3.1 General information	23
3.2 Sleipner	25
3.2.1 Background	25
3.2.2 Base Case: assumptions and boundary conditions	25
3.2.3 Transient Scenarios	28
3.2.4 Other Components	29
3.2.5 Parameter Study	29
3.3 Snøhvit	31
3.3.1 Background	31
3.3.2 Base Case: assumptions and boundary conditions	32
3.3.3 Transient scenarios	34
3.3.4 History Matching and Model Optimization	35
3.4 In Salah	38
3.4.1 Background	38
3.4.2 Base Case: assumptions and boundary conditions	38
3.4.3 Transient scenarios	39
3.5 Ketzin	40
3.5.1 Background	40
3.5.2 Base Case: assumptions and boundary conditions	41
3.5.3 TransienT scenarios	43
3.5.4 Grid Sensitivity	43
4 RESULTS	47
4.1 Sleipner	49
4.1.1 Shut-in Single Component module CO ₂	49

4.1.2	Shut-in CO ₂ VIP Module	58
4.1.3	Blowout CO ₂ With Reservoir Backflow	63
4.1.4	Blowout CO ₂ Without Reservoir Backflow	68
4.1.5	Shut-in Sleipner With Various Components	74
4.2	Snøhvit	77
4.2.1	Shut-in Single Component module CO ₂	77
4.2.2	Blowout CO ₂ With Reservoir Backflow	82
4.2.3	Blowout CO ₂ Without Reservoir Backflow	87
4.2.4	History Matching and Model Optimization	92
4.3	In Salah	96
4.3.1	Shut-in Single Component module CO ₂	96
4.3.2	Blowout CO ₂ With Reservoir Backflow	101
4.3.3	Blowout CO ₂ Without Reservoir Backflow	105
4.4	Ketzin	109
4.4.1	Shut-in Single Component module CO ₂	109
4.4.2	Blowout CO ₂ With Reservoir Backflow	114
4.4.3	Blowout CO ₂ Without Reservoir Backflow	118
5	DISCUSSION	123
6	CONCLUSION	133
7	RECOMMENDATIONS	137
8	REFERENCES	141
9	APPENDICES	147
A	Sleipner Figures	149
I.	Shut-in Single Component Module CO ₂	150
II.	Shut-in CO ₂ VIP Module	153
III.	Blowout CO ₂ with Reservoir Backflow	159
IV.	Blowout CO ₂ Without Reservoir Backflow	163
V.	Shut-in Sleipner With Various Components	167
B	Snøhvit Figures	177
I.	Shut-in Single Component Module CO ₂	178
II.	Blowout CO ₂ With Reservoir Backflow	181
III.	Blowout CO ₂ Without Reservoir Backflow	184
C	In Salah Figures	189
I.	Shut-in Single Component Module CO ₂	190
II.	Blowout CO ₂ With Reservoir Backflow	193
III.	Blowout CO ₂ Without Reservoir Backflow	197
D	Ketzin Figures	201
I.	Shut-in Single Component Module CO ₂	202
II.	Blowout CO ₂ With Reservoir Backflow	207
III.	Blowout CO ₂ Without Reservoir Backflow	211
E	Discussion	215
F	Theory	219
I.	Joule-Thomson Coefficient	220
II.	Isobaric CO ₂ Density	221
G	Model specifications	223
I.	Sleipner	224
II.	Snøhvit	225
III.	In Salah	226
IV.	Ketzin	227

ABBREVIATIONS

BH	Bottomhole
BWR	Benedict-Webb-Rubin
MD	Measured Depth
EOR	Enhanced Oil Recovery
EOS	Equation of state
CCS	CO ₂ Capture and Storage
ETP	Energy Technology Perspectives
g	Gravity
GERG	The European Gas Research Group
IEA	Temperature
LNG	Liquefied natural gas
LPG	Liquefied Petroleum gas
MEG	Monoethylene Glycol
MFC	Mixed Fluid Cascade
P	Pressure
PR	Peng-Robinson
PVT _{xy}	Pressure - Volume - Temperature -Composition
R	Gas Constant
R&D	Research and Development
RK	Redlich--Kwong
SAFT	Statistical Associating Fluid Theory
SRK	Soave-Redlich-Kwong
T	Temperature
TEG	Triethylene Glycol
U	International Energy Agency
UN	United Nation
G _f	Gas Fraction
H _l	Liquid Enthalpy
H _g	Gas Enthalpy
VLE	Vapor-Liquid Equilibrium
WEO	World Energy Outlook
WH	Wellhead
ρ	Density
NTNU	Norwegian University of Science and Technology
NIST	Institute of Standard and Technology

LIST OF FIGURES

Figure 2-1 Phase Diagram Pure CO ₂ (Lawrence J. Pekot, 2011b)	7
Figure 2-2 – PT Phase Envelope for a composition of 95% Carbon Dioxide and 5% Methane. Created with PVTsim and PR Peneloux EOS	15
Figure 2-3 – PH Phase Envelope for a composition of 95% Carbon Dioxide and 5% Methane. Created with PVTsim and PR Peneloux EOS	16
Figure 2-4 Blowout Hungary 1998 (Bíró, 2009)	20
Table 3-1 Wall Specification: Thermal properties and dimensions	26
Table 3-2 - Quantifying the accuracy of important parameters used in the model. Red color indicates values that are expected to have a higher discrepancy, as they are estimated from other estimates.	27
Figure 3-1 Applied Well Geometry Sleipner	28
Figure 3-2 Parameter Study: Injection Stream Vapor Fraction	30
Table 3-3 - Quantifying the accuracy of important parameters used in the model. Red color indicates values that are expected to have a higher discrepancy, as they are estimated from other estimates.	33
Figure 3-3 Geometry Snøhvit Injection Well	34
Figure 3-4 Operational Data at Wellhead and Gauge Snøhvit Shut-in	35
Table 3-4 Parameters used in the iteration process	37
Figure 3-5 In Salah Well Geometry	39
Figure 3-6 Ketzin Injection and Monitoring System (GFZ, 2012)	40
Table 3-5 Quantifying the accuracy of important parameters used in the Ketzin model. Red color indicates values that are expected to have a higher discrepancy, as they are estimated from other estimates. -1 sets the vapor fraction to be determined by OLGA.	42
Figure 3-7 Ketzin Well Geometry	42
Figure 3-8 Grid Sensitivity: Pressure at Wellhead For Various Section Lengths	44
Figure 3-9 Grid Sensitivity for Temperature at Wellhead	44
Figure 3-10 Deviation in pressure for various section lengths at the wellhead at 500 hours	45
Figure 3-11 Deviation in temperature for various section lengths at the wellhead at 500 hours	45
Figure 4-1 Pressure Profile Sleipner for constant injection and selected instants after shut-in. Shut-in start is set to 30h and is the injection stream is completely choked after 32h	49
Figure 4-2 Temperature Profile Sleipner for constant injection and selected instants after shut-in. Shut-in start is set to 30h and is the injection stream is completely choked after 32h.	50
Figure 4-3 Total Mass Flow Profile Sleipner Shut-in	51
Figure 4-4 Flow Profile Separate Phases Sleipner Shut-in after 2000h	52
Figure 4-5 Density Profile Sleipner Shut-in for various points in time	53
Figure 4-6 PH Diagram Sleipner Shut-in at Various Times	56
Figure 4-7 PT Diagram Sleipner Shut-in for Constant injection and after 2000h	57
Figure 4-8 Temperature Profile Sleipner Shut-in with CO ₂ VIP module	58
Figure 4-9 Flow Profile Sleipner Shut-in with CO ₂ VIP module at 500h	59
Figure 4-10 Density Profile Sleipner Shut-in CO ₂ VIP	59
Figure 4-11 PH Diagram Sleipner Shut-in Comparing standard OLGA with CO ₂ VIP	61
Figure 4-12 PT Diagram Sleipner Shut-in Comparing standard OLGA with CO ₂ VIP	62
Figure 4-13 Pressure Profile Sleipner Blowout With Backflow	63
Figure 4-14 Temperature Profile Sleipner Blowout With Backflow	64
Figure 4-15 PH Diagram Sleipner Blowout With Reservoir Backflow	66
Figure 4-16 PT Diagram Sleipner Blowout With Reservoir Backflow	67
Figure 4-17 Pressure Profile Sleipner Blowout NO Backflow	68

Figure 4-18 Temperature Profile Sleipner Blowout NO Backflow	69
Figure 4-19 Mass flow Trend Sleipner Blowout NO Backflow. Downwards Flow is Positive.	69
Figure 4-20 Blowout Details No Backflow 29.0864h	70
Figure 4-21 PH Diagram Sleipner Blowout NO Backflow	72
Figure 4-22 PT Diagram Sleipner Blowout NO Backflow	73
Figure 4-23 Pressure Profile Sleipner Various Components at Constant Injection	74
Figure 4-24 Temperature Profile Sleipner Various Components at Constant Injection	75
Figure 4-25 Heat Loss Per Unit Length From Pipe Wall to Fluid at Constant Injection	76
Figure 4-26 Pressure Profile Snøhvit Shut-in.....	77
Figure 4-27 Temperature Profile Snøhvit Shut-in	78
Figure 4-28 PH diagram Snøhvit Shut-in.....	80
Figure 4-29 PT Diagram Snøhvit Shut-in	81
Figure 4-30 Pressure Profile Snøhvit Blowout With Backflow.....	82
Figure 4-31 Temperature Profile Snøhvit Blowout With Backflow	83
Figure 4-32 Density Profile Snøhvit Blowout With Backflow.....	84
Figure 4-33 PH Diagram Snøhvit Blowout With Backflow.....	85
Figure 4-34 PT Diagram Snøhvit Blowout with Backflow.....	86
Figure 4-35 Pressure Profile Snøhvit Blowout Without Backflow.....	88
Figure 4-36 Temperature Profile Snøhvit Blowout Without Backflow	88
Figure 4-37 PH Diagram Snøhvit Blowout NO Backflow.....	90
Figure 4-38 PT Diagram Snøhvit Blowout NO Backflow	91
Figure 4-39 Wellhead Pressure History Matching	92
Figure 4-40 Wellhead Temperature History Matching.....	93
Figure 4-41 Gauge Pressure History Matching.....	94
Figure 4-42 Gauge Temperature History Matching.....	94
Table 4-1 Parameter values after 1 st and 2 nd iteration cycle	95
Figure 4-43 Pressure Profile In Salah Shut-in.....	96
Figure 4-44 Temperature Profile In Salah Shut-in	97
Figure 4-45 Density Profile In Salah Shut-in (Liquid and gas densities are equal).....	98
Figure 4-46 PH Diagram In Salah Shut-in.....	99
Figure 4-47 PT Diagram Snøhvit Shut-in	100
Figure 4-48 Pressure Profile In Salah Blowout With Backflow.....	101
Figure 4-49 Temperature Profile In Salah Blowout With Backflow	102
Figure 4-50 Isothermal Density at 23°C	102
Figure 4-51 PH Diagram In Salah Blowout with Backflow.....	103
Figure 4-52 PT Diagram In Salah Blowout with Backflow	104
Figure 4-53 Start of Instability In Salah Blowout Without Reservoir Backflow at 29.1583h	105
Figure 4-54 Pressure Profile In Salah Blowout Without Reservoir Backflow	106
Figure 4-55 Temperature Profile In Salah Blowout Without Reservoir Backflow	106
Figure 4-56 PH Diagram In Salah Blowout NO Backflow	107
Figure 4-57 PT Diagram In Salah Blowout NO Backflow	108
Figure 4-58 Pressure Profile Ketzin Shut-in	110
Figure 4-59 Temperature Profile Ketzin Shut-in.....	110
Figure 4-60 PH Diagram Ketzin Shut-in	112
Figure 4-61 PT Diagram Ketzin Shut-in.....	113
Figure 4-62 Pressure Profile Ketzin Blowout With Backflow	115
Figure 4-63 Temperature Profile Ketzin Blowout With Backflow.....	115
Figure 4-64 PH Diagram Ketzin Blowout with Backflow	116
Figure 4-65 PT Diagram Ketzin Blowout with Backflow.....	117

Figure 4-66 Pressure Profile Ketzin Blowout Without Reservoir Backflow	119
Figure 4-67 Temperature Profile Ketzin Blowout Without Reservoir Backflow	119
Figure 4-68 PH Diagram Ketzin Blowout NO Backflow	120
Figure 4-69 PT Diagram Ketzin Blowout NO Backflow	121
Figure 5-1 PH Diagram Constant Injection Sleipner, Snøhvit, Ketzin and In Salah	126
Figure 5-2 Extreme values Temperature at Wellhead All Cases	130
Figure 5-3 Extreme Values Mass Flow at Wellhead All Cases	131
Appendix A-1 Flow Profile Plot Separate Phases Sleipner Shut-in at 32h	150
Appendix A-2 Gas Fraction Profile Plot Sleipner Shut-in at various times	150
Appendix A-3 Flow Regime Sleipner Shut-in at Various Times	151
Appendix A-4 Pressure Trend Sleipner Shut-in at Various Positions	151
Appendix A-5 Temperature Trend Sleipner Shut-in at Various Positions	152
Appendix A-6 Pressure Profile Sleipner with CO2 VIP module	153
Appendix A-7 Total Mass Flow Profile Sleipner Shut-in CO2 VIP	153
Appendix A-8 Flow Profile Sleipner Shut-in 32h CO2 VIP	154
Appendix A-9 Gas Fraction Profile CO2 VIP	154
Appendix A-10 Flow Regime Profile Sleipner Shut-in CO2 VIP	155
Appendix A-11 Flow Regime vs. Change in Enthalpy at 32h	155
Appendix A-12 Pressure Trend Sleipner Shut-in CO2 VIP	156
Appendix A-13 Temperature Trend Sleipner Shut-in CO2 VIP	156
Appendix A-14 PH diagram Sleipner Shut-in CO2 VIP	157
Appendix A-15 PT diagram Sleipner Shut-in CO2	158
Appendix A-16 Density Profile Sleipner Blowout With Reservoir Backflow	159
Appendix A-17 Total Mass Flow Profile Sleipner Blowout With Reservoir Backflow	159
Appendix A-18 Gas Fraction Profile Sleipner Blowout With Reservoir Backflow	160
Appendix A-19 Flow Regime Profile Sleipner Blowout With Reservoir Backflow	160
Appendix A-20 Pressure Trend Sleipner Blowout With Backflow	161
Appendix A-21 Temperature Trend Sleipner Blowout With Backflow	161
Appendix A-22 Total Mass Flow Trend at Wellhead Sleipner Blowout With Backflow	162
Appendix A-23 Total Mass Flow Profile Sleipner Blowout NO Backflow. Downwards flow is positive	163
Appendix A-24 Flow Profile Sleipner Blowout NO Backflow. Downwards flow is positive	163
Appendix A-25 Gas Fraction Profile Sleipner Blowout NO Backflow	164
Appendix A-26 Flow Regime Profile Sleipner Blowout NO Backflow	164
Appendix A-27 Density Profile Sleipner Blowout NO Backflow	165
Appendix A-28 Pressure Trend Sleipner Blowout NO Backflow	165
Appendix A-29 Temperature Trend Sleipner Blowout NO Backflow	166
Appendix A-30 Mass Flow Trend Sleipner Blowout NO Backflow. Downwards flow is Positive	166
Appendix A-31 Pressure Profile Sleipner Various Components at Constant Injection	167
Appendix A-32 Pressure Profile Sleipner Various Components at 32h	167
Appendix A-33 Pressure Profile Sleipner Various Components at 150h	168
Appendix A-34 Temperature Profile Sleipner Various Components at Constant Injection	168
Appendix A-35 Temperature Profile Sleipner Various Components at 32h	169
Appendix A-36 Temperature Profile Sleipner Various Components at 150h	169
Appendix A-37 Heat Loss Per Unit Length From Pipe Wall to Fluid at Constant Injection	170
Appendix A-38 Heat Loss Per Unit Length From Pipe Wall to Fluid at 32h	170
Appendix A-39 Heat Loss Per Unit Length From Pipe Wall to Fluid at 150h	171
Appendix A-40 Flow Regime Profile Sleipner Various Components at Constant Injection	171
Appendix A-41 Flow Regime Profile Sleipner Various Components at 32h	172
Appendix A-42 Flow Regime Profile Sleipner Various Components at 150h	172

Appendix A-43 Gas Fraction Profile Sleipner Various Components at Constant Injection	173
Appendix A-44 Gas Fraction Profile Sleipner Various Components at 32h	173
Appendix A-45 Gas Fraction Profile Sleipner Various Components at 150h	174
Appendix A-46 Pressure Trend Sleipner Shut-in at Wellhead	174
Appendix A-47 Rich Gas Composition (TEP4185, 2011)	175
Appendix B-1 Total Mass Flow Profile Snøhvit Shut-in	178
Appendix B-2 Gas Fraction Profile Sleipner Shut-in	178
Appendix B-3 Density Profile Snøhvit Shut-in	179
Appendix B-4 Flow Regime Profile Snøhvit Shut-in	179
Appendix B-5 Pressure Trend Snøhvit	180
Appendix B-6 Temperature Trend Snøhvit	180
Appendix B-7 Total Mass Flow Profile Snøhvit Blowout With Backflow	181
Appendix B-8 Gas Fraction Profile Sleipner Blowout With Backflow	181
Appendix B-9 Flow Regime Profile Snøhvit Blowout With Backflow	182
Appendix B-10 Pressure Trend Snøhvit Blowout With Backflow	182
Appendix B-11 Temperature Trend Snøhvit Blowout With Backflow	183
Appendix B-12 Total Mass Flow Trend at Wellhead Snøhvit Blowout With Backflow	183
Appendix B-13 Density Profile Snøhvit Blowout Without Backflow	184
Appendix B-14 Total Mass Flow Profile Snøhvit Blowout Without Backflow	184
Appendix B-15 Flow Regime Profile Snøhvit Blowout Without Backflow	185
Appendix B-16 Gas Fraction Profile Sleipner Blowout Without Backflow	185
Appendix B-17 Flow Profile Snøhvit Blowout Without Backflow at 36h	186
Appendix B-18 Pressure Trend Snøhvit Blowout Without Backflow at Wellhead	186
Appendix B-19 Temperature Trend Snøhvit Blowout Without Backflow at Wellhead	187
Appendix B-20 Mass Flow Trend Snøhvit Blowout Without Backflow at Wellhead	187
Appendix C-1 Total Mass Flow Profile In Salah Shut-in	190
Appendix C-2 Flow Profile In Salah Shut-in 32h	190
Appendix C-3 Gas Fraction Profile In Salah Shut-in	191
Appendix C-4 Flow Regime Profile In Salah Shut-in	191
Appendix C-5 Pressure Trend In Salah Shut-in	192
Appendix C-6 Temperature Trend In Salah Shut-in	192
Appendix C-7 Density Profile In Salah Blowout With Backflow	193
Appendix C-8 Total Mass Flow Profile In Salah Blowout With Backflow	193
Appendix C-9 Flow Profile In Salah Blowout With Backflow 29.0167h	194
Appendix C-10 Gas Fraction Profile In Salah Blowout With Backflow	194
Appendix C-11 Flow Regime Profile In Salah Blowout With Backflow	195
Appendix C-12 Pressure Trend Snøhvit Blowout Without Backflow at Wellhead	195
Appendix C-13 Temperature Trend In Salah Blowout Without Backflow at Wellhead	196
Appendix C-14 Mass Flow Trend In Salah Blowout With Backflow at Wellhead	196
Appendix C-15 Density Profile In Salah Blowout Without Reservoir Backflow	197
Appendix C-16 Gas Fraction Profile In Salah Blowout Without Reservoir Backflow	197
Appendix C-17 Flow Regime Profile In Salah Blowout Without Reservoir Backflow	198
Appendix C-18 Total Mass Flow Profile In Salah Blowout Without Reservoir Backflow	198
Appendix C-19 Flow Profile In Salah Blowout Without Reservoir Backflow 29.0417h	199
Appendix C-20 Pressure Trend Snøhvit Blowout Without Backflow at Wellhead	199
Appendix C-21 Temperature Trend Snøhvit Blowout Without Backflow at Wellhead	200
Appendix C-22 Mass Flow Trend In Salah Blowout With Backflow at Wellhead	200
Appendix D-1 Density Profile Ketzin Shut-in	202
Appendix D-2 Gas Fraction Profile Ketzin Shut-in	202

Appendix D-3 Total Mass Flow Profile Ketzin Shut-in	203
Appendix D-4 Flow Profile Ketzin Shut-in 32h.....	203
Appendix D-5 Flow Regime Profile Ketzin Shut-in.....	204
Appendix D-6 Pressure Trend Ketzin Shut-in.....	204
Appendix D-7 Temperature Trend Ketzin Shut-in	205
Appendix D-8 Sensitivity: Pressure at Wellhead for Various Section Lengths after 31h	205
Appendix D-9 Sensitivity: Temperature at Wellhead for Various Section Length after 31h	206
Appendix D-10 Total Mass Flow Profile Ketzin Blowout With Backflow	207
Appendix D-11 Flow Profile Ketzin Blowout With Backflow 29.0167h	207
Appendix D-12 Density Profile Ketzin Blowout With Backflow	208
Appendix D-13 Gas Fraction Profile Ketzin Blowout With Backflow.....	208
Appendix D-14 Flow Regime Profile Ketzin Blowout With Backflow.....	209
Appendix D-15 Pressure Trend Ketzin Blowout Without Backflow at Wellhead.....	209
Appendix D-16 Temperature Trend Ketzin Blowout Without Backflow at Wellhead	210
Appendix D-17 Mass Flow Trend Ketzin Blowout With Backflow at Wellhead.....	210
Appendix D-18 Total Mass Flow Profile Ketzin Blowout Without Reservoir Backflow	211
Appendix D-19 Density Profile Ketzin Blowout Without Reservoir Backflow	211
Appendix D-20 Gas Fraction Profile Ketzin Blowout Without Reservoir Backflow	212
Appendix D-21 Flow Regime Profile Ketzin Blowout Without Reservoir Backflow	212
Appendix D-22 Pressure Trend Ketzin Blowout Without Backflow	213
Appendix D-23 Temperature Trend Ketzin Blowout Without Backflow	213
Appendix D-24 Mass Flow Trend at Wellhead Ketzin Blowout Without Backflow	214
Appendix E-1 Blowout Comparison: Black is with and orange is without backflow	216
Appendix E-2 PH Diagram Snøhvit Blowout Comparison final state in simulation	216
Appendix E-3 PT Diagram Constant Injection Snøhvit, Sleipner, Ketzin and In Salah	217
Appendix F-1 Joule-Thompson Coefficient CO ₂ at 1 bar (NIST)	220
Appendix F-2 Joule-Thompson Coefficient CH ₄ at 1 bar (NIST)	220
Appendix F-3 Joule-Thompson Coefficient CO ₂ at 25 bar (NIST)	220
Appendix F-4 Joule-Thompson Coefficient CH ₄ at 25 bar (NIST)	220
Appendix F-5 Isobaric CO ₂ density at 10 bar (NIST).....	221
Appendix F-6 Isobaric CO ₂ density at 60 bar (NIST).....	221
Appendix F-7 Isobaric CO ₂ density at 70 bar (NIST).....	221
Appendix F-8 Isobaric CO ₂ density at 80 bar (NIST).....	221
Appendix F-9 Isobaric CO ₂ density at 200 bar (NIST).....	221

LIST OF TABLES

Table 3-1 Wall Specification: Thermal properties and dimensions.....	26
Table 3-2 - Quantifying the accuracy of important parameters used in the model. Red color indicates values that are expected to have a higher discrepancy, as they are estimated from other estimates.	27
Table 3-3 - Quantifying the accuracy of important parameters used in the model. Red color indicates values that are expected to have a higher discrepancy, as they are estimated from other estimates.	33
Table 3-4 Parameters used in the iteration process.....	37
Table 3-5 Quantifying the accuracy of important parameters used in the Ketzin model. Red color indicates values that are expected to have a higher discrepancy, as they are estimated from other estimates. -1 sets the vapor fraction to be determined by OLGA.	42
Table 4-1 Parameter values after 1 st and 2 nd iteration cycle.....	95

1 INTRODUCTION

INTRODUCTION

Over the last two decades, CO₂ capture and storage (CCS) has experienced increasing interest as a viable climate mitigation option. The concept is considered well proven through existing projects, but the potential is still far from being fully utilized. The International Energy Agency (IEA) estimates CCS to account for approximately 19% of the reduced emissions, if 2050 levels should remain below 50% of the emissions from 2005 (OECD/IEA, 2011). The main potential of CCS is associated with large stationary sources of emission, such as power generation, natural gas sweetening, hydrogen production for ammonia and ethylene oxide, oil refineries, iron and steel production and cement manufacturing plants, to mention some. Of these, power generation is a major contributor and holds the largest potential for CCS (Koorneef et al., 2010). In this context, the major challenge is to develop competitive techniques for separating CO₂ from low pressure sources such, as the flue gas from coal fired power plants. Most current projects separate the CO₂ from high pressure sources. At Sleipner and Snøhvit for instance, the CO₂ is removed directly from the well stream, where the partial pressure of CO₂ is much higher than typically encountered for flue gas at near atmospheric pressures. This gives a more efficient removal process, but still, the CO₂ removal units are among the most energy intensive components of the production facilities.

The focus of this work is directed towards the injection and storage part of the CCS value chain. It aims to illustrate why dynamic simulations are of particular relevance in relation to transport and storage of carbon dioxide, and to investigate the current capabilities and limitations of the multiphase flow simulator OLGA. In this context, four existing injection wells, Sleipner, Snøhvit, In Salah and Ketzin, were modeled in order to show how various operating and boundary conditions may change how the wells respond to different scenarios. For all the models, a steady state solution was obtained assuming normal operating conditions. Using this as the initial conditions, typical transient scenarios such as blowout and shut-in were simulated for all the wells. This should intentionally illustrate how dynamic simulations can be used to increase the general understanding of the behavior of CO₂ under various conditions. All simulations were performed using the dynamic multiphase flow simulator OLGA and the single component module. When viewing the results however, it is important to acknowledge the limitations of the module and the assumptions made in the design of the models. Due to license issues it was not possible to run all the simulations with the CO₂ VIP module as initially intended. This would likely have given a more stable result (ref. section 2.2.4).

Implementation of CCS on a global scale, will involve a wide range of operating conditions and environments, where depleted oil and gas fields and saline-water saturated formations are highly relevant candidates for the CO₂ storage. In this context, depleted oil and gas reservoirs have some characteristics that make them particularly attractive. They have an extensive data history from the production era and are well studied. They have already proven their ability hold large amounts of oil and gas over an extensive time period, which might indicate that they could do the same for CO₂. Furthermore, they are often located near large CO₂ sources and other infrastructure (Lawrence J. Pekot, 2011b). However, they also represent some challenges that need to be addressed. This includes the initially low pore pressure which may lead to two-phase flow in the wellbore. Depleted reservoirs are typically abandoned at pressures below the critical pressure of CO₂, and may also be below the critical temperature (Lawrence J. Pekot, 2011b). Two-phase flow is not necessarily a project killer however, something which the

experience from Sleipner largely confirms, as it has two-phase flow at the wellhead (Håvard Alnes, 2011). The main arguments why two-phase flow should be avoided, has been that it would lead to unstable conditions in the well, and complicate the injection. This is justified by the rapid changes in fluid properties which might occur in the region near the critical point. Which, for small variations in wellhead pressure and temperature can have a major impact on the bottomhole pressure (Lawrence J. Pekot, 2011b). Transient scenarios will therefore be particularly exposed, as the conditions are constantly changing. They may also give rise to two-phase flow, even in wells that initially are operating completely outside the two-phase region. Transient scenarios involving a rapid drop in pressure, may also give rise to low temperatures in the wells, if the heat transfer with the surroundings are insufficient to maintain the temperature in the well. This in turn, might be both an operational and safety issue. Accurate simulations can therefore be a powerful tool in establishing good operational and safety routines, as a validated model can be used to predict how the well respond to changes in conditions.

Traditional oil and gas simulators are not particularly well suited for pure components, or mixtures of high purity, as they are designed for complex mixtures of hydrocarbons. This will be discussed further in section 2.2.4, but it should be clear that there is a need for a solution that can accurately predict the behavior of fluids of high purity. In this context, the CO₂ VIP module in OLGA did show promising results, but could unfortunately not be used in all the case studies included in this work.

In agreement with the respective supervisors, it was decided to use the linear equation for reservoir inflow in the models. Thus, other reservoir descriptions were not studied in detail. Also, due to the license issues regarding the CO₂ VIP module, the simulations with impurities were not the main focus of this work. However, for details beyond what is covered in this work, it is referred to the specialization project leading up to this report (Thu, 2012). The CO₂-N₂ experiments also expired, as it was desired by Statoil to do the simulations in-house.

2 THEORY

2.1 CARBON DIOXIDE PROPERTIES

2.1.1 BASIC PROPERTIES

The properties of pure CO₂ have been extensively studied and are considered well known. In this section relevant properties will be presented and discussed. Although there is a lot of experience with pipeline transport in general, it cannot simply be transferred to CO₂. Relative to common substances like oil, gas and water, it behaves different at normal operating conditions due to the location of the critical and triple point.

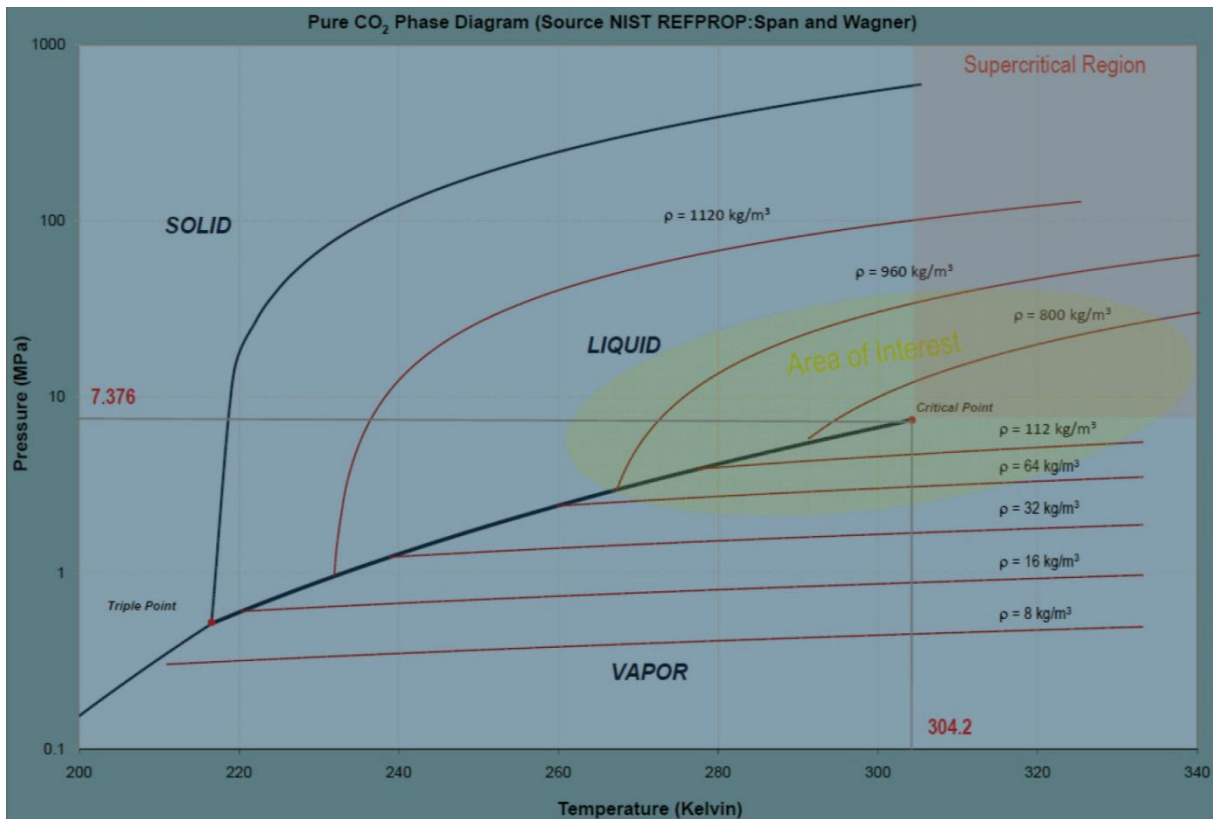


Figure 2-1 Phase Diagram Pure CO₂ (Lawrence J. Pekot, 2011b)

The phase diagram for pure CO₂ is given in Figure 2-1. The triple point can be identified -56.6°C and 5.18 bar, and the critical point at 30.9782°C and 73.773 bar (Oosterkamp and Ramsen, 2008). It can also be noted from the diagram that liquid CO₂ only can exist at pressures above 5.1 bar, and that for pressures below this, CO₂ will go directly from solid to vapor phase. The triple point is defined as the temperature and pressure at which all three phases can coexist in equilibrium and the critical point defines the highest temperature and pressure at which liquid and gas can exist in separate phases. Above the critical temperature and pressure, it is not possible to distinguish liquid from vapor. This is commonly referred to as the supercritical region and has approximately the viscosity of a gas but the density of a fluid (UK, 2007). These properties make it both economically and technically beneficial to transport the CO₂ under

these conditions (Vahedi and Hinsley, 2011). Typical operating conditions for offshore pipelines range between 100 and 300 bar and 0°C to 50°C (Oosterkamp and Ramsen, 2008). Although two-phase flow is technically feasible (Sleipner has two-phase flow at well head), it is often desirable to transport the CO₂ in supercritical and liquid phase to ensure reliable and efficient transport. Especially in the region near the critical point, may small changes in operating conditions lead to large changes in the physical properties.

CO₂ is colorless, odorless and is in gaseous phase at standard atmospheric conditions. It is non-combustible and non-toxic. However at high concentrations, typically 7% to 10% in air, it can cause unconsciousness. The relative density of 1.529 compared to air, may cause the CO₂ to accumulate on the ground and displace the air in the event of an uncontrolled release (UNION, 2007).

2.1.2 CO₂ WITH IMPURITIES

The effect of impurities is another aspect that is being studied, and depending on the amount and type of components present in the stream, it can alter the thermo-physical properties. This is highly relevant, as virtually all industrial sized projects operate with CO₂ that contains some degree of impurities. If the impurities increase the vapor pressure for instance, a higher operational pressure would be needed to keep the fluid in the dense phase during transport. Impurities will also reduce the capacity of the pipeline or well, as they take up space that otherwise could be used to transport CO₂. Other effects include among others; changes in the solubility of water and corrosion rate of the mixture, reactions between the various components and in general in may introduce new safety issues. For further studies on the topic of impurities, it is referred to the report leading up to this work (Thu, 2012).

2.1.3 EQUATION OF STATE FOR PURE CO₂

The detailed knowledge of pure CO₂, has made it possible to establish reference equations of state (EOS) and viscosity relations, capable of estimating properties at a high level of accuracy. Span and Wagner is an empirical EOS specifically developed to cover the region above the triple point of CO₂, and is capable of predicting thermodynamic properties in equilibrium up to 1100 K and 800 MPa (including the immediate vicinity of the critical point (UK, 2007)). With appropriate binary interaction coefficients it can to some extent also be used for CO₂ mixtures.

2.1.4 EQUATION OF STATE FOR CO₂ MIXTURES

Regarding the thermodynamic models used for predicting PVT_{xy} properties of CO₂ mixtures, there seems to be no real consensus on which EOS to use. The cubic equations i.e. Peng-Robinson (PR) and Soave-Redlich-Kwong (SRK) (UK, 2007) offer the advantage of simplicity along with reasonable results in the calculations. More complicated equations like the Benedict-Webb-Rubin (BWR) and SAFT equations have shown to give better results for volume calculations. However, cubic equations seem to be better suited for calculating the vapor-liquid equilibrium (VLE). Considering the claimed accuracy of the GERG equation, this would be the preferred alternative. But the fact that the equation was developed for natural gas components, its application for CO₂ mixtures will be limited to a set of impurities. In other words there is currently no EOS offering sufficient accuracy for both VLE and volume calculations. Establishing a reference equation for CCS applications is highly desirable, but to do so, more experimental data is needed for validation. In addition it will be necessary to determine the desired accuracy for the equation.

2.1.5 JOULE-THOMSON EFFECT

Whenever a real gas or liquid expands freely through a valve or throttling device, such that no heat is exchanged with the environment and no external work is extracted, the fluid will experience a temperature change. This is commonly referred to as the Joule-Thomson effect (Hendricks et al., 1972), which may be expressed by the Joule–Thompson coefficient as shown below.

$$\begin{array}{l} \text{Joule-} \\ \text{Thomson} \\ \text{Coefficient} \end{array} \quad \mu_{JT} = \left(\frac{\partial T}{\partial P} \right)_h \quad (2.1)$$

μ_{JT} represents the rate of change of the temperature, with respect to pressure (at constant enthalpy), and has the dimensions [°C/bar]. Provided that the gas temperature is in the region below the inversion temperature (where μ_{JT} goes from positive to negative), an expansion will lead to cooling of the fluid. As ∂P is negative by definition during an expansion, and μ_{JT} is positive below the inversion temperature, ∂T must also be negative for the equation to be valid. This is relevant for CO₂ transport as the typical operating conditions suggest that the fluid will experience additional cooling while it is expanded through the pipe. This is also valid for well operations, but may have a particular impact during transient scenarios such as shut-ins and blowouts. CO₂ also tend to have a higher Joule–Thompson coefficient than other components typically present in relation to pipe transport. Hence for CO₂ dominated compositions, it can have a larger influence on the temperature development, especially when the pressure is low enough for the fluid to be in gaseous state (ref. Appendix F-1 to Appendix F-4).

2.2 OLGA

2.2.1 HISTORY

OLGA is a dynamic simulation tool for multiphase flow in pipelines. The intended application of the model was to better predict typical transient problems of interest, such as terrain slugging, startup and shut-in of pipelines, variable production rates and pigging. The first version was financed by Statoil and was ready in 1983. Further developments were carried out as a joint research program between the Institute for Energy Technology (IFE) and SINTEF and were supported by Conoco Norway, Esso Norge, Mobil Exploration Norway, Norsk Hydro A/S, Petro Canada, Saga Petroleum, Statoil and Texaco Exploration Norway (Kjell H. Bendiksen, 1991). IFE was then responsible for the development of the model, while the experiments were carried out by SINTEF. Today the OLGA license is maintained by SPT group and the model is under continuous development to verify and improve accuracy of the existing functionality, as well as extending the application of the software. The very foundation however, is still to a large extent based on the work performed in the joint research program.

2.2.2 CONSERVATION EQUATIONS

Early models of OLGA used the extended two-fluid model, as described by Kjell H. Bendiksen et al. in 1991 (Kjell H. Bendiksen, 1991). This approach models the fluid by using separate continuity equations (conservation of mass) for the gas, liquid bulk and droplet phase. The equations are then coupled by equations for the interphasial mass transfer.

$$\begin{array}{l} \text{Continuity} \\ \text{equation gas} \end{array} \quad \frac{\partial}{\partial t} (V_g \rho_g) = -\frac{1}{A} \frac{\partial}{\partial z} (A V_g \rho_g v_g) + \psi_g + G_g \quad (2.2)$$

$$\begin{array}{l} \text{Continuity} \\ \text{equation liquid} \\ \text{phase at wall} \end{array} \quad \frac{\partial}{\partial t} (V_L \rho_L) = -\frac{1}{A} \frac{\partial}{\partial z} (A V_L \rho_L v_L) - \psi_g \frac{V_L}{V_L + V_D} - \psi_e + \psi_d + G_L \quad (2.3)$$

$$\begin{array}{l} \text{Continuity} \\ \text{equation} \\ \text{Liquid} \\ \text{droplets} \end{array} \quad \frac{\partial}{\partial t} (V_D \rho_L) = -\frac{1}{A} \frac{\partial}{\partial z} (A V_D \rho_L v_D) - \psi_g \frac{V_D}{V_L + V_D} + \psi_e - \psi_d + G_D \quad (2.4)$$

In the above equations V_g, V_L and V_D represents the gas, liquid film and liquid droplet volume fractions, $\rho =$ density, $v =$ velocity, $A =$ pipe cross-section area, $\psi_g =$ mass transfer between the phases, ψ_e and ψ_d entrainment and deposition rates and $G_f =$ possible mass source of phase f. In order to allow for stepwise time integration, the equations have been reformulated to obtain a pressure equation, which together with the momentum equations may be solved simultaneously with regards to phase velocities and pressure (Kjell H. Bendiksen, 1991). By doing this, the equations are simplified to express the density explicit as a linear function of pressure only. The density error is corrected by a source in the next section. Since Kjell H. Bendiksen et al. published their paper in 1991, the model has been expanded to account for a third fluid in the calculations. Consequently, the present model applies separate continuity equations for gas, oil and water liquids, as well as equations for oil and water droplets (SPTgroup, 2012b). In the calculations, gas is always assumed to be lighter than oil and water, but oil may be both lighter and heavier than water. Note however that the model only has been verified for fluids where oil is lighter than water. It is also worth noting that for the table based thermodynamics, the total composition of the mixture is assumed to be constant. Phase fractions on the other hand, may vary with time. In reality, the composition may vary along the pipeline due to amongst others different phase velocities, holdup, changes in the injected stream, interphasial mass transfer. To overcome this, it is required to use the compositional tracking module in OLGA which solves the continuity equations separately for each component and each phase. By doing this, the material properties of the fluid are continuously calculated based on the current conditions in the pipeline.

The interphasial mass-transfer may be computed from equations below, where R_s represents the gas mass fraction at equilibrium conditions.

$$\begin{array}{l} \text{Gas mass} \\ \text{fraction} \end{array} \quad R_s = \frac{m_g}{(m_g + m_L + m_D)} \quad (2.5)$$

$$\begin{array}{l} \text{Interphasial} \\ \text{mass transfer} \end{array} \quad \psi_g = \left[\left(\frac{\partial R_s}{\partial p} \right)_T \frac{\partial p}{\partial t} + \left(\frac{\partial R_s}{\partial p} \right)_T \frac{\partial p}{\partial z} \frac{\partial z}{\partial t} + \left(\frac{\partial R_s}{\partial T} \right)_P \frac{\partial T}{\partial t} + \left(\frac{\partial R_s}{\partial T} \right)_P \frac{\partial T}{\partial z} \frac{\partial z}{\partial t} \right] \cdot (m_g + m_L + m_D) \quad (2.6)$$

The momentum equations are expressed for the continuous liquid phase (oil and water), as well as one for gas with liquid droplets. These equations are presented in equation 2.7 and 2.8 respectively.

$$\begin{aligned}
 \text{Momentum} & \quad \frac{\partial}{\partial t} (V_L \rho_L v_L) = -V_L \left(\frac{\partial p}{\partial z} \right) - \frac{1}{A} \frac{\partial}{\partial z} (AV_L \rho_L v_L^2) - \lambda_L \frac{1}{2} \rho_L |v_L| v_L \frac{S_L}{4A} + \\
 \text{equation for} & \quad \lambda_i \frac{1}{2} \rho_g |v_r| v_r \frac{S_i}{4A} + V_L \rho_L g \cos \alpha - \psi_g \frac{V_L}{V_L + V_D} v_a - \psi_e v_i + \psi_d v_D - \\
 \text{liquid at the} & \quad V_L d (\rho_L - \rho_g) g \frac{\partial V_L}{\partial z} \sin \alpha \\
 \text{wall} & \quad
 \end{aligned} \tag{2.7}$$

$$\begin{aligned}
 \text{Combined} & \quad \frac{\partial}{\partial t} (V_g \rho_g v_g + V_D \rho_D v_D) = -(V_g + V_D) \left(\frac{\partial p}{\partial z} \right) - \frac{1}{A} \frac{\partial}{\partial z} (AV_g \rho_g v_g^2 + \\
 \text{momentum} & \quad AV_D \rho_L v_D^2) - \lambda_g \frac{1}{2} \rho_g |v_g| v_g \frac{S_g}{4A} - \lambda_i \frac{1}{2} \rho_g |v_r| v_r \frac{S_i}{4A} + (V_g \rho_g + \\
 \text{equation for} & \quad V_D \rho_L) g \cos \alpha + \psi_g \frac{V_L}{V_L + V_D} v_a + \psi_e v_i - \psi_d v_d \\
 \text{gas and liquid} & \quad \\
 \text{droplets} & \quad
 \end{aligned} \tag{2.8}$$

Here α represents the pipe inclination with the vertical plane, S_g, S_L and S_i the wetted perimeters of the gas, liquid and interface, λ_g, λ_L and λ_i the friction factors and v_r the relative velocity. In the three-fluid model, separate momentum equations are applied for each of the continuous liquid phases (oil/condensate and water). One mixture energy equation is applied, which implies the assumption that all phases are at the same temperature.

$$\begin{aligned}
 \text{Mixture} & \quad \frac{\partial}{\partial t} \left[m_g \left(e_g + \frac{1}{2} v_g^2 + gz \right) + m_L \left(e_L + \frac{1}{2} v_L^2 + gz \right) + m_D \left(e_D + \frac{1}{2} v_D^2 + \right. \\
 \text{energy} & \quad \left. gz \right) \right] = - \frac{\partial}{\partial z} \left[m_g v_g \left(h_g + \frac{1}{2} v_g^2 + gz \right) + m_L v_L \left(h_L + \frac{1}{2} v_L^2 + gz \right) + \right. \\
 \text{equation} & \quad \left. m_D v_D \left(h_D + \frac{1}{2} v_D^2 + gz \right) \right] + h_s + U
 \end{aligned} \tag{2.9}$$

Here e represents the internal energy per unit mass, z the elevation, h_s the enthalpy from possible sources and U the heat transfer from the pipe walls. To close the system of equations, fluid properties and boundary and initial conditions are required. The experimental verification of the model is mainly applied to determine friction factors (both for wall friction and interphasial friction), flow regimes and transitions between the different flow regimes. This in turn leads to a better prediction of the pressure drop and heat transfer in the pipeline.

2.2.3 THERMAL CALCULATIONS

Thermal calculations in OLGA assume that radial conduction is the dominating factor. Hence, the heat flux through the pipe wall can be specified either with an estimated overall heat transfer coefficient, or by modeling the pipe wall (and surroundings) by one or several concentric wall layers. This is done by specifying thermal conductivity, specific heat capacities, densities and thickness of each layer, which is used to calculate the heat transfer through the wall. As the ambient conditions may change along the pipeline, it may be desirable to apply different wall descriptions to different sections of the pipeline. For instance, if the model comprises a wellbore, connected to a platform based process facility, there might be a significant difference in the heat transfer experienced, between the wellbore and the surrounding formation, and the riser and the surrounding sea water. In the latter case convection may be more dominant, and hence increase the heat transfer with the surroundings. Depending on various factors such as phase fractions, velocities, thermal gradients etc., OLGA calculates the heat transfer coefficient from the flowing fluid to the internal pipe wall, whereas the outer heat transfer coefficient is specified by the user. Circumferential symmetry is assumed in the calculations, but if this is not the case an overall heat transfer coefficient needs to be specified. During a depressurization for instance, or any other situation where the fluid rapidly expands from high to low pressure, the Joule-Thompson effect may have a significant effect on the heat transfer. Particularly for transient simulations where the heat storage in the pipe walls and surroundings may be important, it might be necessary to use a finer discretization of the wall layers (SPTgroup, 2012b). If a more detailed description of the heat transfer is required, the FEMTherm model can be used. However, this may increase the complexity of the model significantly and should therefore only be used if the concentric wall layer approach cannot describe the case at a satisfactory level.

2.2.4 SINGLE COMPONENT AND CO₂-VIP

The numerical approach used in standard OLGA is designed for multi-component hydrocarbon fluids (SPTgroup, 2012b). Such fluids typically have wide phase envelopes, which allows for a gradual transition when the operational range is within the two-phase area. Single component fluids on the other hand, are often suspect to rapid changes in thermo physical properties when crossing the saturation line or operating in the near critical region. This is also true for multi-component fluids with narrow phase envelopes. Typical such fluids are predominated by one component, and the behavior is approaching the behavior of a single component. This can be seen from the tightly stacked quality lines, which are approaching each other to form a single saturation line, as the case is for single component fluids. As a consequence of this, the numerical approach used in standard OLGA may become unstable when performing simulations with such fluids. According to Monika Håvelsrud in SPT Group (Håvelsrud, 2012a), standard OLGA should be able to handle mixtures with up to 80% of one component, as long as the mixture has a significant two-phase area. However, initial simulations performed prior to this work, were not able to confirm this statement (Thu, 2012). Most likely this was a consequence of the chosen compositions, but regardless it makes the model very dependent on the composition, which in practical terms excludes it from being used in most of the existing industrial size CO₂ storage projects.

The single component module has built in fluid property calculations for H₂O and CO₂. However, for other single component fluids, it is necessary to specify a set of input parameters. As fluid property calculations are both time consuming and in demand of a high computational capacity, tables are generated at the start of each simulation and used for linear interpolation during the simulations. As the fluid property tables are limited to a maximum of 100 grid points, it is important to limit the pressure and temperature span in order to get a good resolution of the tabulated values (Staff, 2012). In the calculations, the single component model assumes that both the liquid and gas phase are at the *same* pressure and temperature, and that if the fluid temperature is above the saturation temperature, boiling will occur. A similar assumption is used for condensation, which occurs if the fluid temperature is below the saturation temperature (SPTgroup, 2012b). The saturation line is determined by solving the equation of state (EOS) for equal fugacity for the gas and liquid phase. The saturation line is then extrapolated above the critical point by using the slope of the saturation line at the critical point. In this region (close to the critical point) properties such as the thermal capacity and density of CO₂ is extremely sensitive to small changes in temperature and pressure. As a consequence of this, numerical smoothing has been applied in the near critical region and accordingly; unphysical behavior may be expected when operating in this region. For CO₂, which is of prior importance in this work, the single component module takes use of the Span and Wagner EOS which is recognized by industry as the most accurate representation of the available PVT data for CO₂ and its mixtures (UK, 2007). It was developed with special interest in the critical region, and is valid for equilibrium thermodynamic properties of carbon dioxide from the triple point at 5.18 bar and -56.6°C, up to about 827°C and 8000 bar. Even so, the single component module has some clear limitations when addressing challenges that are frequently encountered in real CCS projects. As any other multiphase flow model, the single component module, rely heavily on experimental data for verification. Due to scarcity of such data however, the functionality of the model has not been sufficiently validated (Håvelsrud, 2012b). Another challenge is the need for expansion of the functionality to also cover the effects of impurities in the CO₂ flow. In reality, it may be technically feasible to purify the CO₂ prior to injection, but economically, such restrictions can rule out CCS as a viable alternative. To address these challenges, the CO₂-VIP project was established in 2010, to verify and improve the CO₂ functionality in OLGA. Resulting from this is the CO₂-VIP version of OLGA, based on pressure and mixture enthalpy as the two independent variables. In standard OLGA, pressure and temperature are used. This is normally a reasonable assumption for multiphase flow involving oil and gas, as the physical properties change gradually with P and T. This however, is as mentioned in the beginning of this section, not the case for pure components or mixtures that are approaching the behavior of pure components. For such fluids, pressure and temperature cannot be treated as independent variables near the saturation line and near the critical point, as a small change in pressure may lead to completely different conditions, depending on whether the temperature is assumed to be constant or not.

As a consequence of this, the governing equations have been rewritten to a Pressure-Enthalpy (PH) format, improving the performance of the simulator (Håvelsrud, 2012b). During calculations, the enthalpy is now assumed constant for small changes in pressure, but with better accuracy than the corresponding assumption with regards to temperature. This can be seen in Figure 2-2 and Figure 2-3 for a mixture of 95% CO₂ and 5% CH₄. Notice how the quality lines are virtually on top of each other in the Pressure-Temperature (PT) diagram, whereas in the Pressure-Enthalpy (PH) diagram, the lines are more spread out. From this it can be seen that the approach of assuming constant temperature for small changes in pressure, potentially may lead to a larger discrepancy, as opposed to a similar assumption for the enthalpy

in a PH diagram. The PH formulation is designed to work with both the single component and compositional tracking module, and as a consequence of this it is applicable for both pure components and mixtures. For the single component module, the Span & Wagner EOS is built in and used to calculate the fluid properties of CO₂. The compositional tracking module on the other hand, uses input files from PVTsim to calculate fluid properties of the mixture (Håvelsrud, 2012c). The applied EOS is then chosen when defining the fluid in PVTsim. Available equations of state are different variations of PR and SRK.

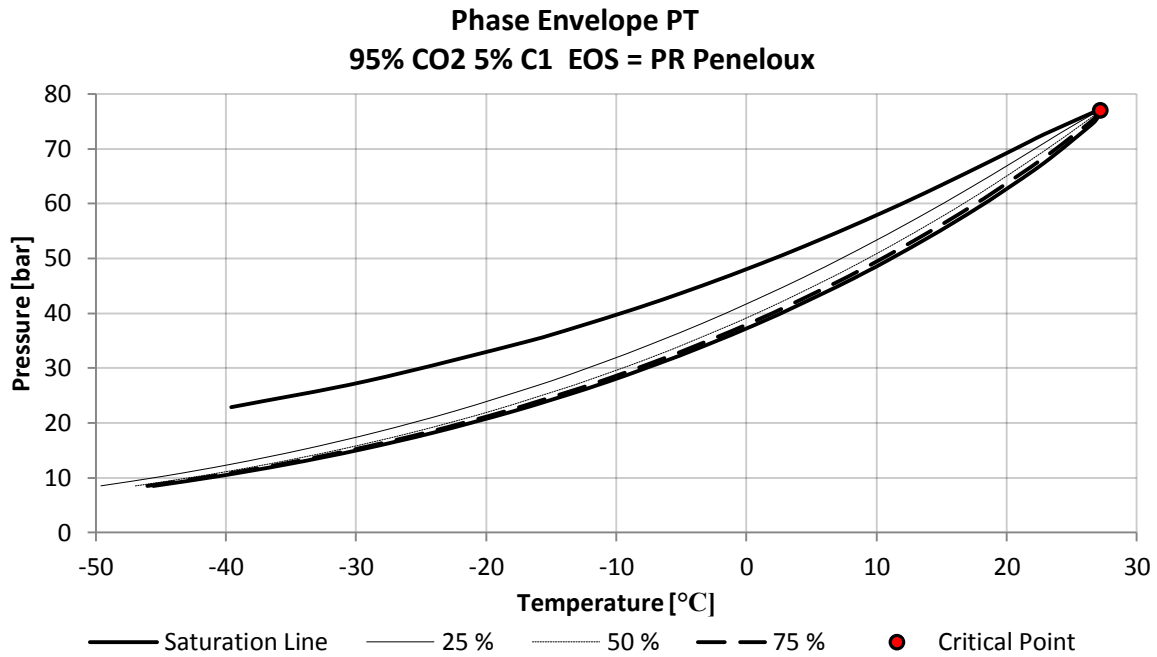


Figure 2-2 – PT Phase Envelope for a composition of 95% Carbon Dioxide and 5% Methane.
Created with PVTsim and PR Peneloux EOS

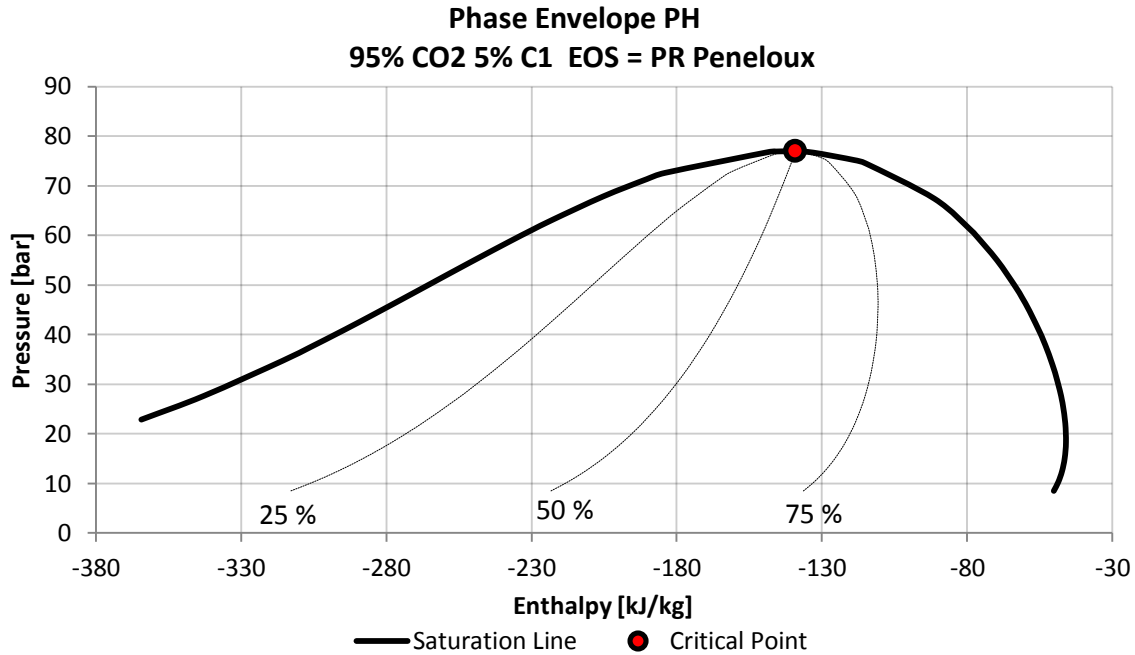


Figure 2-3 – PH Phase Envelope for a composition of 95% Carbon Dioxide and 5% Methane.
Created with PVTsim and PR Peneloux EOS

2.2.5 RESERVOIR MODELING

Depending on the available reservoir information and the desired degree of accuracy, there are various alternatives to define a reservoir in OLGA. For the purpose of this work, the simulations will be performed assuming a linear relation between the mass flow rate and pressure difference between the well and the reservoir.

$$\begin{array}{l} \text{Linear well} \\ \text{model} \end{array} \quad G_w = A + B(P_{wf} - P_r) \quad (2.10)$$

In the above equation G_w represents the mass flow rate into the reservoir, B the injectivity index, A the minimum required pressure difference for the fluid to start flowing and P_{wf} and P_r the bottom hole flowing pressure and reservoir pressure respectively. Note that A , in most cases, is less than or equal to zero. Other available flow relations are for instance the Forchheimer and backpressure equations which require a more detailed knowledge of the reservoir and well properties. An alternative to the standard well in OLGA, is to use inflow zones instead. The functionality is more or less the same, but with the possibility to specify a start and end position for the inflow to happen. This is in contrast to the well, which is point specific, and thus, it allows for interpolation in reservoir properties between the boundary positions. It is worth noting that the steady state pre-processor does not handle injection wells and in these cases it is required to use the dynamic solver (SPTgroup, 2012b).

None of the above alternatives include the actual reservoir in the simulations, but use inflow/outflow correlations instead. To perform transient simulations of the wellbore and reservoir, it is required to use the ROCX module, which can be coupled to OLGA through the near well option under boundary and initial conditions. It can be used as input to the OLGA simulation, or used to run standalone simulations from an OLGA restart file. This naturally requires detailed knowledge of the reservoir characteristics and will increase the complexity of the model, but if the transient behavior of the near-well region is of particular interest, this is the way to implement it in the OLGA model. Another alternative would be to include the simulation results from OLGA in the more comprehensive reservoir simulation software ECLIPSE (Schlumberger, 2012), but in general there is a need for a solution that couples wellbore and reservoir simulations. In addition to the transient behavior in the near-well region, ROCX may amongst others give a more precise prediction of the well at shut-in and start-up, better prediction of the onset of flow instabilities, distribution of fluid in the reservoir and cross flow between the different layers in the formation (SPTGroup, 2012a). For the purpose of this work however, it was considered more important to establish the basic models, as it would make the models significantly more complex. With this in place, future work may focus on further development of the models.

2.3 GEOLOGICAL STORAGE

With regards to geological storage of CO₂, several types of geological formations may be applicable. For the North Sea Basing, the largest potential capacity for CO₂ storage will be in depleted oil and gas fields or deep saline-water saturated formations (Directorate, 2012). Most of the available literature on the topic stresses that the CO₂ should be in supercritical or liquid state during transport and injection. However, the Sleipner CO₂ injection is highly likely to operate well within the two-phase area for the upper part of the well, indicating that this not necessarily need to be an absolute requirement (Svend Tollak Munkejord and Mølnevik, 2013). In some cases, two-phase flow may in fact be inevitable, for instance for formations at shallow depth and depleted oil and gas reservoirs with a low pore pressure (Lawrence J. Pekot, 2011a). With regards to efficient transport however, supercritical or liquid transport may be desirable, as it increases the transport capacity of the pipeline as the density is increased. In a typical well the increasing pressure and temperature with depth, ensures a transition to supercritical state at about 800 meters below surface level. At these conditions, the density of both liquid and gas approach each other and is about 500 to 600 times the density at surface conditions. In terms of volume this corresponds to about 0.27% of the atmospheric volume (Directorate, 2012).

Suitable formations for CO₂ injection typically have high porosity and permeability, to allow large volumes to be injected at the required rate. To ensure that the CO₂ is safely stored, it is an absolute requirement that the formation is overlain by an impermeable layer to prevent CO₂ migration upwards. As opposed to the storage formation, the cap rock must have low porosity and low permeability. Typical cap rock formations are shale, mud and evaporatives (salts). In general, there are five trapping mechanisms that may impact the storage capacity of a reservoir: stratigraphic, structural, residual, solubility and mineral trapping. Typically, stratigraphic and structural trapping are the most dominant mechanisms initially. Residual trapping is caused by the capillary pressure of water, which traps the CO₂ in the small pores. The solubility of the saline water affects the rate at which the CO₂ dissolves in the water, a process that forms a weak carbonic acid. The process also increases the density of the fluid and may enhance the dissolution process, as the internal fluid movement increases when the denser fluid move down as the gravitational forces increases. Mineral trapping depends on the rock formation as the dissolved CO₂ may react chemically with the surrounding rock to form stable minerals. This is a very slow process (thousands of years), but will in the long term offer the most secure form of storage.

The porosity of a formation is a measure of the pore space of the rock, which may be used to store fluids. The permeability on the other hand, measures the interconnectivity of the reservoir, or the rock's ability to allow fluids to flow through. This is naturally strongly affected by the size, shape and connectivity of the pores spaces in the rock. The main advantage of depleted oil and gas reservoirs, are their proven ability to safely store oil and gas for an extended period of time.

2.4 TRANSIENT SCENARIOS

2.4.1 SHUT-IN

Shut-in is another term for stopping the production or injection. This might be done in relation to operational issues, but is also done as a way of gathering information about the well and reservoir. In this context, experience from designing the models showed that a shut-in pressure curve was of high value when determining the injection coefficient of the inflow equation. The injection coefficient was then varied to determine a solution that gave better correspondence with the measure fall of pressure. Depending on the rate of change in pressure, low temperatures might be encountered in the well. This is particularly relevant for CO₂, due to the location of the critical point. From an operational point of view it is therefore desirable to close the valve gradually to allow the well to exchange heat with the ambient. An emergency shut-in would likely be of a more instant nature and may therefore lead to lower temperatures.

2.4.2 BLOWOUT

Blowout is a more intuitive term, and is characterize by a rapid discharge of CO₂ (or well content in general) from the well and reservoir. This is solely an undesired scenario and might involve a significant security risk. If the discharge rate is high, and the surface conditions allow little dispersion of the fluid, high concentrations may be experienced near the outburst. CO₂ is, as indicated in section 2.1.1, non-combustible and non-toxic, but can cause unconsciousness at concentrations between 7% and 10% in air. The density of CO₂ compared to air, may also cause the CO₂ to accumulate on the ground and displace the air in the event of an uncontrolled release (UNION, 2007). In this context it is of high value to estimate the expected discharge rate, in order to establish appropriate safety routines. Furthermore, the rapid expansion of the well content may give rise to low or very low temperatures, especially near the wellhead. The reason for this is the location of the critical and triple point of CO₂, but will also depend on the initial state of the well, and the conditions at the wellhead. Typical operating conditions suggest that the well enters the two-phase region during a blowout. The subsequent evaporation will then lead to decreasing temperatures in the well, if the heat transfer with the surroundings is insufficient to maintain the temperature at the given rate of evaporation. The relatively large Joule-Thomson for CO₂ also contributes to additional cooling. A worst case scenario would typically involve that the wellhead, for some reason, is completely removed. This has also been assumed in all the blowout simulations included in this work. Further complications may also be experienced if the conditions fall below the triple point and dry ice is formed. In Figure 2-4, pictures from a CO₂ blowout in Hungary is presented. Although the well and boundary conditions is not known, it should still give a good indication of the extent. I can also be seen how a jet was used to heat the surface in order to reduce the formation of dry ice.



Figure 2-4 Blowout Hungary 1998 (Bíró, 2009)

3 METHOD

3.1 GENERAL INFORMATION

Common for all the case studies covered by this work, is the general approach in the design of the models. It was in each case desirable to design a base case, from which various scenarios could be simulated. To achieve this, it was necessary to gather all relevant information regarding the wells, and make reasonable assumptions for the information that was not readily available. Initial simulations were used to check the results against expected values and boundary conditions. If necessary, parameter studies were performed and relevant parameters adjusted until the output was satisfactory. All base cases were simulated with constant parameter values (i.e. pressure, temperature and mass flow at wellhead), and the simulation time were set long enough for the simulation to approach the steady state solution. Assumptions and boundary conditions used in the various base case models are described in the assumption and boundary condition sections for the respective cases.

In order to verify the models however, operational data is required in order to tune the parameters. A validated well model may then be used to simulate transient scenarios such as start-up, shut-in and blow out. If measured values for pressure, temperature and flow rates only are available at the wellhead, the verified model can be used as a virtual downhole gauge to calculate all bottomhole flowing conditions. However, if a downhole gauge is installed in the well, bottomhole temperature and pressure measurements can be used in addition to the surface conditions to improve the capabilities of the verified model to also function as a virtual downhole multiphase flow meter (Mantecon, 2007).

A basic set of simulations were performed in all the case studies. This includes constant injection, shut-in and blowout. In addition to this, some of the case studies were selected for additional simulations. For the purpose of comparing the results, constant reservoir pressure was assumed unless otherwise is stated. For Sleipner, In Salah and Ketzin wellhead properties are considered known for an instant of time (constant values). For Snøhvit on the other hand, operational data from a performed shut-in were available from both the wellhead and the downhole measurement gauge (time series).

Regarding the blowout simulations, two sets of simulations were performed for all the different cases, one with, and one without backflow. For the cases with backflow, the production coefficient was set equal to the injection coefficient. For the cases without backflow on the other hand, the production coefficient was set to zero. In reality, a blowout is likely to induce water production from the reservoir, an effect that currently is not possible to include in OLGA, as the used single component module only is valid for pure components. The CO₂ VIP module, might give better results on this (as the component tracking module could be used), but due to license issues, this could not be tested out within the given time limit of the project. Furthermore, as the injected CO₂ is expected to migrate upwards in the formation, it may be expected to reduce the backflow of CO₂ during the event of a blowout. However, this would be a far more complex situation and is not addressed as the production coefficient is constant. Also, if water is produced, this might counteract the backflow from the reservoir as it will remain in liquid phase even at atmospheric pressure. This way it could act as a liquid plug with a significant hydrostatic pressure contribution. Again however, such effects were not possible to implement in the model, but the actual scenario might be expected to lie between the two extreme cases which was modeled.

Unless anything else is stated, all shut-in simulations have constant injection from 0 to 30 hours, when the injection stream starts to choke down over 2 hours. Similarly, all blowout simulations have constant injection from 0 to 29 hours, when the valve opens instantly. It was also assumed a response time of 1 hour, before the injection stream chokes down as in the shut-in cases.

3.2 SLEIPNER

3.2.1 BACKGROUND

The Sleipner field was discovered in 1974 and is located about 250 km offshore southern Norway and produces about 26 MSm³ of gas and 8000 Sm³ of condensate per day (Iain Wright, 2009). It is the largest and longest running CO₂ capture and storage project in the world, and was the first of its kind to implement an offshore gas treatment and CO₂ removal (amine based) unit, Sleipner T. This was necessary as the CO₂ content of the produced reservoir exceeds the requirements for export to Europe. The wellstream contains approximately 9% CO₂ and is reduced to approximately 2.5% to meet export and customer specifications (Institute, 2012). Furthermore, the injected CO₂ is wet, contains between 0.5% and 2% methane (Eiken et al., 2011) and is within the two-phase region at the wellhead (Håvard Alnes, 2011). Since 1996, about one million tons of carbon dioxide has been captured annually from the produced gas, and reinjected into the Utsira formation about 800 to 1000 meters below the seabed (Directorate, 2012). Accumulated over the life time of the fields, the injected CO₂ represents about a 3% reduction in the total Norwegian CO₂ emissions, as opposed to venting the CO₂ to atmosphere. The formation contains a 200-300 m thick saline sandstone layer with high porosity (38%) and permeability (1-8 Darcy) (Iain Wright, 2009), and is covered by a thick layer of shale rock, which prevents the CO₂ from migrating upwards. The storage capacity of the formation is about 16 Gigatonnes (Directorate, 2012). The decision to reinject the CO₂ was to a large extent driven by the imposition of the Norwegian CO₂ tax in 1991 (Iain Wright, 2009).

3.2.2 BASE CASE: ASSUMPTIONS AND BOUNDARY CONDITIONS

The Sleipner injection well does not have a downhole measurement gauge, and the only known conditions are therefore at the wellhead (WH). For pure CO₂, the injection stream was modeled as a source at approximately 65 bar, 24 °C and a mass flow rate of 103354 kg/h (H. Hansen, 2005) and (Alnes, 2012). The gas fraction at the inlet is not measured however, but of particular interest, as it is likely that the fluid enters the well within the two-phase area. Accurate prediction of the gas fraction and transition to supercritical phase in the pipeline, is crucial in determining the bottomhole pressure. To achieve this, it is important to precisely define the well geometry and the corresponding heat transfer of the different parts of the well. To do this the geometry was made up of 22 separate pipes, which in OLGA may be interpreted as parts of constant slope. The pipes can be further divided into sections to achieve better accuracy in the calculations (variables such as pressure, temperature and density are average values for each section). PIPE-1 was defined to go from wellhead to sea level, PIPE-2 from sea level to seabed, and the remaining pipes from seabed and down to the bottom of the well. By doing this it was possible to apply different heat transfer conditions to the different parts of the well. For the part above sea level, a constant ambient temperature of 10°C was assumed and the surrounding medium was set to air. In the same manner, the surrounding medium and a constant ambient temperature of 7°C were assumed for the part submerged in water. A geothermal gradient was specified for the wellbore, giving an ambient temperature at the seabed and bottomhole of 7°C and 47.3°C respectively.

The applied geothermal gradient is expressed by the linear equation as shown in the equation below (Håvard Alnes, 2011).

$$\begin{array}{l} \textit{Geothermal} \\ \textit{Gradient} \end{array} \quad T(z) = 31.7 \cdot z + 3.4 \quad (3.1)$$

Further considerations with regards to the heat transfer, are the thermal properties and dimensions of the materials used to specify the pipe walls and surrounding formation. For simplicity, all casing and tubing were assumed to be made of stainless steel. According to this, the riser was specified by a 20.6 mm thick uninsulated layer of stainless steel, with its accompanying thermal properties. Heat transfer was modeled as described in section 2.2.3. Whether the section is above or below sea level, air or water was specified as the surrounding medium. The layer of stainless steel in the wellbore was assumed to be of the same thickness as the riser, but to account for the effect of the surrounding formation, additional layers of formation were added to the wall. It should be noted however, that the annulus was not included in the wall model, something which clearly may affect the results to some extent. As the concentric layers of surrounding formation were added in a significant radial circumference, it may be reasonable to assume that the outer wall temperature approaches the ambient formation temperature. An inner diameter of 6.27 inches were assumed for the whole system, except for the last pipe where a 4 inch diameter was assumed. Please see Table 3-1 for properties used in the model.

Section	Material	Thickness	Capacity	Conductivity	Density
Riser	Stainless Steel	0.0206 m	450 J/KgK	20 W/mK	7850 kg/m ³
Riser	Air	∞	1000 J/KgK	0.023 W/mK	1.29 kg/m ³
Riser	Water	∞	4186 J/KgK	0.56 W/mK	1000 kg/m ³
Wellbore	Stainless Steel	0.0206 m	450 J/KgK	20 W/mK	7850 kg/m ³
Wellbore	Formation	0.05 , 0.1, 0.2, 0.4, 0.8, 1.5, 3 and 6 m	880 J/KgK	2 W/mK	2500 kg/m ³

Table 3-1 Wall Specification: Thermal properties and dimensions

The reservoir was modeled by the use of zones in OLGAs. By doing this the perforations along the wellbore was added, and the inflow calculated between the boundary positions, as opposed to the well option which is modeled as a point source/leak. The application of zones also allows for interpolation of the reservoir properties, but for simplicity, the reservoir temperature and pressure was assumed constant. The reservoir pressure and temperature was set to 103 bar and 41°C respectively (H. Hansen, 2005), and was assumed to be constant during the whole simulation period. As the Utsira formation is known for its excellent reservoir properties, and the injection has been stable during the whole operational period, this seems to be a valid assumption. With regards to the reservoir inflow, a linear relation was assumed (ref section 2.2.5) and the injection coefficient B was estimated based on the work done by Lawrence J. Pekot et al. (Lawrence J. Pekot, 2011b). Due to the excellent reservoir properties (in terms of porosity and permeability), the upper value of 400 000 Sm³/d/bar was chosen as an initial estimation. The density of

CO₂ was calculated at 1 atmosphere and 15°C, and the injection coefficient then converted to 8.6694e-005 kg/s/Pa, as required by OLGA.

As the chosen model configuration did not allow for initialization with the steady state pre-processor, initial conditions were necessary to run the model¹. An initial estimation used the conditions of the injected CO₂ as inlet conditions and assumed the fluid to approach ambient conditions at the end of the well. An initial bottomhole pressure of 105 bar was also assumed (Håvard Alnes, 2011). As operation is expected to be within the two phase region, small temperature variations may affect the density of the fluid significantly. This will in turn affect the bottomhole pressure of the well and illustrates the importance of accurate property predictions and determination of the transition to supercritical phase. As mentioned in the beginning of this section, the vapor fraction at the wellhead was unknown and had to be estimated. This was done by running a parameter study (ref. section 3.2.5) for the vapor fraction. The resulting vapor fraction which give a satisfactory match for the wellhead pressure was approximately 0.85.

As the degree of accuracy may vary significantly, it is important to know on which basis the assumptions have been made. This is illustrated in Table 3-2 for some essential values used in the model.

Position	Variable	Value	Data Source
Wellhead	Pressure	65 bar	Measured
Wellhead	Temperature	24 °C	Measured
Wellhead	Mass Flow	28.7 kg/s	Measured
Wellhead	Void Fraction	0.85	Estimated
Reservoir	Injection Coefficient	8.6694 e-005 kg/s/Pa	Estimated
Reservoir	Pressure	103	Estimated
Reservoir	Temperature	41 °C	Estimated
Reservoir	Phase	Supercritical	NIST

Table 3-2 - Quantifying the accuracy of important parameters used in the model. Red color indicates values that are expected to have a higher discrepancy, as they are estimated from other estimates.

¹ To use the steady state pre-processor the reservoir needs to be in the last section of the last pipe

The simulation time were set to 29 hours as the solution then seemed to approach the steady state solution. The case was then used as a restart case to simulate other transient scenarios. The applied geometry can be studied in Figure 3-1. For further model specifications it is referred to Appendix G.

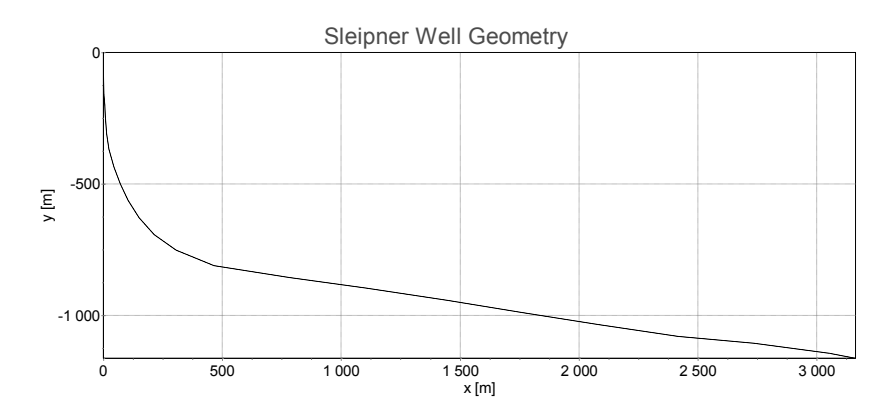


Figure 3-1 Applied Well Geometry Sleipner

3.2.3 TRANSIENT SCENARIOS

Shut-in

The shut-in of the Sleipner well was modeled by letting the injected mass stream decrease linearly to zero over two hours. The base case was used as a restart file, and from this it follows that the simulation starts at 29 hours. Choking of the source was initiated at 30 hours. Simulation end time was set to 150 hours, giving 5 days of simulation time from the time the injected mass starts to decrease. When using the single component module with PT-flash (ref. section 2.2.4), OLGA ran into some numerical issues that caused the simulation to terminate. For this reason MINDT was set to 1s in order to attempt to bypass the troublesome PT area (normally it should not be greater than 0.001).

Blowout

To model blowout of the well, some adjustments had to be done to the model. This involved adding a valve at the first section boundary of the first pipe. To represent the worst case scenario, the valve was specified to be activated during injection, with a back pressure of 1 atmosphere (specified as a pressure node) and a diameter equal to the pipe diameter. Furthermore, the discharge coefficient of the valve was set to 1. To be consistent with the previous models, the valve was activated at 29 hours of simulation time by a manual controller, and it was assumed a response time of 1 hour before the source was choked in the same manner as for the shut-in (starting at 30h). As for the shut-in case, numerical instability caused by operation close to the saturation line and critical point, required the minimum time step to be set to 1s for both blowout scenarios. The PVT-table range also had to be increased, to increase the tolerance in the calculations. It should be noted however, that this leads to decreasing resolution of the PVT data, and thus decreases the accuracy of the calculations.

3.2.4 OTHER COMPONENTS

To illustrate the behavior of CO₂, a shut-in of the Sleipner well was simulated using various components and mixtures. The fluids used in the simulations were as follows: H₂O, CH₄, a typical rich gas composition, a typical heavy oil composition and a mixture of 95 mol% CO₂ and 5 mol% CH₄. As the single component module only is available for CO₂ and H₂O, compositional tracking had to be used for the other fluids. This involves defining the fluids in PVTsim and creating an input file for use in OLGA. For the heavy oil, a typical northern oil composition was chosen from the PVTsim database, and the rich gas was specified according to the composition given in Appendix A-47. The transient scenarios were to a large extent modeled as for CO₂, but for the purpose of comparison, the wellhead pressures had to be adjusted in order to match the specified reservoir pressure of the Utsira formation. All other variables (i.e. injection coefficient, geometry, heat transfer, reservoir pressure etc.) were left unchanged, with an exception for the H₂O case. Due to the relatively low reservoir pressure, and the corresponding high hydrostatic pressure contribution of water, the low wellhead pressure caused negative pressures to occur in the pipeline. Consequently, the wellhead and reservoir pressures had to be increased in order to get a physical result and successfully run the model. In some models it was also required to adjust the stroke time of the leak to avoid numerical instabilities.

3.2.5 PARAMETER STUDY

Gas Fraction of Injection Stream

After defining the initial model according to the procedure described above, it was possible to run the model. However, as the initial simulations failed to match the known wellhead pressure, a parameter study was performed in order to determine a vapor fraction, which together with the other assumed model parameters, gave a reasonable agreement with the conditions at both the wellhead and reservoir. By default, the vapor fraction is set to be determined by OLGA, which calculates the fraction based on the fluid table, pressure and temperature at the source location (Mohanaraj, 2012). This can be overridden by manually specifying the gas fraction (gas properties are still taken from the generated property tables).

The initial simulations gave a vapor fraction at the wellhead of approximately 0.69. However, the resulting wellhead pressure turned out significantly lower than expected at 41.5 bar. The reason for this may be more complex than just a miscalculated vapor fraction, but as operational data would be needed in order to validate the model, other values were assumed reasonable for the purpose of this study. Accordingly, all parameters except the vapor fraction of the injection stream were assumed constant in the parameter study, and simulations were then performed for vapor fractions ranging from 0 to 1, with a step size of 0.1.

The result from the parameter study can be seen in Figure 3-2. Where vapor fraction -1, represents the case where OLGA determines the fraction from the tabulated values. It can be seen that the resulting wellhead pressure is lowest for the OLGA determined fraction, and that the measured wellhead pressure is obtained for a vapor fraction slightly above 0.8. It should be noted however, that these values are averaged over the first section. Accordingly, the vapor fraction was set to 0.85 as indicated in section

3.2.2. It can also be seen that the output fluctuations are increasing for high vapor fractions, and for a vapor fraction of 1, the simulation failed to converge.

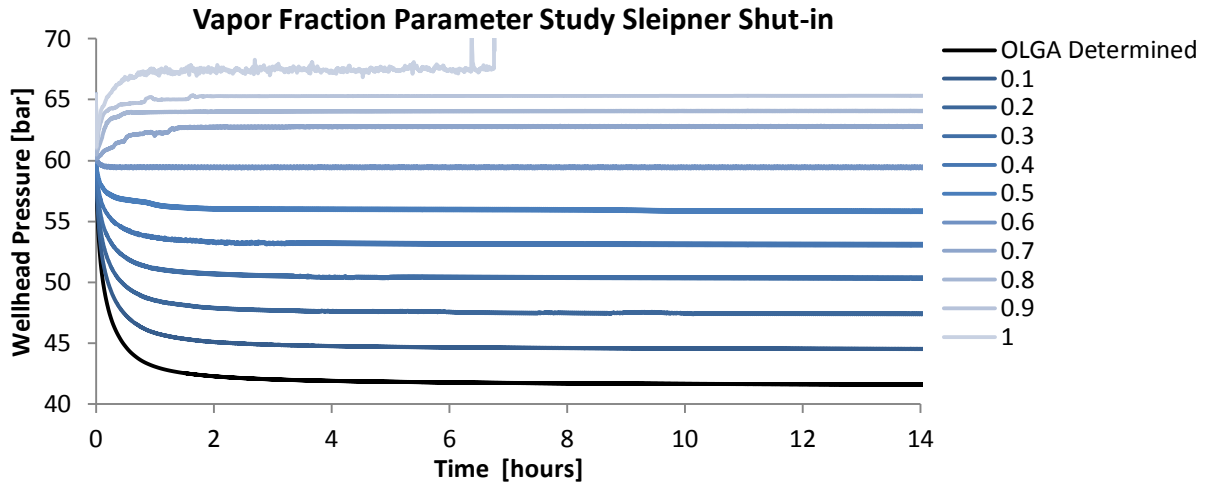


Figure 3-2 Parameter Study: Injection Stream Vapor Fraction

3.3 SNØHVIT

3.3.1 BACKGROUND

The Snøhvit unit is located approximately 150 km of the coast of Norway and is connected to three major gas fields, Snøhvit, Askeladd and Albatross, discovered in 1984, 1981 and 1982 respectively. The LNG plant got operational in August 2007 and CO₂ reinjection into the Tubåen formation started in April 2008. It is operated by Statoil and is the first Oil and Gas development in the Barents Sea. The production strategy is a phased development starting off with eight production wells and one CO₂ injector. Askeladd and thereafter Albatross will be phased in to maintain the required production plateau. The project has made significant technology advances when it comes to for instance long distance transport of the unprocessed well stream, remote controlled field facilities from onshore, production of the main process on a barge and being the world's first offshore CO₂ pipeline with subsea well. Many of these were necessary to adapt to the conditions on site, but also in order to meet the strict environmental and emission regulations given by the authorities.

The plant was the world's most efficient liquefaction plant when built, producing LNG at about 0.243 kWh/kg LNG (Rødum, 2011). The liquefaction is done by a mixed fluid cascade process (MFC) developed by Statoil and Linde, and is separated in a pre-cooling, liquefaction and sub-cooling cycle. This approach gives better temperature adaption (compared to pure refrigerants) between the cooled gas flow and the evaporating liquefaction flow, thus reducing the power input to the liquefaction process. It also reduces the complexity of the system compared to a conventional cascade process, as it requires amongst others fewer pressure levels, compressor stages and heat exchanger units. However, the refrigerants need to be produced and controlled, as the efficiency is highly linked with the composition. Another important factor affecting the overall efficiency is the availability of cooling water at low temperature. Estimations show that power input to the liquefaction process increases about 1 % per °C the cooling water temperature increases. The liquefaction process reduces the volume with a factor of about 610, ideal for long distance transport where transportation by pipeline is uneconomic. On annual basis the production facilities export approximately 5.7 billion Sm³ of natural gas, 460 000 tons condensate and 220 000 tons LPG (Rødum, 2011).

Furthermore, about 700 000 tons CO₂ is removed from the feed stream and reinjected into the Tubåen formation annually. Accumulated over the 30 year design life of the development, this is expected to count for approximately 12 GSm³ CO₂ (Olav Hansen and Ringrose, 2013) or about 2 % of the total Norwegian CO₂ emissions (Maldal and Tappel, 2004). The CO₂ is separated in an amine process operating at high pressure and low temperature (approximately 66 bar and 45 °C) in the absorber, and low pressure and high temperature in the regenerator (approximately 1.5 bar and 113 °C). The amine process is one of the most energy intensive processes, utilizing waste heat from the power production. The gas in the Snøhvit, Askeladd and Albatross field contains about 5-8 % CO₂, which must be reduced to less than 50 ppm before the liquefaction process. The separated CO₂ is then dried and recompressed to ensure that free water does not form, and that the CO₂ remains in the liquid region, during the whole transport. The technology for the CO₂ storage is considered proven by the CO₂ storage at Sleipner, but the different conditions resulted in some challenges when designing the injection system. Due to its high permeability

and porosity, the Utsira formation at Sleipner is virtually an ideal formation for storing CO₂. The Tubåen formation on the other hand, has both lower permeability and porosity and also lacks a huge water-bearing, similar to the Utsira formation at Sleipner. In addition, the Utsira and Tubåen formation are located at different depths, 800-1000 m and 2400-2600 m respectively. This leads to higher operational pressures in the injection system at Snøhvit.

During the autumn of 2008 a rapid pressure increase was experienced in the Tubåen formation. This was interpreted to be caused by salt precipitation in the near wellbore region, which reduced the injectivity, or communication between reservoir and formation (Olav Hansen and Ringrose, 2013). As the CO₂ is dehydrated prior to injection, formation water will likely dissolve into the fluid and thus increase the salinity of the remaining water. Eventually, this may lead to salt precipitation, reduction of pore space and reduced injectivity. Weekly injection of Methyl Ethyl Glycol (MEG) did counteract the loss of injectivity, but as the problems persisted and the pressure approached the estimated rock fraction pressure, Tubåen was abandoned in favor of the Stø formation. For the purpose of this work however, the Tubåen formation will be used.

3.3.2 BASE CASE: ASSUMPTIONS AND BOUNDARY CONDITIONS

As opposed to the other cases included by this study, operational data were available for the Snøhvit case. The available data are from a shut-in performed in August 2008 and were for convenience averaged over 5 minutes to reduce the fluctuations. Furthermore, the time series were converted to hours, in order to easily be compared with results from OLGA. In the design of the base case, the main target was to establish a model that gave reasonable accordance with the operational data for constant injection rate, while maintaining the simplicity of the model. Further use of the operational data would require in-depth analysis and optimization of the model, and will be discussed further in section 3.3.4.

One of the main challenges in the design of the Snøhvit base case, was to establish reasonable estimates for the reservoir properties. Initial estimates suggests a reservoir pressure and temperature of 290 bar and 98-100°C (Olav Hansen, 2011). In April 2011 however, the estimated reservoir pressure in Tubåen were estimated to approximately 388 bar (Hansen, 2012). Thus, in order to be in accordance with the available operational data from August 2008, an initial estimate of 320 bar (based on the presentation by Ringrose et al. (Philip Ringrose, 2011)) was assumed.

Another challenge that got evident when tuning the model with regards to measurements at both wellhead and gauge, was the discrepancies caused by compositional differences between the actual and simulated fluids. To quantify the expected discrepancy, a density estimate from the Snøhvit data was compared to densities obtained for wellhead and gauge conditions, using the NIST database. This gave an average density difference between the wellhead and gauge of approximately 35.5 kg/m³, which represents a hydrostatic pressure contribution of about 5.1 bar. Consequently, as the single component module assumes pure CO₂ in the calculations, the simulated pressures might be expected to lie about 5 to 6 bars above measured values. Note that this assumes a linear relation for the density profile in the well, but when considering that the fluid will remain in liquid phase during normal operation, the assumption should not be too far off. As the hydrostatic pressure contribution is expected to be greater at larger depths, an injection coefficient of 5.41944e-006 kg/s/Pa was chosen, as this gave better coherence with

the simulated and measured wellhead pressures, while the gauge pressure was within the expected deviation at approximately 4.5 bar. The coefficient was established by performing a parameter study with various injection coefficients. The production coefficient was then set equal to the injection coefficient to allow backflow from the reservoir.

The operational data were used as input at the wellhead, and according to this, the injection stream was specified with a mass flow of 17.31 kg/s at 113.3 bar and 3.72 °C. The gauge measurements were not directly used in the model, but were used to optimize the model parameters along with the wellhead measurements. Table 3-3 presents some of the essential design parameters and values of the model.

Position	Variable	Value	Data Source
Wellhead	Pressure	113.3 bar	Measured
Wellhead	Temperature	3.72 °C	Measured
Wellhead	Mass Flow	17.31 kg/s	Measured
Wellhead	Phase	Liquid	NIST
Gauge	Pressure	247	Measured
Gauge	Temperature	17.4 °C	Measured
Gauge	Phase	Liquid	NIST
Reservoir	Injection Coefficient	5.41944e-006 kg/s/Pa	Estimated
Reservoir	Pressure	320	Estimated
Reservoir	Temperature	98.7 °C	Estimated

Table 3-3 - Quantifying the accuracy of important parameters used in the model. Red color indicates values that are expected to have a higher discrepancy, as they are estimated from other estimates.

With regards to the heat transfer with the surroundings, the ambient temperature at the top of the well was assumed to be approximately equal to the sea water temperature at the seabed at 4°C. Furthermore, the ambient temperature at bottom of the well was assumed to be slightly higher than the reservoir temperature estimate and set to 102°C. The initial conditions were set equal to the measured wellhead conditions at the inlet, and estimated roughly to be 326.5 bar and 102°C at the bottom of the well. The model was then set to run for 29 hours to let the solution approach steady state conditions.

Priority was given to make the geometry as simple as possible, without excessive loss of accuracy. Accordingly, the applied geometry was made up of 53 pipes and 133 sections. Pipe walls and formation were specified in a similar manner as for the wellbore part of the Sleipner case, described in section 2.2.3. The applied geometry can be seen in Figure 3-3 and a summary of the model specifications in Appendix G.

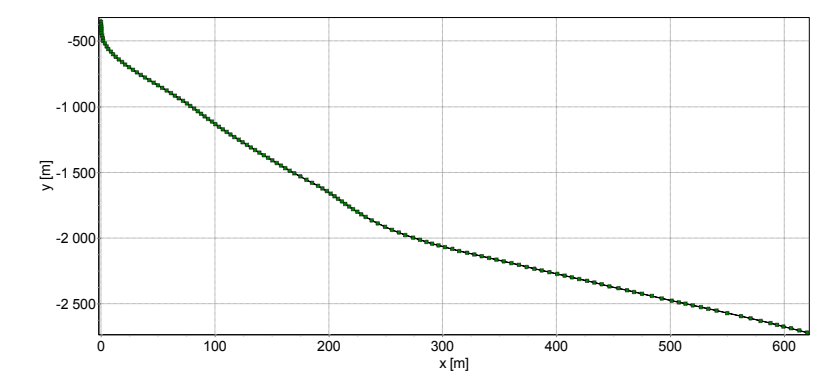


Figure 3-3 Geometry Snøhvit Injection Well

3.3.3 TRANSIENT SCENARIOS

Shut-in

The shut-in was modeled in a similar manner as for the Sleipner case. Accordingly the base case was used as a restart case for the simulation and the simulation starts at 29 hours. The injected CO₂ was choked down over 2 hours, starting at 30 hours simulation time. As opposed to the Sleipner shut-in, the Snøhvit shut-in was able to run with a minimum time step of 0.001. No Further adjustments were done.

Blowout

Blow down was modeled using a valve at the first section boundary of the first pipe. The pressure node on the other side, was specified with approximate values for the conditions at the subsea wellhead. Accordingly the conditions were set to approximately 31 bar and 4°C. The blowout valve was set to open at 29 hours, and the injection was choked down over two hours, starting at 30 hours. The large and instant changes occurring once the valve opened, caused the model to run into numerical issues for the same configuration as for the shut-in. As a consequence of this, the minimum time step was set to 1s for both blowout scenarios. However, the model with reservoir backflow still experienced major problems, and eventually terminated. Most likely this was caused by the rapid pressure drop and subsequent evaporation of the CO₂ in the well. Consequently, the time constant TBOILING was increased from 1s (standard value) to 10s. In general, large values will slow down the mass transfer, allowing for non-equilibrium in chemical potential. Small values will force the phases towards equilibrium. Too small values might however lead to instabilities, which in turn may give a non-physical result (SPTgroup, 2012b). The PVT-table limits were, as for the Sleipner blowouts, increased in order to increase the tolerance during the calculations.

3.3.4 HISTORY MATCHING AND MODEL OPTIMIZATION

The OLGA Risk management and optimization module (RMO) was used to match the simulation output from the Snøhvit shut-in model with respect to operational data. In this process operational data from a shut-in of the CO₂ injection well at Snøhvit in 2008 was used. This included pressure, temperature and mass flow measurements at the wellhead, and pressure and temperature measurements at the gauge. The operational data were then averaged over 5 minutes to reduce some of the fluctuations, and the measured data can be seen in the figures below.

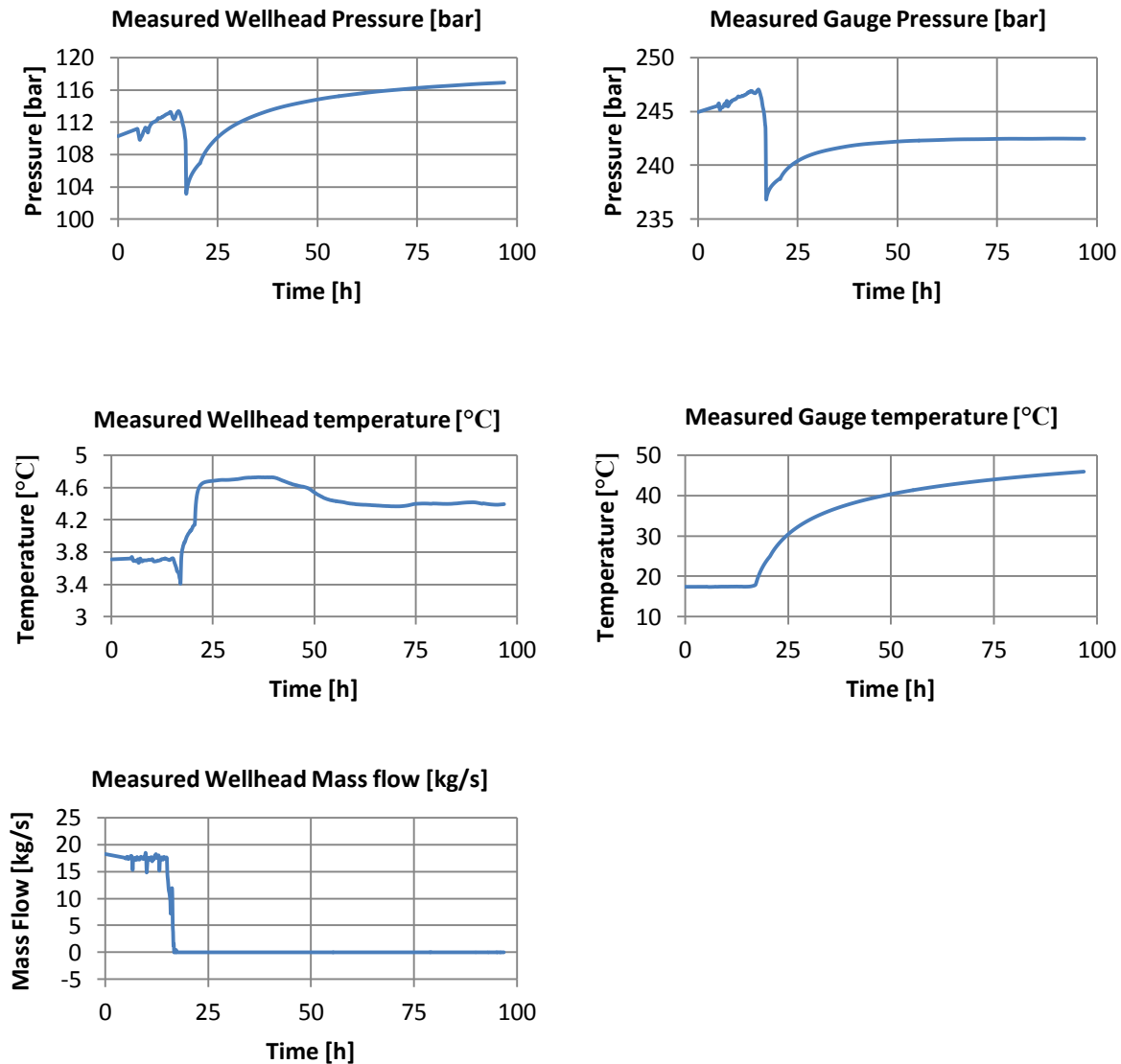


Figure 3-4 Operational Data at Wellhead and Gauge Snøhvit Shut-in

The wellhead measurements were then used directly used as input to the source at the wellhead. This way, the shut-in was implicit modeled by the changing conditions. It was however considered necessary to apply some simplifications. Initial simulations revealed some trouble likely caused by mismatch between the specified initial conditions and the nearly steady state conditions in the well leading up to the shut-in. However, as adjusting the initial conditions failed to solve the problem, it was decided to increase the initialization time of the model, in order to give some time for the output to stabilize. From experience, the steady state pre-processor seems to give a better result in determining the initial state, but it comes with some absolute requirements in order to run. One of these is that the well has to be placed in the last section of the last pipe. During the design of the model however, it was considered desirable to include the openhole in the end of the well, as this could affect the results in some of the transient simulations. Accordingly, the steady state pre-processor could not be applied, and initial conditions had to be used. The initialization time was then increased from 30 hours (which was used in all the other shut-in models) to 130h. The operational data were also modified to be in accordance with the time scheme used in OLGA.

Furthermore, as RMO only takes into account the last value in a specified time series, the model was further simplified by assuming constant values for the first 130 hours of the simulation. Thus, the pressure buildup seen in the measured wellhead and gauge data were neglected, and set equal to the state just before the shut-in was initiated. To allow for variations in the parameter values, the shut-in can be divided into sections, but would require running a new iteration process for each section. A linear relation will then be assumed for the selected parameters. However, as the process is both time consuming and more complicated, it may be desirable evaluate the benefit before proceeding. In this context, it was therefore considered sufficient to assume constant parameters prior to the shut-in, but allow them to change linearly between 130 hours and the end of the simulation.

The operational data were then used as input to the RMO module. At first it was considered best to match the simulation result with respect to pressure and temperature at both locations, but after some initial testing it was decided only to optimize only on the wellhead pressure and temperature. This was also recommended by SPT group. Due to the density differences between the pure CO₂ used in the simulations, and the actual composition at Snøhvit, it was considered more appropriate to optimize on the wellhead conditions, as the pressure differences will be larger with increasing depth. This was also indicated in section 3.3.2, where an expected pressure difference of 5-6 bar was calculated at the gauge. One option could be to introduce either a valve, or the pipe roughness, as an input parameter, to offset the deviation.

RMO calculates a global value based on the deviance between simulation results and measured data for all the parameters specified to be part of the objective function. The iteration process may then either maximize or minimize this global value. During these simulations the latter choice was specified. As indicated, the iteration process was then run to match the model with regards to the measured pressure and temperature data from the wellhead, up to 130h. However, due to the already mentioned initialization problems, it was decided not to optimize on the very first part of the simulation. Neither was it considered a good solution to only optimize on a single pressure and temperature value at 130h. The reason for is that the angle of the pressure and temperature curves would not be considered, and might therefore give a misleading result. The model was then optimized with regards to the time span between 120 and 130 hours, and the simulation ran until the global value seemed to stabilize. To allow the parameters to change

during the shut-in, a new iteration process was run, based on the results from the previous iteration. This was done by editing the time series in OLGA for the respective parameters, by copying the 130h values to the end time of the simulation. This should allow the parameters to change linearly in this interval, but could just as well remain unchanged as if it gives a smaller global value. As the initial simulations seemed to be a bit misleading, it was decided to disregard the temperature measurements in this iteration process. The reason for this, is a general suspicion that the measured wellhead temperature seems to be influenced by some other factors not accounted for in the model. This can be seen from the measure wellhead temperature in Figure 3-4, and might be caused by interference with the measuring device. The parameters included in the iteration process include the coefficients of the reservoir inflow and outflow equations, initial conditions and reservoir conditions. Other parameters could naturally also be of interest, but in this work the parameters listed in Table 3-4 were considered of prior importance.

Parameters
AINJ
APROD
BINJ
BPROD
HMININNERWALL
INPRESSURE
INTAMBIENT
INTEMPERATURE
OUTAMBIENT
OUTPRESSURE
OUTTEMPERATURE
RESERVOIR PRESSURE
RESERVOIR TEMPERATURE

Table 3-4 Parameters used in the iteration process

3.4 IN SALAH

3.4.1 BACKGROUND

The In Salah project reinjects carbon dioxide which is removed from the production stream from several gas fields. The CO₂ content of the gas fields lie between 1 and 10 percent and has to be reduced in order to meet export specifications. It is then stored in a deep saline formation about 1.9km below the surface at the Krechba formation in central Algeria. Injection started in 2004 and has since then injected more than 3.8Mt CO₂ (MIT, 2012). Due to the relatively low permeability, three long horizontal wells is used for the injection, however, in this study only the 501 well will be investigated. A wide range of monitoring techniques has been implemented in the project to assure that the CO₂ remains in place and to demonstrate that CCS is a viable greenhouse gas mitigation option.

3.4.2 BASE CASE: ASSUMPTIONS AND BOUNDARY CONDITIONS

The In Salah model was to a large extent built on the published article by Bissel et al. (R.C.Bissell, 2011). However as the available data was scarce, several estimations and assumptions had to be made, in order to run the model. To make up for some of the missing data, the Snøhvit model was used as basis and used if no data, or reasonable estimates, were available.

Initial and heat transfer conditions were estimated from Bissel et al. (figure 2 and 3). Accordingly, the initial temperature at the inlet and outlet were set to 32°C and 50°C respectively. The inlet and outlet pressures were estimated from the relatively stable interval around 2009 in figure 2, and set to approximately 170 bar at the wellhead and 325 bar at the bottomhole. The ambient formation temperature on the other hand were taken from figure 3 and set to 34°C at the surface and 95°C at the bottomhole. It should be noted that the surface conditions is subject to relatively large fluctuations as the facility is situated in the desert (may experience large temperature differences between day/night and also on a seasonal basis). This was not considered of major importance in this work, nonetheless, a parameter study was conducted with surface temperatures ranging from 30°C to 40°C. This showed a negligible change in pressure (the fluid is already in supercritical state) and more significant changes with regards to temperature. Still, for the purpose of this study, the surface temperature was set to 34°C. The injected mass flow was set constant to approximately 5.6 kg/s at 170 bar, 32°C.

With regards to the reservoir conditions, little information was available and a rough estimation was used based on the available information. Accordingly, the reservoir temperature was set to 95°C according to the initial formation temperature from Bissel et al. (R.C.Bissell, 2011) and the reservoir pressure was set to 320 bar, slightly lower than the flowing bottomhole pressure at 325 bar.

The applied geometry comprised roughly two parts, an initial steep part down to reservoir depth at approximately 1900 meters, and a long horizontal part at roughly the same depth.

It should be noted that the estimations and assumptions done in order to make the model, might affect the result significantly.

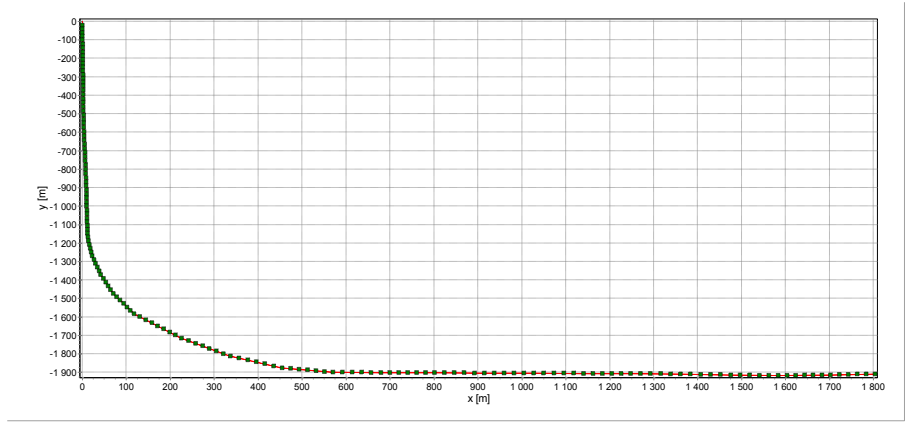


Figure 3-5 In Salah Well Geometry

3.4.3 TRANSIENT SCENARIOS

Shut-in

The shut-in was modeled by choking the valve over 2 hours, starting at 30 hours and similar to the Snøhvit case it was able to run with minimum time step of 0.001s without further adjustments.

Blowout

Blowout was modeled by adding a valve at the first section boundary of the first pipe. The connected pressure node was specified with surface conditions at 1 atm and 34°C. As for the previous cases, two blowout scenarios were modeled, with and without backflow. The blowout valve was opened at 29 hours, and the injection stream was choked from 30 to 32 hours. For the case with backflow, a minimum time step of 0.001s was used, but to run the model TBOILING had to be increased to 10s. For the case without backflow on the other hand, TBOILING was left at 1s, but the minimum time step was increased to 0.1s. The PVT range also had to be increased.

3.5 KETZIN

3.5.1 BACKGROUND

The Ketzin pilot site is the longest operating on-shore CO₂ storage site in Europe (S. Martens, 2011), aiming to improve the scientific understanding of the geological storage of CO₂ and study the subsurface processes of the CO₂ injection and distribution (GFZ, 2012). Injection began in June 2008 and by September 2011 approximately 53.000 tons of CO₂ had been injected. Based on existing data from previous seasonal storage of natural gas, further site characterization were performed and three wells were drilled for CO₂ injection and monitoring of the reservoir. The targeted saline aquifer for CO₂ storage is the Stuttgart Formation at about 630 -710 meters depth. The Ktzi 201 well is used for both injection and observation, while the latter two (Ktzi 200 and Ktzi 202) are solely used for observing the injection and migration of the CO₂ in the formation. In addition to this, a shallow groundwater observation well (Ktzi P300) was installed above the 210 meters thick cap rock of the Stuttgart Formation in 2011. In terms of the injected mass, the size of the project is considerably smaller than industrial scale projects, and is limited by legal regulations (in order to be considered as a research and development project). Since startup, the average injection has been approximately 45 tons per day and the facility was designed to allow for injections ranging from 0 to 78 tons per day. The majority of the injected CO₂ is of high purity (>99.9 %) which is a by-product from hydrogen production (S. Martens, 2011).

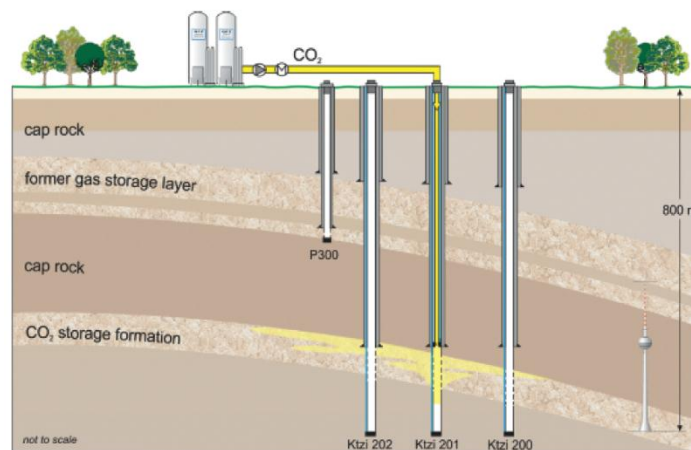


Figure 3-6 Ketzin Injection and Monitoring System (GFZ, 2012)

3.5.2 BASE CASE: ASSUMPTIONS AND BOUNDARY CONDITIONS

For the Ketzin base case, available data for the Ktzi 201 well were gathered to make a reasonable model of the well. Based on the work done by A. T. Singhe et al (A. T. Singhe, 2013), the model was discretized into three pipes. All section lengths specified to be approximately 20 meters. However, as the Ktzi 201 well is a vertical well, it gives a larger degree of freedom with regards to the discretization. As a consequence of this it would also be an excellent candidate for sensitivity analysis due to the simplicity. The reservoir is located at approximately 630 meters depth and the initial temperature and pressure were around 33.5 °C and 61 bar respectively (A. T. Singhe, 2013). The geothermal gradient used for the heat transfer was taken to be $3.7 \frac{^{\circ}\text{C}}{100\text{m}}$ and the vertical pressure gradient $1.1 \frac{\text{bar}}{10\text{m}}$ (Bernd Wiese, 2010). By then using the thermal gradient and a surface temperature of 10 °C, the initial bottomhole temperature was estimated to 37.94 °C. The vertical pressure gradient gives a higher reservoir pressure on the other hand, but as Singe et al. provides some measurements in their reports, 61 bar were considered to be in best possible accordance with this.

Wellhead pressure and temperature were set to 55.37 bar and 37.09 °C respectively (A. T. Singhe, 2013). The volume flow was also obtained from the same article (26375 m³/day), but had to be converted to mass flow in order to be used as input in OLGA. It was however not specified if the flow rate was at standard or wellhead conditions. Density was therefore calculated for both the wellhead and standard conditions (15°C, 1 atm) and used to calculate the respective mass flows. This gave a mass flow of 151910 kg/h at wellhead conditions and 2057.9 kg/h if standard conditions were assumed. However, as the mass flow at wellhead conditions was even greater than the injection rate at Sleipner, this value was disregarded. Also, the lower value was in reasonable accordance with the average injection rate of 45 tons per day. The high purity of the injected CO₂ at Ketzin, should reduce the discrepancies caused by compositional differences. As a consequence of this it should be reasonable to expect a good match between reservoir and wellhead pressure, but this is also highly dependent on whether the operation is within the two-phase area, and whether the computational algorithm is capable of accurately predicting the transition to supercritical. The latter is naturally highly dependent on the definition of the well model and the specified parameter values. This is attempted quantified in Table 3-5. As can be seen, the wellhead conditions are assumed to be known. It also seems to be reasonable to assume that the obtained reservoir pressure and temperature are within acceptable limits, as all values used in the model are based on published work. This leaves amongst others the injection coefficient and heat transfer as some of the parameters that have to be tuned to meet the boundary conditions of the base case. With regards to the injectivity coefficient of the inflow equation, a value from Michael Zettlitzer et al. (Michael Zettlitzer, 2010), was attempted converted from volume to mass basis in order to be used in OLGA. Both standard and downhole conditions were assumed, but as the obtained injectivity coefficient were too small, it caused the simulations to terminate. An estimate from Lawrence J. Pekot et al. was also applied, but as the resulting wellhead pressure was about 3 bars too low, a parameter study was run with values in between the two studies. As a result from this, an injection coefficient of 1.58e-006 kg/s/Pa was established, and seemed to give reasonable results according to the given boundary conditions.

Position	Variable	Value	Data Source
Wellhead	Pressure	55.37 bar	Measured
Wellhead	Temperature	37.09 °C	Measured
Wellhead	Mass Flow	2057.9 kg/h	Measured
Wellhead	Vapor Fraction	-1	OLGA determined
Reservoir	Injection Coefficient	1.58e-006 kg/s/Pa	Estimated
Reservoir	Pressure	61 bar	Estimated
Reservoir	Temperature	33.5 °C	Estimated

Table 3-5 Quantifying the accuracy of important parameters used in the Ketzin model. Red color indicates values that are expected to have a higher discrepancy, as they are estimated from other estimates. -1 sets the vapor fraction to be determined by OLGA.

The pipe wall and surrounding formation were specified as described in section 2.2.3, but with minor variations with regards to thickness of the layers and thermal properties of the formations. Tubing and casing were assumed to be of stainless steel, but modified with the conductivity used by Singhe et al. The content of the annulus was assumed to be oil based mud (Espen Krogh, 2012), as no other information was available. Thermal capacity and density of the formations were also difficult to obtain, and was therefore also based on the values provided by Espen Krogh et al. The thermal conductivities on the other hand, were taken from Singhe et al. Detailed description of the model can be seen in Appendix G.

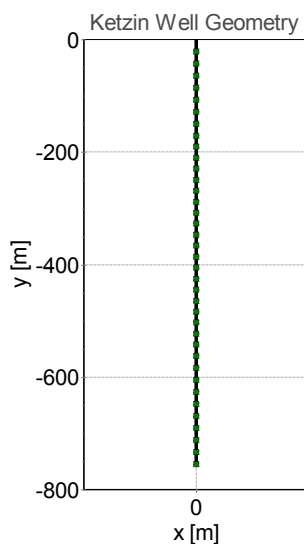


Figure 3-7 Ketzin Well Geometry

3.5.3 TRANSIENT SCENARIOS

Shut-in

The Ketzin shut-in was modeled in the same manner as the other cases, by choking the injection stream over two hours, starting at 30 hours. Both the minimum time step and the evaporation time constant were left as in the base case at 0.001s and 1s respectively.

Blowout

Blowout was modeled by adding a controlled valve, set to open fully, with a discharge coefficient of 1, at 29 hours. The injected CO₂ was choked down as describe for the shut-in after 30 hours. As the wellhead is on the surface, a pressure node was used to model the surface conditions at 1 atm and 10°C. As the operational range of the Ketzin injection system is in the superheated region, a blowout will not involve phase change, unless the fluid is cooled enough for it to enter the two-phase area. Consequently, less trouble was experienced with the blowout simulations, as opposed to the other cases covered by this work. Accordingly, both blowout simulations were able to run with a minimum time step of 0.001s. The temperature range of the PVT tables had to be increased however, as the temperature got below the tabulated values.

3.5.4 GRID SENSITIVITY

A grid sensitivity analysis was performed on the Ketzin well, to investigate the impact of the model discretization on the temperature and pressure. Ketzin was chosen as it is a virtually vertical well and thus offers great flexibility with regards to varying pipe and section lengths. In OLGA, the geometry is divided into pipes (parts of constant slope) and then again into sections (for which the calculations are performed). Thus, the discretization into sections is limited by the pipe length. For the Ketzin well however, the vertical geometry allowed for defining the whole well by a single pipe, which then could be divided into sections. Uniform section lengths were then applied, and simulations were performed using section lengths ranging from 1 to 256 meter, by increasing the length by a factor of two. Simulation time was not considered in this analysis, although it was seen to increase significantly with decreasing section length. The study is primarily meant to indicate how the simulation result in general, is affected by the discretization of the model. However, it should be noted that the source is linked to the first section and thus moves when the section lengths is altered. This will clearly affect the result. As volume variables such as pressure and temperature are calculated as averages for the sections, the value is expected to increase with increasing section length as pressure and temperature increases with depth.

The performed simulations where identical to the Ketzin shut-in simulation, apart from the discretization, and as can be seen from both Figure 3-8 and Figure 3-9, pressure and temperature seems to approach a numerical solution when the section length is decreasing. According to this it should be possible to quantify the error caused by the discretization of the model. However, most real cases have a more complex geometry than the Ketzin case, and it is therefore not possible to directly transfer this result.

Nonetheless it should be possible to establish some guidelines and with regards to discretization, and estimate the expected error for this particular case.

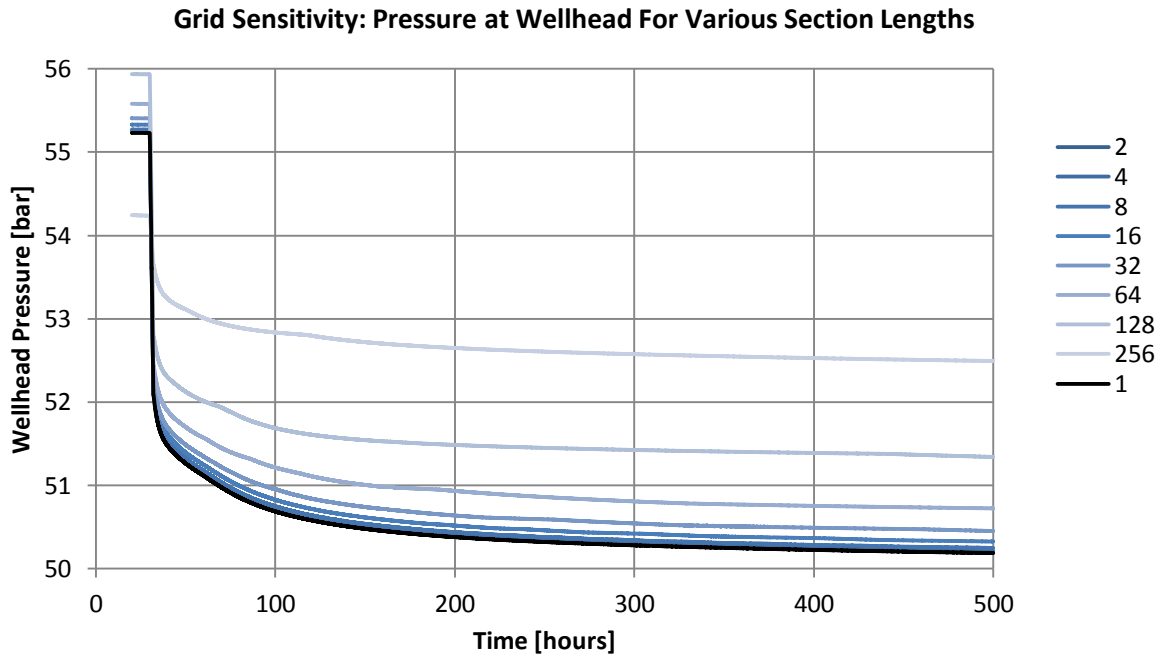


Figure 3-8 Grid Sensitivity: Pressure at Wellhead For Various Section Lengths

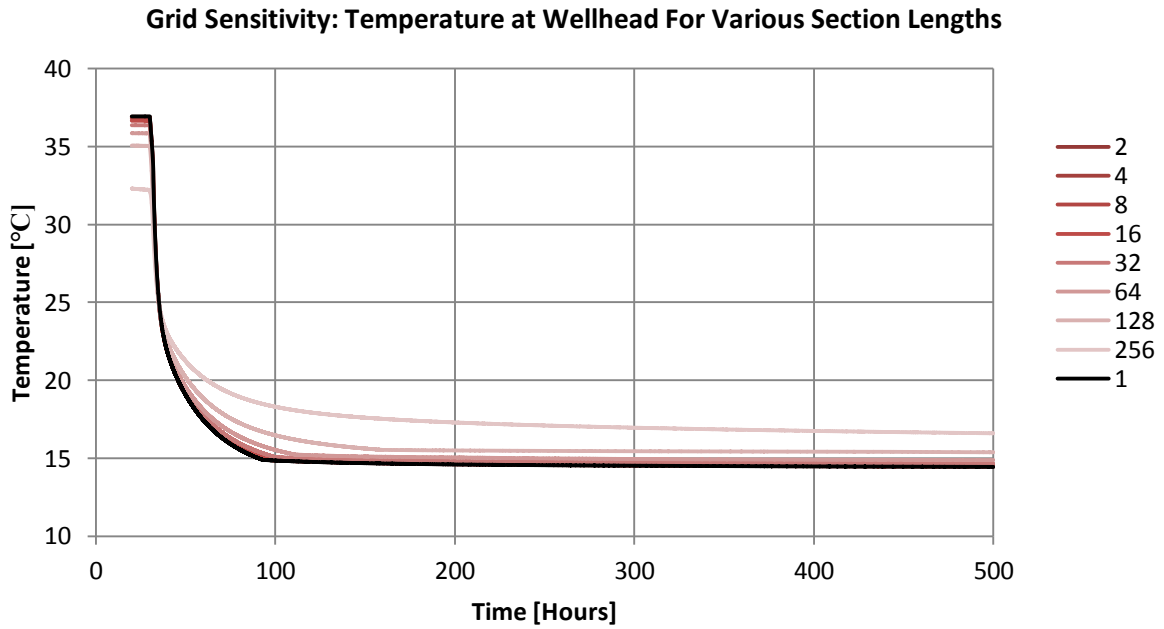


Figure 3-9 Grid Sensitivity for Temperature at Wellhead

To obtain an estimate for the error caused by increasing section length, pressure and temperature values at 500 hours were plotted against section lengths. This showed an approximately linear relation for both properties, but is in Figure 3-10 and Figure 3-11 presented with a logarithmic scale on the horizontal axis to increase the readability. The result was then extrapolated to zero meters and the result was used to estimate an approximate error for the various section lengths simulated. This gave approximately 4.6% deviation in pressure and 15% deviation in temperature for the 256 meter section lengths. It can also be seen that to keep the deviation below 1% for both pressure and temperature in this example, section lengths should not be longer than approximately 20 meters. However, as the simulation time is highly dependent section lengths and number of sections, it is generally not recommended to use section lengths shorter than 20 meters. This however, needs to be evaluated in each case (Håveldsrud, 2012). By increasing the minimum section length from 1 to 5 meters, the simulation will run approximately 5 times faster. All models covered by this work, used approximately 20 meters in sections of interest (typically at wellhead and gauge) and larger sections in parts where the geometry allowed to do so.

Pressure deviation in percentage at wellhead after 500h

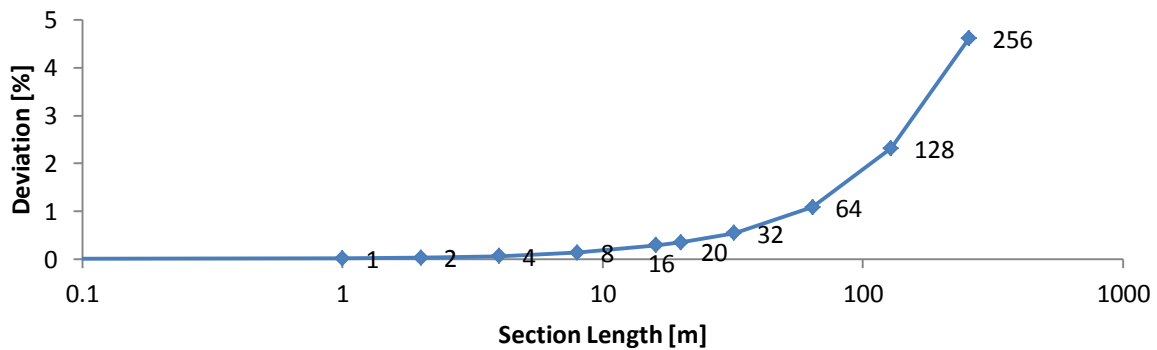


Figure 3-10 Deviation in pressure for various section lengths at the wellhead at 500 hours

Temperature deviation in percentage at wellhead after 500h

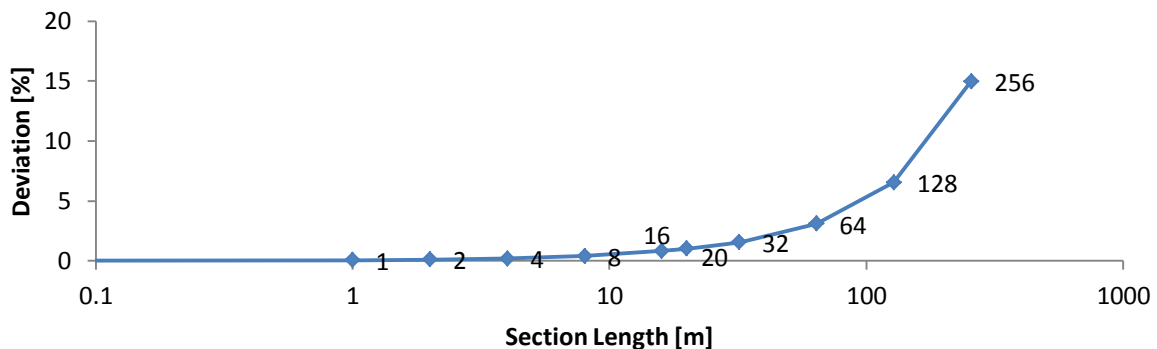


Figure 3-11 Deviation in temperature for various section lengths at the wellhead at 500 hours

A profile comparison was also conducted and can be seen in Appendix D-8 and Appendix D-9 where it has been plotted one hour into the shut-in. From this it can be seen how increasing section lengths leads to a more linear result, which is reasonable as the result is averaged over larger sections. Furthermore, the pressure curve appears to be less affected. However, it seems highly likely that this is not generally representative. Firstly, as will be discussed in section 4.4, the well is almost fully within the superheated region throughout the simulation. Consequently, there is no significant phase change which may rapidly affect the pressure. Also, the conditions throughout the well are relatively far away from the critical region, which should give more gradual transitions in fluid properties. The nature of the shut-in is another likely factor that might affect the result, as the system is relatively small compared to the other systems included in this study. Still, the same shut-in procedure was used for all the simulations, which gives a choking time of two hours. As this is a relatively gradual transition for such a small system, the subsequent pressure wave will be less pronounced than a more instant shut-in, or blowout procedure would be. In general it can be said that rapid changes are evened out for large section lengths. This can also be seen from the temperature plot, as the result get more linear with increasing length, even though the fluid is cooled in the upper part of the well, and heated in towards the bottom. Especially near the inflow zone where a rapid drop in temperature is experienced, it can be seen that the accuracy is significantly reduced when the section length is increased from 16 to 32 meters.]

4 RESULTS

4.1 SLEIPNER

The results from the Sleipner simulations are presented in this section. It was not considered necessary to include the base case simulations in separate diagrams, as these are included as the initial state in most of the diagrams. The model has not been verified against experimental data, but has been tuned to give reasonably accordance with the available data. Also, as the operating range covered by the simulations is within the two phase area and around the critical point of CO₂, it stresses the capabilities and limitations of the single component module (ref. section 2.2.4). Due to license limitations, only the Sleipner shut-in for pure CO₂ could be simulated with the CO₂-VIP module. This will be discussed in section 1.1.1.

4.1.1 SHUT-IN SINGLE COMPONENT MODULE CO₂

As indicated, the following diagrams contain information for both constant injection and shut-in of the Sleipner well.

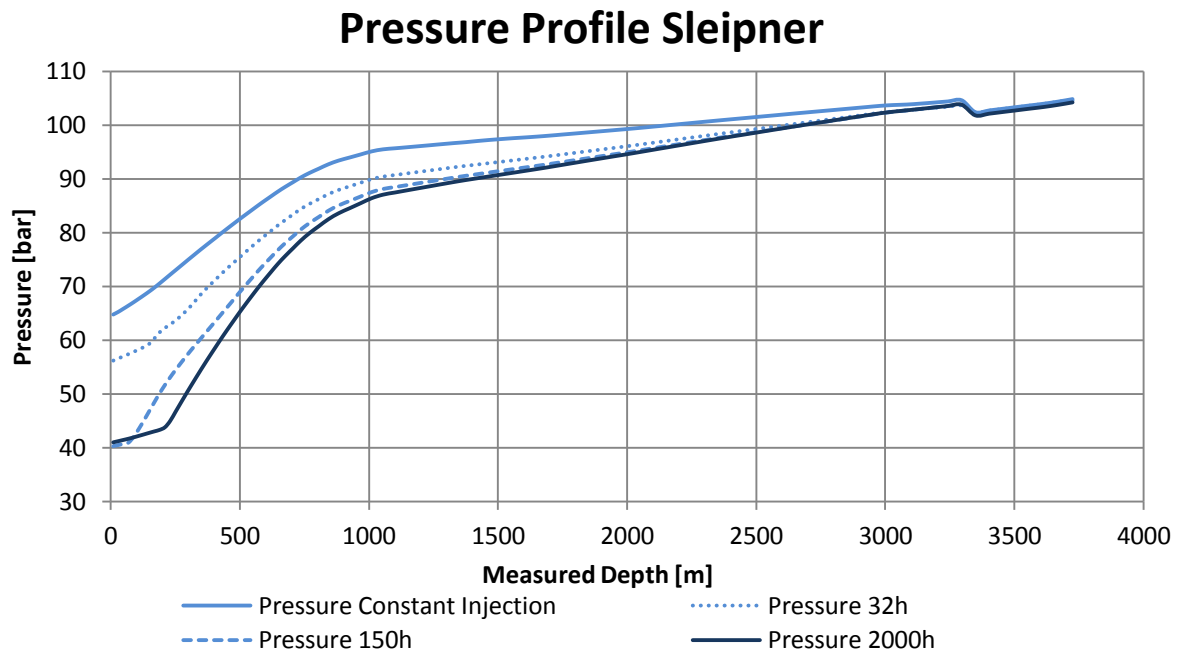


Figure 4-1 Pressure Profile Sleipner for constant injection and selected instants after shut-in. Shut-in start is set to 30h and is the injection stream is completely choked after 32h.

From Figure 4-1 it can be seen that the conditions in the well approaches the specified boundary conditions at constant injection. The pressure at the wellhead is approximately 65 bar as intended, and the inflow zone can also be seen to lie slightly above the assumed reservoir pressure of 103 bar. The relatively sharp increase in pressure in the first part of the well, can to a large extent be explained by the geometry of the well, which has the largest increase in depth in this section. However, as the conditions change down the well, the hydrostatic pressure contribution is also dependent on the density of the fluid, which may change significantly for small changes in pressure and temperature. The state of the fluid will

naturally also affect the pressure contribution. Furthermore, when looking at the density plot in Figure 4-5, it can be seen that after around 900h, the liquid and gas densities approach each other and form an approximately straight line. This may indicate that the compressibility of the CO₂ after this point is significantly reduced. This might also explain the approximately linear pressure increase in the last part of the well, as the depth in this part of the well also increases in a similar linear manner. The results for the constant injection line were extracted at 29h. This gave enough time for the results to approach a steady solution and also ensured that the results were not affected by the choking of the injection stream which was initiated at 30h and completed at 32h. After 32h it can be seen that the pressure at the wellhead has decreased with about 8.6 bar and that the pressure wave has worked its way all the way down the well. The shape of the pressure curve is however more or less the same. This is not the case at 150h and 2000h on the other hand, which show a more distinguished section in the first part of the well. This might be explained by the state of the fluid in this particular part of the well, which is directly affected by how the heat transfer is modeled. As explained in section 3.2.2, the heat transfer has been divided into three sections, one for the riser above sea level, one for the riser in water and one for the wellbore. This effect will be further discussed shortly. The dip in pressure is caused by the inflow zones in which the CO₂ expands into the reservoir as long as the pressure difference between the inflow zone and the reservoir is positive. If the pressure in the inflow zone falls below the specified reservoir pressure, backflow may be experienced in the well. This is a direct consequence of the coupling between the reservoir and the well, where the production coefficient was set equal to the injection coefficient.

Temperature Profile Sleipner

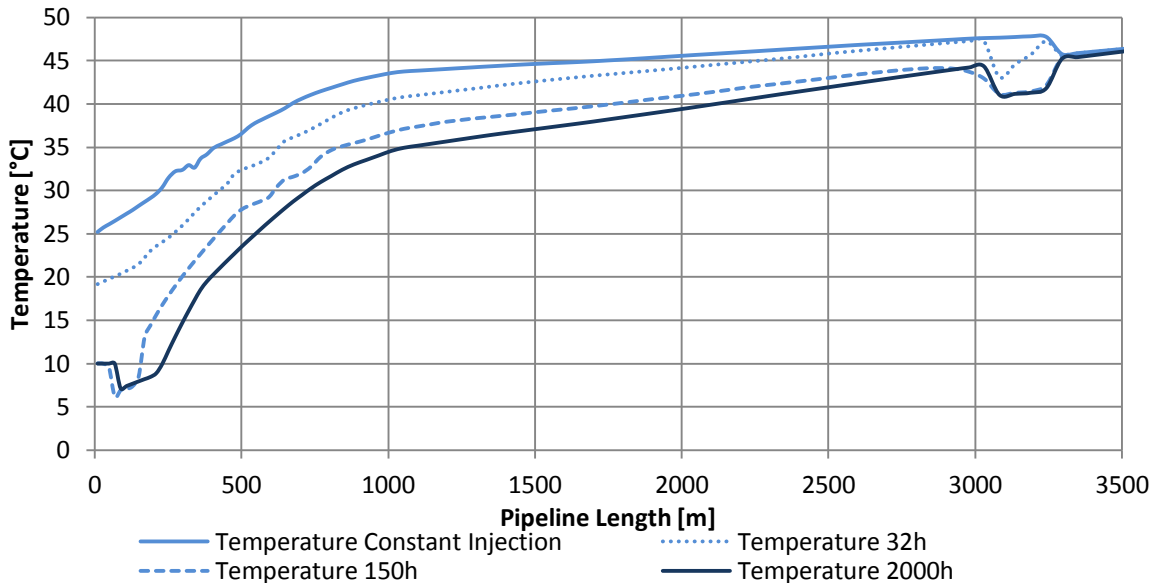


Figure 4-2 Temperature Profile Sleipner for constant injection and selected instants after shut-in. Shut-in start is set to 30h and is the injection stream is completely choked after 32h.

In the temperature profile plot in Figure 4-2, output fluctuations get more pronounced, especially up to about 800m measured depth, between 20°C and 40°C. This is likely to be caused by numerical instabilities that are related to the operational range in this part of the well. As explained in section 2.2.4, OLGA’s original approach is not particularly well suited for fluids with narrow phase envelopes, when

operation is close to the saturation line or near the critical point at approximately 31°C and 73.8 bar. Identifying the same temperature interval in a PT diagram for the shut-in (ref. Figure 4-7) seems to support the suspicion about the fluctuations, as the well conditions in this interval lie in the near critical region. This graph will be further discussed shortly. From the temperature plot it can also be seen that the temperature of the first section approaches the ambient temperature of 10°C after 2000 hours. According to this, the fluid is superheated at the wellhead. The temperature then drops to approximately 7°C for the riser section submerged in water. Opposed to the riser above sea level, the temperature is slightly higher than the ambient temperature of 7°C in this section. The fluid in this section is on the saturation line (this may also be seen in the PT diagram in Figure 4-7). Since the temperature increases down the well, it is likely that condensation occurs in this section, forming a thin liquid film on the inner pipe wall. Even so, the pipeline flow is close to stable at this point.

Total Mass Flow Profile Sleipner

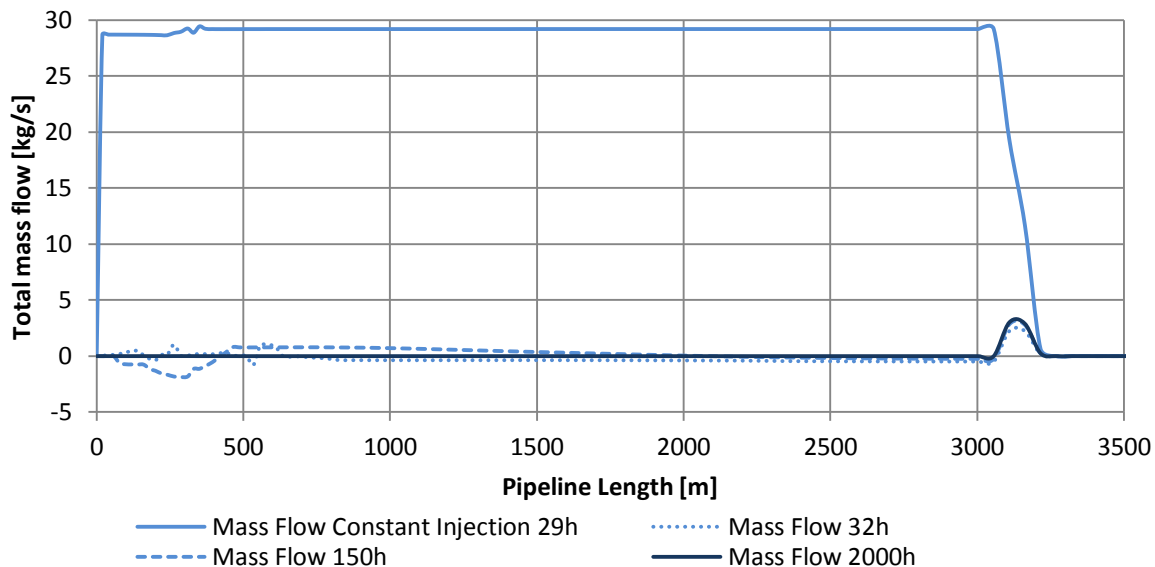


Figure 4-3 Total Mass Flow Profile Sleipner Shut-in

This also seems to be confirmed by the total mass flow plot in Figure 4-3, as it appears to be no flow in the well at this point². However, when looking closer at the data after 2000 hours, there is indeed a small countercurrent flow of gas and liquid (Figure 4-4). The inflow of “warm” gas from below explains the elevated temperature, as the heat outflow through the wall is converted from latent heat when the fluid condenses. The fluid continues to move down until it reaches the point where the fluid enters the subcooled region. Continuous evaporation along the well gives the countercurrent gas flow at approximately the same rate. At 32h it can be seen that the total mass flow varies between positive and negative flow. A better understanding of this may be experienced by plotting the liquid and gas mass flow separately. This can be seen in Appendix A-8, where they have been plotted along with the total mass

² Disregard the inflow zone between 3000 and 3200 meters at this point. Also note that the reason why there is no flow in the first section, is because OLGA measures flow across both section boundaries. In this case however, the flow comes from the injection stream which is placed mid-section with the uppermost section boundary closed

flow. Here, the same countercurrent flow pattern is experienced in the first part of the well, although with an overall positive trend (downwards flow). It should be noted that the conditions are under continuous change at this point, and the resulting output fluctuates considerably. After 2000h on the other hand, the flow rates are close to steady state (Figure 4-4).

Flow Profile Sleipner 2000h

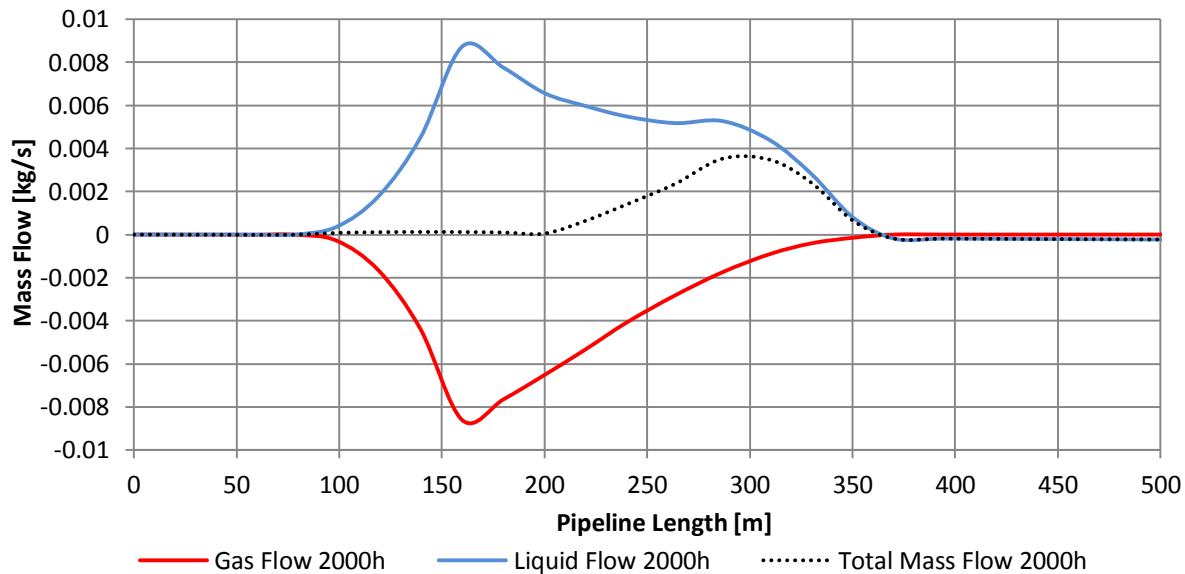


Figure 4-4 Flow Profile Separate Phases Sleipner Shut-in after 2000h

After about 800 meters in the 32h plot (Appendix A-1), it can also be seen that the total mass flow becomes more stable. However, it also reveals something interesting: how OLGA defines the fluids with either gas or liquid properties, as there currently is no separate indication for supercritical phase. At first the total mass flow equals the gas mass flow (from about 800 meters), but after about 2300 meters, it equals the liquid mass flow. In reality, it has been in the supercritical phase the whole time, which can be seen from the density plot in Figure 4-5. That predicts the transition to supercritical phase at approximately 475m MD at 32h. At constant injection, the transition takes place around 275m MD and after 2000h (at stable conditions), the transition to supercritical has shifted down the well to approximately 650m MD. Plotting the liquid and gas densities is currently the best way of determining the transition to supercritical phase in OLGA (Håvelsrud, 2012d). It also shows that using liquid holdup or gas fraction might be a bit misleading, when the operational range is near the critical region. A profile plot for the gas fraction is included in Appendix AI.

Density Profile Sleipner

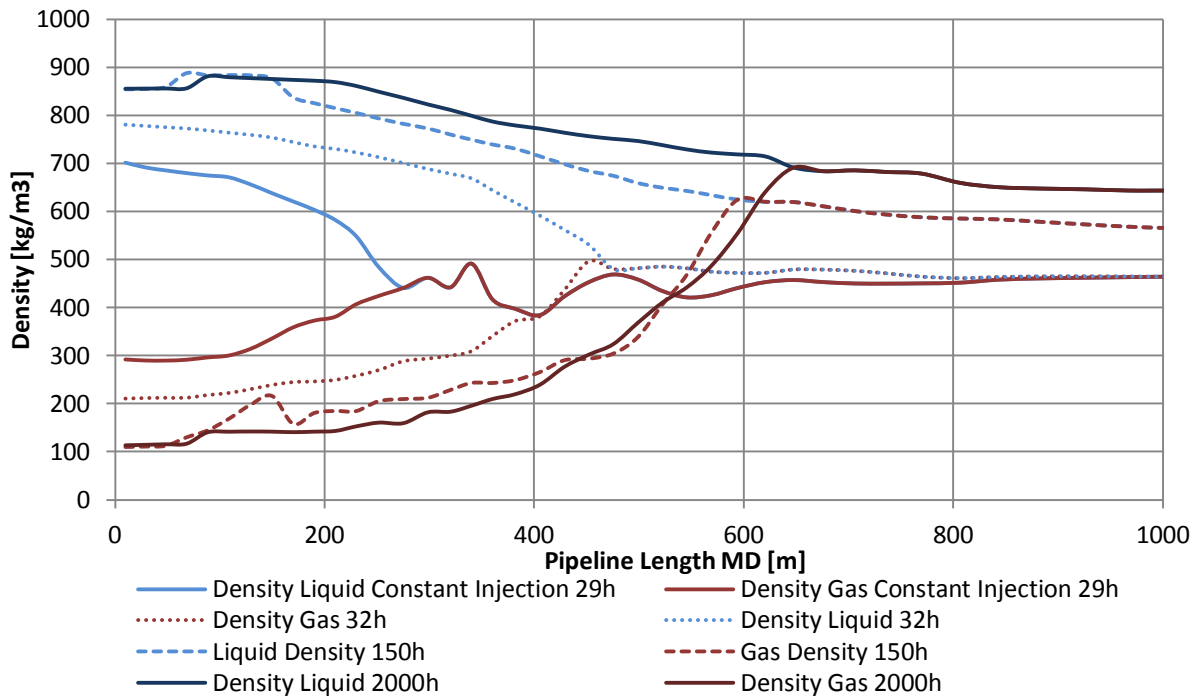


Figure 4-5 Density Profile Sleipner Shut-in for various points in time

The mass flow plots also revealed some misleading results caused by the assumption of constant reservoir conditions. This would have been satisfying if only one inflow zone had been used, but as the different perforations of the well was modeled as separate inflow zones, the conditions should have been varied according to the conditions at each perforation. The inflow zones are in the interval from approximately 3070m to 3220m, which can be identified in both the temperature, pressure and mass flow diagrams above (Figure 4-1, Figure 4-2 and Figure 4-3). From the mass flow plot it can be seen that a positive (downwards flow) appears in the inflow zone. What happens is that the reservoir pressure is equal for the different perforations, but as the perforations are located at varying depth, the hydrostatic pressure difference induces a net flow from the upper to the lowermost perforation. This naturally affects both the pressure and temperature in the same area. After the inflow zones, there is no flow, and the conditions approaches the defined boundary conditions.

To give a better perspective about the operational range of the well during the shut-in, it was desirable to plot the results in a PH and PT diagram. To do this, the temperature, pressure, vapor fraction and phase enthalpies were plotted in a profile plot in OLGA and exported to Excel. The total enthalpy was then calculated by multiplying the gas fraction with the gas enthalpy, liquid holdup with the liquid enthalpy and then adding the results³. Saturation, isothermal and isobaric properties were then obtained from the

³ It was also attempted to use the total enthalpy [W] from OLGA, divide it by the mass flow, and plot it in a similar manner. However, as the mass flow goes to zero, it turned out not to be a good solution.

NIST library (NIST, 2011) and used to create the basic PH and PT diagrams. To make the calculated OLGA enthalpy correspond to the NIST values, the pressure and temperature at the wellhead were used to retrieve the NIST enthalpy at wellhead conditions. For vapor fractions between 0 and 1, the enthalpy was calculated from the equation below, where the following relation for the vapor fraction and liquid fraction has been assumed: $G_f + L_f = 1$.

$$\begin{array}{l} \text{Two-Phase} \\ \text{Enthalpy} \end{array} \quad Hl + Gf \cdot (Hg - Hl) \quad (4.1)$$

If the wellhead was outside the two-phase area on the other hand, the enthalpy was obtained from the isobaric NIST properties. The difference between the OLGA and NIST enthalpies was then used to match the data. The adjusted enthalpy was then plotted for various instants of the shut-in and the result can be seen in Figure 4-7. As there is a lot of information in this diagram, some explanation is in place. First of all, the plotted constant injection line was taken just before the injection stream is starting to choke down at 30h. 31 hours is then one hour into the shut-in and so on. The choking is completed at 32 hours, making it fully closed at the wellhead. However, there may still be reservoir inflow/outflow, depending on the conditions at the perforations. For the various time series, the conditions at the wellhead are marked by a circle in one end, and an arrow representing the bottomhole conditions in the other end. The yellow square represent the reservoir conditions and the red squares and triangles represent the riser sections at 500h. Furthermore, the yellow shaded areas represent the conditions in the inflow zones.

At constant injection in can be seen that the wellhead is clearly within the two-phase area, which seems to agree with the work done by Alnes et al. (Håvard Alnes, 2011). The gas fraction then decreases until the two-phase region is left fairly close to the critical point. At this point the results starts to show signs of instability, which most likely is caused by the numerical scheme in OLGA (ref. section 2.2.4). As the fluid properties may change radically for small changes in pressure and temperature in the near critical region, the current method of solving the conservation equations in OLGA fails. The results get back on track when the conditions moves further away from the critical region on the other hand. From this point on the results seem to be relatively stable.

After 32h (when the injection stream is completely choked), the results are fluctuating significantly within the two-phase region. The validity of the results is definitely a question, but is hard to quantify as no measurements are available. The flow regime on the other hand may, give some explanation to the fluctuations. In general, the flow regime seems to vary between annular, bubble and stratified flow throughout the simulation. At 32h however, there is a tendency to slug flow (ref Appendix A-3). This might be parts of the explanation. The gas fraction also varies at 42h, but more gradual than at 32h, and there is no indication of slug flow in the well. It is also interesting how the results at both 42h and 150h first enter the subcooled region before it reenters the two-phase area, where bubble flow is the dominating flow regime. It seems possible that the two-phase bubble flow should be capable of sustaining the subcooled liquid above. Still, it is not a stable condition. It was notice from the profile plot from the shut-in, that there seem to be a shift around 300h, from changing conditions to more or less stable. Even so, it can be seen that the simulation after 500h, still show signs if numerical instabilities when the near critical region is approached. Again it is emphasized that the operating range of the simulation stresses the capabilities of the current version of OLGA, and that it is hard to quantify the accuracy of the simulations.

At 500h it can also be seen that the conditions of the inflow zone, is approaching the reservoir conditions, which might indicate that the conditions are approaching the specified boundary conditions.

Figure 4-7 shows the same simulation in a PT-diagram at constant injection and after 2000h. Also here it can be seen how the initial and final conditions close in on the critical point and how two-phase flow exists in the first part of the well. The transition to supercritical was retrieved from the plot data to be at 252m MD at constant injection and 770m MD after 2000h. This differs slightly from the results in Figure 4-5, but is still in the same range. Furthermore, the transition to subcooled liquid was identified at 382m MD at 2000h. Although a bit difficult to read from the diagram, it is interesting to see how the constant injection line seems to be lead around, and not through the critical point. Most likely, this is caused by the numerical smoothing which has been applied to avoid trouble when the derivatives become undefined at the critical point.

PH Diagram Sleipner Shut-in

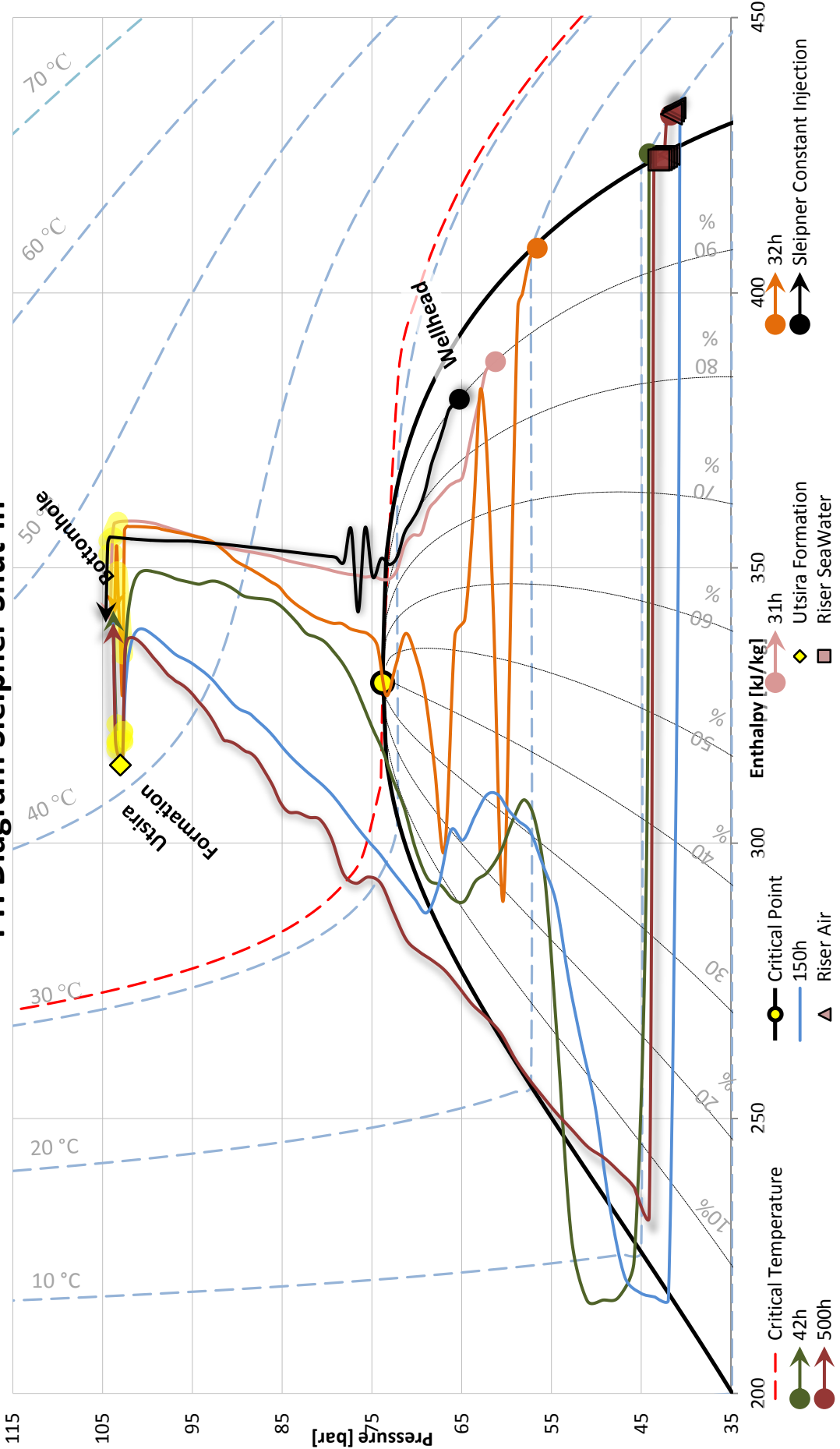


Figure 4-6 PH Diagram Sleipner Shut-in at Various Times

PT Diagram Sleipner Shut-in

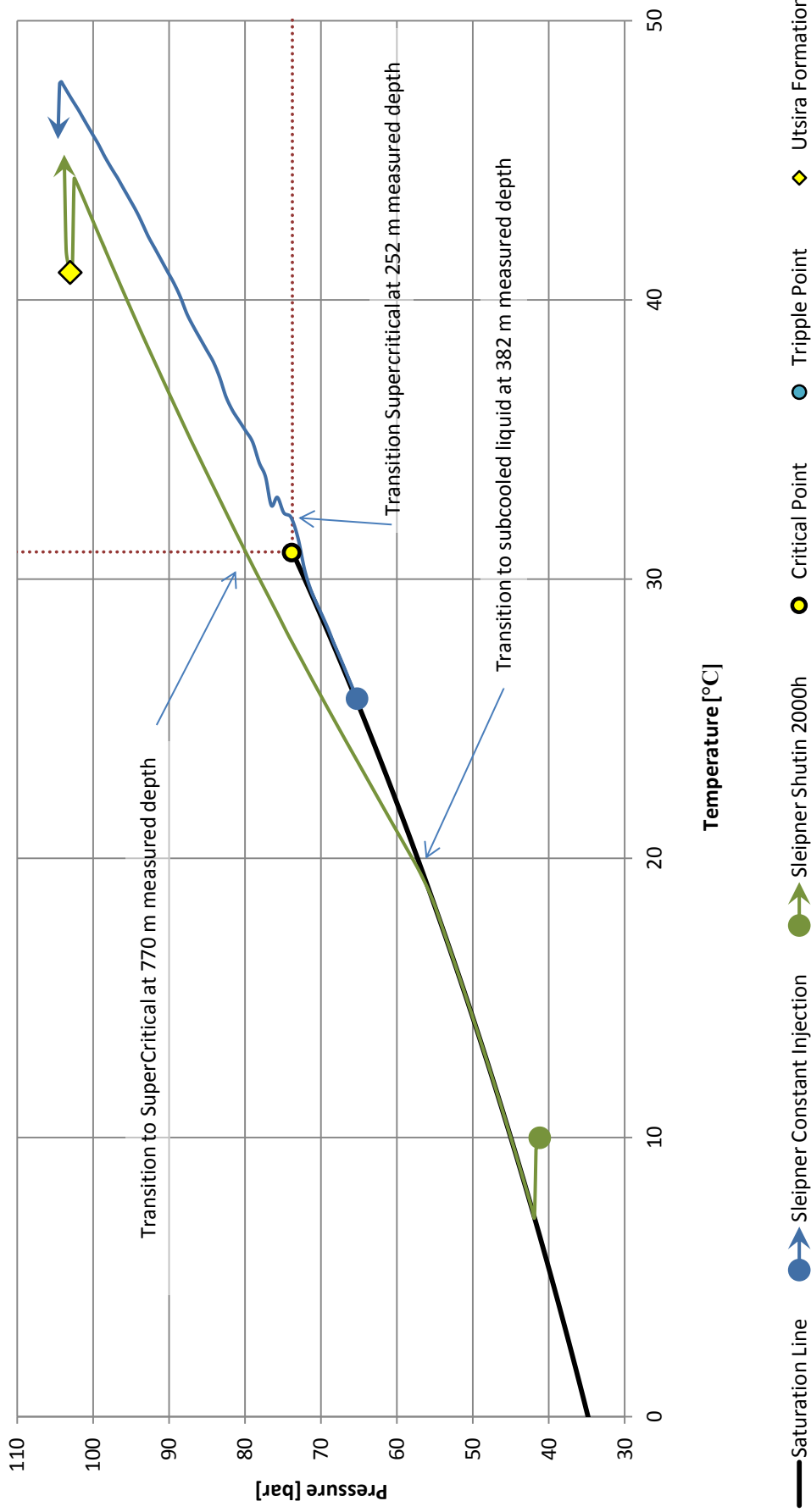


Figure 4-7 PT Diagram Sleipner Shut-in for Constant injection and after 2000h

4.1.2 SHUT-IN CO₂ VIP MODULE

The initial thought was to do all the simulations using the CO₂-VIP module (ref. section 2.2.4). However, due to license issues, this was not possible. But thanks to Monica Håvelsrud in SPT group it was still possible to get some results for the Sleipner shut-in. The simulated model was identical to the one presented in the previous section, apart from the simulation approach using PH instead of PT flash.

In terms of pressure, the differences are minor, but a slight increase in pressure was observed at the wellhead (Appendix A-6). Due to some adjustments in the plotting frequency, the simulation at 150h cannot be directly compared, but showed the largest difference. Also, the CO₂ VIP simulation was terminated at 500h, which explains why there are minor differences between the final results.

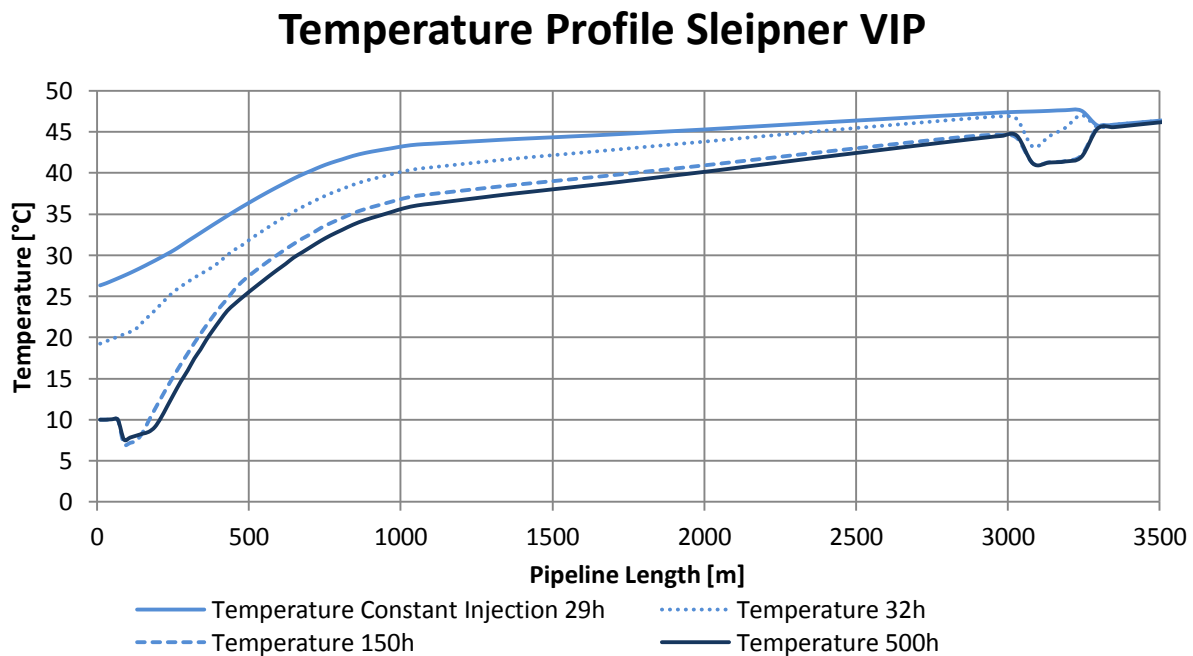


Figure 4-8 Temperature Profile Sleipner Shut-in with CO₂ VIP module

The temperature profile on the other hand, showed more pronounced distinctions between the two simulations. Most noticeable is the significant reduction of the temperature fluctuations between 20°C and 40°C, up to 800m MD. This can be seen by comparing Figure 4-8 and Figure 4-2.

Flow Profile Sleipner Shut-in CO2 VIP 500h

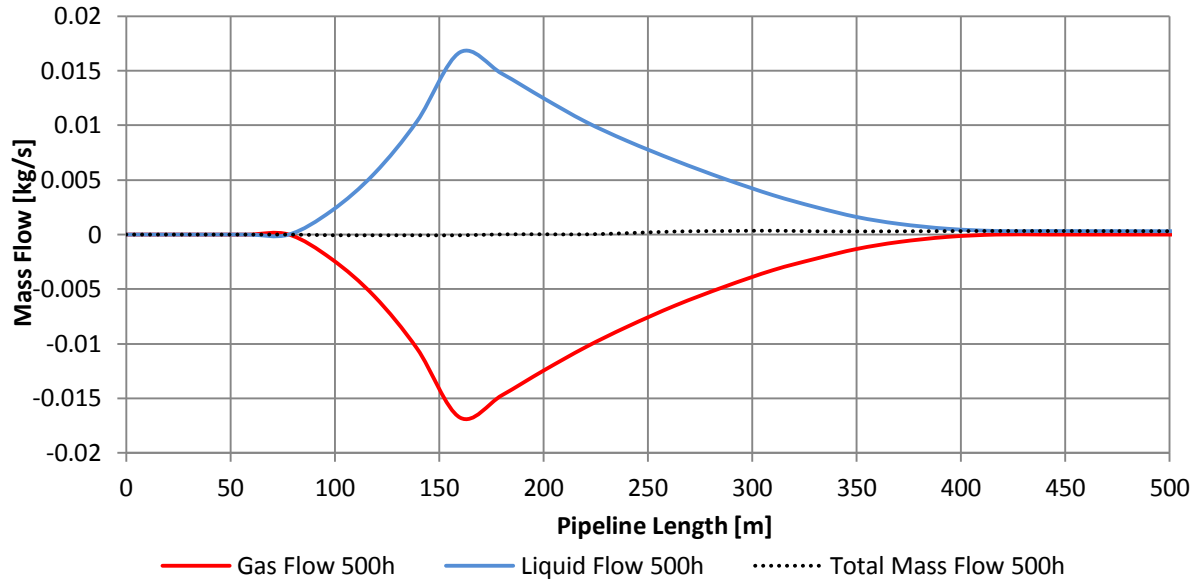


Figure 4-9 Flow Profile Sleipner Shut-in with CO2 VIP module at 500h

Density Profile Sleipner Shut-in CO2 VIP

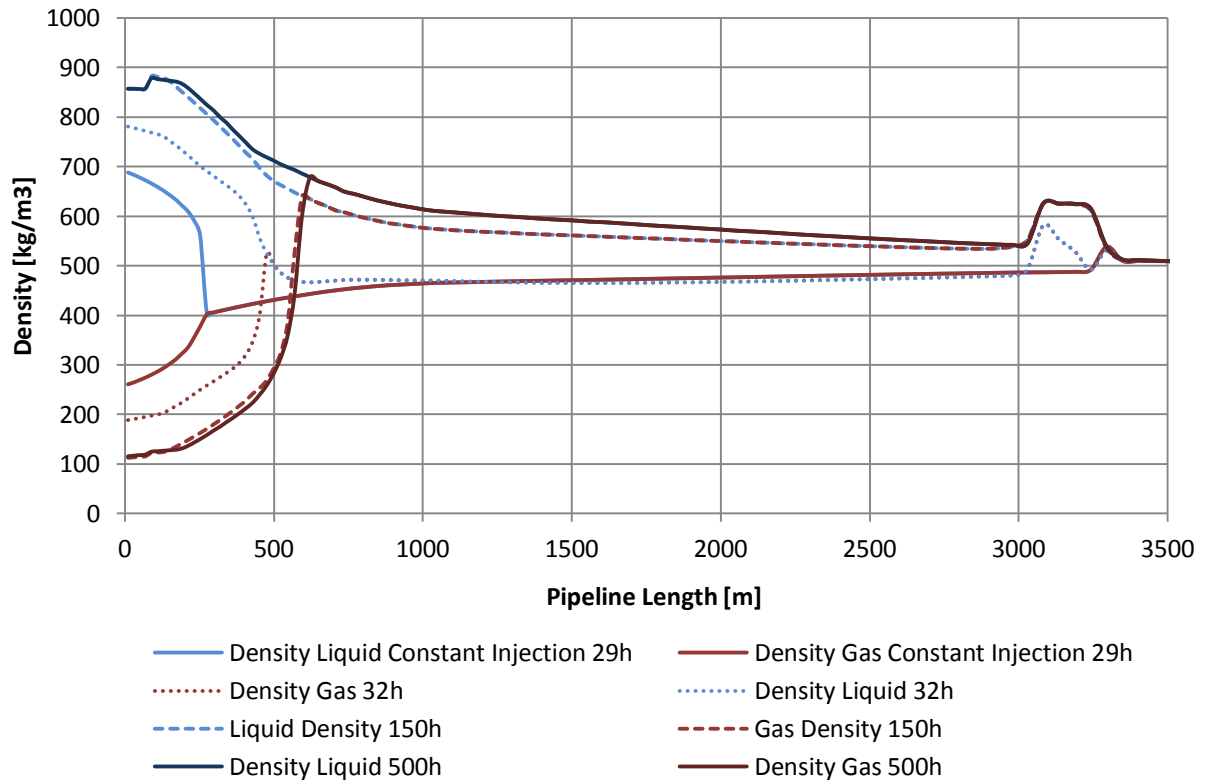


Figure 4-10 Density Profile Sleipner Shut-in CO2 VIP

Comparing the flow profiles at 500h and 2000h (Figure 4-9 and Figure 4-4 respectively) also showed indications of a more stable results, even though the CO₂ VIP simulation where at 500h. Looking at the diagram above, it can be seen that the liquid and gas mass flows are virtually mirror images of each other, indicating that there is a balance between evaporation and condensation in the first part of the well. The calculated gas fractions also turned out remarkably more stable for the PH than the PT flash (Appendix A-9 and Appendix A-2). Especially at 32h, where the PT simulation rapidly fluctuates between 1 and 0. The PH simulation on the other hand shows a more stable transition from gas to liquid.

The transition to supercritical phase is best determined by plotting the liquid and gas densities. This is displayed in Figure 4-10, where the most obvious difference from Figure 4-5, again is the reduced fluctuations. The measured depth at which the transition takes place on the other hand, only shows minor differences.

To get a more complete picture, the results were then compared in a PH diagram, by following the same method as explained in the previous section. The resulting diagram is presented in Figure 4-11, where the results have been plotted for constant injection rate and after 32 and 500 hours. Circles indicate the wellhead conditions, arrows the conditions at the bottom of the well and PH and PT simulations have been indicated by solid and dotted lines respectively. From this it seems like the fluctuations caused by numerical instabilities have been more or less eliminated. For constant injection for instance, the fluctuations in the near critical region is reduced to a straight line from the saturation line to the inflow zone. The slight increase in wellhead pressure can also be seen here. Other than that however, the differences are minor. At 32h on the other hand, the same abrupt changes within the two-phase area are present in both simulations. The deviance is significant, but it seems to be mainly in terms of the gas fraction and not so much in terms of pressure and temperature. For convenience, the riser section has been outlined for the CO₂ VIP simulation. This seems to a large extent to explain the initial reduction in gas fraction, caused by cooling of the fluid from the ambient air and water outside the riser. From this point on, the temperature gradient is linearly increasing. Still the gas fraction is fluctuating. There might be several reasons for this, but it does not seem unlikely that the composition vary along the well. It was suspected however, that the fluctuations may be caused by changes in the heat transfer behavior with changes in the flow regimes (M. K. Dobson et al., 1994). Accordingly, the flow regime was plotted with the enthalpy (ref. Appendix A-11). The result seems to a large extent to confirm this. At 500h the same trends can be identified. The numerical instabilities seem to be significantly reduced and different flow regime predictions are likely to affect the heat transfer.

From the PT diagram in Figure 4-12, it can be seen that the CO₂ VIP simulations in general seems to close in on the critical point. In fact, in terms of temperature and pressure, the constant injection line for the CO₂ VIP simulation, goes more or less straight through the critical point, whereas for the PT flash simulation, it seems to be lead outside the troublesome area. This might be caused by the applied numerical smoothing in this region.

In general, the CO₂ VIP results look promising, and seem to a large extent to reduce the numerical instabilities experienced in the near critical region. The change in flow regime prediction also seems to explain some of the deviance between the simulations. However, other factors may also play a significant role here. Again it is emphasized that the results have not been verified against experimental data.

Comparison of Results in PH Diagram Sleipner Shut-in

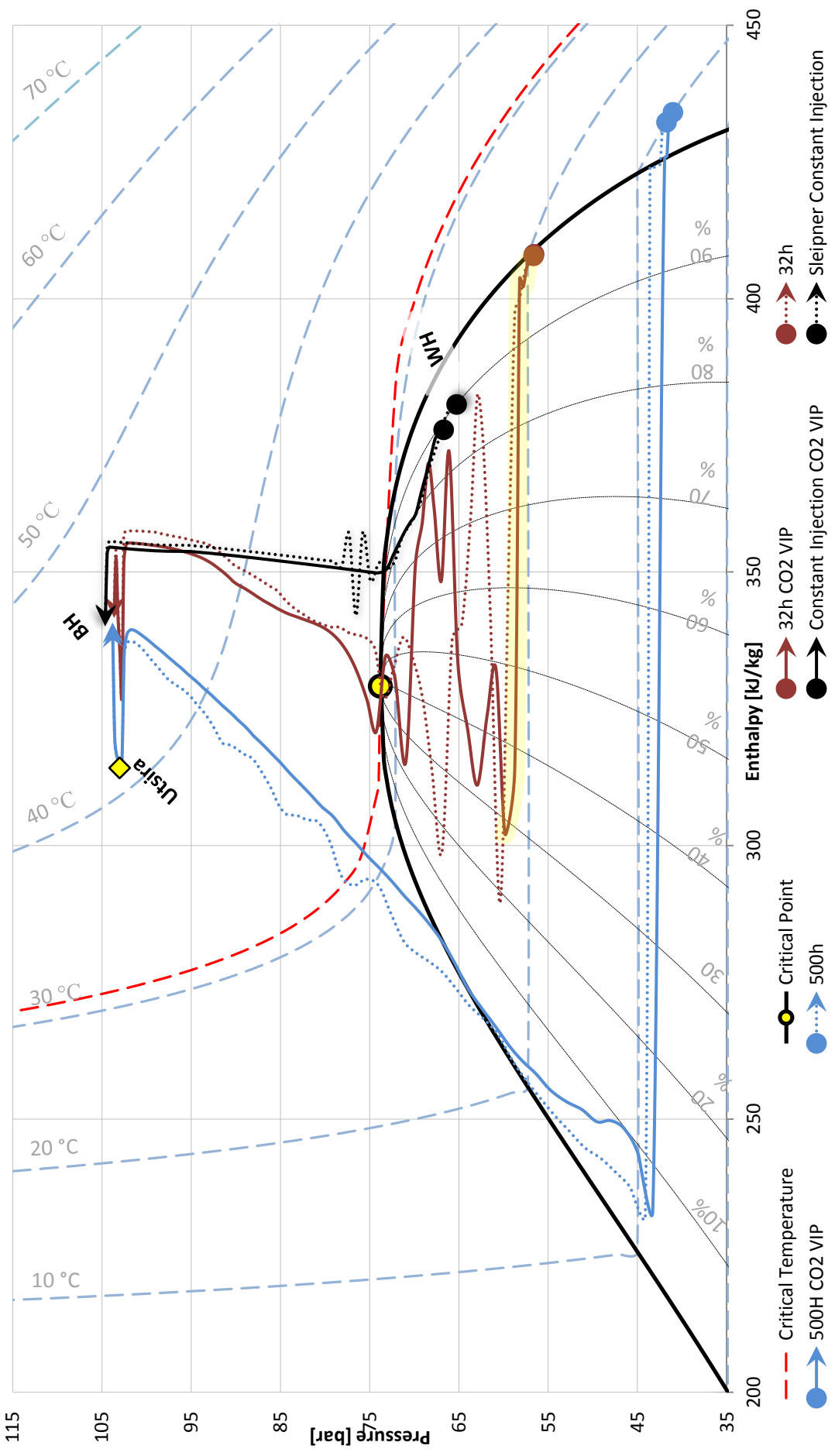


Figure 4-11 PH Diagram Sleipner Shut-in Comparing standard OLGA with CO2 VIP

Comparison of Results in PT Diagrams Sleipner Shut-in

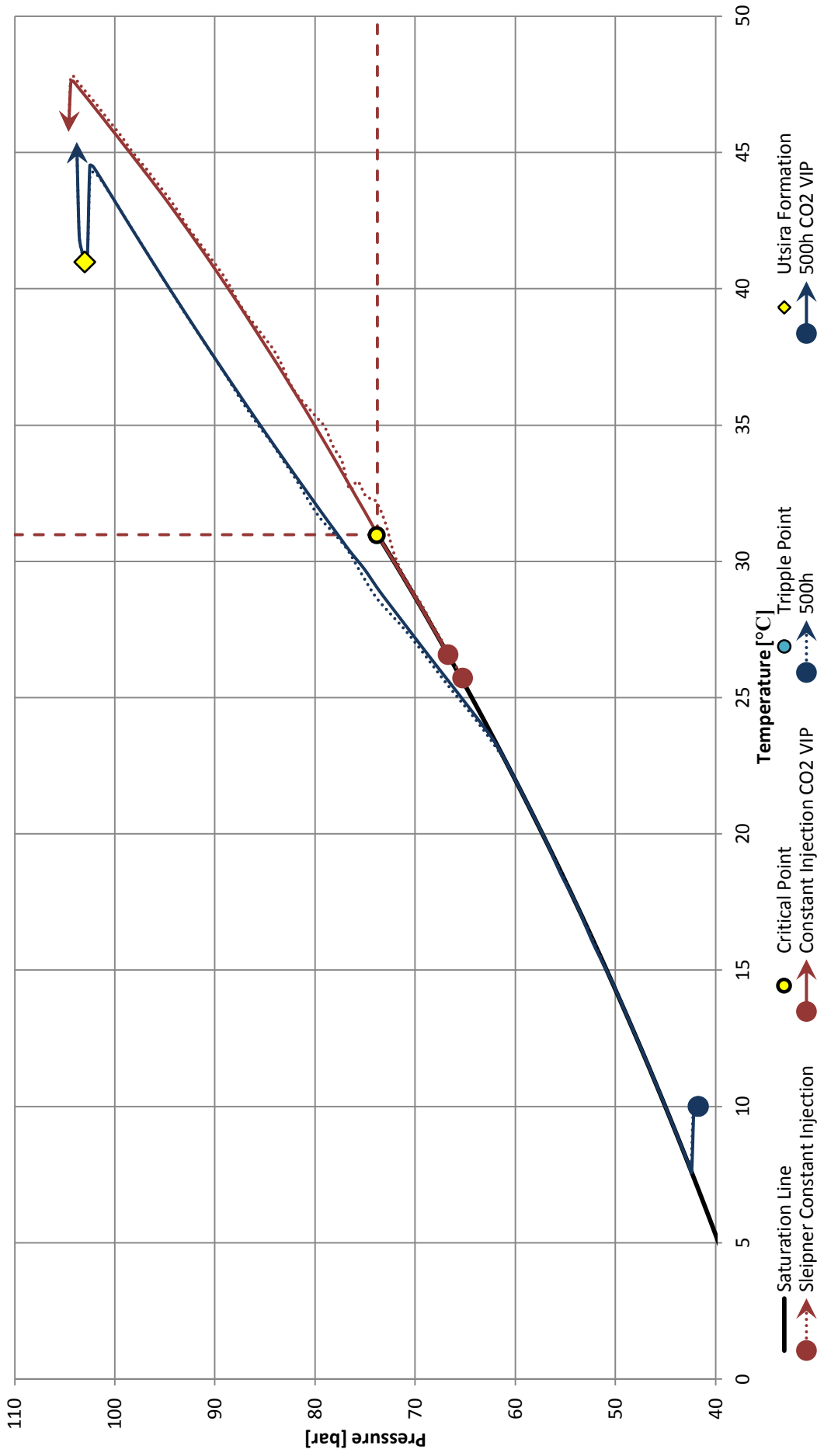


Figure 4-12 PT Diagram Sleipner Shut-in Comparing standard OLGA with CO2 VIP

4.1.3 BLOWOUT CO₂ WITH RESERVOIR BACKFLOW

The blowout simulation with reservoir backflow experienced major trouble for the same settings used during the shut-in. Accordingly, the minimum time step had to be increased to 1s (ref. section 3.2.3). This was done in an attempt to skip the most troublesome areas of the simulation. Even with the adjustments, OLGA experienced severe trouble in the calculations, but managed to complete the simulation. It is expected that the results are significantly affected by the adjustments made to the model, and when considering the simulation time and number of time steps that had to be recalculated, the accuracy is expected to be significantly reduced. With regards to the blowout simulation it is important to keep in mind that factors such as water backflow from the reservoir is expected, and that CO₂ migration may decrease the actual backflow of CO₂ from the reservoir. In that context, this simulation represents the worst case scenario, as CO₂ will continuously flow back from the reservoir. Also, as the reservoir pressure is assumed constant, the blowout will persist indefinitely and the best possible outcome is therefore that a constant backflow is reached. This depends on the conditions at the bottomhole, as the production coefficient is dependent on the pressure difference between the inflow zones and the reservoir.

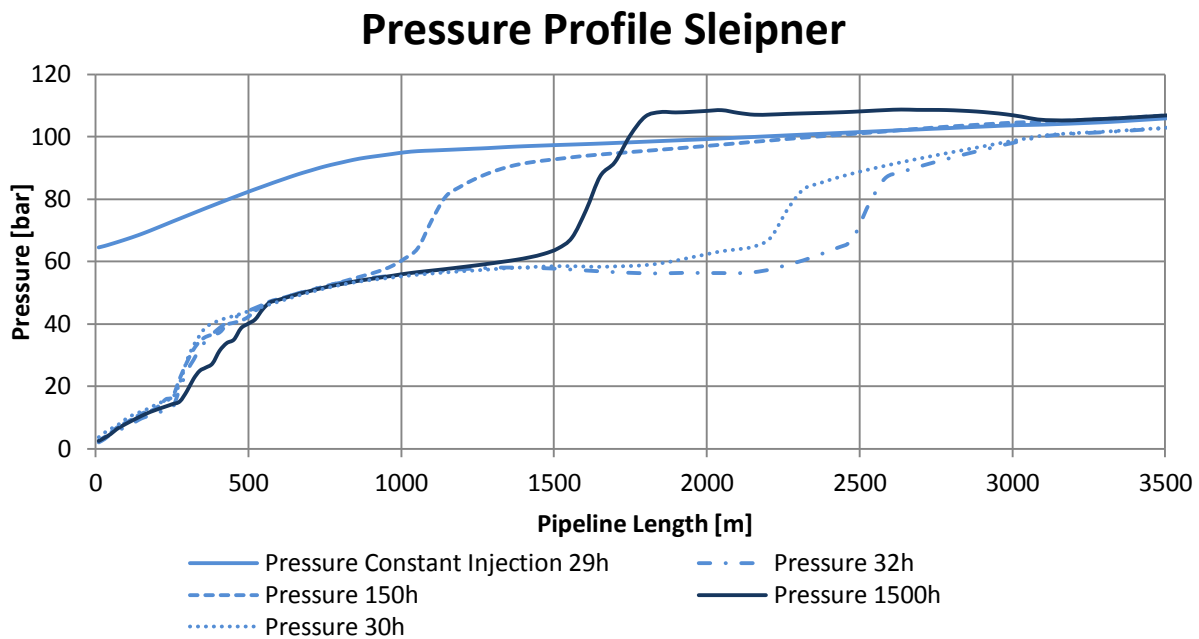


Figure 4-13 Pressure Profile Sleipner Blowout With Backflow

As suspected, the pressure profile (Figure 4-13) shows strong signs of instability, as the pressure front moves back and forth in the well. To some extent this might be the case if large slugs are produced. Nonetheless, the pressure difference of the pressure fronts seems to be very large. It can also be seen that the pressure at 1500h exceeds the reservoir pressure (103 bar) at around 2000 meters, which clearly is an unphysical result. The pressure can also be seen to drop quickly at the outlet, and seems to be relatively stable in the first part of the well. The results showed no signs of converging towards any solution, even after 2000h. Similar trends may also be seen for the temperature profile (Figure 4-14). It can also be seen

that very low temperatures are predicted at the outlet, which just after the blowout valve has opened approaches -100°C . At these temperatures, the integrity of the well is at risk, as such a large and instant temperature decrease would involve high thermal stress in the material that may lead to thermal cracking of the well components.

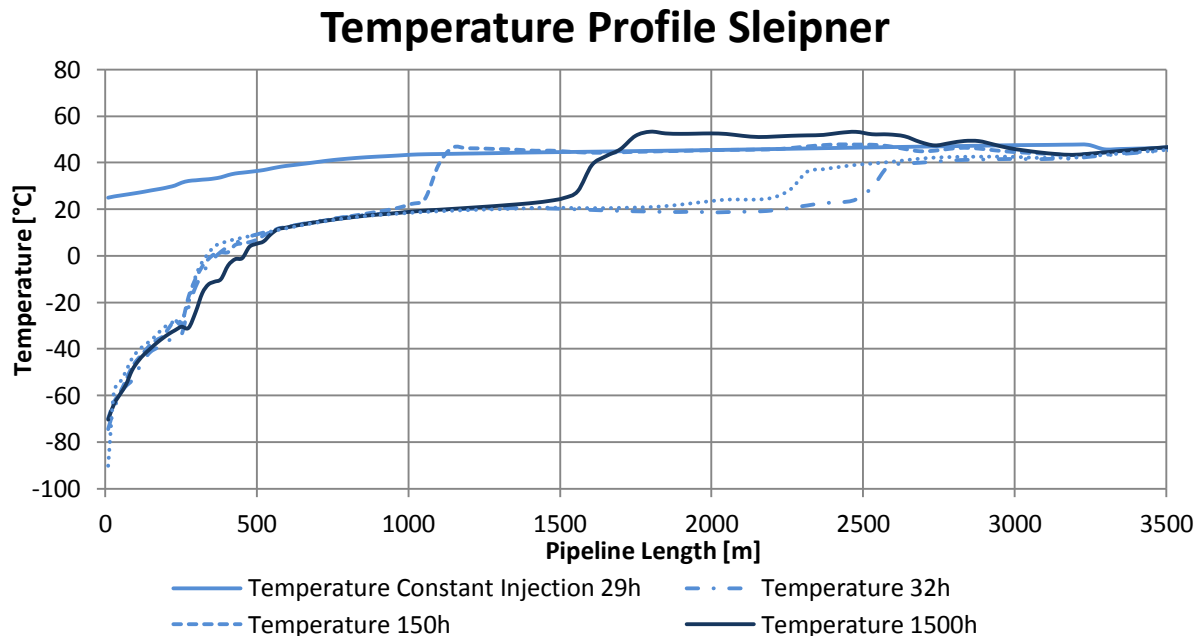


Figure 4-14 Temperature Profile Sleipner Blowout With Backflow

From the above results it is not surprising that also the transition to supercritical phase is continuously changing throughout the simulation. At 30, 150 and 1500 hours the transition can be located at approximately 2260, 1100 and 1600m MD (Appendix A-16). Maybe more interesting is to look at the total mass flow plot (Appendix A-17) as it seems to calculate a *relatively stable* (in terms of this simulation) discharge of approximately 40 kg/s, despite the unstable results for the rest of the well. On the other hand, the extreme values is more than 10 times the injection rate and seems to underpin the impression that the results are far from realistic. Not very surprising, as it was expected to be the most extreme scenario from the very beginning. The question then is if it still is possible to gain some knowledge from it and why OLGAs seems to struggle with the calculations.

To try to answer this, the PH and PT diagrams may be helpful (Figure 4-15 and Figure 4-16). First of all, it was noticed that the enthalpy difference between the OLGAs results and the NIST database changed for the different instants plotted. This might also be an indication that the results are unphysical, as the enthalpy difference in theory should remain unchanged. For this reason, the enthalpy difference was changed before plotting the results, to the value calculated at constant injection (and also the shut-in), to offset the error in an attempt to place the results as correct as possible in relation to each other. It might also be an effect of the existing non-equilibrium conditions in the well.

As shown in the diagrams both pressure and temperature exceeds the given boundary conditions and show no signs of stabilizing behavior. The most interesting observation that can be withdrawn from the

diagrams is probably that the results fall below the triple point of CO₂ and thus outside the validity range of OLGA. This is a highly likely explanation to the unrealistic results. Although the results seems unrealistic, it is interesting to note the maximum discharge flow rate at the wellhead, as this is of particular interest in the design of safety routines. In this case the maximum discharge was measured to about 100 kg/s. By the end of the simulation, the discharge fluctuates between approximately 30 and 60 kg/s (Appendix A-22).

PH Diagram Sleipner Blowout with Backflow

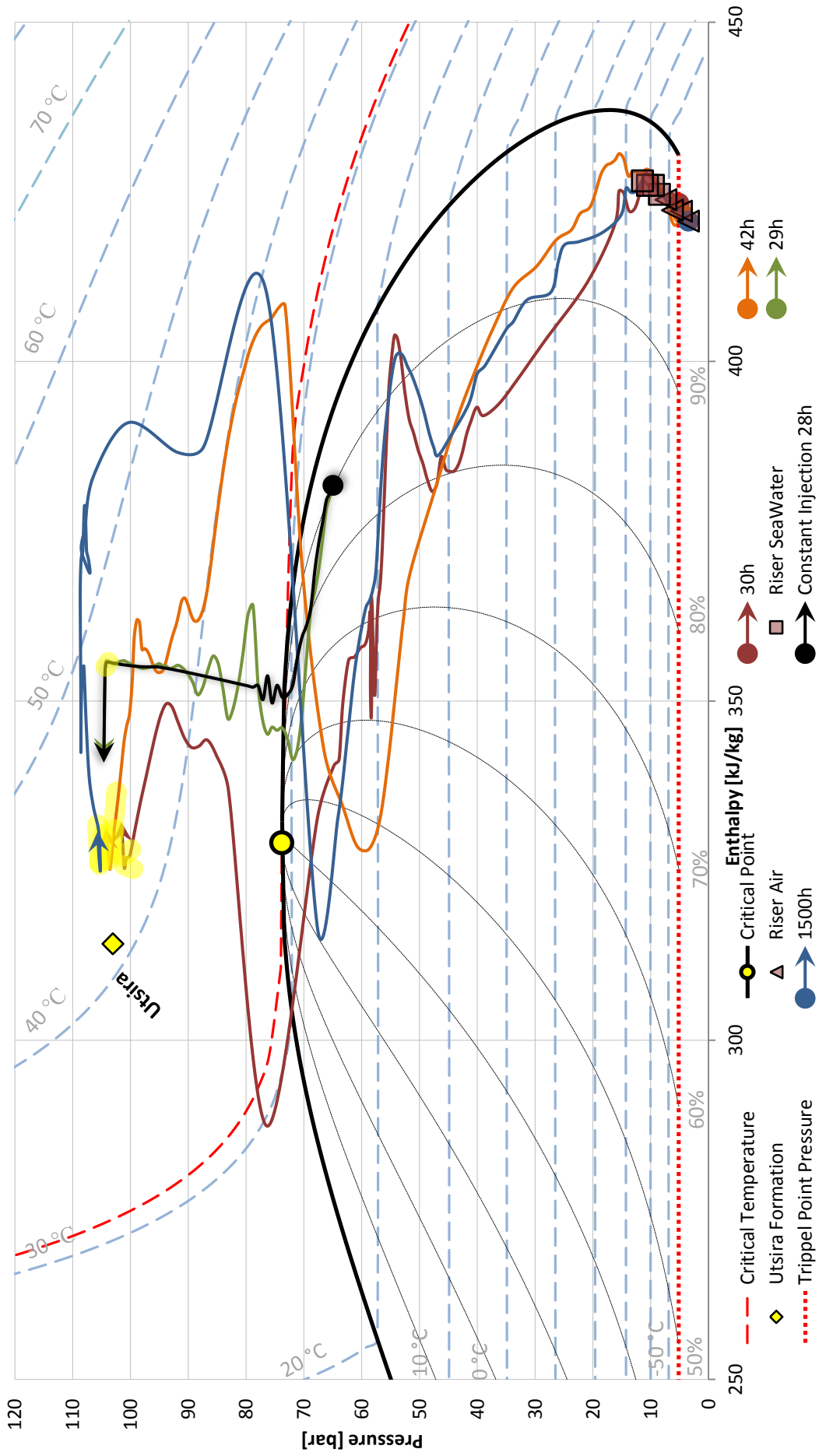


Figure 4-15 PH Diagram Sleipner Blowout With Reservoir Backflow

PT Diagram Sleipner Blowout with backflow

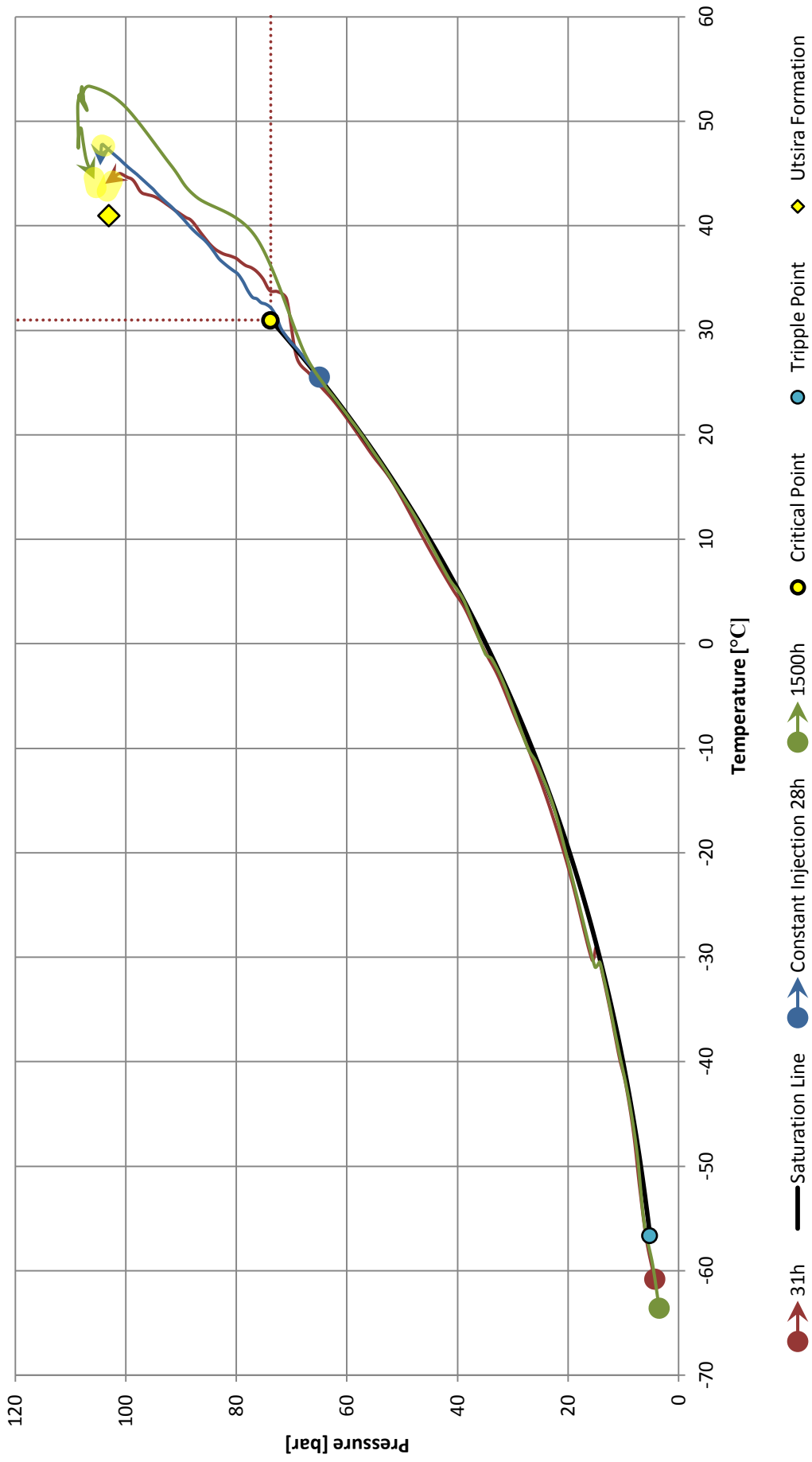


Figure 4-16 PT Diagram Sleipner Blowout With Reservoir Backflow

4.1.4 BLOWOUT CO₂ WITHOUT RESERVOIR BACKFLOW

The other extreme blowout scenario that was simulated was with no backflow from the reservoir. Apart from this, the two cases were identical. No backflow basically implies that the well is fully closed (as long as the pressure in the inflow zone is below the reservoir pressure) at the reservoir and that the only outflow is from the blowout valve which opens instantly at 29.00h. As opposed to the blowout with backflow from the reservoir, this simulation seems to experience less trouble in the calculations. Nonetheless, it required a minimum time step of 1s.

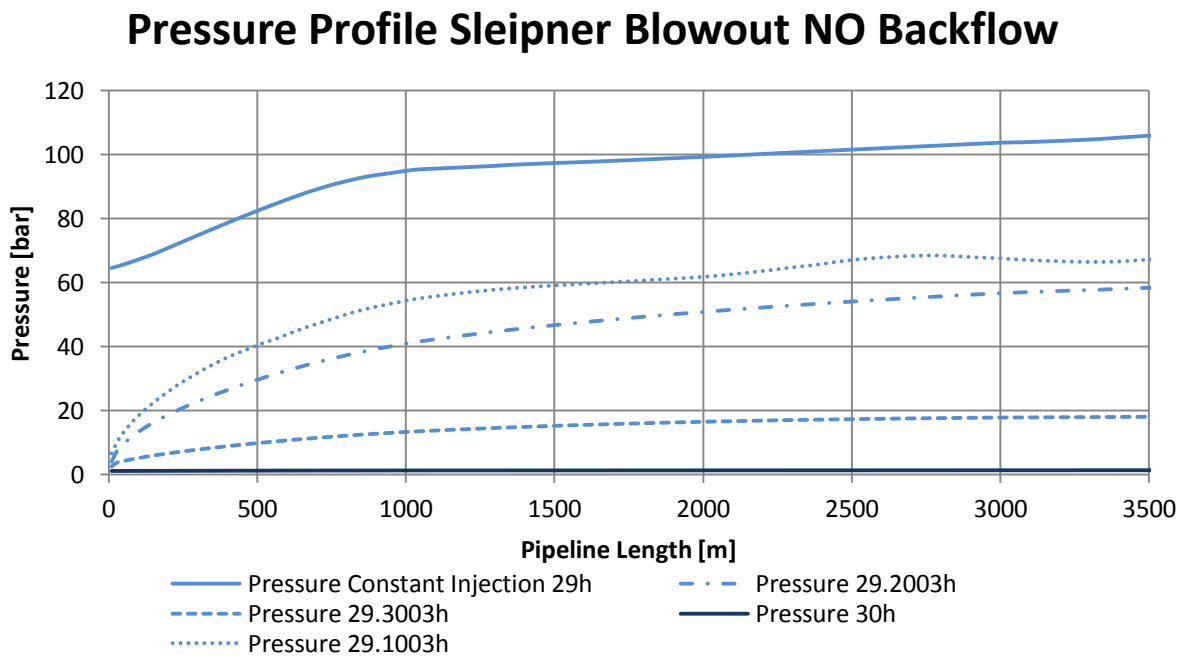


Figure 4-17 Pressure Profile Sleipner Blowout NO Backflow

From the pressure profile in Figure 4-17, it can be seen that the plotting frequency had to be changed in order to capture the trend in the well as the blowout seems to be more or less completed after 1 hour. The intermediate lines are plotted at 6, 12 and 18 minutes after the valve opens. As for the previous blowout case (ref. section 4.1.3), it can be seen from the temperature profile (Figure 4-18) that the outlet temperature seems to lie in the same range. Accordingly very low temperatures are expected, especially in the first section of the riser which is surrounded by air. This can be explained by the heat conductivity of the surrounding air, as the heat transfer in this section is insufficient to maintain the temperature while the fluid is expanding out of the well. Both evaporation and Joule-Thomson cooling contributes to the low temperature. At 30h the temperature seems to have approached steady conditions. This can be seen as the two riser sections seems to have stabilized at 10°C and 7°C which was specified as the ambient temperature.

Temperature Profile Sleipner Blowout NO Backflow

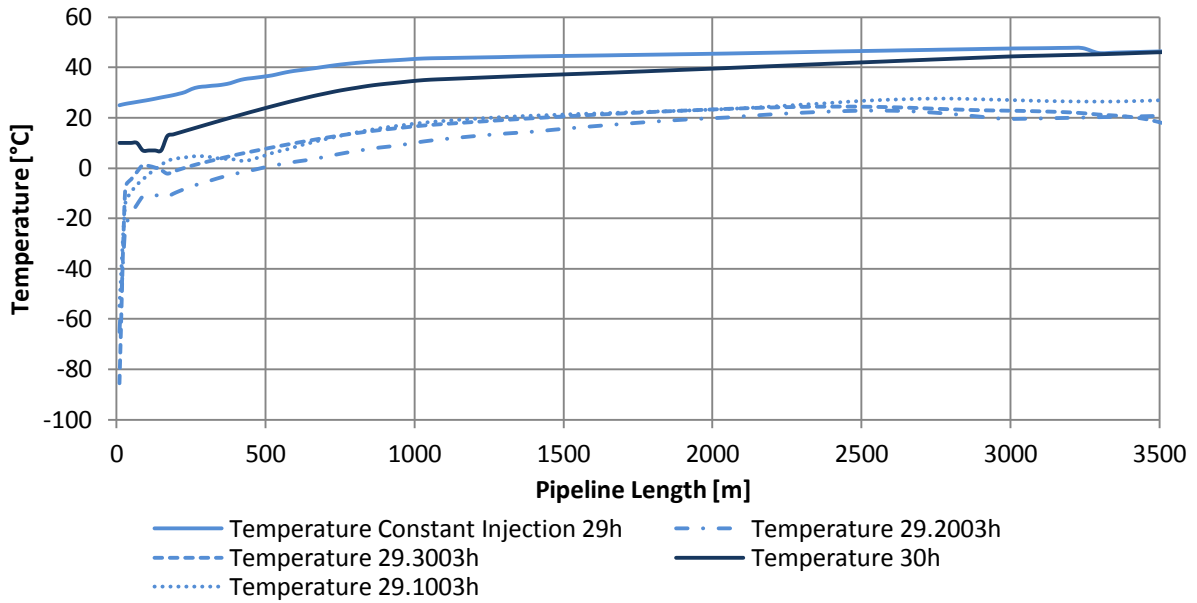


Figure 4-18 Temperature Profile Sleipner Blowout NO Backflow

Mass flow Trend Sleipner Blowout NO Backflow

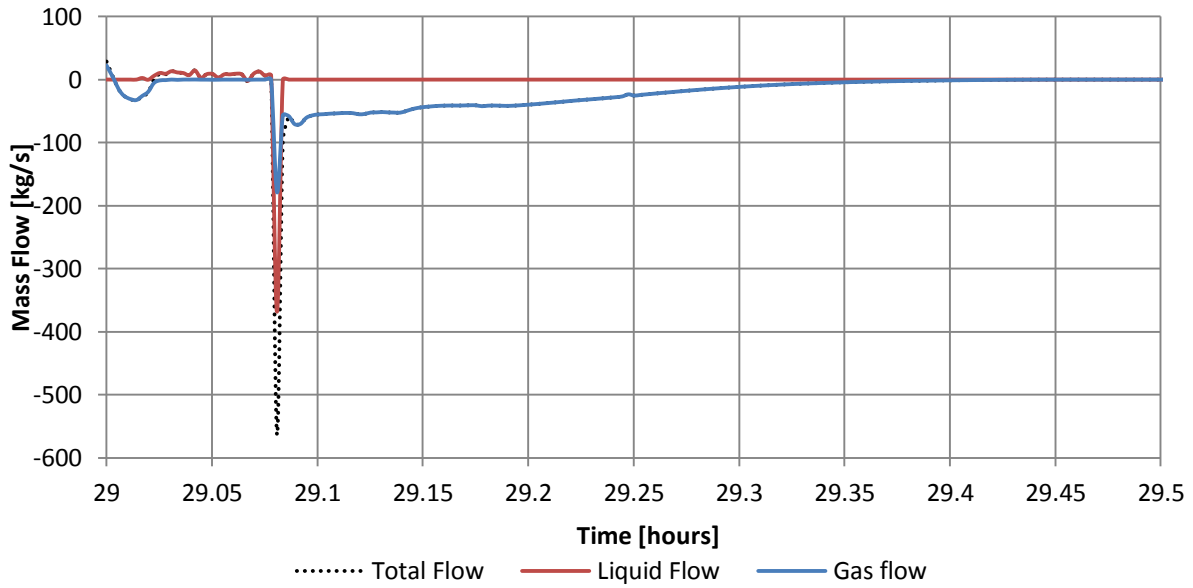


Figure 4-19 Mass flow Trend Sleipner Blowout NO Backflow. Downwards Flow is Positive.

The mass flow profiles have been included in the appendix where it can be studied further (Appendix A-23 and Appendix A-24). In this case however, it was considered more interesting to look at the trend plot for the flow at the wellhead. This can be seen in Figure 4-19. During constant injection (at 29 hours) it can be seen that the injected CO₂ is slightly within the two-phase region, but consist mainly of gas. This is in accordance with previous results. It then decreases relatively fast, but the net flow is still positive about 20 seconds into the simulation. The flow then remains solely gas until about 40 seconds when the gas mass flow starts to increase and the first signs of liquid flow appear. In the next section the gas flow seemingly goes to zero and there is a downwards flow of liquid. This persists up to about 5 minutes when the mass flow instantly increases/decreases to approximately 22 times the constant injection rate, consisting of roughly equal amounts of liquid and gas. After the blowout, the remaining liquid seems to evaporate and the gas mass flow evenly decreases until it reaches zero about 27 minutes into the simulation. One explanation to the instant blowout, might be formation of a liquid plug and an accompanying pressure buildup behind the plug. However, by closely examining the pressure development in the well, the pressure wave was seen to propagate down the well first, and then a second wave moves from the bottomhole and back to the wellhead. This might indicate that the first pressure wave leads to strong evaporation throughout the well. The large increase in volume then effectively empties the well. This also seems to be supported by the low temperatures experienced throughout the well, which might indicate that strong evaporation takes place. It might seem that the blowout has the characteristics of a boiling liquid expanding vapor explosion. The problem with profile plots is that it has to be exported at a certain instant of time in order to present the results in a report. Thus, the results depend heavily on the chosen instants. For this reason a profile plot was created in order to capture some of the effects that have been discussed. The result is displayed in Figure 4-20 and contains information about the pressure, temperature, gas fraction and flow regime, when the pressure wave is propagating down the well. The remaining profile and trend plots have been included in Appendix A-IV. From this it can be seen how the vapor fraction decrease and temperature decreases as the pressure wave propagates down the well. It can also be seen that there is a tendency to slugging in the upper part of the well.

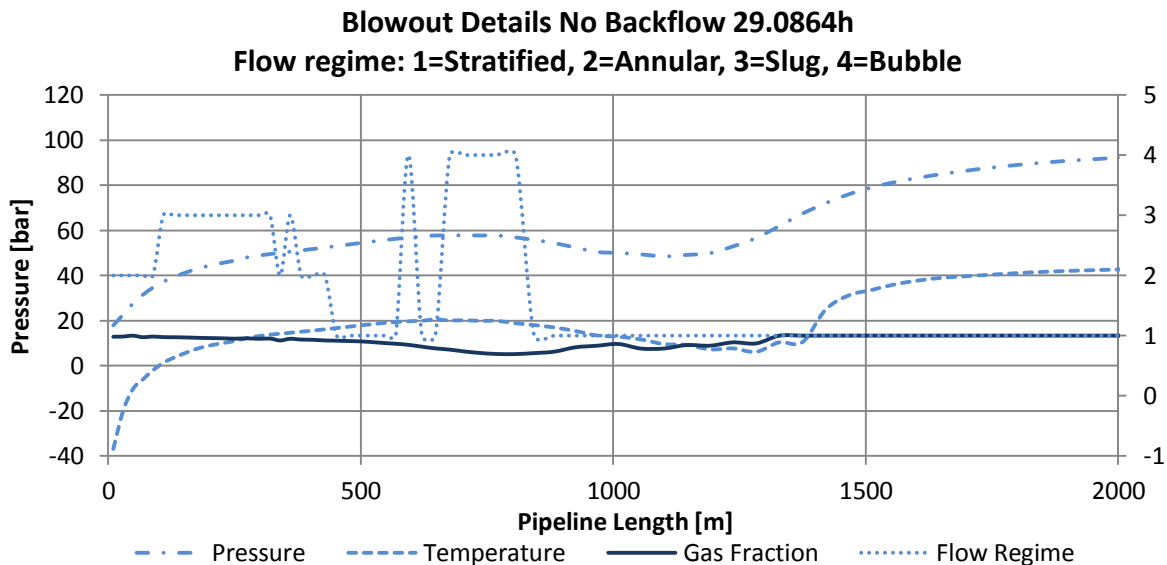


Figure 4-20 Blowout Details No Backflow 29.0864h

As opposed to the blowout with backflow from the reservoir, it can be seen from the PH and PT diagrams (Figure 4-21 and Figure 4-22) that the blowout remains outside the solid formation region, which might be a likely reason why the simulation results seem more reliable, although not validated. In the end the whole well is well within the superheated region, as it should be, as the wellhead pressure goes to atmospheric pressure and there is no backflow from the reservoir. The temperature of the inflow zone also seems to approach the reservoir temperature, which is a good indication that the conditions are stabilizing, as temperature change is much slower than changes in pressure. It can also be seen that the conditions after 30h is relatively close to the solution after 1500h, which underlines the instant nature of this blowout. As for the discharge flow rate at the wellhead, a maximum flow rate of 563 kg/s was calculated (Appendix A-30). This is by far the largest discharge flow rate of all the simulated scenarios, and is likely a combination of the size and initial state of the system and the instant reduction in pressure.

PH Diagram Sleipner Blowout NO Backflow

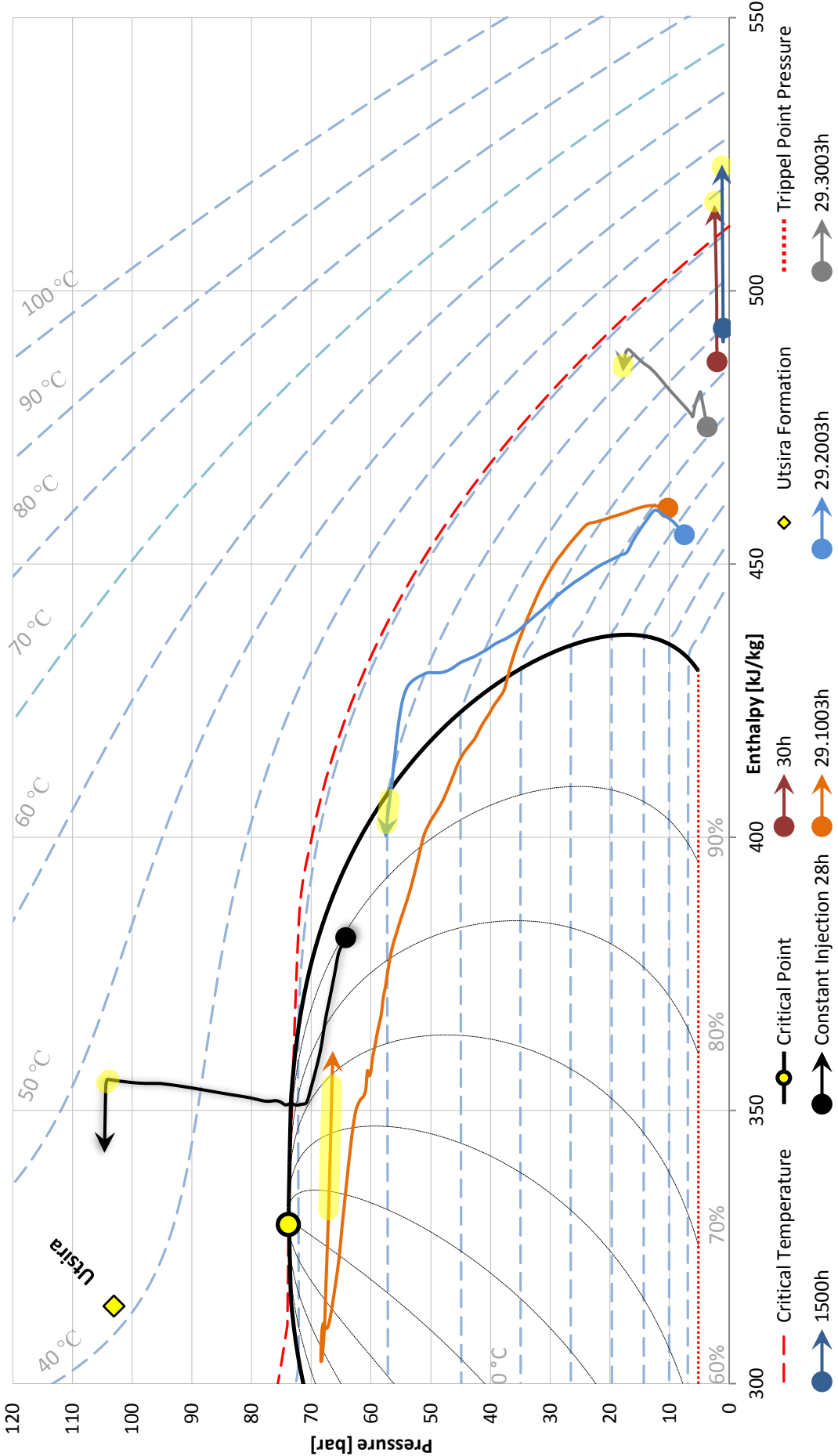


Figure 4-21 PH Diagram Sleipner Blowout NO Backflow

PT Diagram Sleipner Blowout NO backflow

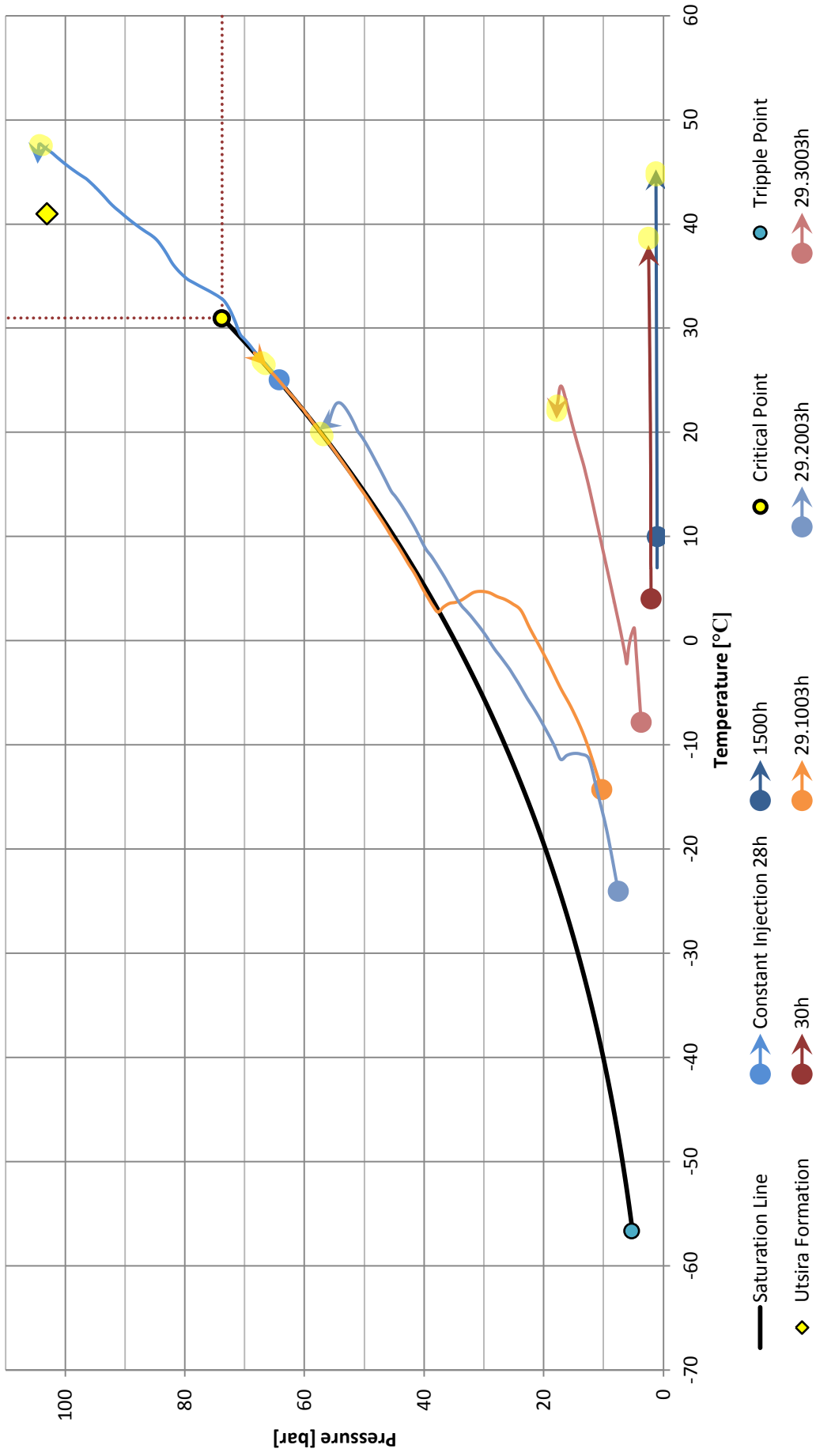


Figure 4-22 PT Diagram Sleipner Blowout NO Backflow

4.1.5 SHUT-IN SLEIPNER WITH VARIOUS COMPONENTS

To illustrate how CO₂ behaves different than other substances commonly encountered with pipe transport/well operations, the Sleipner model was used to simulate shut-ins for a variety of substances. The procedure is described in section 3.2.4 and the results are presented here. As far as possible, the only change made to the models, were adjustments to the wellhead pressure, in order to meet the specified reservoir pressure of 103 bar.

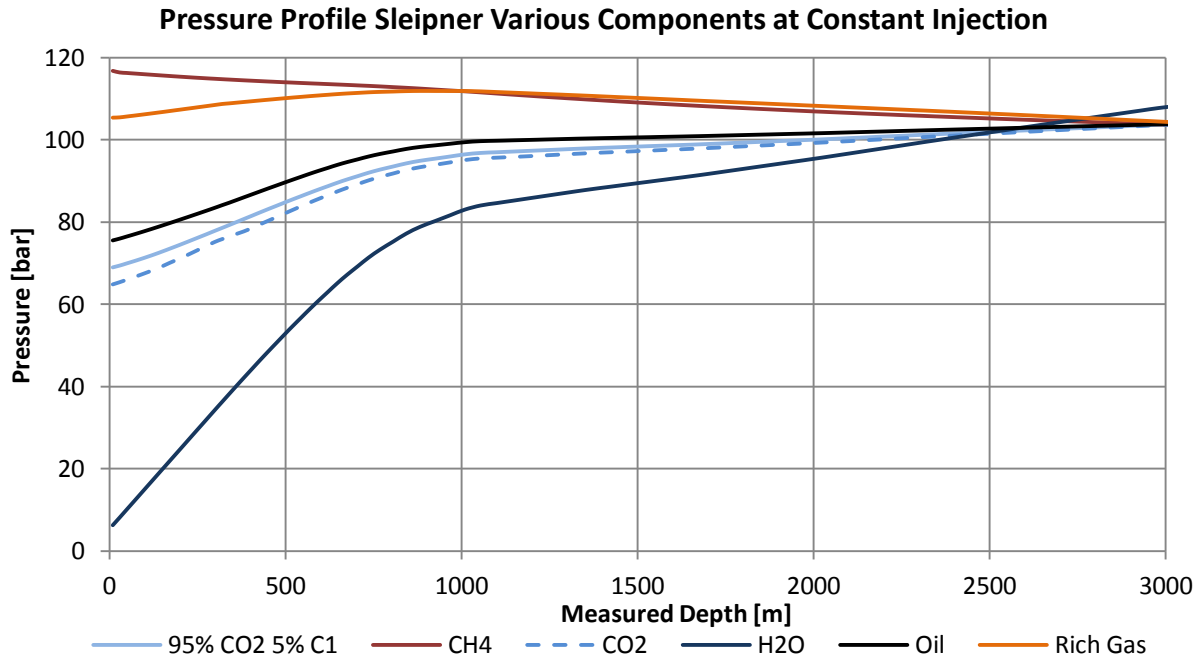


Figure 4-23 Pressure Profile Sleipner Various Components at Constant Injection

As can be seen from the pressure plot during constant injection (Figure 4-23), the CO₂ curve lies approximately mid between the curves for rich gas and water. And if the 95% pure CO₂ curve is disregarded, it actually lies closer to oil than any of the other substances (in terms of pressure). As explained in the method section, the hydrostatic pressure contribution of water is very large, and for this reason the reservoir pressure had to be increased, which explains why the pressure curve for water is higher than the rest at 3000m MD. Also interesting is how the two curves with the highest methane content show a tendency to decrease in pressure with depth. This might be explained by the low molecular weight of methane and the corresponding low gravitational pressure contribution. In fact, during injection, the frictional pressure drop is larger than the gravitational pressure contribution, which is why the pressure is increasing with depth. This is also indicated by the pressure plot at 32h (Appendix A-32), when choking is complete. At this point, the flow in the well is significantly reduced and thus also the frictional pressure drop. Accordingly, the pressure increases slightly throughout. By comparing the pressure profiles for constant injection and at 32h (Appendix A-31 and Appendix A-32), it can be seen that the reduction in pressure at the wellhead is about 8-9 bar. For water, rich gas and methane, the reduction is about 4.5, 13.9 and 21.6 respectively. For oil, the wellhead pressure increases about 14 bar.

As water is relatively incompressible and remains in liquid phase throughout the shut-in, change in pressure is minor. For CO₂, it is expected that the pressure reduction is delayed by the phase changes that takes place as long as the operational range of the well is within the two-phase region. For oil and rich gas the situation is more complex as they are composed of several components which all evaporate/condense at different pressures. Methane remains in gaseous state throughout the shut-in, and the conditions is therefore not affected by any phase changes, but change according to the conditions in the well. If the pressure profile at 32h then is compared to the pressure profile at 150h (Appendix A-32 and Appendix A-33), it can be seen that the pressure curve for CO₂ change significantly more than the other fluids which only show minor changes in pressure. This might indicate that the other fluids will approach a steady solution faster. It should also be noted that the curve for 95% CO₂ and 5% CH₄ is outside the recommendations from SPT Group, and shows the most prominent signs of instability.

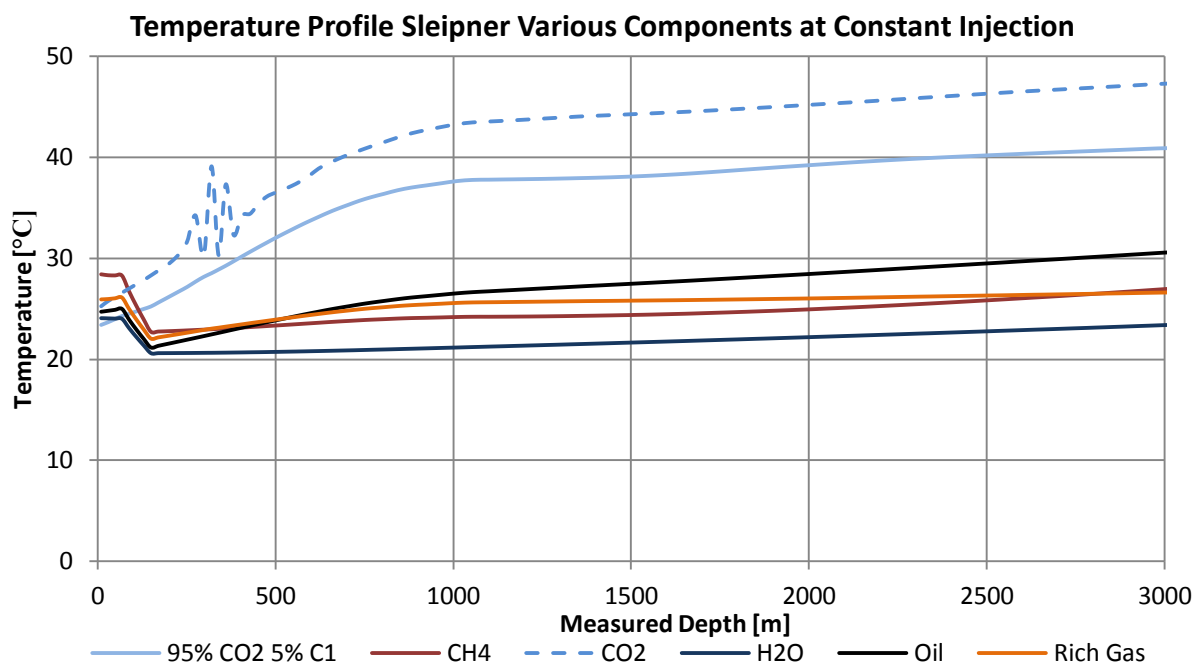


Figure 4-24 Temperature Profile Sleipner Various Components at Constant Injection

The CO₂ temperature also behaves significantly different than the other simulated fluids. In Figure 4-24, the temperature profile for constant injection has been plotted, plots at 32h and 150h are available in Appendix A-35 and Appendix A-36. Again it is expected that the different behavior is caused by the two-phase operation and, how the heat transfer (Appendix A-37 to Appendix A-39) is strongly dependent on factors such as the gas/vapor fraction and the flow regime in the well (Appendix A-40 to Appendix A-45). The gas fraction and flow regime plots show most fluctuations for the CO₂ rich fluids, while the other components are more stable throughout⁴. Even the multi-component fluids show a relatively stable gas fraction, even though the operation is within the two-phase area. Most likely this can be explained by the amount of components which give a more gradual change in conditions. The instabilities from the temperature plot can be identified from section 4.1.1, as the fluid is in the near critical region. At 32h, the

⁴ Keep in mind that the gas fraction may be a bit misleading when the fluid is within the supercritical region

temperature can be seen to approach the set boundary conditions for all fluids except CO₂ (Appendix A-35). At 150h on the other hand, the temperature is closer to the boundary conditions (Appendix A-36).

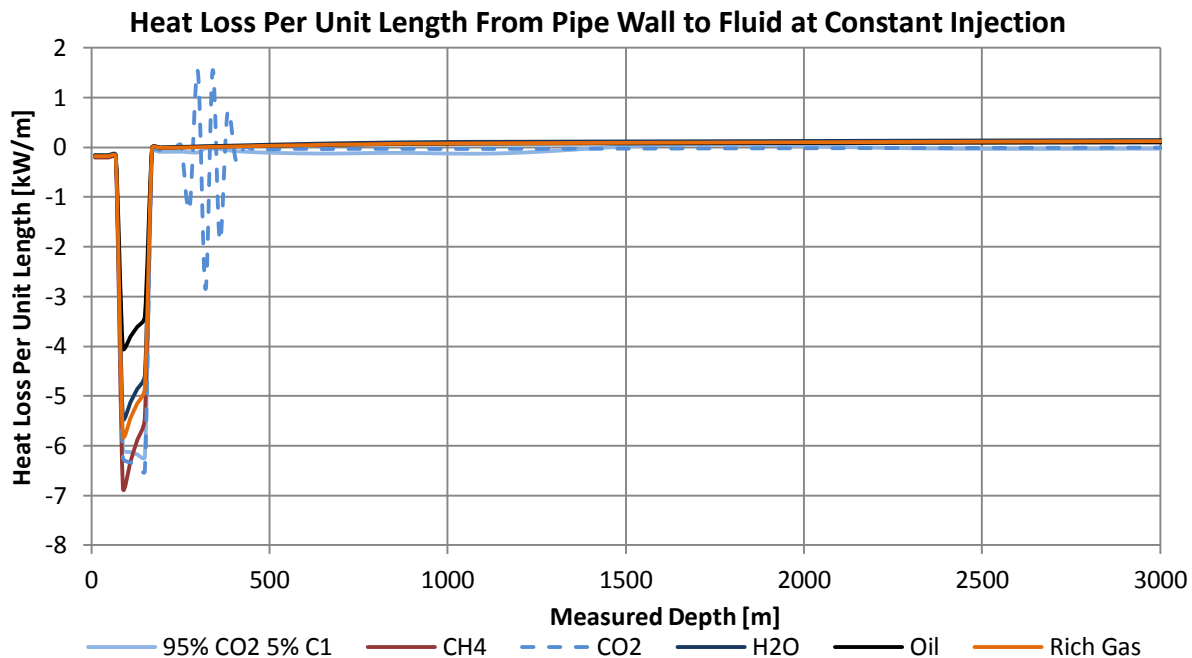


Figure 4-25 Heat Loss Per Unit Length From Pipe Wall to Fluid at Constant Injection

Figure 4-25 indicates that the calculated heat transfer from the pipe wall to the fluids, is in the same range at constant injection. However, for CO₂, the heat transfer is to a larger extent used to evaporate the liquid. Thus the temperature is not affected in the same manner as the remaining fluids. Even at 150h (Appendix A-39), it can be seen that the CO₂-rich fluids have a significantly larger heat transfer than the other fluids. Closer examination of the diagram, show heat transfer from the fluid to the pipe in the first section and heat transfer from the pipe wall to the fluid next. This seems to correspond with results from Figure 4-4 and seems to explain why the CO₂ shut-in, reacts slower in terms of pressure and temperature, than the other simulated fluids. In this particular case, no extreme temperatures were experienced in the well. However, if the reservoir pressure is low (typically common in depleted oil and gas reservoirs), a shut-in might lead to large inflow of the well content to the reservoir, which in turn might lead to a pressure drop in the well. Then, depending on the rate of change in pressure, the evaporation of the liquid content might lead to very low temperatures in the well, if the heat transfer to the well is insufficient to maintain the temperature. This was experienced during the blowout scenarios (ref. section 4.1.3 and 4.1.4) and illustrates some of the challenges related to transport of carbon dioxide. The behavior can to a large extent be explained by the location of the critical points of the respective fluids. However, when comparing with complex fluids (in terms of composition) typically encountered in oil and gas transport, it was also seen that the complex fluids showed a more graduate transition in terms of the fluid properties. Which is why the standard OLGA approach has some clear limitations when it comes to pure, or almost pure fluids near the saturation line and critical point (ref. section 2.2.4).

4.2 SNØHVIT

The results from the Snøhvit simulations are presented in this section. As for the Sleipner cases it was not considered necessary to include the base case simulations in separate diagrams, as these are included as the initial state in most of the diagrams. The model has not been verified against experimental data unless otherwise is stated, but has been tuned to give reasonable accordance with the set boundary conditions. Due to license limitations, the CO₂ VIP module was not available during the simulations. Consequently, all the simulations were performed with the standard single component module (PT-flash module).

4.2.1 SHUT-IN SINGLE COMPONENT MODULE CO₂

As indicated in section 3.3.3, the Snøhvit shut-in simulation did not experience the same trouble as the one for Sleipner, and consequently, a smaller time step could be applied. With regards to the wellhead pressure, this is more or less as expected, as it lies well above the critical pressure of CO₂.

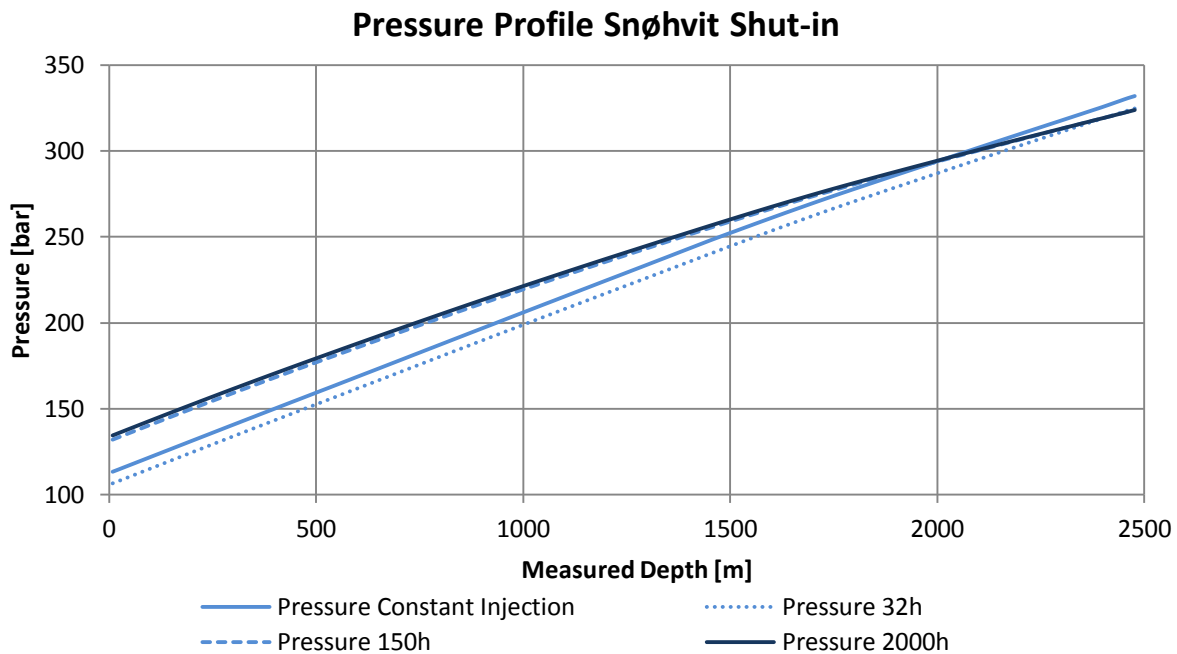


Figure 4-26 Pressure Profile Snøhvit Shut-in

From Figure 4-26 it can be seen that the pressure at constant injection seems to give a reasonable match with the specified boundary conditions. If the pressure profile is compared to the one for the Sleipner shut-in, it is significantly more linear. This is likely a combination of several factors. Firstly, the geometry has a slightly more even inclination than the Sleipner well, with two long relatively linear sections. The transition between the sections is at approximately 1500m MD, which seems to coincide well with the diagram. Another factor is naturally the state of the fluid, which according to the given boundary conditions is likely to remain in the liquid and supercritical state throughout the shut-in. From the graph it

can also be seen that there is a predicted initial pressure drop in the well and that the pressure then increases again and seems to be close to steady conditions at 150h.

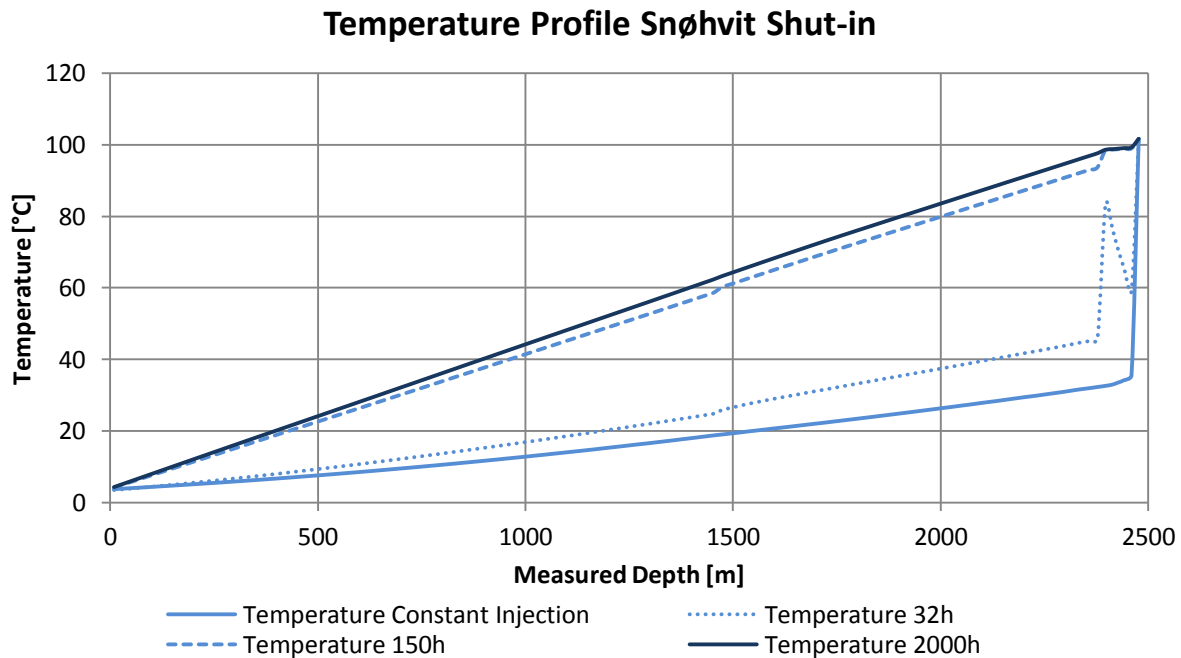


Figure 4-27 Temperature Profile Snøhvit Shut-in

The temperature profile (Figure 4-27), show a relatively large difference between constant injection and 2000h. Especially in the inflow region (approximately 2400m MD) at constant injection, there is a significant temperature difference before and after the reservoir. This indicates that the fluid does not approach the ambient temperature before entering the reservoir. In the last section of the well however, the temperature is significantly higher. This seems reasonable, as the section is located after the inflow zone and is basically just an open hole with little or no flow. Consequently, the temperature in this section is closer to the ambient temperature. At 2000h it can be seen that the temperature increases more or less linearly throughout the well.

Appendix B-2 seems to confirm the suspicion from the pressure profile and indicates that the fluid remains in the liquid state throughout the shut-in. The mass flow profile (Appendix B-1) also seems to indicate that the flow conditions stabilize relatively quickly in the well, something which also is indicated by the flow regime plot (Appendix B-4). The density plot (Appendix B-3) on the other hand, showed a greater change than initially anticipated, but when viewed in context with the temperature change in the well it seems to make sense.

The results was, as for the Sleipner case, processed and plotted in a PH and PT diagram. This can be seen in Figure 4-28 and Figure 4-29. In these diagrams, inflow zones have been marked by yellow shaded areas. Furthermore, the wellhead pressures are marked with circles and the bottomhole pressures with arrows. Reservoir conditions are indicated by a yellow square. From the PH diagram, it can be seen how the wellhead pressure initially falls and then increases again as indicated by the pressure profile (Figure 4-26). In this case, the initial pressure drop showed a close relation to the injected mass flow.

Accordingly, the minimum pressure was registered at 32 hours, when the injection stream was closed. The following increase in temperature, as the fluid approaches the ambient temperature, is then the main contributor to the subsequent increase in pressure. The gradual nature of the shut-in procedure will naturally affect the result, as the fluid has more time to exchange heat with the surroundings. In the event of an emergency shutdown on the other hand, a more instant fall in pressure and temperature might be expected. The used shut-in procedure was taken from the available operational data from Snøhvit. Furthermore it can be seen that the conditions of the inflow zones, approaches the formation conditions when time is increased. After 1500h, the conditions seem to have stabilized in the well and the inflow conditions are more or less equal to the reservoir conditions. Thus, at this point, the line should approximate the geothermal gradient applied in the model. At approximately 1500m MD there is a change in both inner diameter and inclination of the wellbore. This can be seen, relatively pronounced, about halfway for the 32h, 42h and 150h curves. Also noticeable, is the abrupt changes in enthalpy in the inflow zone at 32h. The reason for this seems to be that the pressure in the inflow zone falls below the reservoir pressure. This in turn leads to reservoir inflow in the well which rapidly increases the enthalpy. However, as the inflow only affects the subsequent sections to a limited extent, the enthalpy is reduced again, before it approaches the ambient conditions in the last section (after the inflow zone). The PT diagram (Figure 4-29) has been plotted for both initial and final conditions. Intermediate solutions should lie in between, as for the PH diagram. As the near-critical region does not have any clear boundaries, it is difficult to make any hard conclusions on whether it is affected or not. To do this, it is necessary to investigate how the fluid properties change with temperature and pressure for the various conditions along the well. On the other hand it was a significant difference from the Sleipner shut-in, and the output seems to be more stable. By interpolating in the plot data, the transition from liquid to supercritical was estimated to approximately 2185m MD at constant injection and 632m MD after 1500h.

PH Diagram Snøhvit Shut-in

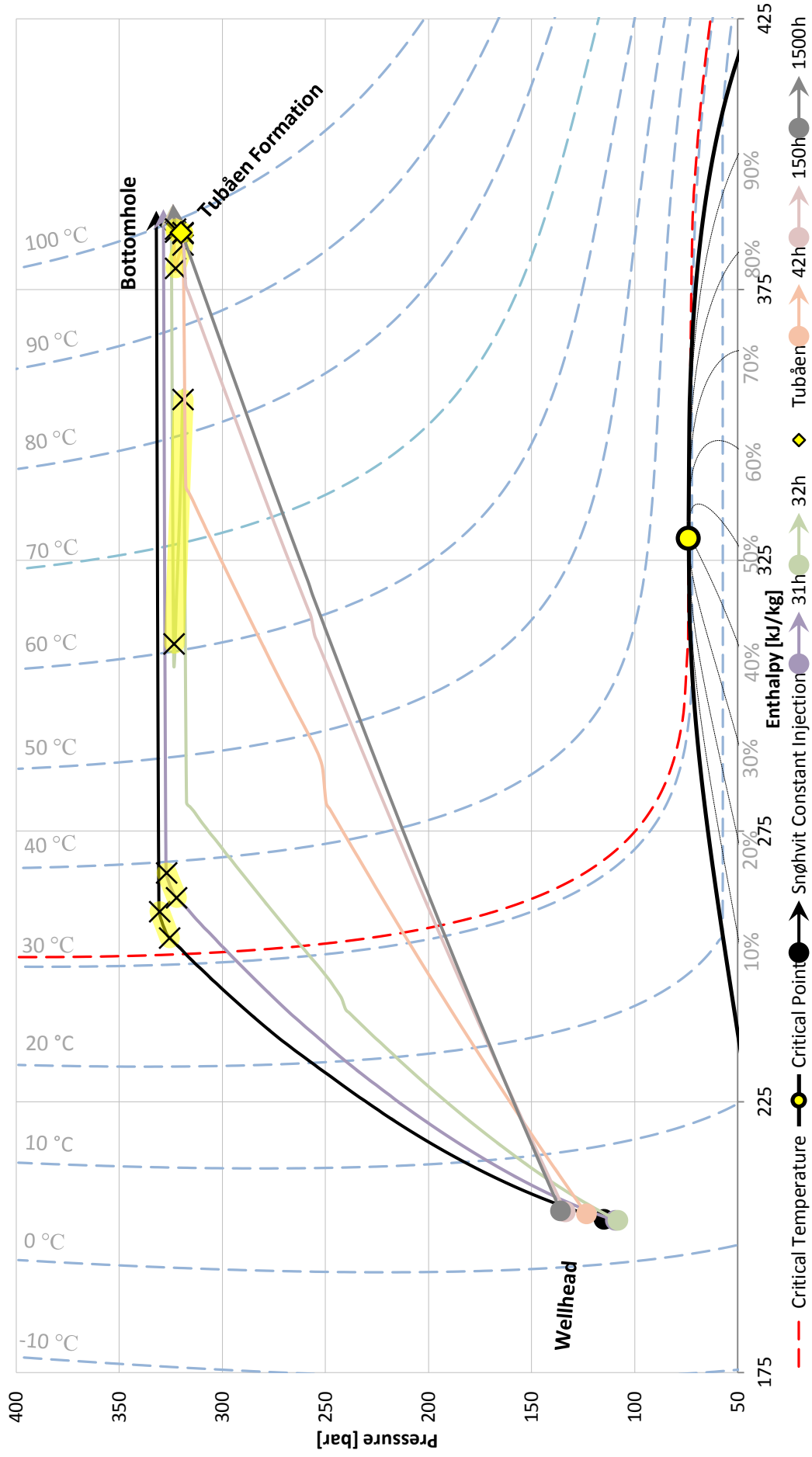


Figure 4-28 PH diagram Snøhvit Shut-in

PT Diagram Snøhvit Shut-in

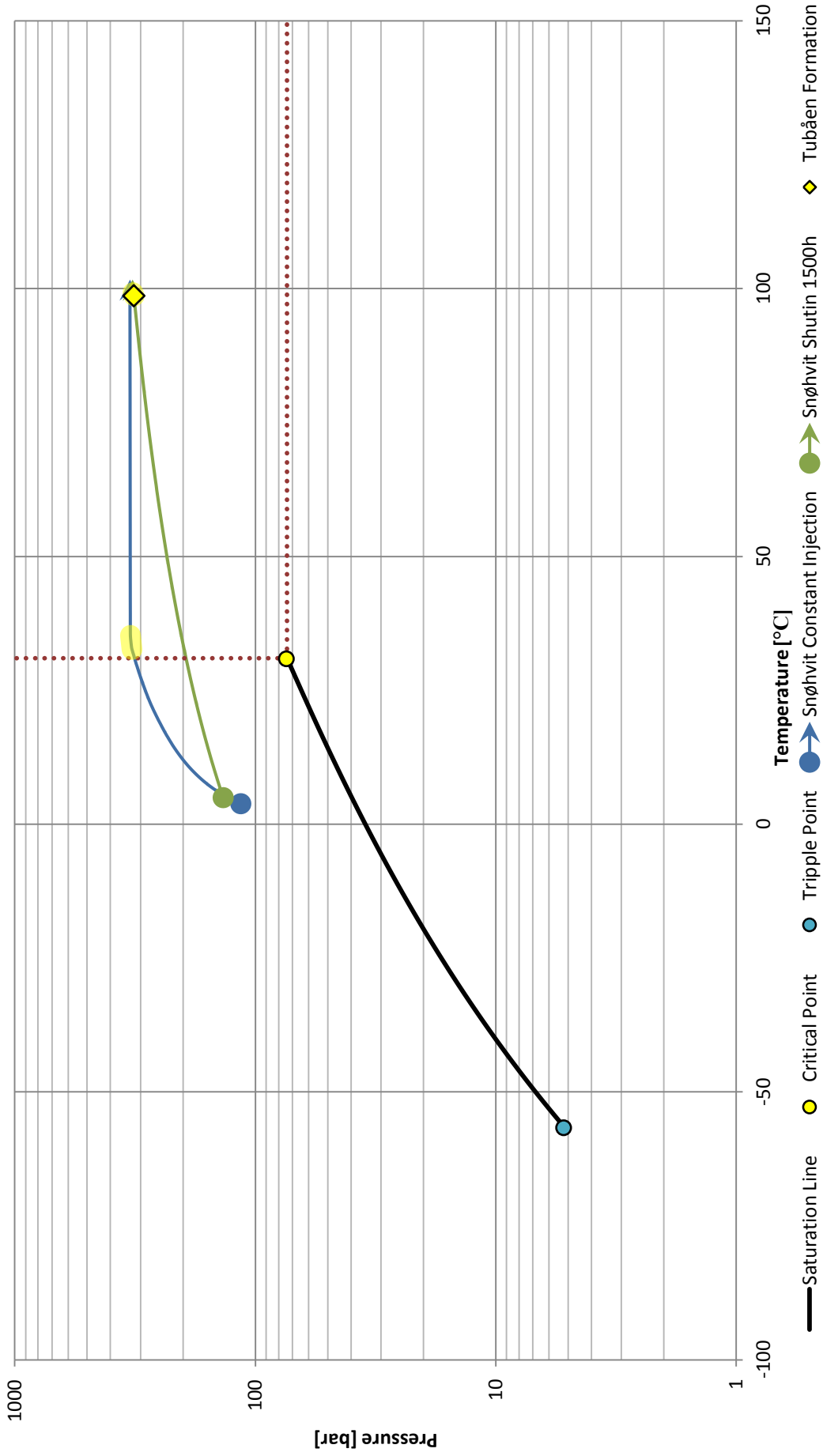


Figure 4-29 PT Diagram Snøhvit Shut-in

4.2.2 BLOWOUT CO₂ WITH RESERVOIR BACKFLOW

As indicated in section 3.3.3, the Snøhvit blowout simulation with reservoir backflow, ran into major numerical problems once the valve opened. Consequently, the time step was set to 1s and the time constant controlling the evaporation was set to 10s. This will clearly affect the result, but was still necessary in order to complete the simulation. As opposed to the similar Sleipner simulation, the backpressure was set to approximately 31 bar, to account for the subsea wellhead conditions. Consequently, the results should not get below the triple point and this is therefore not the reason for the instabilities that were experienced.

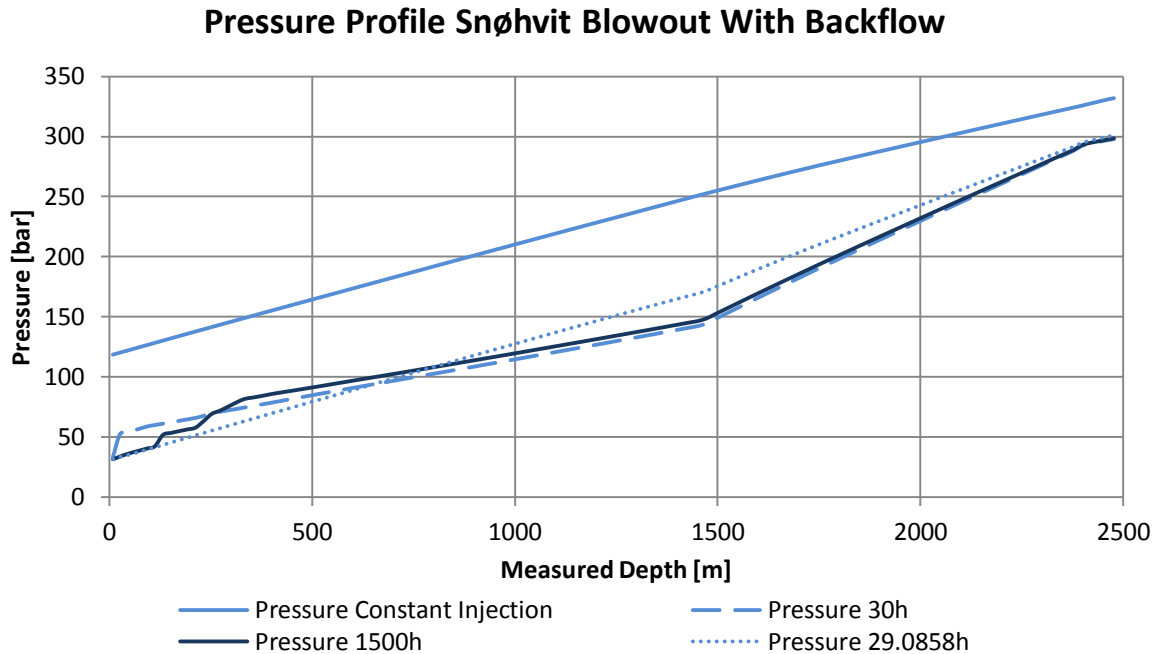


Figure 4-30 Pressure Profile Snøhvit Blowout With Backflow

Figure 4-30 confirms this, and show an instant drop in pressure throughout the system. After 5 minutes (29.0858h) the pressure at the wellhead has dropped to about 32 bar. Again it can be seen that around 1500m MD there is a change in inclination for the plots. Note however that the flow direction is reversed for all the simulations after the valve opens. Interesting is also how the pressure at 1500h show some relatively sharp changes in pressure in the first part of the well. This was expected to some extent for the Sleipner case, as the heat transfer was modeled differently for the wellbore and the two riser sections. In this case however, the geothermal gradient is a linear function from the wellhead to the bottomhole and can thus not explain the behavior.

The same distinctions can also be seen from the temperature plot (Figure 4-31), but there seems to be no clear reason which fully explains the abrupt changes. It might be a complex explanation involving amongst others phase transitions, changes in vapor fraction, numerical instabilities and flow regimes in that particular part of the well. As Appendix B-9 and Appendix B-8 shows, the flow regime is stable in the relevant section, but the vapor fraction is continuously decreasing. Another interesting observation

from the temperature plot, is that the temperature actually increases in almost the whole well. However, when considering the model specifications it might not be that unlikely after all. At constant injection cold CO₂ at 4°C is injected at the wellhead, and by the time the CO₂ reaches the inflow zone, the temperature has increased to slightly above 40°C. This is still about 55°C below the

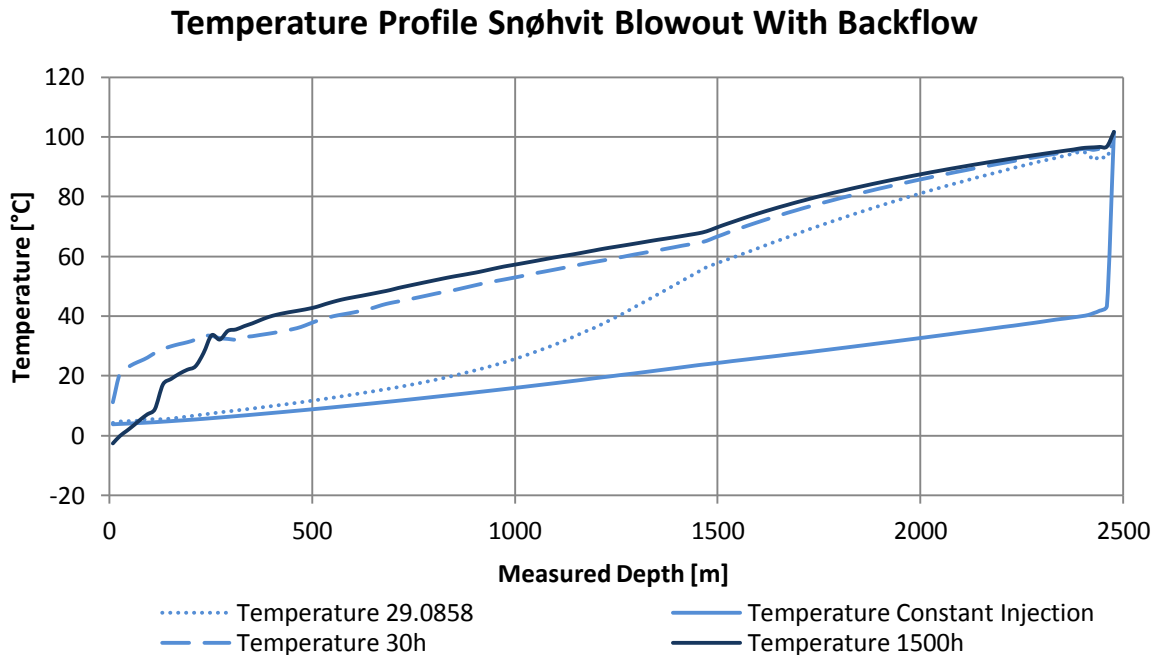


Figure 4-31 Temperature Profile Snøhvit Blowout With Backflow

reservoir temperature, and seems to explain the sudden increase in temperature in the last, non-flowing, part of the well. During the blowout on the other hand, CO₂ is flowing out of the reservoir, at reservoir conditions (98.7°C, 320 bar), which seems to be a likely explanation to the increasing temperature. As the CO₂ flows upwards it is cooled by the decreasing ambient temperature, the Joule-Thomson effect and as it enters the two-phase region, evaporation will lead to additional cooling. The latter might explain the change in the part of the well which is closest to the wellhead. It is clear however, that the cooling affect would be more pronounced if the backpressure was atmospheric, as in the Sleipner case. If the density plot also is included in the analysis (Figure 4-32), it can be seen that the transition to supercritical phase (after 1500h) seems to coincide with the changes in pressure and temperature in the first part of the well. Furthermore, it can be seen how the system enters the two-phase region with time. Both the 30h and 1500h plot estimates a transition to supercritical at about 270m MD.

An interesting observation was made from the trend plots (Appendix B-10 and Appendix B-11), which revealed a sudden change in output, from highly fluctuating, to less fluctuating. This happens at approximately 715h. However, it seems more likely that the simulation engine randomly finds a steadier solution, than this is caused by a specific event at this time in the simulation. In general it can be said that the pressure in the inflow zone has to be relatively stable (in order to find a steady solution), as the outflow from the reservoir is directly coupled to the pressure difference between the inflow zone and the reservoir. This again is dependent on many interconnected factors such as the density of the fluid, the transition between phases and flow regimes, and gas fraction to mention some. Thus, differentiating the

various effects is not an easy task and it seems more likely that the simulation rather swings into a more stable solution. Additional figures have been included in appendix B-II.

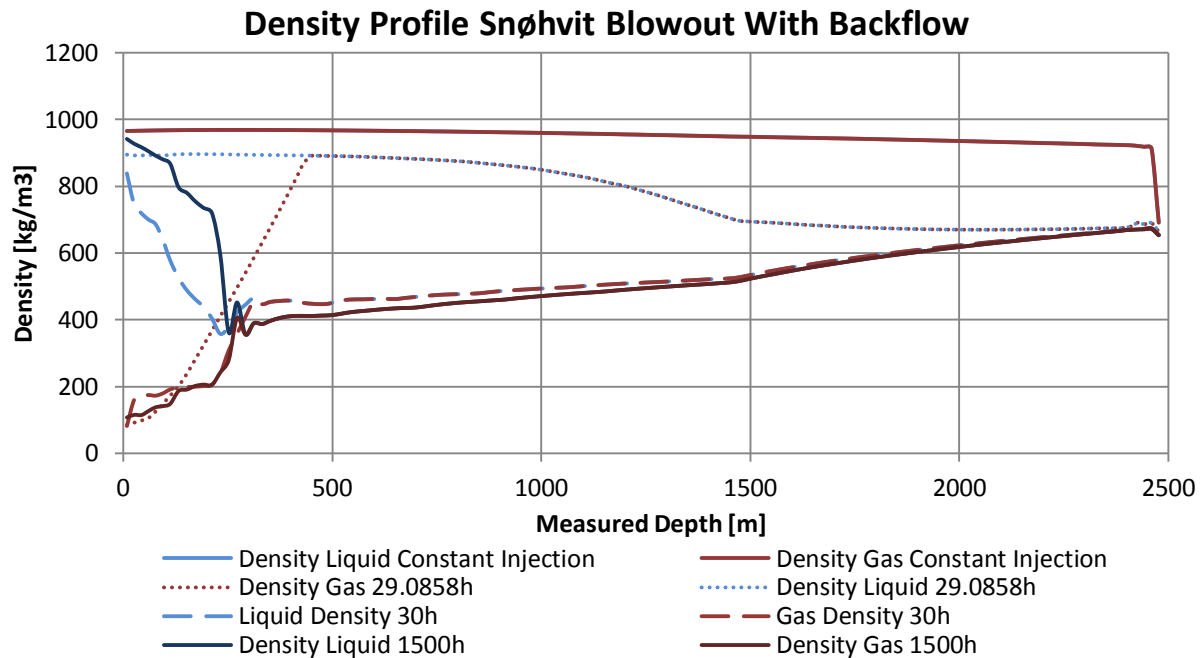


Figure 4-32 Density Profile Snøhvit Blowout With Backflow

With the highly fluctuating output, and the somewhat unexpected behavior in the first part of the well, in mind, it is of particular interest to have a closer look at the PH and PT diagrams for the blowout (Figure 4-33 and Figure 4-34). From this, it seems quite evident, that operation in the near critical region may be the main cause of the abrupt changes observed in the first part of the well, as large parts of the simulation operates in this region. From about 15 minutes into the simulation and throughout, the solution is definitely in, or very close to, the near critical region. In that sense, the standard OLGAs approach appears to meet its limitation (ref. section 2.2.4). Although it is only speculations, it seems likely that the reason why the results seemed to stabilize is that it found a solution which exits the phase envelope far enough to the right to avoid the near critical region (see the 1500h plot). It might also be a possible explanation for the discussed pressure and temperature behavior, as the plot abruptly fluctuates near the saturation line. The fluctuations seen in the pressure trend plot can also be identified in PH diagram. The PT diagram also gives a good perspective of the simulation, as it shows how close the lines are to the critical point. The accuracy of the simulations is naturally highly debatable. It should be kept in mind however, that it is an extreme scenario. Nonetheless, it would be interesting to run the simulation with the CO₂ VIP module to see the difference. As for the discharge flow rate, a maximum flow rate of 234 kg/s was encountered at the wellhead, and seems to end up fluctuating between approximately 50 kg/s and 80 kg/s (Appendix B-12). However, the result was highly unstable.

PH Diagram Snøhvit Blowout with Backflow

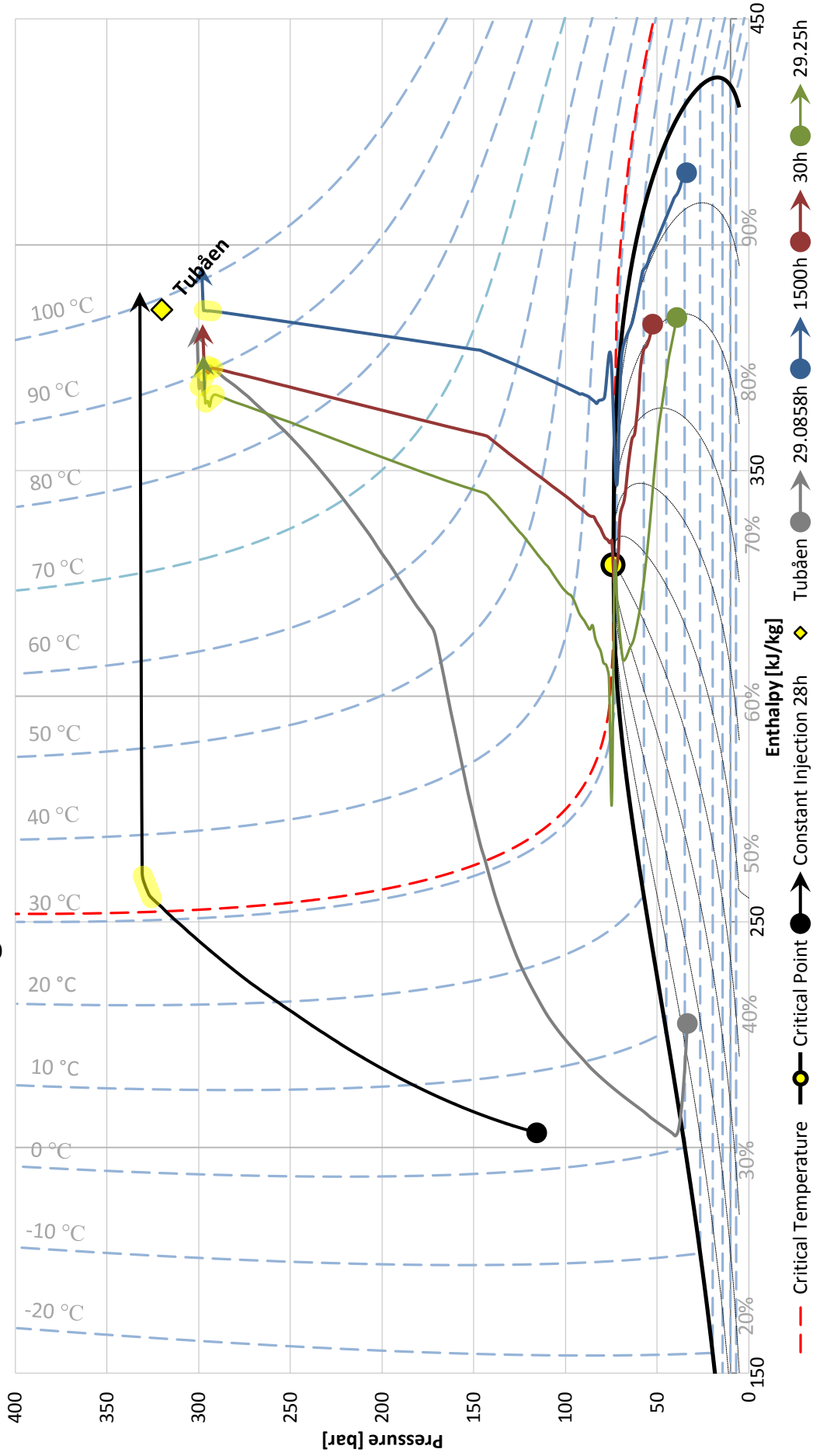


Figure 4-33 PH Diagram Snøhvit Blowout With Backflow

PT Diagram Snøhvit Blowout with Backflow

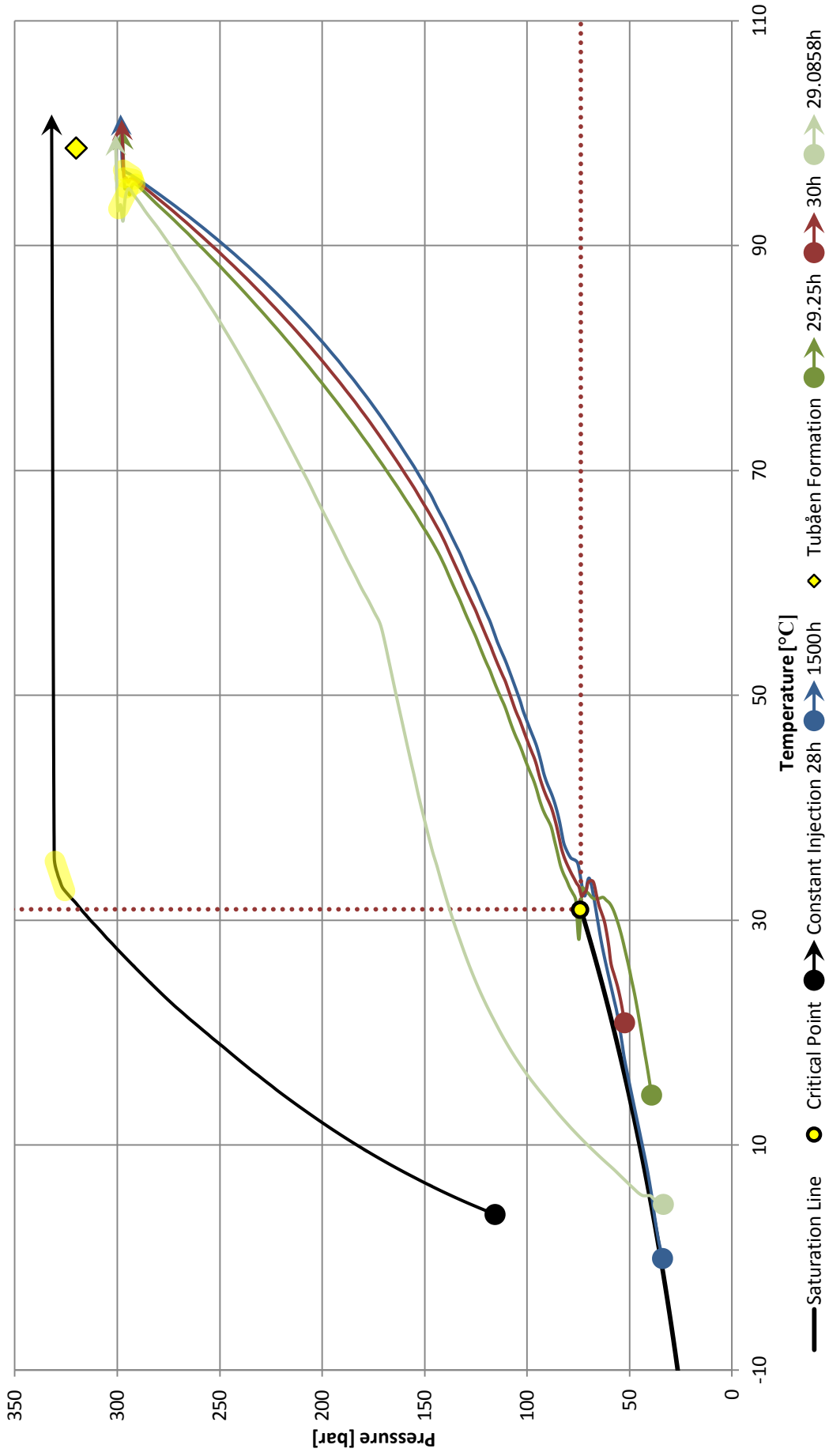


Figure 4-34 PT Diagram Snøhvit Blowout with Backflow

4.2.3 BLOWOUT CO₂ WITHOUT RESERVOIR BACKFLOW

The second scenario was specified as described in section 3.3.3. Accordingly, the minimum time step was set to 1s. As in the previous scenario (section 4.2.2), the backpressure and temperature were specified to approximate the subsea conditions at the wellhead. Also this scenario experienced some numerical trouble, but not in the same extent as the case with reservoir backflow. The pressure and temperature profile plots can be seen in Figure 4-35 and Figure 4-36, additional figures are included in appendix B-III. If the pressure profile is compared to the pressure profile for blowout with backflow from the reservoir (Figure 4-30), it can be seen that the pressure difference between the wellhead and bottomhole is significantly reduced. The resulting bottomhole pressure of approximately 50 bar, seems to indicate that the entire well is in gaseous phase at this point. At 30 and 36 hours, changes in inclination can be identified from the plots. This is likely to indicate phase changes in the well. The temperature plot reveals some more complex effects. Especially after 36 hours, there is a drop in temperature around 1000m MD, which does not appear to have an obvious explanation. It can be seen from Appendix B-17 however, that there is an abrupt change in mass flow at this point. Also the density plot (Appendix B-13) has an abrupt change in density at this point, about 250m before the transition to supercritical. The flow regime plot (Appendix B-15) also reveals a change from slug to annular before it changes again to bubble flow. This is likely to affect the heat transfer with the surroundings and might be parts of the explanation. On the other hand, it seems likely that the pressure and temperature at this point is close enough to the critical point to be affected by numerical instabilities. Furthermore, it can be seen that the well is close to final conditions after 42h (13 hours after the valve opens) and that the well is fully within the superheated region. Although the temperature in the well gets above the critical temperature, the pressure remains below the critical pressure at the end of the simulation. When compared to the similar Sleipner simulation (section 4.1.4) it can be seen that the time to reach steady conditions is significantly longer (the Sleipner simulation was close to the final state after one hour). This is naturally dependent on the size of the

Pressure Profile Snøhvit Blowout Without Backflow

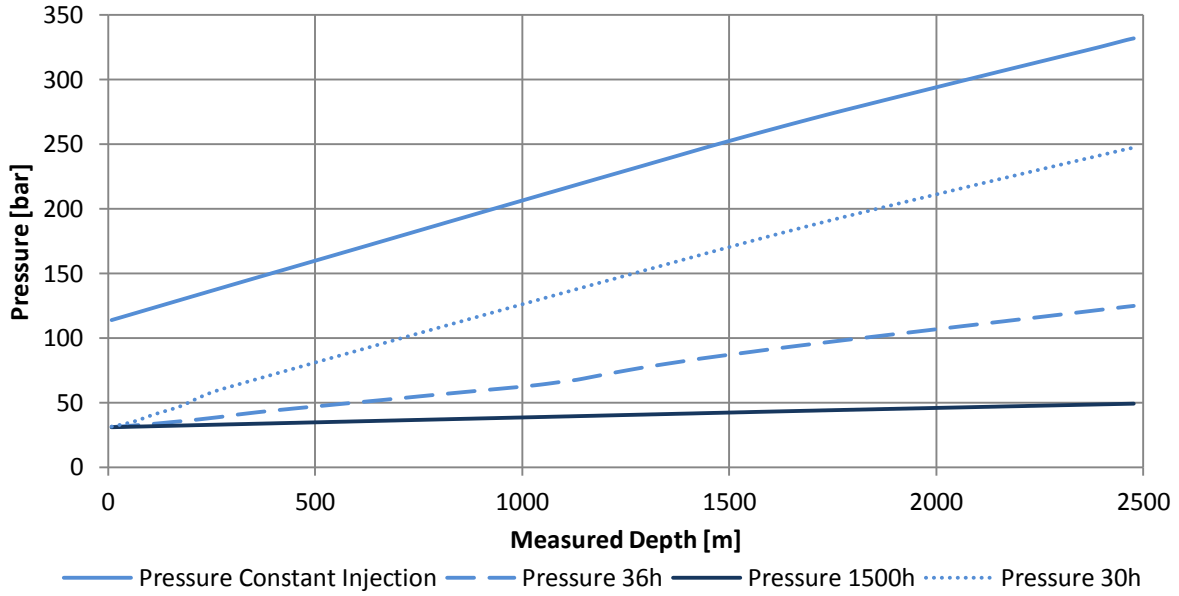


Figure 4-35 Pressure Profile Snøhvit Blowout Without Backflow

Temperature Profile Snøhvit Blowout Without Backflow

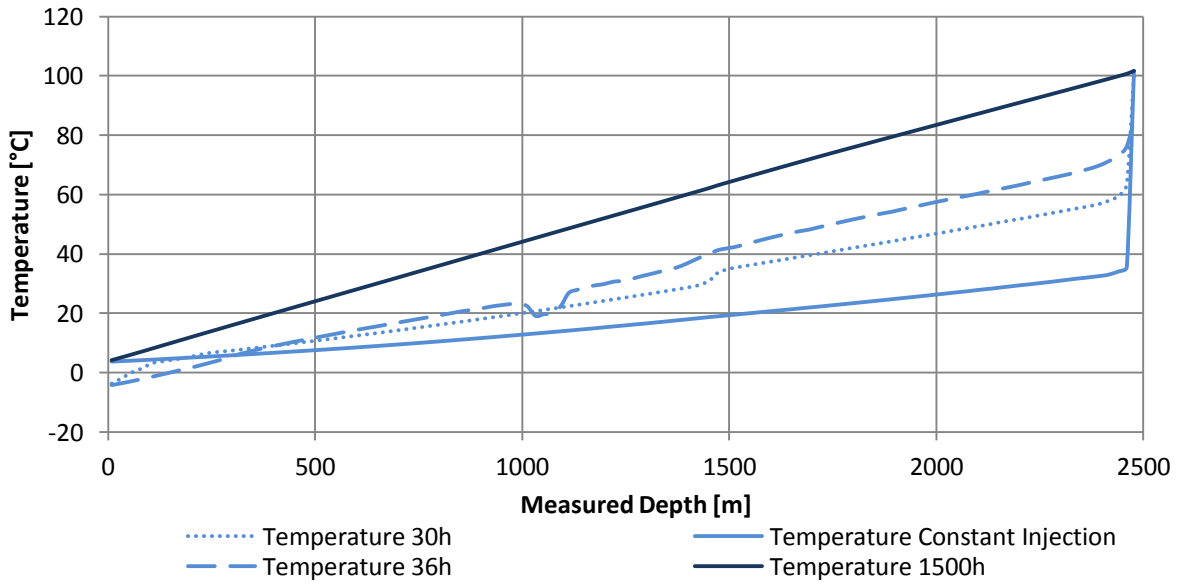


Figure 4-36 Temperature Profile Snøhvit Blowout Without Backflow

systems, but in this, case the main cause seems to be how long the simulation linger in the two-phase region. At Sleipner, the initial state at the wellhead is already close to superheated, which seems to give a more rapid equalization of pressure. The low backpressure in combination with two-phase flow might also appear to speed up the evaporation process. In this case however, the whole well is above the two-phase area and a large part of the well has to traverse the entire phase envelope. This seems to slow down the process. It also has to cross the critical region, which seems to cause some trouble in the calculations. The Sleipner simulation on the other hand, may appear to barely touch the near-critical region, and seemed also to encounter less problems during the calculations. The PT diagram also show the somewhat strange behavior discussed in relation to the temperature profile (Figure 4-36) and seems to back up the impression that it is caused by numerical instabilities. The temperature of the inflow zone can also be seen to approach the formation temperature at the end of the simulation, which seems to indicate that the well is approaching steady state conditions. The maximum encountered discharge flow rate at the wellhead was approximately 104 kg/s (Appendix B-20). As for the Snøhvit case with reservoir backflow, it would be interesting to run the model with the CO₂ VIP module (ref. section 2.2.4).

PH Diagram Snøhvit Blowout NO Backflow

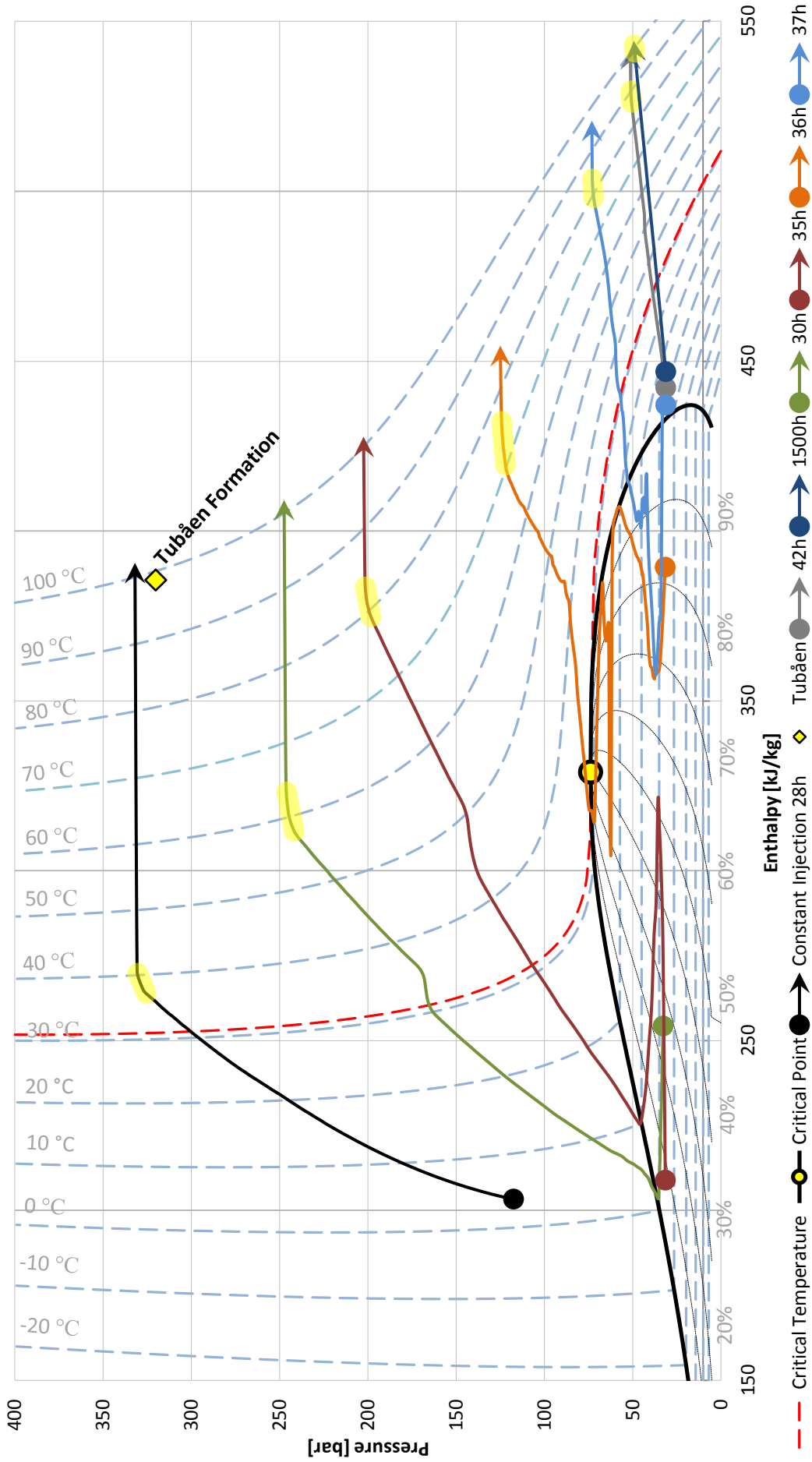


Figure 4-37 PH Diagram Snøhvit Blowout NO Backflow

PT Diagram Snøhvit Blowout NO Backflow

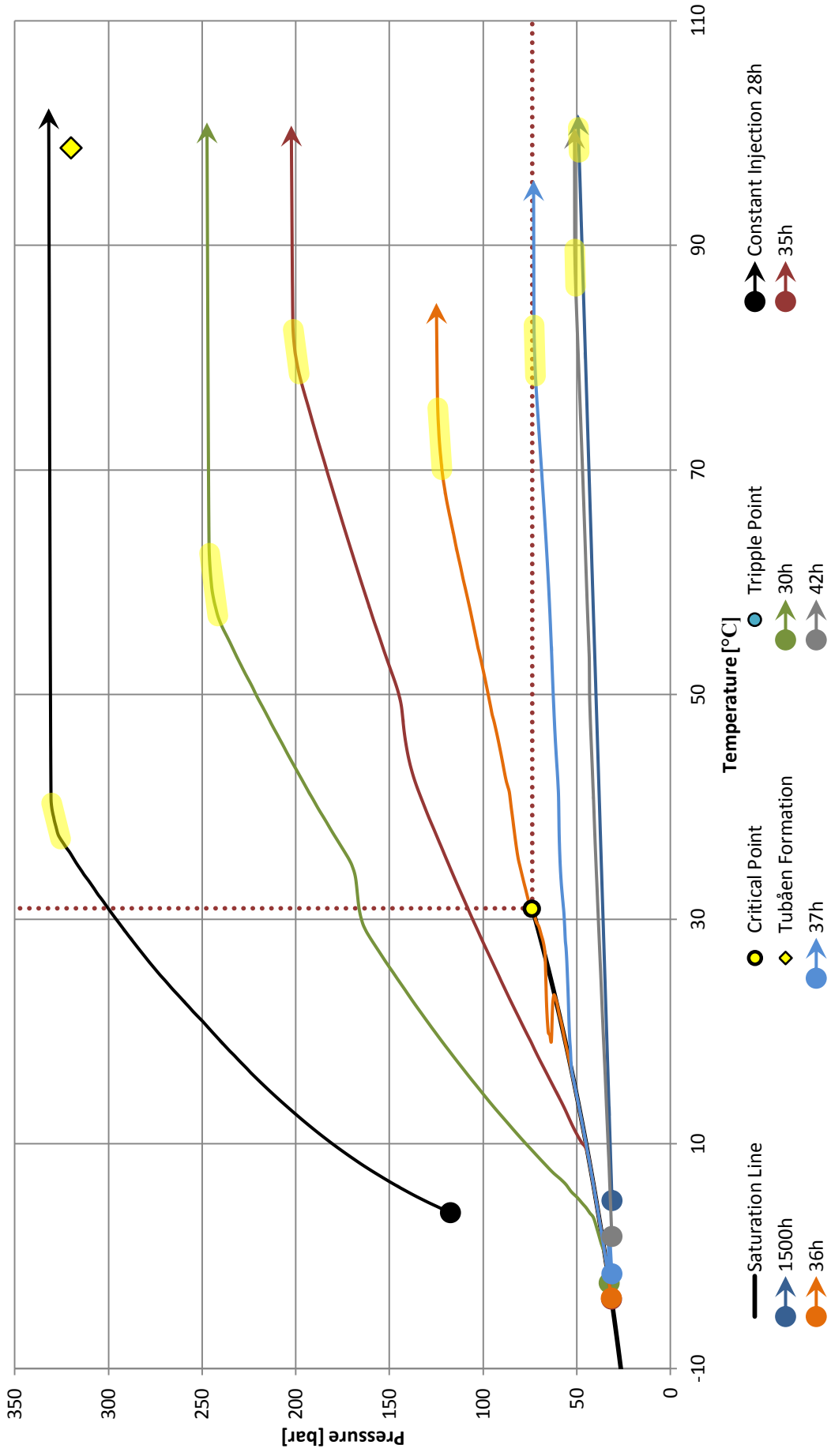


Figure 4-38 PT Diagram Snøhvit Blowout NO Backflow

4.2.4 HISTORY MATCHING AND MODEL OPTIMIZATION

The iteration process was allowed to run approximately 350 iterations, each consisting of four separate experiments. At this point the global value was changing at a very low rate and the iteration process was ended. The steps of the process are outlined in section 3.3.4 and the results are presented here.

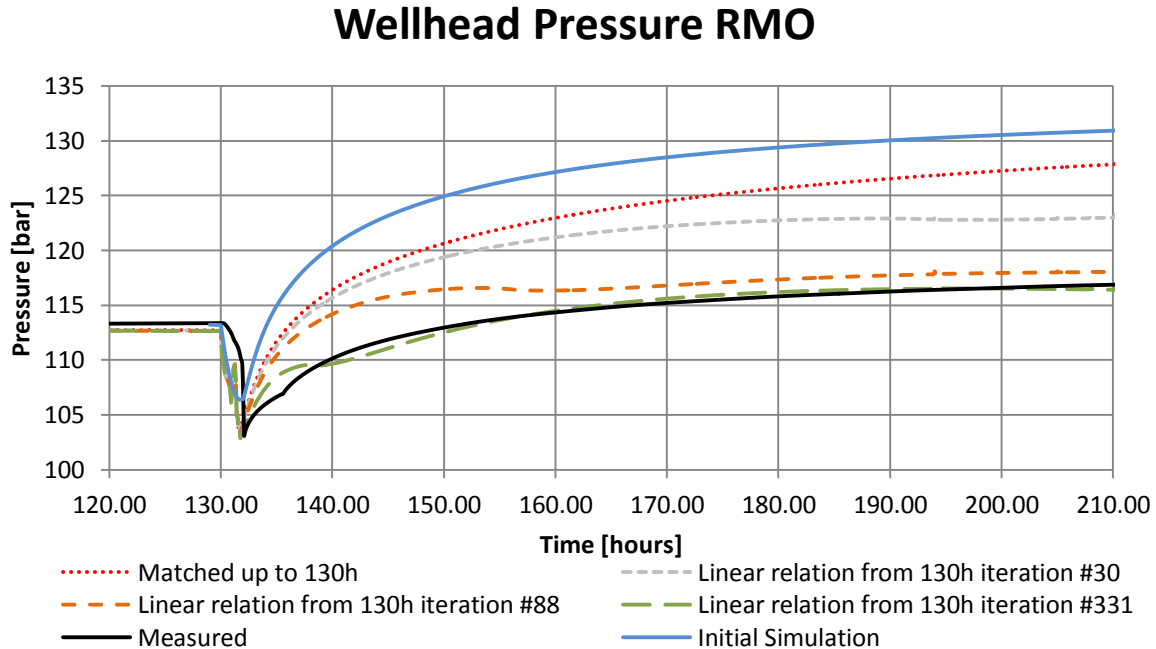


Figure 4-39 Wellhead Pressure History Matching

The resulting wellhead pressure is presented in Figure 4-39, where the initial simulation represents the results from the shut-in simulation from section 4.2.1. The result from the first iteration process has also been plotted separately. In addition to the operational data which are represented by a black line, three results from the second iteration process have been included, where iteration 331 is the result with the lowest global value.

As can be seen, the final results definitely close in on the measured pressure, but also introduce some unexpected changes in pressure after the initial drop in pressure. The same changes are not equally pronounced in the wellhead temperature, but might be explained by the time scale. If heat transfer with the surroundings is sufficient, it should show less variation in the temperature. However, by closely examining the measured pressure curve, it can be seen that there is a marked change in pressure around 136 hours. The reason for this is not entirely understood, but it might be that the different formations have a slightly different response to the shut-in. As the temperature is well above the critical region throughout the well, it seems unlikely that this is caused by abrupt changes in fluid properties.

Wellhead Temperature RMO

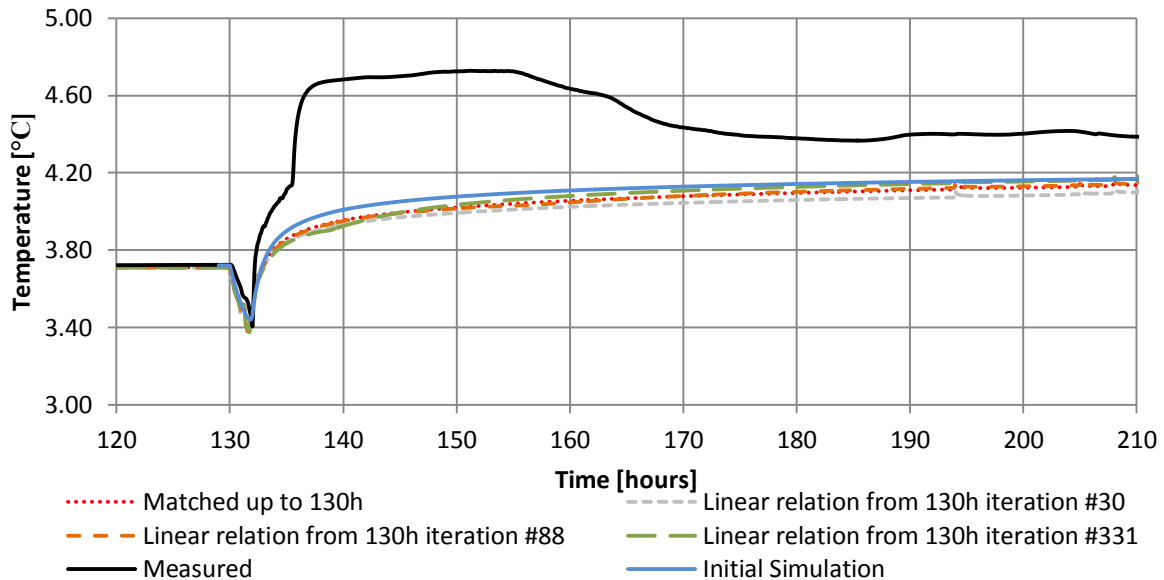


Figure 4-40 Wellhead Temperature History Matching

As mentioned in section 3.3.4, the temperature measurements were disregarded in the second iteration cycle. This was mainly justified by the somewhat unnatural behavior of the temperature, which also can be seen from the black curve in the temperature plot (Figure 4-40). During the first iteration cycle, pressure and temperature was weighted equally, and optimized against the constant pressure and temperature from 120 to 130 hours. Although the results are not following the measured temperature, there is in general not a very large difference between the simulations.

The gauge trend plot (Figure 4-41) also show the same changes in pressure, but slightly more pronounced. This might be an indication that the behavior is caused by the reservoir, as the gauge is located closer. As expected, it can also be seen that the simulated pressure lie about 4-5 bars above the measured pressure (from before the shut-in). Furthermore, it was observed that there is a tendency that the pressure increases faster for the simulations than for the measured data. This is true for both the wellhead and gauge pressure plots. This might be an effect of the simplified linear equation used for the reservoir, but might also indicate that the calculated heat transfer is wrongly estimated. This might also be indicated by the temperature plot (Figure 4-42), as it can be seen that all the simulations experience a more rapid increase in temperature, when compared to the observed values. After about 140 hours however, the simulations are more or less parallel to the measured values. Regarding the gauge pressure there is also a relatively distinct decrease in pressure for the last iterations. This was also the case for the wellhead pressure to some extent, although not as distinct. If this solely is caused by a reduction in reservoir pressure is not entirely understood, but it is only the case for the simulation results from the second iteration process, which allowed for a linear change in the parameters. It might also be an effect of the iteration process itself, as it aims to minimize the global value. This in turn might lead to a final reservoir pressure that is estimated too low, as long as the overall deviance is less.

Gauge Pressure RMO

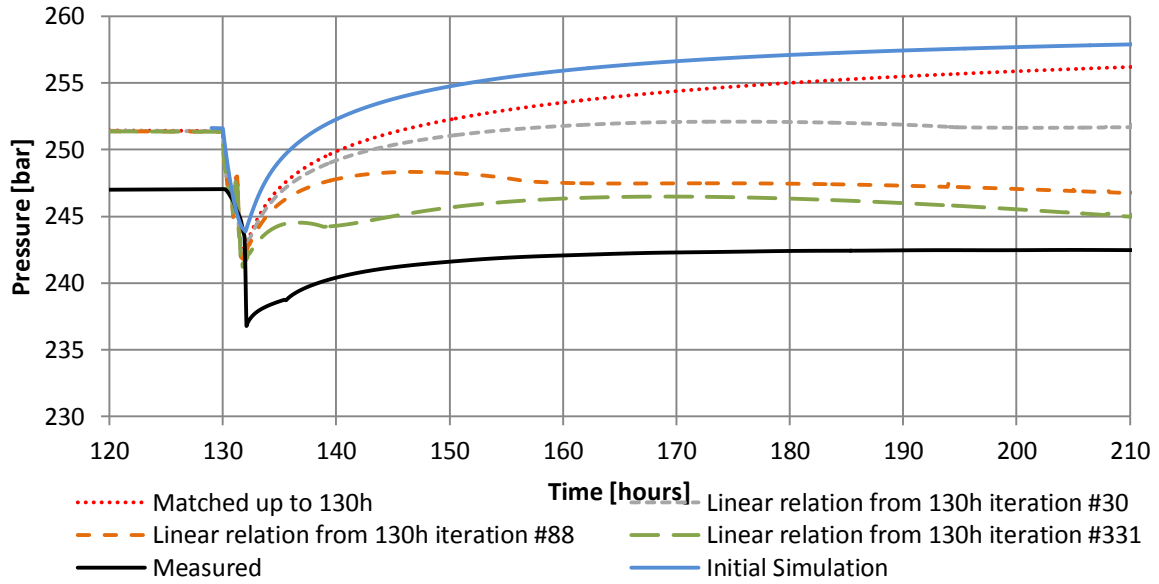


Figure 4-41 Gauge Pressure History Matching

Gauge Temperature RMO

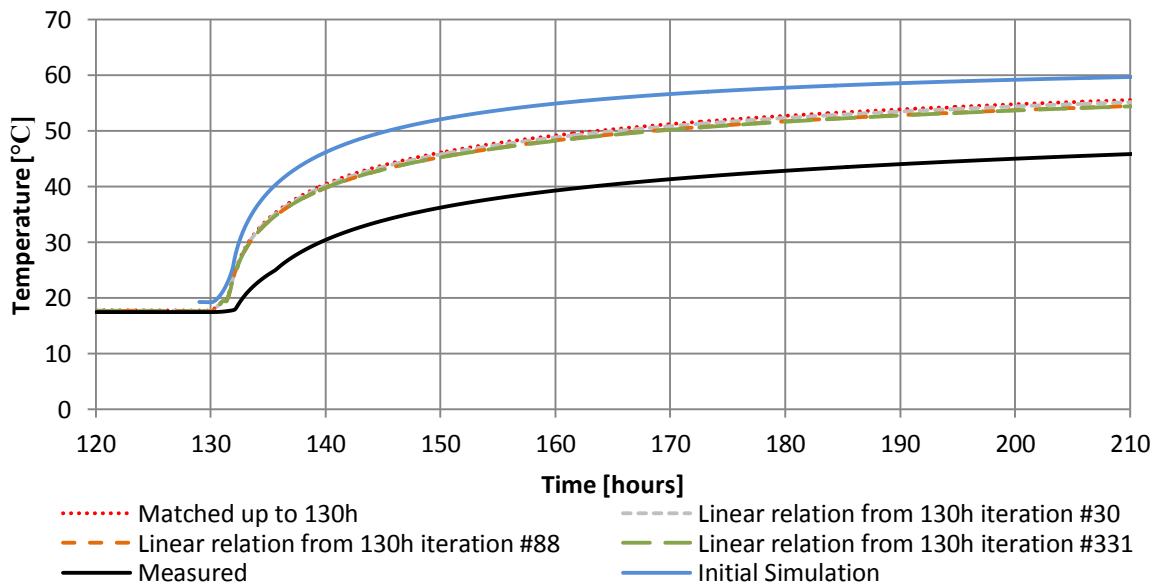


Figure 4-42 Gauge Temperature History Matching

It might seem like the simulated gauge pressure is approaching the measured values, but as mentioned it was only specified to match the wellhead pressure.

The resulting parameter values from the two iteration cycles are presented in Table 4-1. In hindsight it seems reasonable that the values for the initial conditions should have been excluded from the second iteration cycle. However, as it can be seen they are not changing much, and will likely have a minor impact on the final result, as a relatively long initialization time was specified. The ambient conditions are also not likely to change much during the shut-in, and should probably not have been included in both iterations either. However, it would probably make more sense to include it in the second iteration cycle than the first, as the temperature is set constant prior to the shut-in. The largest change was observed for the A coefficients of the inflow and outflow equations and in the reservoir pressure. It seems likely that the decreasing reservoir pressure explains the decreasing pressure experienced at both the wellhead and the gauge, and that the reduction might be a little bit exaggerated. The large increase in the production coefficient might also explain the changes experienced in the pressure. As stated in the OPGA manual (SPTgroup, 2012b), it should be less than zero if a minimum pressure difference is required for fluid flow from reservoir into the well. As it seems to be estimated rather high, the pressure difference may be substantial, and might explain the sudden increase in pressure once fluid starts to flow. To get the most out of the RMO module it is clearly beneficial to be well aware of what to expect from the result, which parameters to use as input, and how/if they are likely to change.

Parameter	1st Iteration	2nd Iteration
AINJ	-0.297	-2.568
APROD	0.00	-15.903
BINJ	5.433e-06	5.906e-06
BPROD	5.378e-06	5.224e-06
HMININNERWALL	45.467	52.951
INPRESSURE	113.309	112.331
INTAMBIENT	4.005	3.913
INTEMPERATURE	3.179	3.807
OUTPRESSURE	326.310	327.362
OUTAMBIENT	101.935	98.783
OUTTEMPERATURE	101.873	99.716
RESERVOIR PRESSURE	320.023	308.308
RESERVOIR TEMPERATURE	98.455	100.637

Table 4-1 Parameter values after 1st and 2nd iteration cycle

4.3 IN SALAH

The results from the In Salah simulations are presented in this section. As for the previous cases it was not considered necessary to include the base case simulations in separate diagrams, as these are included as the initial state in most of the diagrams. The model has not been verified against experimental data, but has been tuned to give reasonably accordance with the set boundary conditions. Due to license limitations, the CO₂ VIP module was not available during the simulations. Consequently, all the simulations were performed with the standard single component module (PT-flash module). All the presented models were specified as indicated in section 3.4.2 and 3.4.3. As only one of the injection wells were modeled, the injection rate is relatively low compared to Sleipner and Snøhvit.

4.3.1 SHUT-IN SINGLE COMPONENT MODULE CO₂

The figures of the In Salah Shut-in has been plotted for constant injection (after 30 hours), and at 32, 150 and 1500 hours. Figure 4-43 presents the pressure profile of the well at these instants. Here it can be seen that there is an initial pressure drop in the well, which at first sight seems to be more or less like a vertical shift of the constant injection curve. Then, as time increase, the pressure seems to stabilize around the initial wellhead pressure.

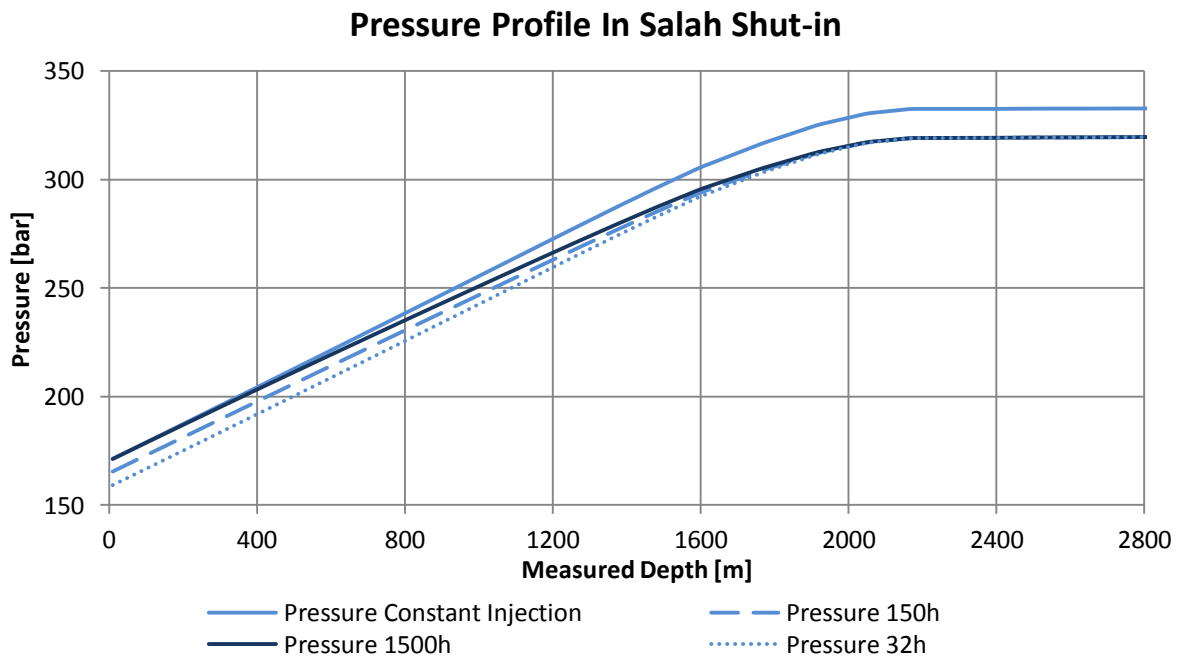


Figure 4-43 Pressure Profile In Salah Shut-in

The horizontal orientation of the In Salah well can be seen as the more or less horizontal part of the pressure curves at the end of the well. Although the initial and final wellhead pressures are approximately the same, the conditions can be seen to change along the well. At the bottomhole, the 32, 150 and 1500

hour lines merge and seem to stabilize at approximately 13 bar below the constant injection pressure in this section.

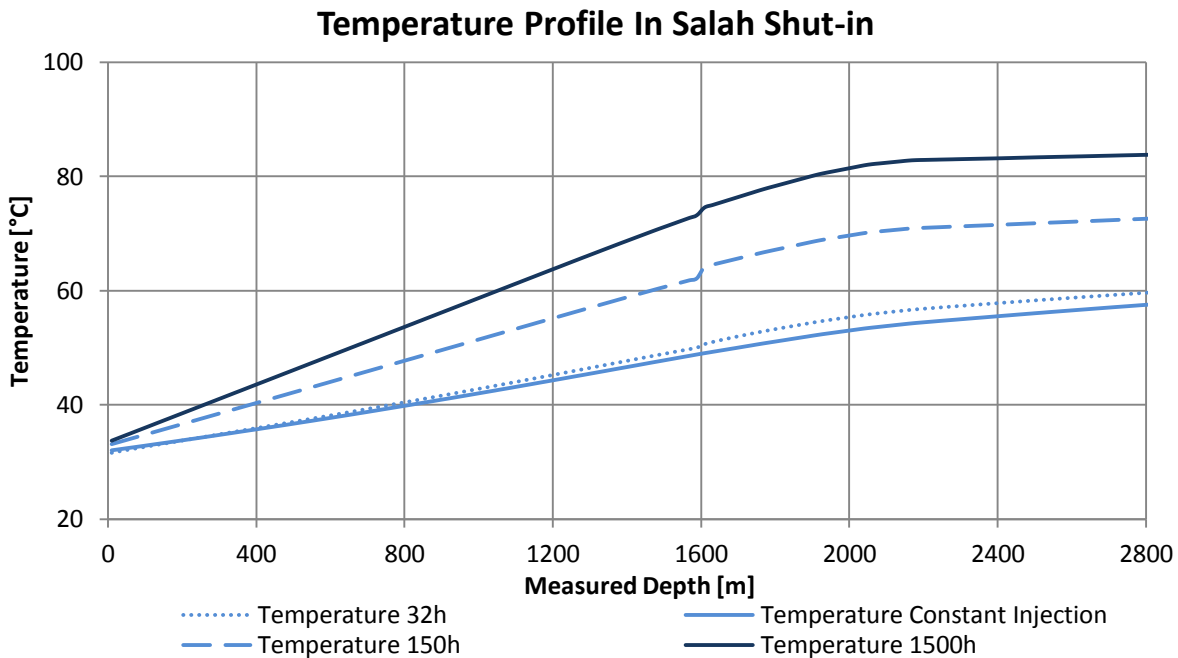


Figure 4-44 Temperature Profile In Salah Shut-in

Furthermore, the temperature profile shows a slight increase in temperature at the wellhead. This is pretty much like expected, as the injected CO₂ was specified two degrees below the ambient temperature. A small decrease in temperature can be seen after 32 hours and follows from the reduction in pressure. The increasing temperature difference down the well, indicates that the injected CO₂ does not approach the ambient temperature before reaching the reservoir. Thus, the temperature rises once the shut-in is complete. At 1600m MD an instant change in temperature is observed, which is explained by reduction of the inner tubing diameter, and the subsequent reduction in heat transfer caused by the reduction of the surface area. As the last section is more or less horizontal, the ambient temperature remains more or less unchanged in this section, which explains why the temperature curves flatten out, especially as time is increased. From Appendix C-2, which shows the mass flow at the instant the choking is completed, it can be seen that there is still a positive flow towards the reservoir. When considering the quantity however, it is not expected to affect the conditions in the well significantly. As the specified wellhead pressure is well above the critical pressure, two phase flow was not expected to occur in the well, which also seems to be confirmed by Appendix C-3. Thus, it is expected that the pressure profile should be closely linked to the density profile (Figure 4-45). After 32h, the density is reduced, but still relatively parallel to the density at constant injection. This is a direct consequence of the pressure reduction which follows the shut-in. On the other hand, as heat transfer is a more gradual process than changes in pressure, the temperature related density changes get more evident as time increases. This can also be seen from the density plot, as the density decreases with the change in temperature over time.

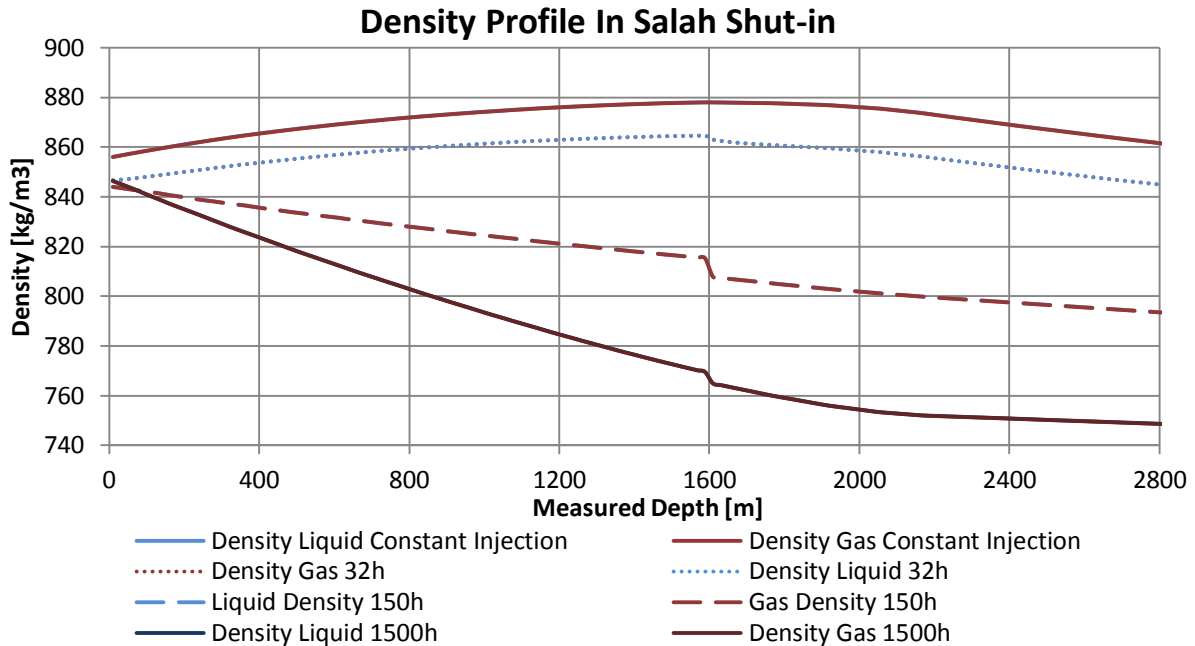


Figure 4-45 Density Profile In Salah Shut-in (Liquid and gas densities are equal)

From the PH and PT diagrams (Figure 4-46 and Figure 4-47), it can be seen that the well remains in the supercritical region throughout the shut-in. It can also be seen that the initial temperature of the inflow zone, is about 35°C below the reservoir temperature, but approaches the reservoir conditions with time. It was noticed however, that the approach seems to be remarkable slower than the previously simulated shut-ins. One possible explanation is that the model was specified with only one perforation. Both the Sleipner and Snøhvit model had several perforations on the other hand, and in these models, constant reservoir properties were assumed. This turned out to induce a flow that would not have been there otherwise. If warm CO₂ from the reservoir flows back into the well, it might just happen that this caused the conditions of the inflow zone to approach the ambient conditions faster. However, as the flow is limited to the perforations (and by magnitude), it should not necessarily affect the conditions excessively in the rest of the well. Another likely explanation might be the long horizontal section of the well, as it in this section, only will be minor changes in the ambient conditions (when considering the geothermal gradient). There is also a relatively large temperature difference between the fluid during constant injection and after 1500h. This might indicate that the wall and surrounding formation has experienced significant cooling during the injection, which needs to be reheated for the fluid to approach ambient conditions. In general, the fluid properties and the corresponding heat transfer will vary according to the conditions of the respective wells.

The PH diagram also gives a good presentation of the wellhead conditions, as it includes both the pressure and temperature changes. Consequently, it can be seen how the pressure drops as the inflow is choked, and how it increases again as the temperature increases. Although a clear definition of the near critical region is missing, it seems unlikely that this should affect the result considerably in this case. This was also indicated during the simulations, as no significant trouble was encountered.

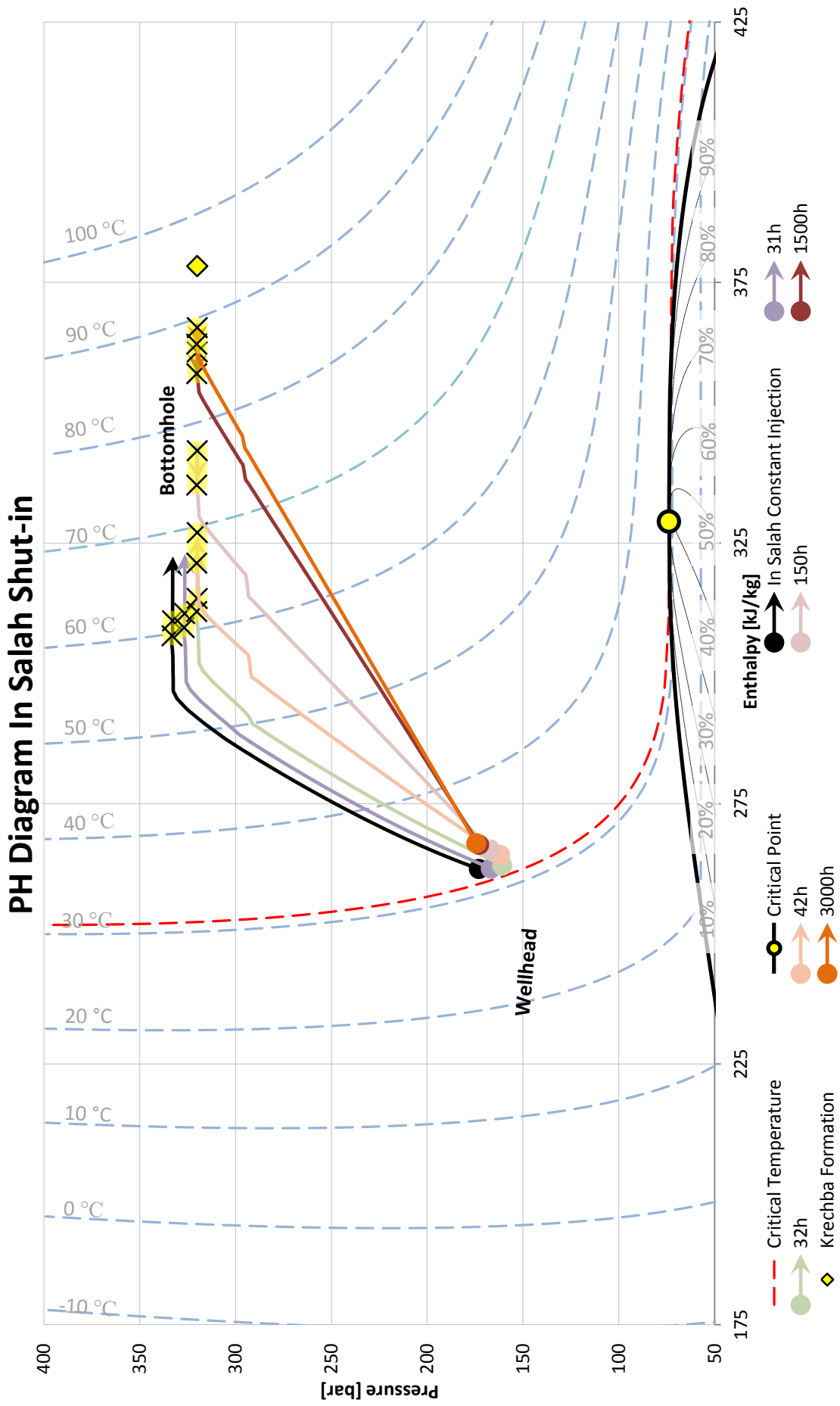


Figure 4-46 PH Diagram In Salah Shut-in

PT Diagram Snøhvit Shut-in

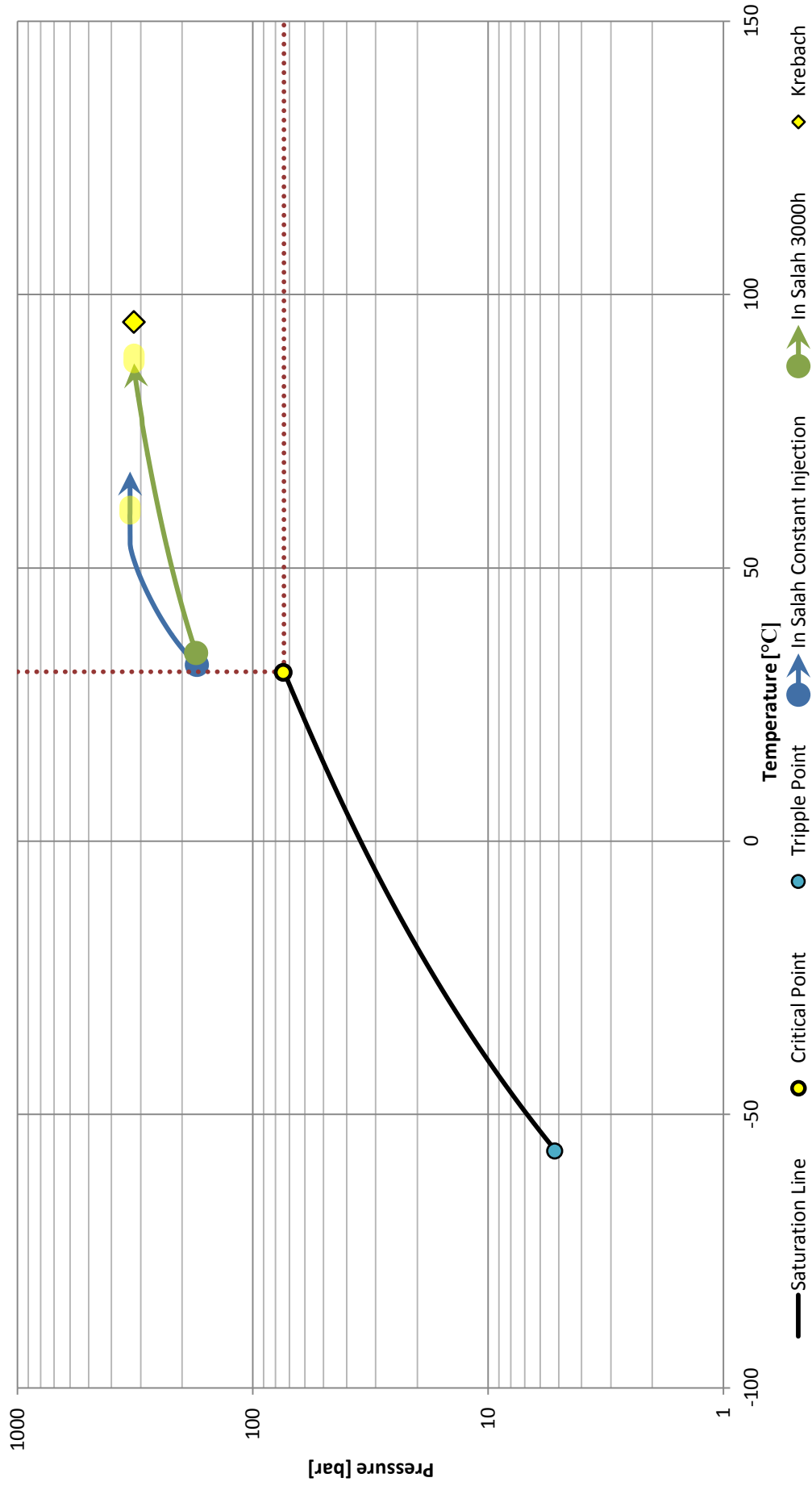


Figure 4-47 PT Diagram Snøhvit Shut-in

4.3.2 BLOWOUT CO₂ WITH RESERVOIR BACKFLOW

Measured in simulation time, this was by far the most time consuming simulation. There is however no reason to believe that this was caused by how the model was specified as it seems to be caused solely by numerical issues encountered by the simulation engine. The simulation terminated after 526h (simulation time), but for the purpose of this study it was considered sufficient. The pressure profile is presented in Figure 4-48 and gives the results for the final and initial state, as well as after 1 and 15 minutes after the valve opens (29.0167 and 29.25 hours).

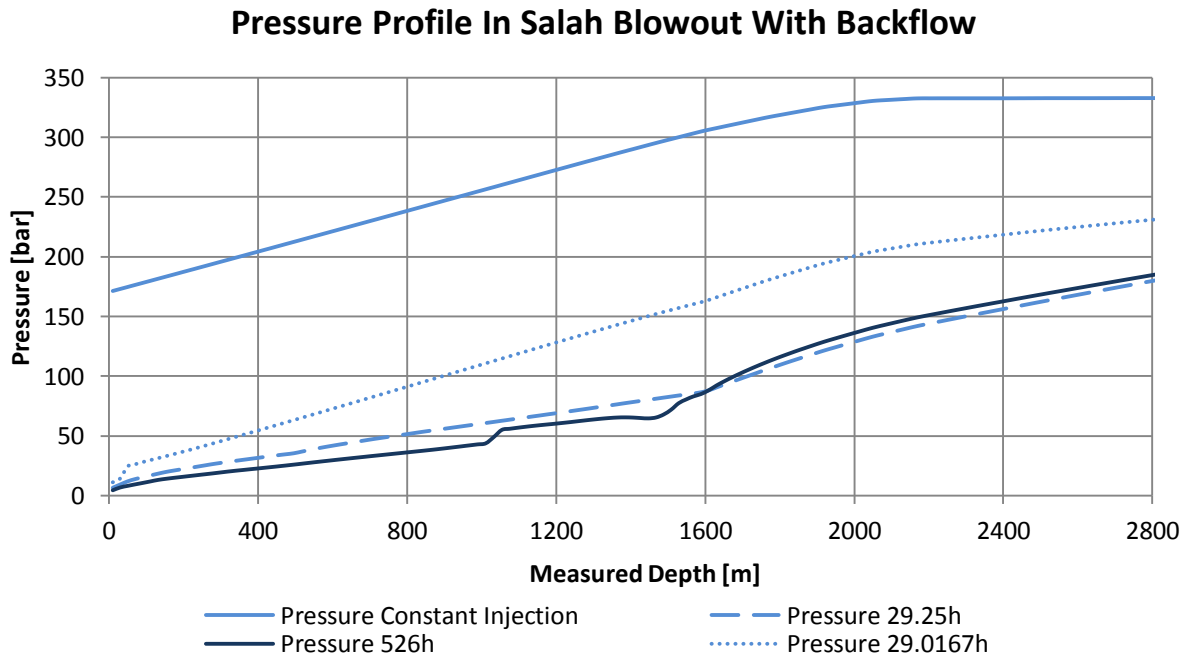


Figure 4-48 Pressure Profile In Salah Blowout With Backflow

Around 1200m MD something strange seems to happen after 526h. This is expected to be caused numerical instability near the critical region. The pressure is still about 8 bar below the critical pressure, but the fluid properties are known to change abruptly throughout the near critical region. To investigate this suspicion, the temperature at 1200m (Figure 4-49) was used to plot isothermal properties from the NIST database. The resulting density plot can be seen in Figure 4-50 and seems to a large extent to explain the increasing pressure seen in the pressure plot.

The PH and PT diagram of the blowout are presented in Figure 4-51 and Figure 4-52 and show, as expected, that the operational range of the well is close to, or in, the near critical region for a large part of the simulation. This seems to persist from about 5 minutes after the valve opens (29.0833h) and throughout. The low pressure and temperature experienced at the wellhead also leads the solution close to the solid formation line. Although this is not explicitly captured by the selected plots, it seems likely that the solution might fall below the triple point in the upper part of the well. As for the similar Sleipner simulation, the enthalpy difference between the OLGA results and the NIST values showed a significant

Temperature Profile In Salah Blowout With Backflow

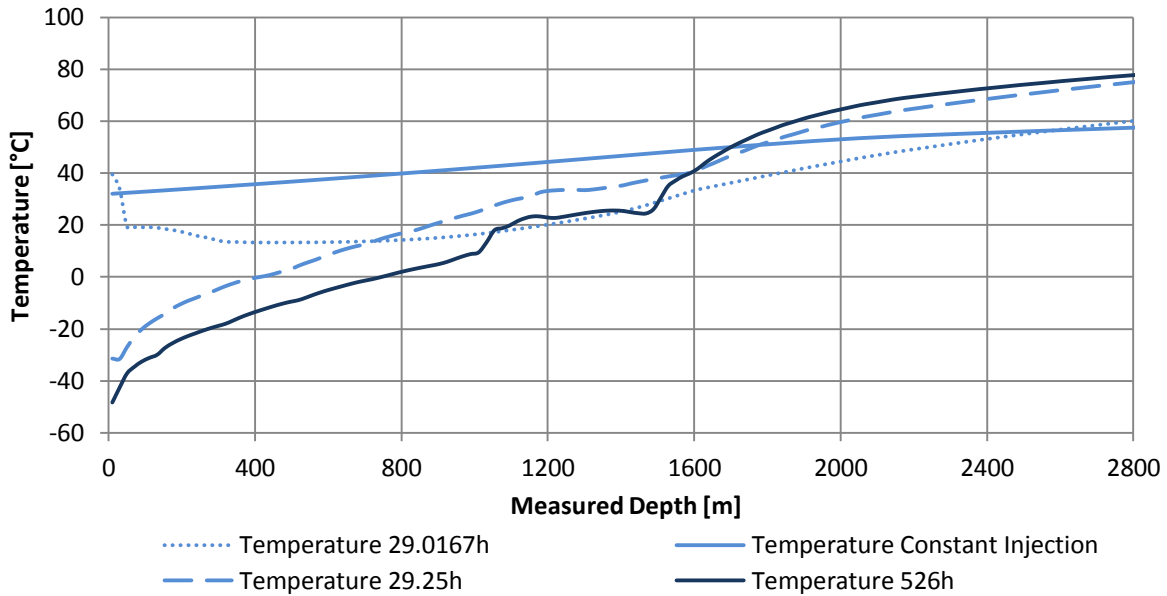


Figure 4-49 Temperature Profile In Salah Blowout With Backflow

discrepancy compared to the difference from the steady state solutions. It seems likely that this might be a direct consequence of operation outside the validity range of OLGA. In general, it may seem like the In Salah blowout combines the problems encountered with both the Sleipner and Snøhvit blowout (ref. section 4.1.3 and 4.2.2). But then again, the initial state lies between Sleipner and Snøhvit, on the opposite side of the critical point from Sleipner. Again it is not possible to estimate the accuracy of the results, but due to the previously discussed problems it would not be surprising if the accuracy is the lowest of all the cases. A maximum discharge rate of 111 kg/s was encountered at the wellhead and seemed to settle at approximately 49 kg/s after about 13 minutes (Appendix C-14).

Isothermal Density at 23°C

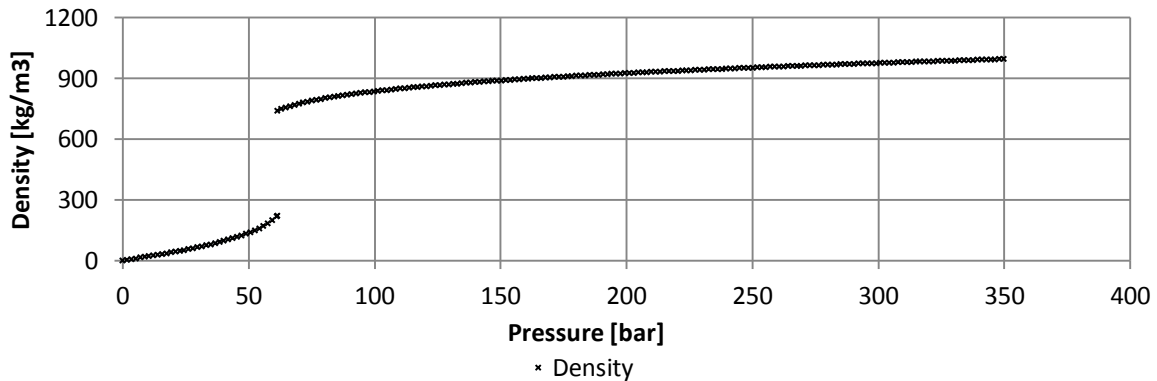


Figure 4-50 Isothermal Density at 23°C

PH Diagram In Salah Blowout with Backflow

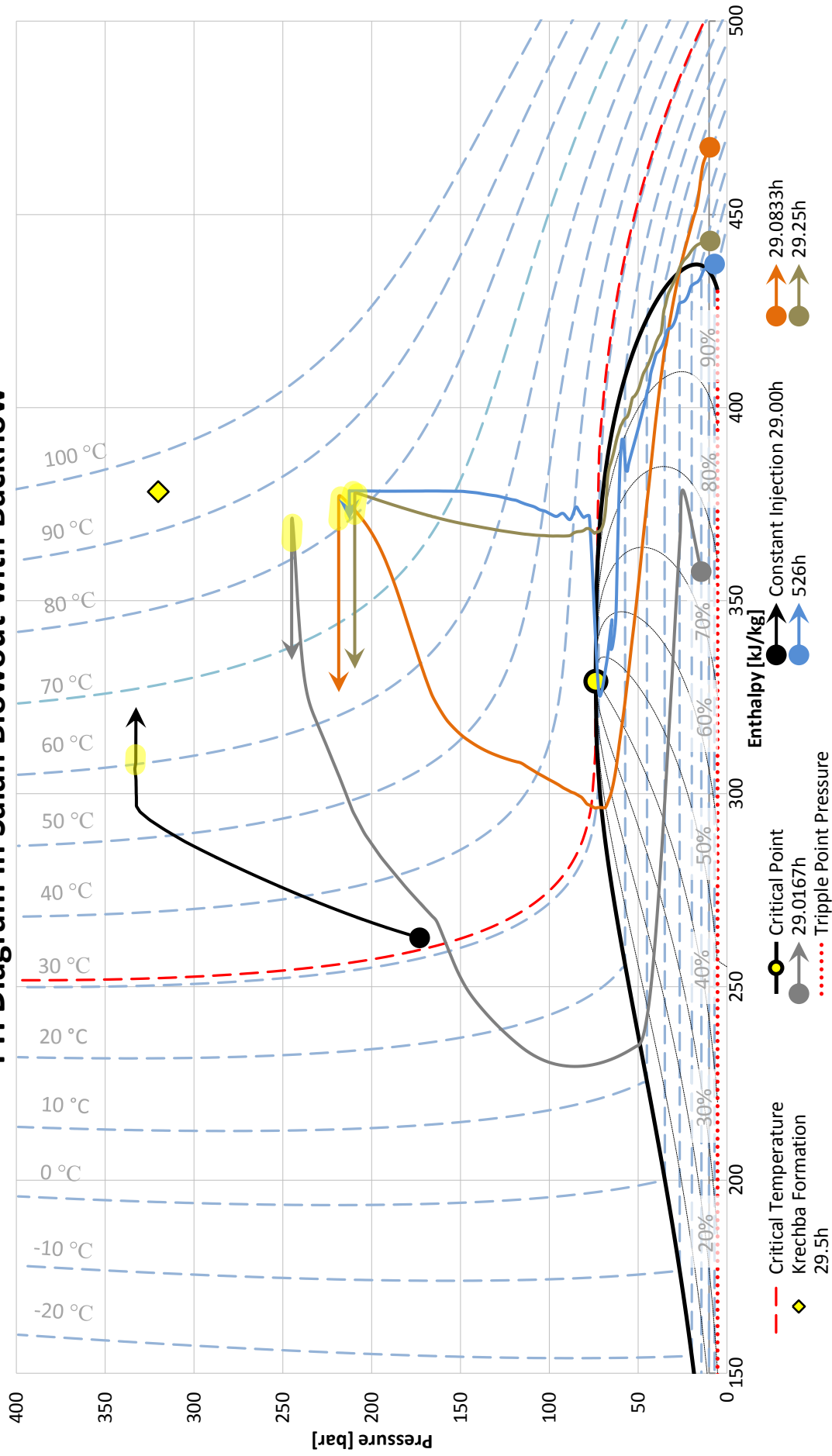


Figure 4-51 PH Diagram In Salah Blowout with Backflow

PT Diagram In Salah Blowout with Backflow

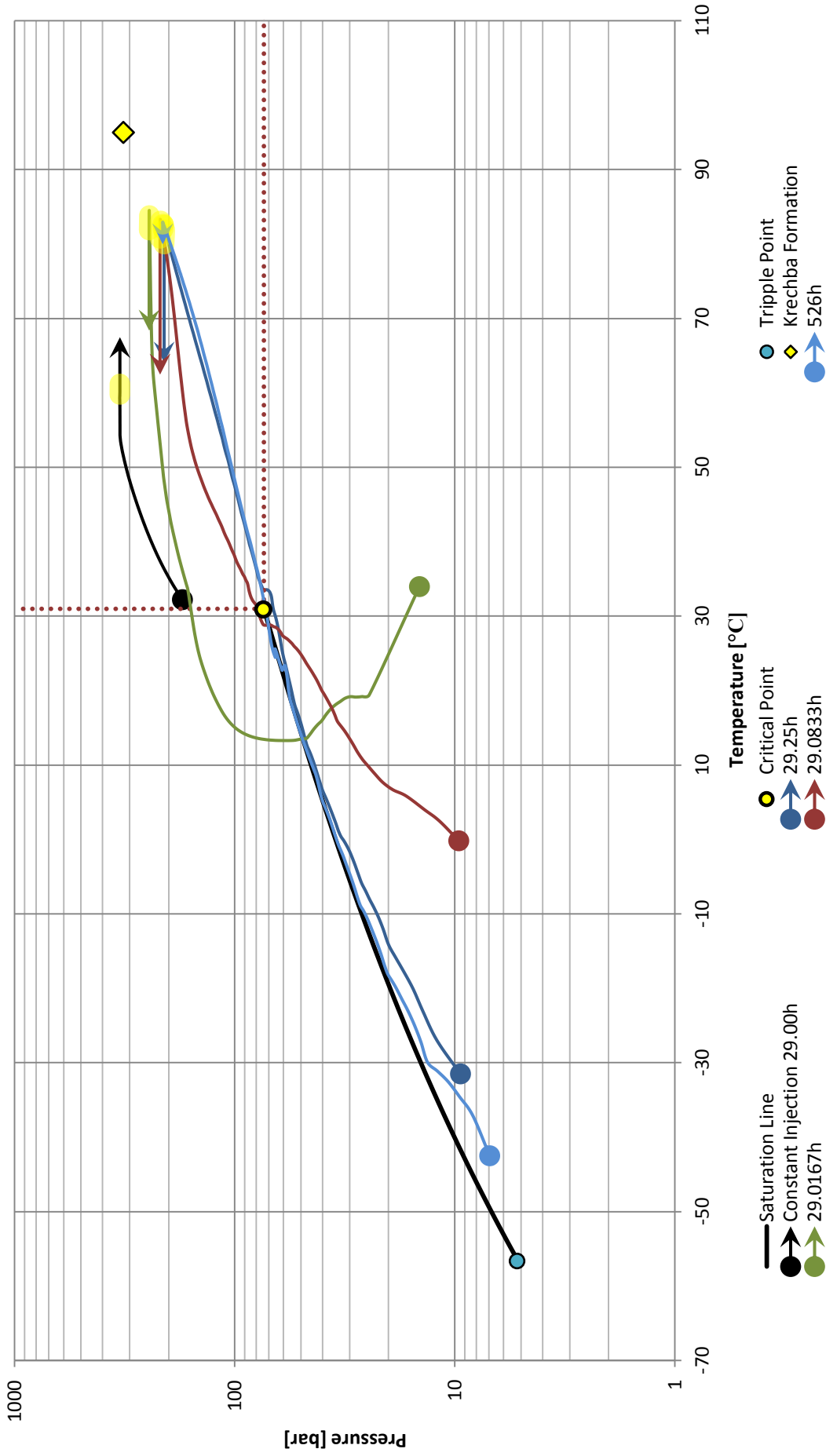


Figure 4-52 PT Diagram In Salah Blowout with Backflow

4.3.3 BLOWOUT CO₂ WITHOUT RESERVOIR BACKFLOW

The blowout simulation without reservoir backflow, was run with a minimum time step of 0.1s and the default time constant for mass transfer. Compared to the blowout simulation with reservoir backflow, the actual simulation seemed to run significantly more efficient. Even so, it can be seen from Figure 4-54, that numerical instabilities were experienced towards the end of the wellbore. At this point it can be seen that both the pressure and temperature at both sides of the pressure and temperature wave do not enclose the critical point. Closer examination of the profile plot in OLOGA, showed that the instabilities occur approximately 9.5 minutes after the valve opens, at approximately 1500m MD. Pressure and temperature were extracted at this point and is presented in a separate diagram in Figure 4-53. In this figure the pressure and temperature fronts have been outlined along with the critical properties. As the diagram shows, both the critical pressure and temperature lies within the shaded areas. Accordingly, it seems highly likely that the near critical region is causing the instabilities, and it would be very interesting to run the simulation with the CO₂ VIP module. As the pressure decreases further, the instabilities vanish.

The PH and PT diagrams (Figure 4-56 and Figure 4-57) show that the depressurization is more or less complete after 20 min. The whole well is then in the superheated region, but has not come to equilibrium with the specified ambient conditions yet. It can also be seen that the PT diagram indicates that the conditions after five minutes are below the triple point. This was not initially noticed from the PH diagram as the wrongly estimated enthalpy difference shifted the wellhead conditions into the superheated region. The enthalpy difference was therefore adjusted to 507 kJ/kg, as all stable simulations seem to approach this value. Under these conditions, the maximum calculated discharge rate of approximately 212 kg/s was encountered at the wellhead (Appendix C-22). Additional figures are included in appendix C-III.

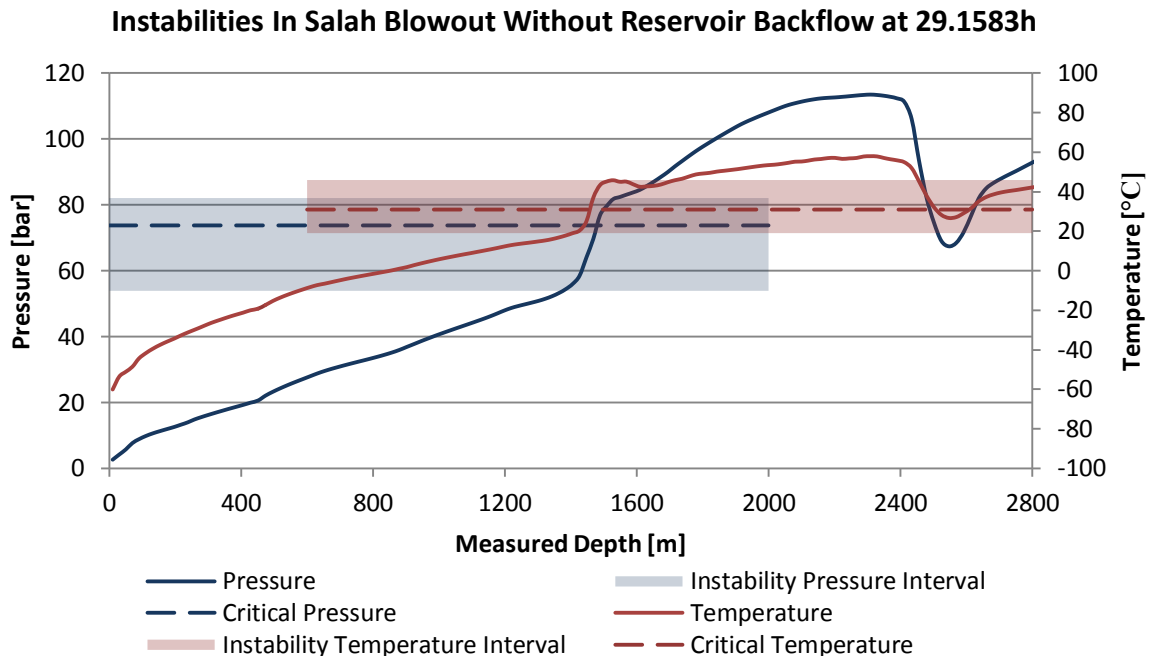


Figure 4-53 Start of Instability In Salah Blowout Without Reservoir Backflow at 29.1583h

Pressure Profile In Salah Blowout Without Reservoir Backflow

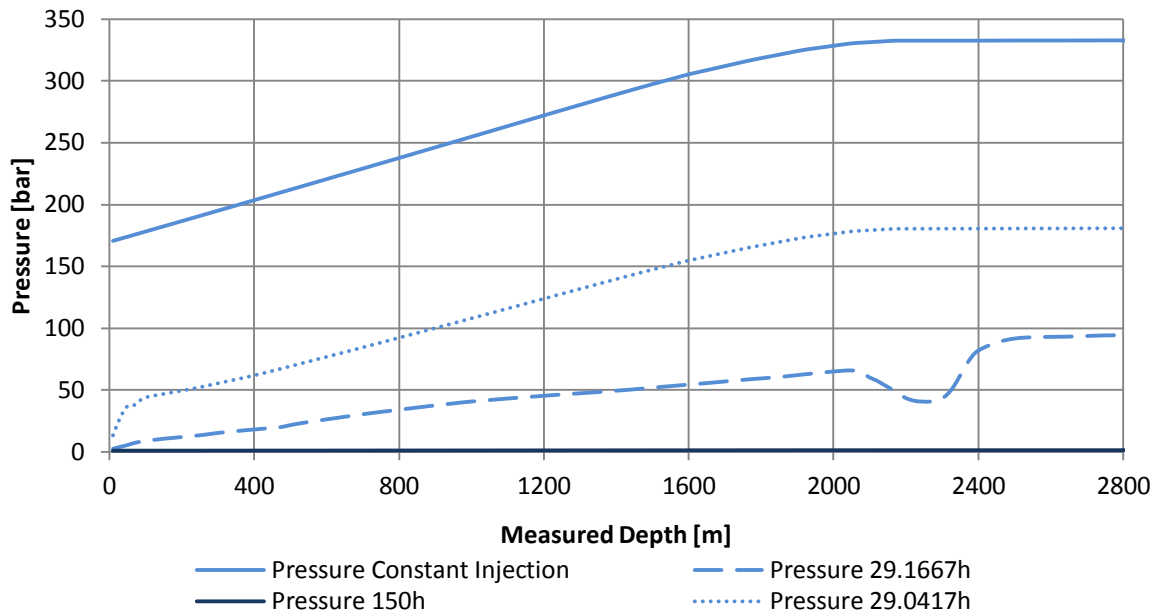


Figure 4-54 Pressure Profile In Salah Blowout Without Reservoir Backflow

Temperature Profile In Salah Blowout Without Reservoir Backflow

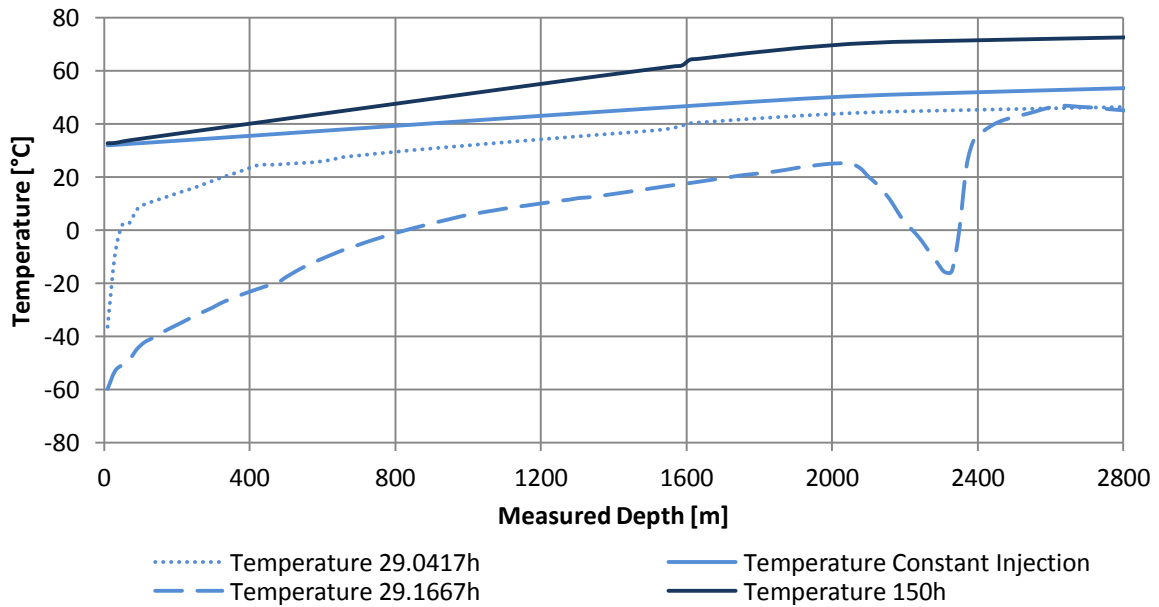


Figure 4-55 Temperature Profile In Salah Blowout Without Reservoir Backflow

PH Diagram In Salah Blowout NO Backflow

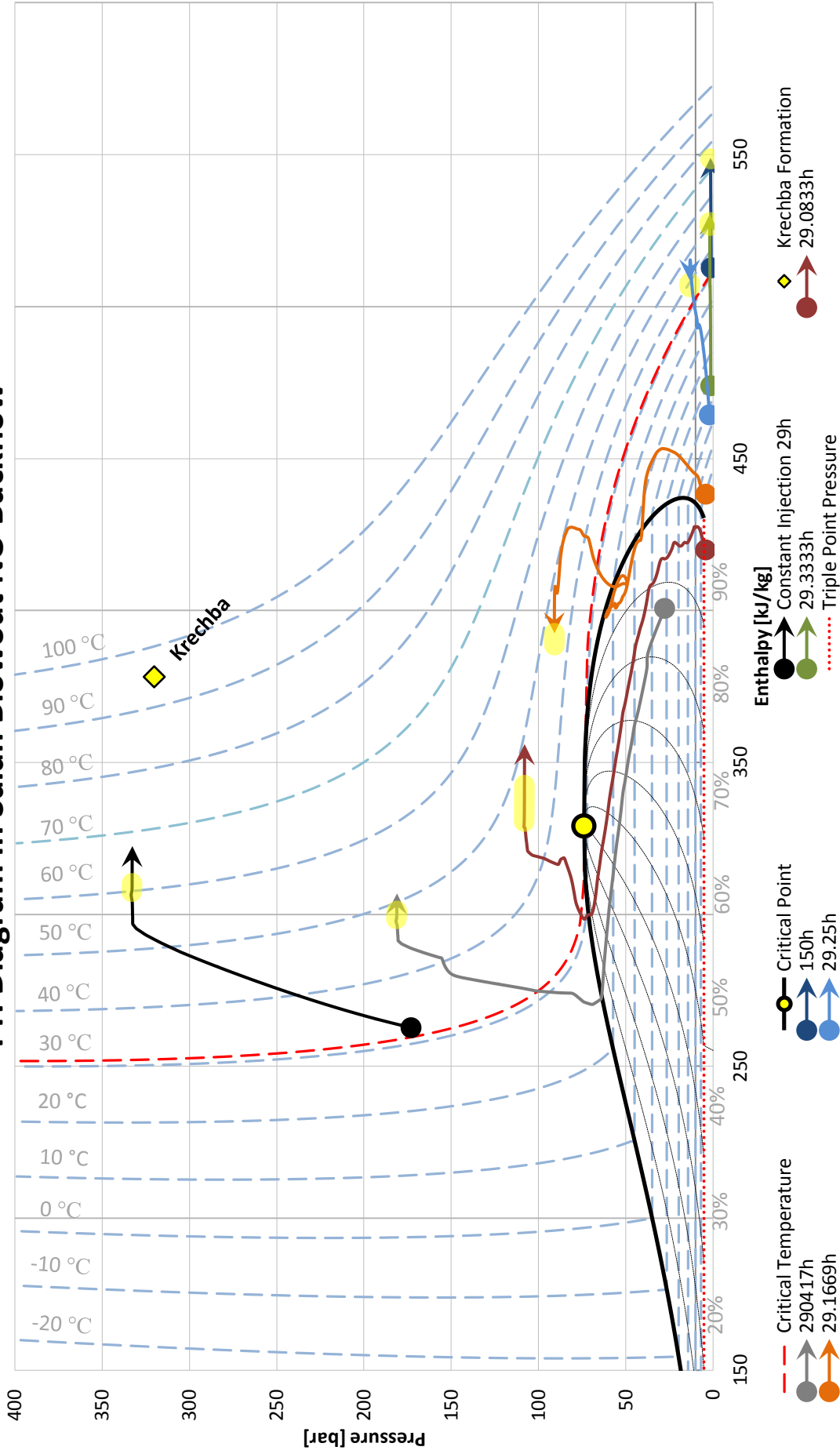


Figure 4-56 PH Diagram In Salah Blowout NO Backflow

PT Diagram In Salah Blowout NO Backflow

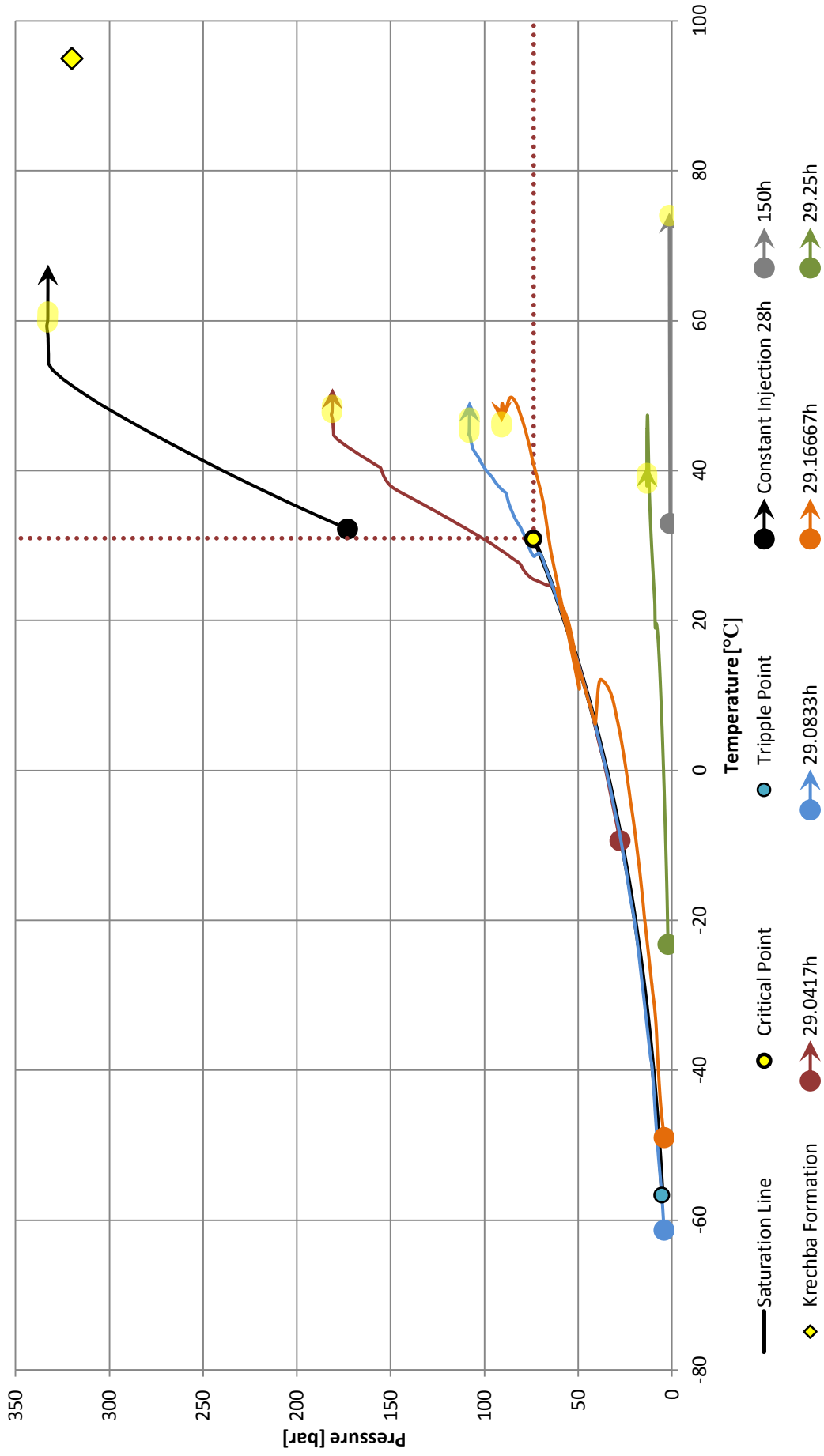


Figure 4-57 PT Diagram In Salah Blowout NO Backflow

4.4 KETZIN

The results from the Ketzin simulations are presented in this section. As for the previous cases it was not considered necessary to include the base case simulations in separate diagrams, as these are included as the initial state in most of the diagrams. The model has not been verified against experimental data, but has been tuned to give reasonably accordance with the set boundary conditions. Due to license limitations, the CO₂ VIP module was not available during the simulations. Consequently, all the simulations were performed with the standard single component module (PT-flash module). All the presented models were specified as indicated in section 3.5.2 and 3.5.3. As Ketzin is a research well, it is considerable smaller than the previously discussed industrial sized projects, especially in terms of the injected mass, but also in extent. Also, as the Ketzin well is a vertical well, the pipeline length or measured depth is equal to the vertical depth. This may in some cases make the analysis more logical, as the results are not complicated further by the geometry of the well.

4.4.1 SHUT-IN SINGLE COMPONENT MODULE CO₂

The shut-in profile plots have been plotted for constant injection and at 32, 42 and 3000 hours. The pressure and temperature profiles are presented in Figure 4-58 and Figure 4-59 and the remaining plots can be seen in appendix D-I. The pressure profile shows a relatively linear curve throughout the well at constant injection. Experience from previous simulations, suggest that no phase change occur in the well. The specified wellhead conditions also indicate that the well is in the superheated region. Consequently, it was expected that less trouble should be encountered during the transient simulations. As the pressure remains below the critical pressure throughout the well, it seems highly unlikely that any of the scenarios should approach the near critical region. However, depending on how much the temperature decreases, the solutions might enter the two-phase region.

After 32 hours, the pressure curve is roughly shifted vertically about 4 bar. After 3000 hours however, a change in inclination can be seen at approximately 300m MD. The same can also be seen from the temperature plot. The temperature plot also shows that the temperature is further reduced after the initial temperature drop related to the drop in pressure. This is reasonable, as the ambient temperature at the wellhead was specified lower than the temperature of the injected CO₂. The changes in temperature around 600m MD is caused by the inflow zone. At the end of the well there is little or no flow and the temperature approaches the ambient temperature.

Pressure Profile Ketzin Shut-in

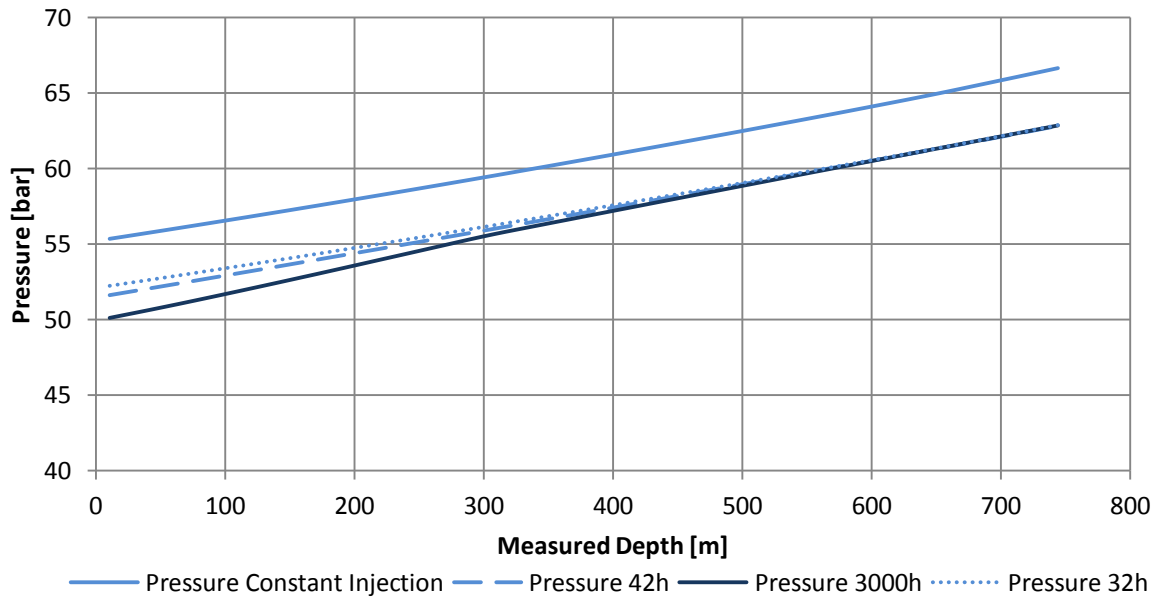


Figure 4-58 Pressure Profile Ketzin Shut-in

Temperature Profile Ketzin Shut-in

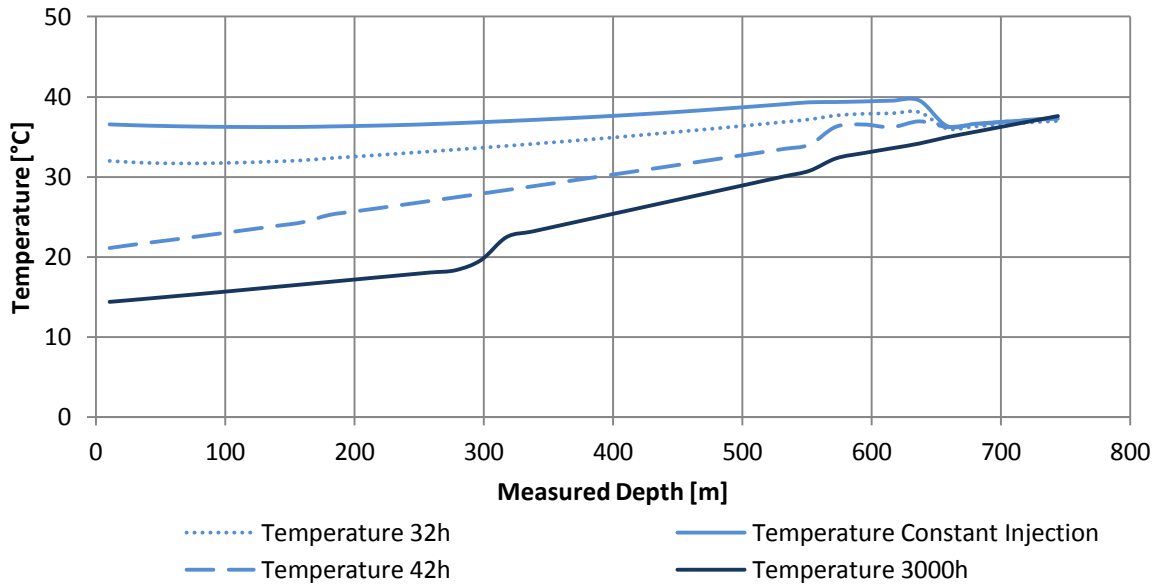


Figure 4-59 Temperature Profile Ketzin Shut-in

From the PH diagram (Figure 4-60) it can be seen that the pressure conditions in the bottom of the well is more or less settled after 32h. After this it is mainly heat transfer with the ambient is the dominating effect, and it can be seen how the temperature of the inflow zone approaches the reservoir temperature as time increases. After 150h however, the upper part of the well slightly enters the two-phase region. As illustrated by Appendix D-2, condensation occurs in the first 300m of the well (after 3000h), but the extent of the condensation is very limited. However, even after 3000h, it can be seen from the temperature plot that the fluid temperature at the wellhead still is about 15°C, which is approximately 5°C above the specified ambient temperature. It might thus seem like the condensing fluid prevents the well from achieving full equilibrium with the surroundings. The saturation line is met at approximately 18°C, thus it seems likely that the well might be subject to seasonal variations during prolonged shut-ins.

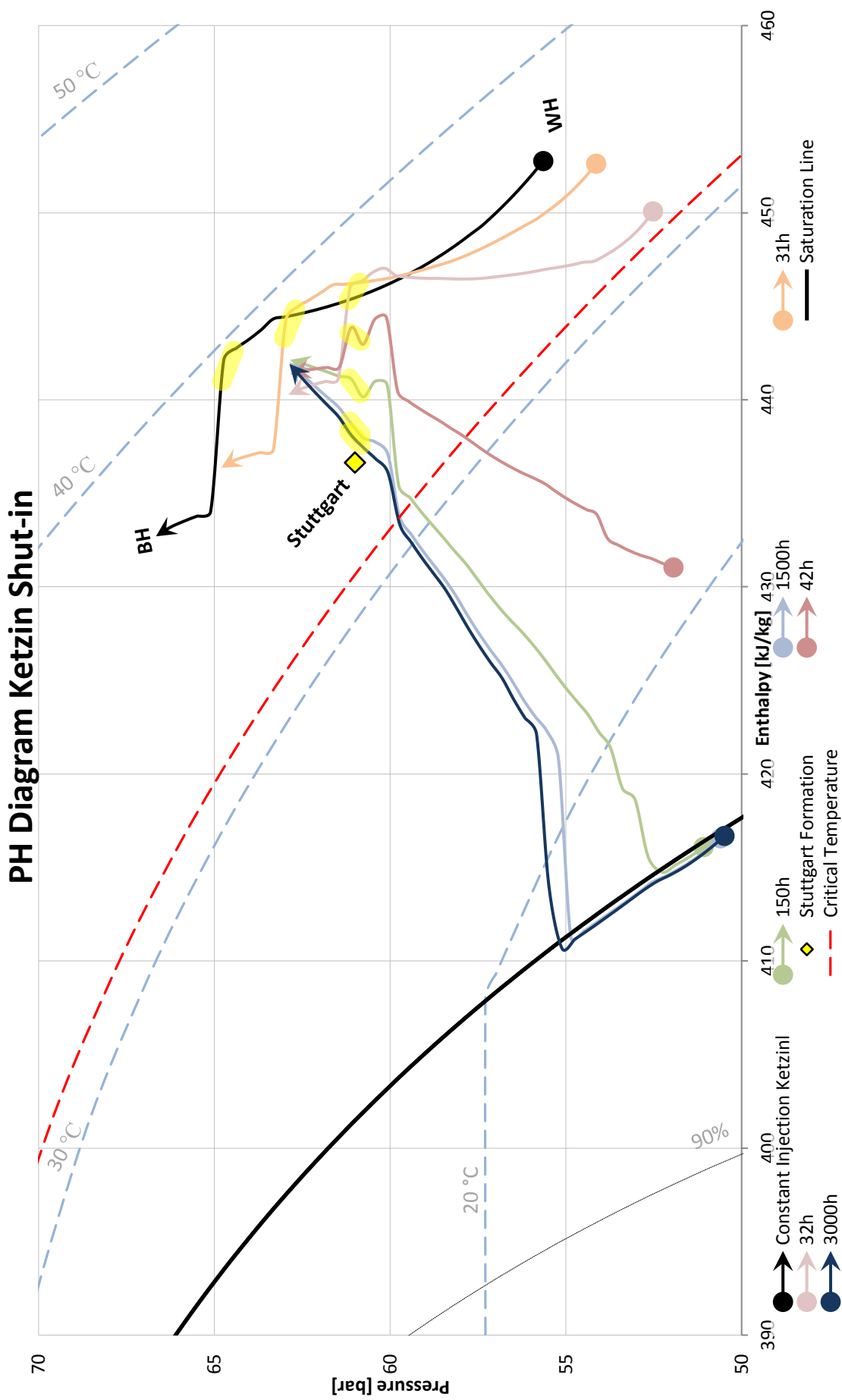


Figure 4-60 PH Diagram Ketzin Shut-in

PT Diagram Ketzin Shut-in

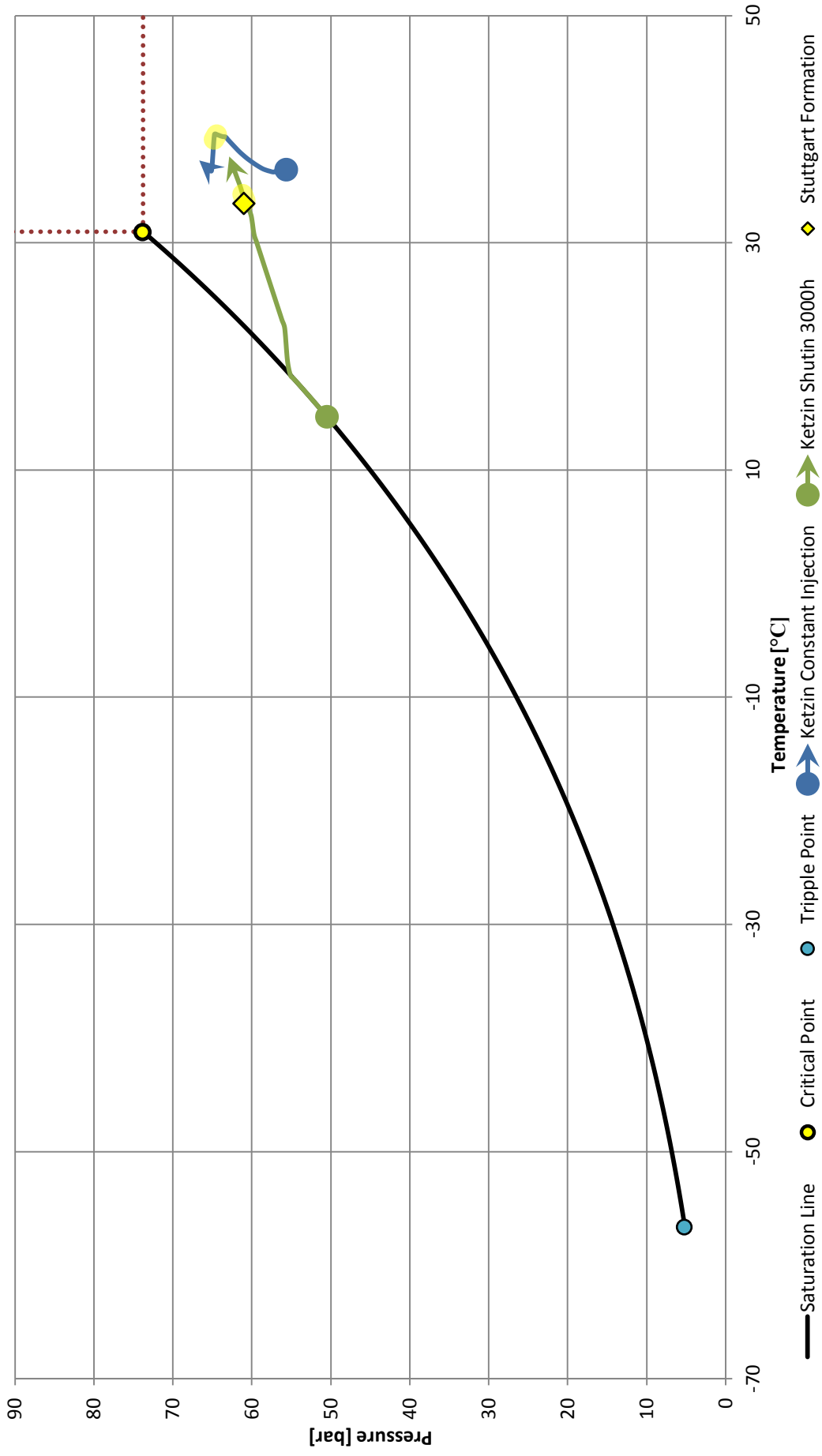


Figure 4-61 PT Diagram Ketzin Shut-in

4.4.2 BLOWOUT CO₂ WITH RESERVOIR BACKFLOW

Compared to the previously discussed blowout cases (with reservoir backflow), the Ketzin blowout did not encounter any problems of significance. Most likely this is caused by the initial state of the well, which is solely in the superheated region. The pressure and temperature plot from the Ketzin blowout with reservoir backflow are presented in Figure 4-62 and Figure 4-63. Additional profile and trend plots have been included in Appendix D-II. As the pressure profile shows, the result is not as linear as for the shut-in. This seems to be caused by increased variations in fluid properties, as the conditions vary to a larger extent along the well. It can also be seen that the well seems to stabilize relatively quickly in terms of pressure, as the pressure curve after 10 minutes (29.1708h) is approximately equal to the pressure curve at 1500 hours. At this point the bottomhole pressure is about 30 bar. The temperature on the other hand is still changing after 10 minutes. This is also clearly expressed in the PH diagram (Figure 4-64), as both the wellhead and bottomhole pressure remains approximately at the same level from this point and throughout the simulation. As CO₂ is flowing out of the reservoir, at reservoir conditions, the inflow zone remains relatively stable at the reservoir temperature, while the rest of the well experiences cooling from the expanding fluid. The well also seems to approach a steady solution after 1500h. As already mentioned, the simulation did not encounter any problems of significance. This seems reasonable when looking at the PH and PT diagrams, as the solution remains in the superheated region throughout the simulation. As the reservoir outflow is strictly dependent on the bottomhole pressure, it is also sensitive to phase changes and correct prediction of the phase transitions. Although the Sleipner, Snøhvit and In Salah simulations (section 4.1.4, 4.2.2 and 4.3.2) experienced operation in both the near critical region and below the triple point, it seems likely that two-phase operation in general might complicate the simulation further. This seems particularly relevant in these cases with reservoir backflow, as a stable bottomhole pressure is the very foundation of a steady solution. Under these circumstances, the maximum calculated discharge rate was approximately 7.5 kg/s and seems to stabilize at approximately 5 kg/s after about 7 minutes.

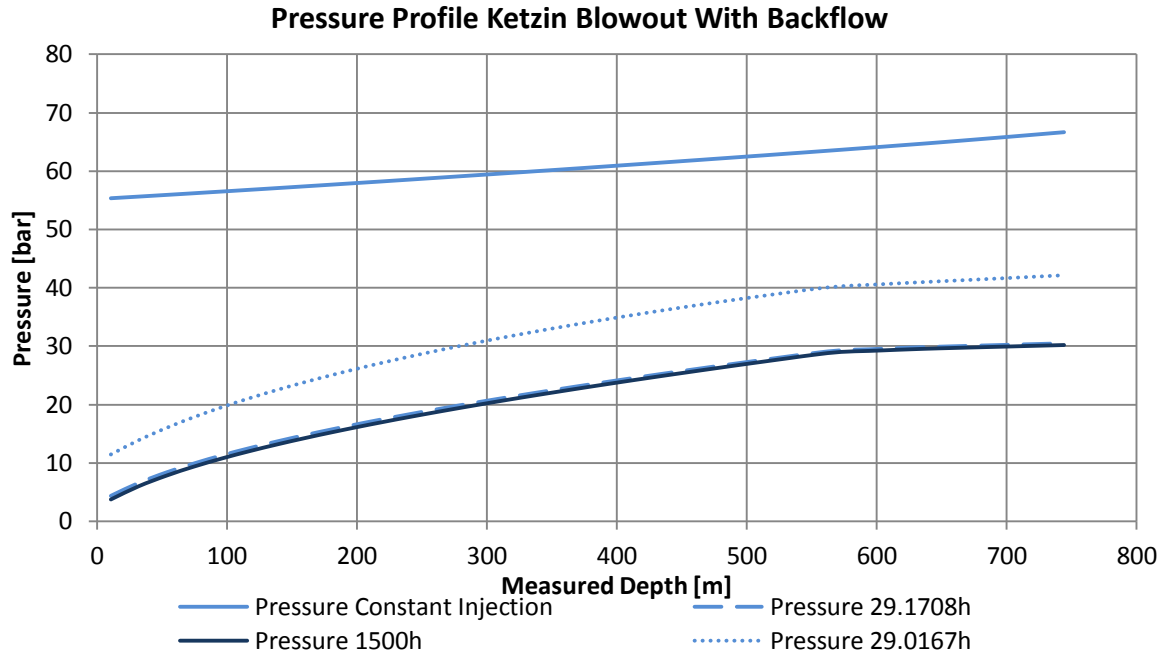


Figure 4-62 Pressure Profile Ketzin Blowout With Backflow

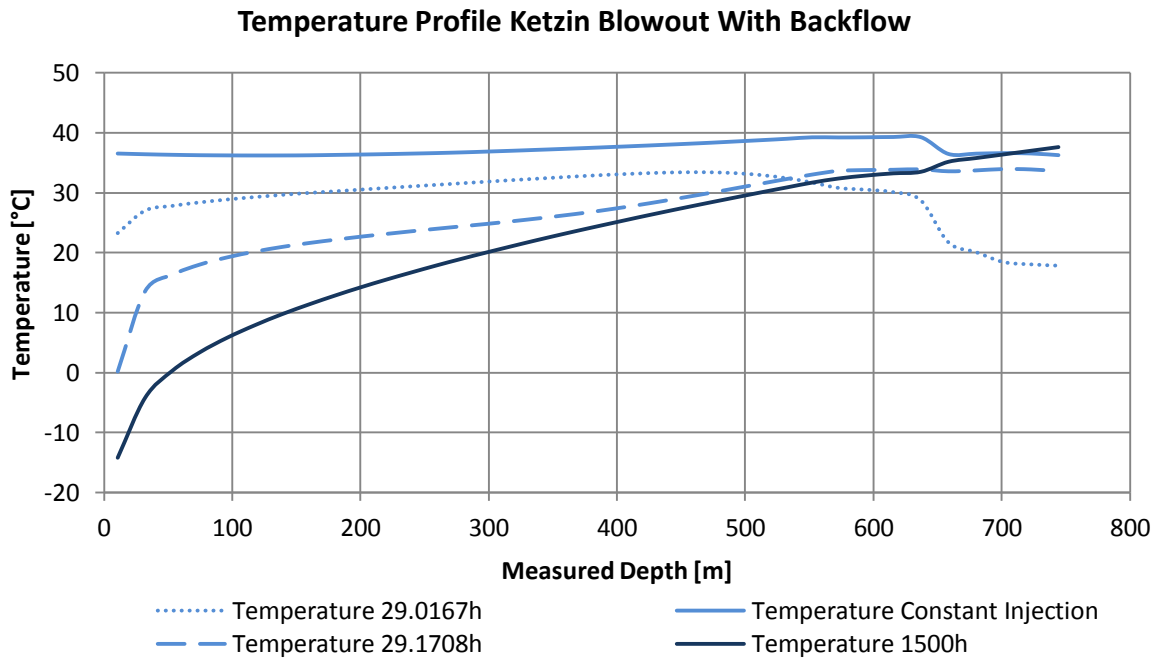


Figure 4-63 Temperature Profile Ketzin Blowout With Backflow

PH Diagram Ketzin Blowout with Backflow

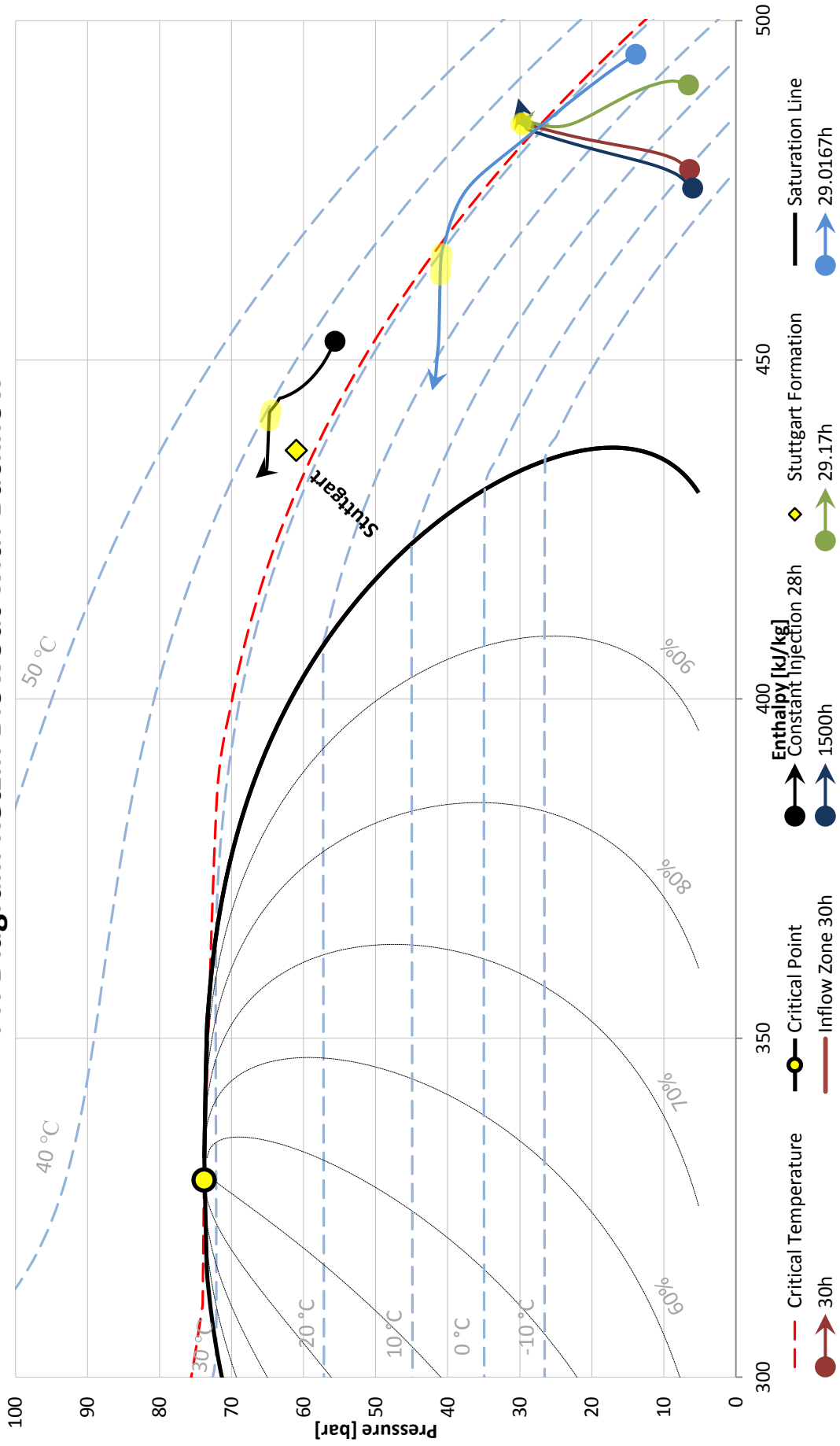


Figure 4-64 PH Diagram Ketzin Blowout with Backflow

PT Diagram Ketzin Blowout with Backflow

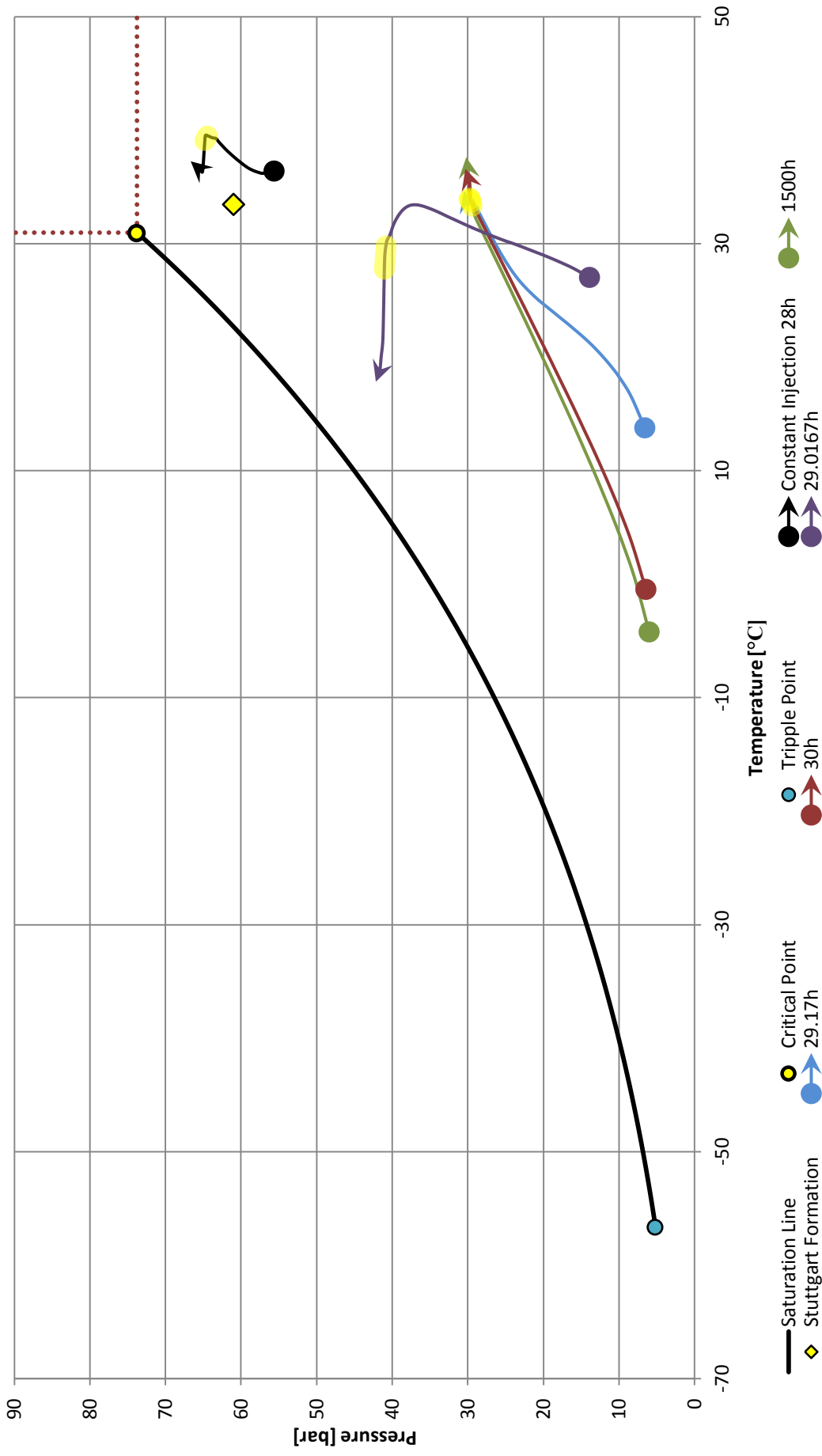


Figure 4-65 PT Diagram Ketzin Blowout with Backflow

4.4.3 BLOWOUT CO₂ WITHOUT RESERVOIR BACKFLOW

As for the previous scenario (ref. section 4.4.2), also this case ran seemingly without encountering any significant problems. As the pressure trend reveals (Appendix D-22), the well is in equilibrium in terms of pressure after about 3.3 minutes. Temperature wise, it takes a bit longer, but after 1 hour, the temperature curves at both the wellhead and bottomhole seems to flatten out (Appendix D-23). The temperature profile (Figure 4-67) also shows, more pronounced than the previous two scenarios, how the fluid is cooled in the first part of the well and then heated towards the end. It also indicates that the temperature at the selected instants is lower at the bottomhole than at the wellhead. It seems likely that this is caused by the pressure drop, which is largest at this point of the well. After 1500 hours, there is a sudden increase in pressure at approximately 560m depth, which corresponds well to the change in diameter of the inner tubing. Furthermore, it can be seen from the PH and PT diagrams, that no phase changes are encountered and that the well relatively quickly seems to approach equilibrium with the surroundings. Under these circumstances, a maximum discharge rate of approximately 9.4 kg/s was encountered at the wellhead (Appendix D-24).

Pressure Profile Ketzin Blowout Without Reservoir Backflow

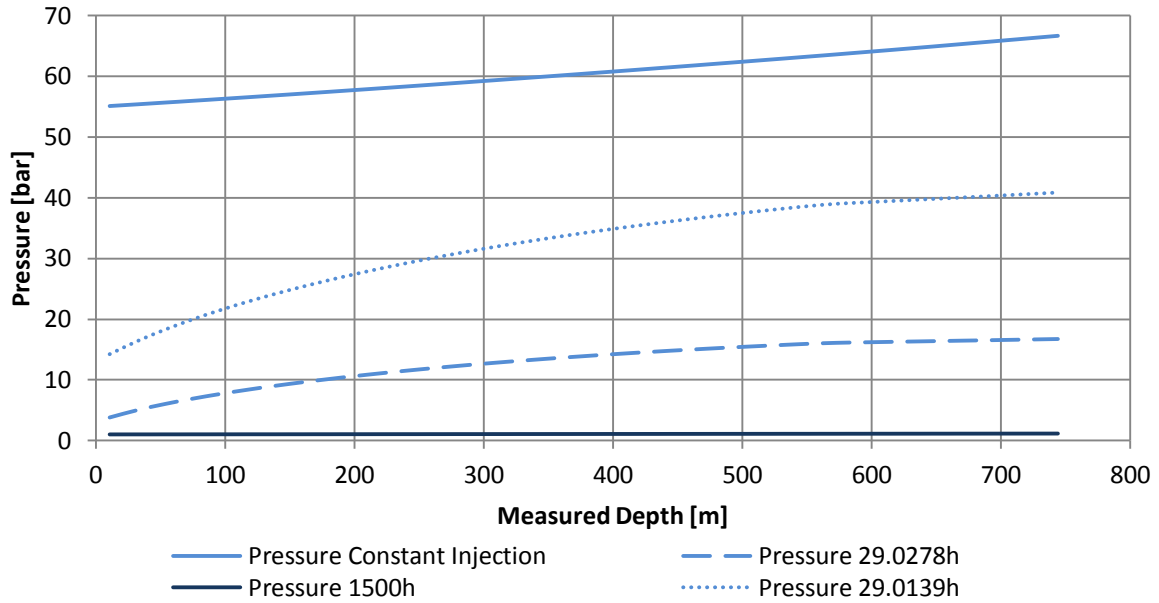


Figure 4-66 Pressure Profile Ketzin Blowout Without Reservoir Backflow

Temperature Profile Ketzin Blowout Without Reservoir Backflow

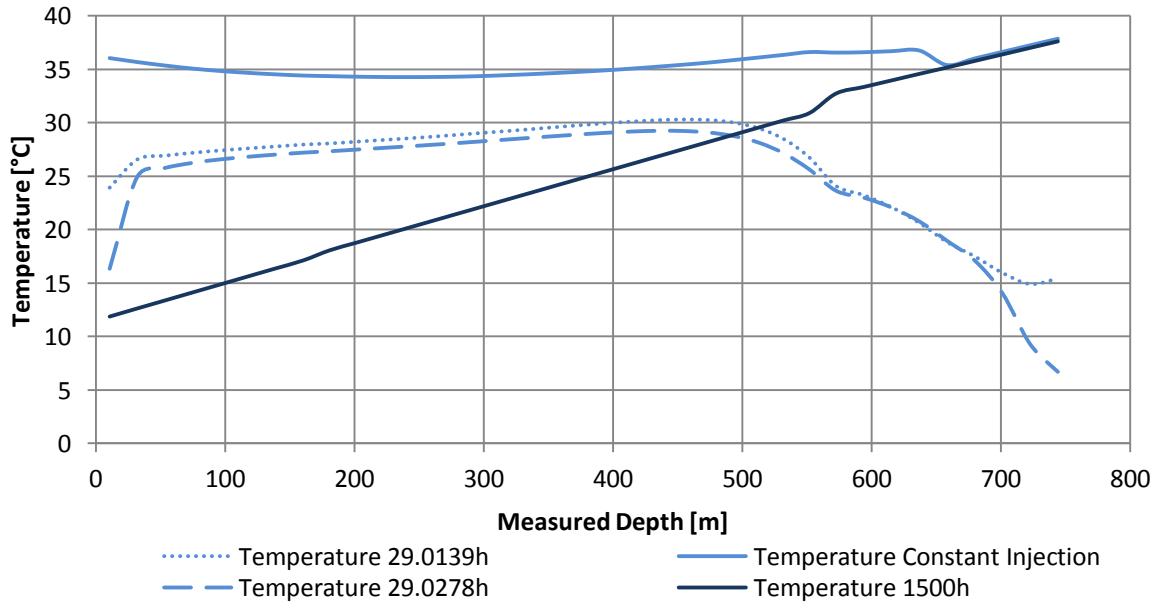


Figure 4-67 Temperature Profile Ketzin Blowout Without Reservoir Backflow

PH Diagram Ketzin Blowout NO Backflow

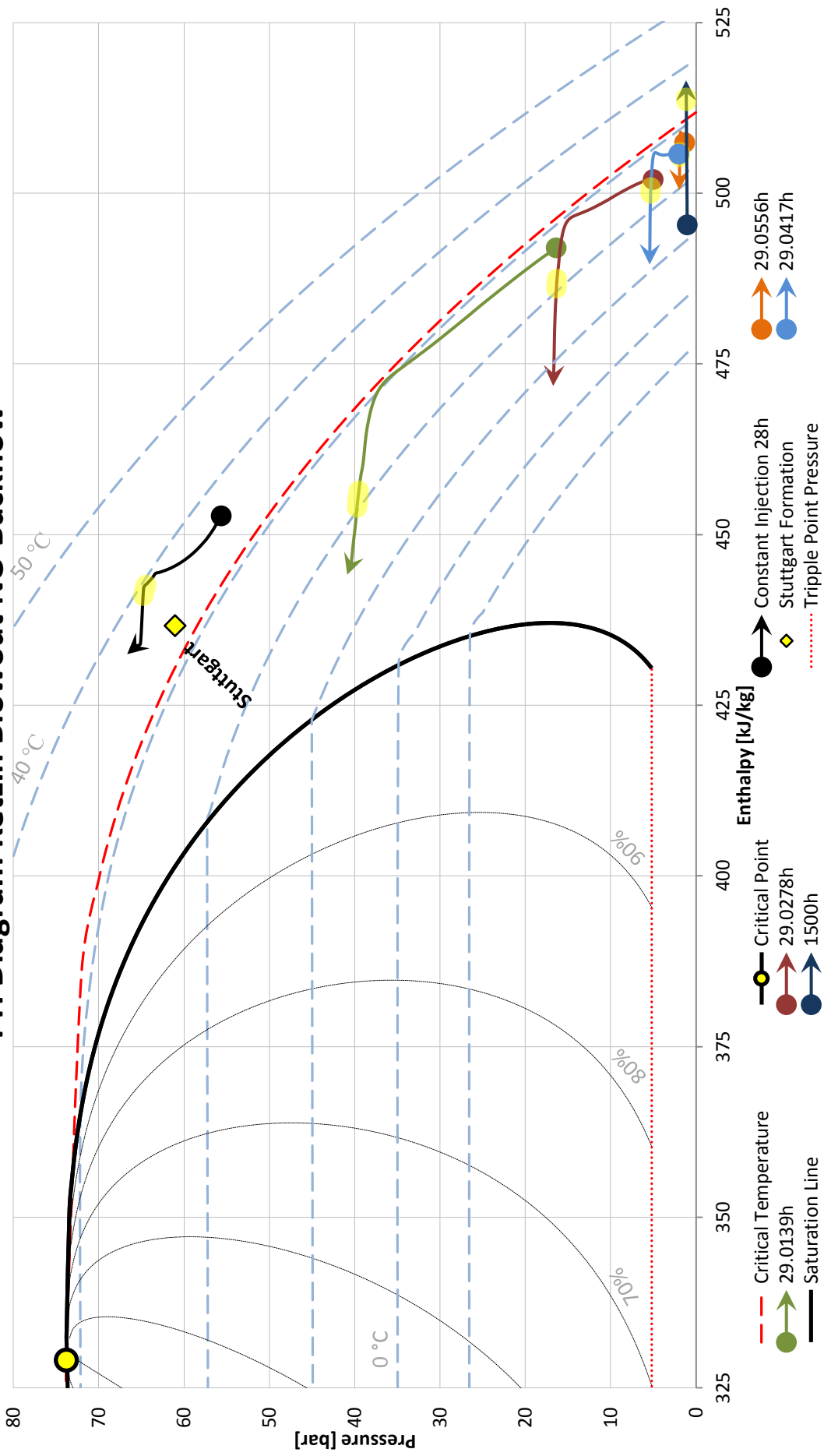


Figure 4-68 PH Diagram Ketzin Blowout NO Backflow

PT Diagram Ketzin Blowout NO Backflow

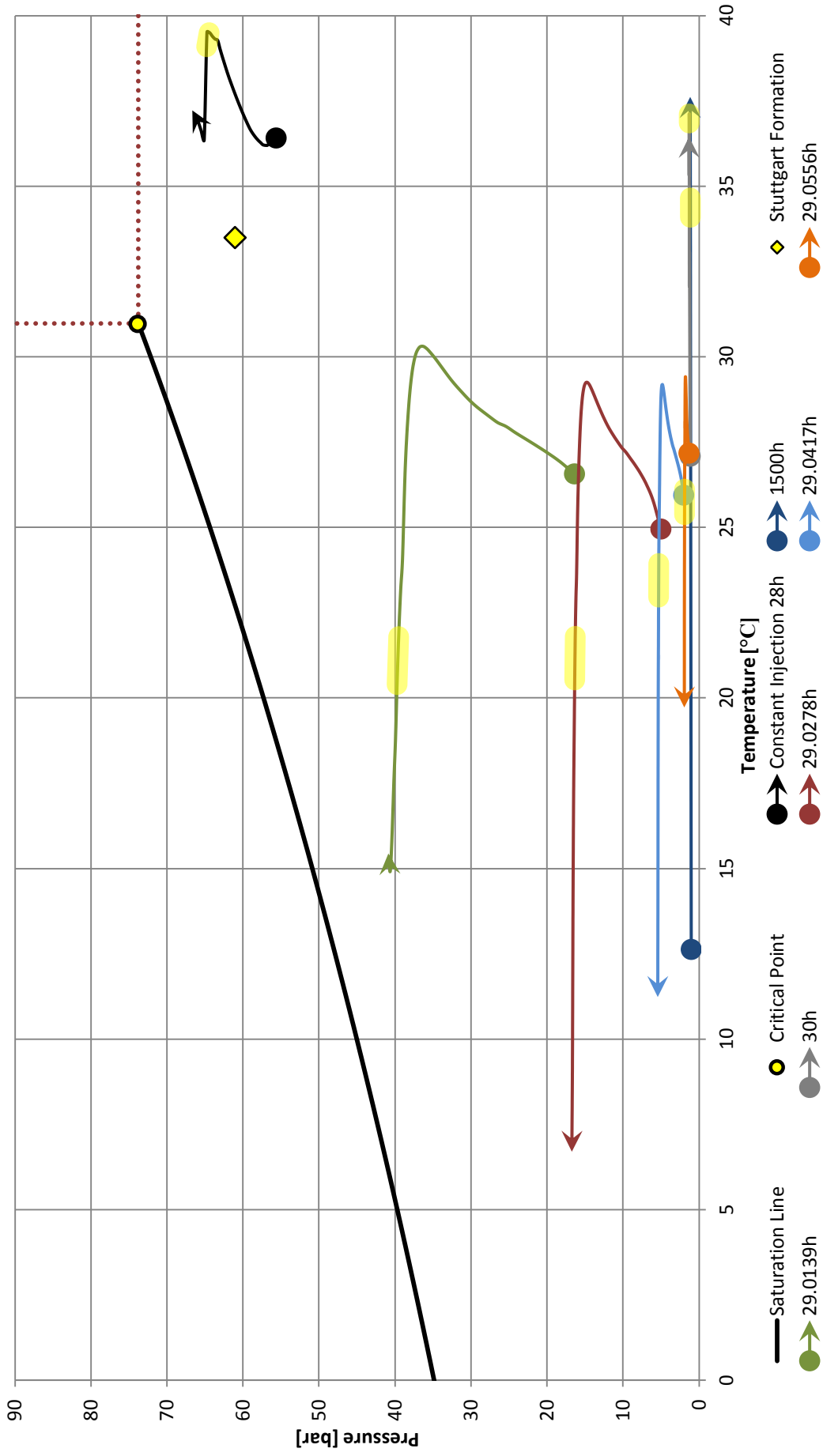


Figure 4-69 PT Diagram Ketzin Blowout NO Backflow

5 DISCUSSION

DISCUSSION

The simulation results in general, did to a large extent, confirm the discussed theoretical limitations of the model (ref. section 2.2.4). As a consequence of this, numerical instabilities were encountered for all simulations operating in the near critical region. Additional problems were also encountered by the simulations entering the solid formation region. This seemingly gave rise to a more unphysical behavior, but should also be expected in this region, as it is outside the validity range of OLGA. The CO₂ VIP module on the other hand, did show promising results, but could unfortunately not be used in all the simulations due to license restrictions. As seen in Figure 4-11, it did significantly reduce fluctuations in the near critical region for both the initial and final conditions. At 32 hours, the output did fluctuate more, especially within the two-phase area and near the critical point. However, when considering the transient behavior at this point of the simulation, it might not be unreasonable to expect the vapor fraction to vary significantly along the well. It should also be noted that the results for constant injection, and after 500 hours, were approaching a steady solution. Thus it seems reasonable to expect a more stable result for these plots. In general, it is also worth mentioning that none of the OLGA modules used in these simulations, have been sufficiently validated. Thus, the only way to quantify the expected uncertainty would be to optimize the models with respect to operational data. Nonetheless, some cases were numerically more stable than others.

At constant injection, all the models converged to a steady state. The Sleipner simulation did admittedly encounter numerical instabilities in the near critical region, but the overall result was relatively stable. Comparing the standard OLGA and CO₂ VIP simulation, the overall result did not differ significantly, apart from the reduced fluctuations in the near critical region. An overview of the wells at constant injection is presented in the PH diagram in Figure 5-1 (PT diagram can be seen in Appendix E-3). From this it seems relatively obvious that the numerical instabilities are caused by operation in the near critical region, as all the other simulations appear to give stable results throughout, and are located relatively far away from the critical point. Furthermore, it illustrates how the initial conditions may vary significantly for various projects and locations, which in turn forms the basis for how the wells respond to the different transient scenarios. Thus, it can be used to increase the general understanding of the expected behavior based on initial and specified boundary conditions.

Sleipner was the only well that encountered numerical issues of significance during the shut-in (Figure 4-6), but as can be seen from the respective PH diagrams, it was also the only well where the critical region was within the operational range. It can also be seen that the cooling of the fluid, which followed the shut-in, caused the fluid to traverse large parts of the critical region while approaching the ambient conditions. As for the other wells, no numerical issues of significance were encountered, and the conditions did remain outside the immediate vicinity of the critical point throughout the simulations. Although the Ketzin shut-in did enter the two-phase region, the relatively low initial pressure, lead the solution outside the critical region. For the same reason, no significant numerical issues were encountered for the Ketzin well during the blowout simulations.

PH Diagram Constant Injection Sleipner, Snøhvit, Ketzin and In Salah

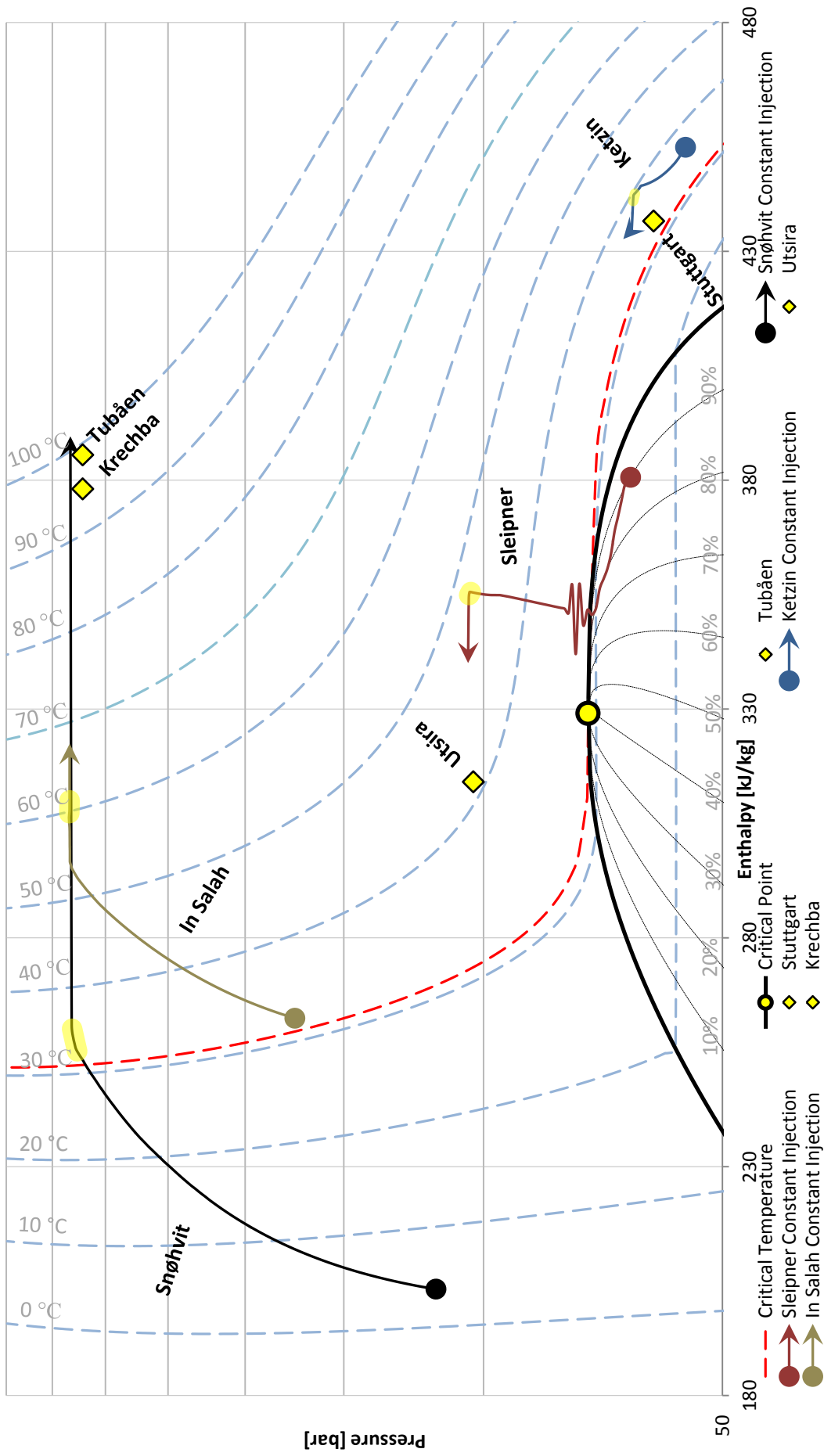


Figure 5-1 PH Diagram Constant Injection Sleipner, Snøhvit, Ketzin and In Salah

This was not the case for the remaining wells however. For the Sleipner case with reservoir backflow (Figure 4-15), it was seen that the low backpressure caused the upper part of the well to cross the sublimation line and enter the solid region. The continuous backflow also worked to maintain a certain pressure down the well, which caused the well to remain within the two-phase/near critical region throughout the simulation. The same trend was experienced for the Snøhvit (Figure 4-33) and In Salah (Figure 4-51) blowout simulations (with reservoir backflow), and kept the well within the two-phase/near critical region throughout the simulations. The elevated wellhead pressure at Snøhvit did keep the solution clear of the solid region. Thus, the main cause of the fluctuations in this case, seems to be caused by operation near the critical point. The In Salah simulation results did not explicitly indicate that the solution entered the solid region, as the solution seemed to enter the superheated region, before the pressure got below the triple point pressure. This was also confirmed by investigating the trend plot for the wellhead pressure and temperature. Nonetheless, the simulation did experience more numerical issues than the corresponding Snøhvit simulation, but the reason for this is not entirely understood.

Compared to the blowout simulations with reservoir backflow, the blowout simulations without backflow showed more stable results. Numerical instabilities were still encountered for the simulations operating in the critical region, but the combination of a low final bottomhole pressure and unchanged ambient conditions, seemed to lead the solutions out of the most critical region. Eventually all simulations approached a steady solution within the superheated region as expected. Initially, the results from the Sleipner simulation seemed surprisingly more stable than the other Sleipner cases included in this study. However, when viewed in the PH diagram (Figure 4-21), with the boundary conditions it mind, it gave more sense. As can be seen from the plot, the initial state (at constant injection) exits the phase envelope to the right of the critical point. Thus, once the valve opens, the solution immediately starts to move away from the critical region. Although it still seems likely that the solution at some point enters the critical region, the unchanged ambient conditions, and low bottomhole pressure, assures that the solution does not remain in the near critical region, as the case was with backflow. Both the In Salah and Snøhvit simulation did experience some instabilities caused by operation in the near critical region. As opposed to the initial state of the Sleipner simulation, the initial state for both Snøhvit and In Salah is located on the far side of the critical point. Consequently, both solutions had to cross the near critical region to some extent. At best (if the depressurization were controlled, to allow sufficient heat transfer with the surroundings), the In Salah simulation would have passed approximately 3°C above the critical point. Similarly, the Snøhvit wellhead would not get above 4°C. It was also observed that the In Salah blowout did enter the solid formation region (which seemed to give rise to unphysical behavior in the well) and that the Snøhvit blowout (still without backflow) was considerably slower than the similar simulations for the other wells. This might be caused by numerical instability, but it seems likely that the higher backpressure might affect the rate of flashing from liquid to gas and this way slowed down the process.

From an operational point of view, ensuring safe operation is of major concern. In this context transient scenarios are of particular interest, as they often involve rapid changes to the temperature and pressure in the well or pipeline. Typical transient scenarios in a well are for instance a planned shut-in, start-up, or an undesired event such as a blowout or an emergency shutdown. This is highly relevant for CO₂, as a rapid drop in pressure might lead to critically low temperatures. This naturally depends on several factors such as the initial state of the well, the rate of change in pressure, phase changes, expansion cooling and heat transfer with the surroundings to mention some. If the temperature should fall below the design temperature of the components, the terms of the guarantee provided by the manufacturer are violated.

Even lower temperatures will also imply a significant security risk, as the temperature approaches the physical tolerance limit of the materials. In the event of a blowout, an estimation of the expected discharge rate might be helpful in establishing appropriate safety routines, according to expected concentration levels near the outburst. Low temperatures will also increase the risk of ice and hydrate formation, but as the single component module is restricted to pure CO₂, this is not accounted for in the simulations.

By reviewing the simulation results from all the shut-ins, it was observed that no critically low temperatures were experienced in either of the wells included in this study. In this context, there are some important points to have in mind. First of all, the shut-in procedure was determined from the available Snøhvit data. This resulted in a relatively gradual transition from normal injection to fully closed, over two hours. Accordingly, it is probably a good representation of an actual shut-in procedure, but a different result should be expected in case of an emergency shutdown. In such an event, a more rapid pressure drop might be expected and could this way result in low temperatures in the well. The applied procedure is likely determined with this in mind, as it gives a gradual decrease in pressure, and plenty of time for heat exchange with the surroundings. This was also seen from the results, as none of the simulations experienced temperatures significantly below the ambient wellhead temperature. Another valid point in this discussion is the coupling between the reservoir and the wellbore, which in all the simulations included in this study, was simplified to a linear relation. Including a model of the reservoir in the simulation (for instance by modeling the near well region in ROCX) would likely give better prediction of the flowing conditions in the well. It would however increase the complexity of the model significantly.

Depleted oil and gas reservoirs are highly relevant in terms of CO₂ storage, but might involve additional challenges during operation. This is due to the low pore pressure such reservoirs may have and the corresponding low bottomhole pressure. However, two-phase flow in the well should not necessarily be a project killer, as the experience from Sleipner indicates. It might however, lead to less predictable conditions in the well, as small changes in pressure and temperature might lead to large changes in fluid properties. In this context, accurate simulations are of high value during planning and operation. In relation to shut-ins, in combination with low pressure reservoirs, one scenario might be that the liquid content of the well is drained into the reservoir (until the pressure is equalized). This will in turn lead to a pressure drop in the well. The corresponding change in temperature is then highly dependent on the rate of the inflow to the reservoir and the heat transfer with the surrounding formation.

As for the shut-in simulations, the simplified relation between the wellbore and reservoir is likely to affect the result during a blowout. For instance, due to the density differences between CO₂ and the formation water, the CO₂ is expected to migrate upwards once injected into the reservoir. This could clearly affect the result in the event of a blowout, as it could give a reservoir backflow with high water content. This could in theory also reduce the outburst in some cases, as water remains a liquid even at atmospheric pressure, and has a relatively high density. Thus if the water content is high, it could form a liquid plug in the well. To include such effects, it would therefore be necessary to include both the reservoir in the simulations, and impurities in the fluid composition. However, at this point it is not possible to include water in the simulation (the single component module is limited to pure CO₂). The CO₂ VIP module should in theory be able to handle other components, but this has not been verified. It would however limit the fluid property calculations to the equations of state available in PVTsim. Hydrate formation is

another issue that is not considered in this study. Nonetheless, it could be highly relevant in many of the simulated scenarios.

Two blowout scenarios were simulated, with and without reservoir backflow. Here the scenario with reservoir backflow was thought to represent the worst case scenario. As the reservoir pressure was set constant, the best possible outcome would be a stable flow out of the well. However, as all the simulations, except Ketzin, ended up fluctuating in the near critical region, none of the simulations seemed to find a stable solution. The scenario without reservoir backflow on the other hand, was thought to represent the best possible scenario. In this case, the well is emptied without further contribution from the reservoir. Although numerical instabilities were encountered for the simulations entering the near critical and/or solid formation region, all the simulations seemed to approach a steady solution towards the end. Most of the discussed effects, not accounted for by the simulations, would likely contribute to a reduction of the reservoir outflow (reduction in reservoir pressure, water production, solid formation etc.). A more realistic result may therefore lie somewhere in between the two extreme scenarios. However, due to the highly fluctuating output and uncertain accuracy, it is difficult to identify any clear trends. At least not before any of the solutions are approaching a steady solution. The most meaningful cases to compare would therefore probably be the Ketzin well, as these simulations encounter least numerical trouble. This has also been included in Appendix E-1, where it can be seen that the two scenarios seem to follow each other until the rate of change in pressure decreases for the case with backflow. The case without backflow continues to decrease in both pressure and temperature until the pressure difference between the well and bottomhole is significantly reduced. The temperature starts to increase when the depressurization is nearly completed. It is however difficult to predict how water production would affect the result.

Even though the accuracy is highly debatable, the calculated extreme values for discharge flow and temperature might indicate at least the scale of what might be expected if a blowout should occur. In this context it is important to keep in mind that the scenarios themselves are extreme scenarios, and that the simulations assume that the well is completely open. The extreme values of both temperature and discharge flow was determined at the wellhead, for all shut-in and blowout simulations. With regards to safety procedures, the maximum discharge rate might be used to determine expected concentration levels, which can provide guidelines in the determination of safety routines. The lowest temperature were for all the cases registered at the wellhead, and might indicate if there is a risk of violating warranties, thermal cracking or dry ice from the discharge. The results can be seen in Figure 5-2 and Figure 5-3. They show, as mentioned before, that none of the shut-in scenarios encounter significantly low temperatures, as all remain above 0°C. Furthermore it can be seen that both Sleipner and In Salah encountered critically low temperatures during the simulations. Ketzin also experienced significant cooling during the blowout without reservoir backflow, but then again, CO₂ has a strong Joule-Thomson effect, and the pressure equalization was completed in just about 3 minutes. The Snøhvit blowout simulations on the other hand, seem to experience a surprisingly low cooling effect. This can to a large extent be explained by the higher backpressure due to the subsea wellhead. However, it might also seem like the initial conditions play a significant role here. By studying the PH diagrams of the blowouts (Figure 4-33 and Figure 4-37), it may seem like the low initial temperature gives a nearly isenthalpic depressurization in the liquid region, until the upper part of the well reaches the saturation line. It can also be noted how the isothermal lines in this region, are relatively vertical. Also, when the wellhead reaches the saturation line, it seems to be close to the specified backpressure. As for In Salah, the initial temperature is higher, and it seems to reach the saturation line at a higher pressure. Therefore, a larger part of the depressurization is done within the two-

phase region. This seems to be the case also for Sleipner, although the initial conditions already are within the two-phase region. The extreme temperatures are not fully captured in the PH-diagrams, and might be caused by operation below the triple point.

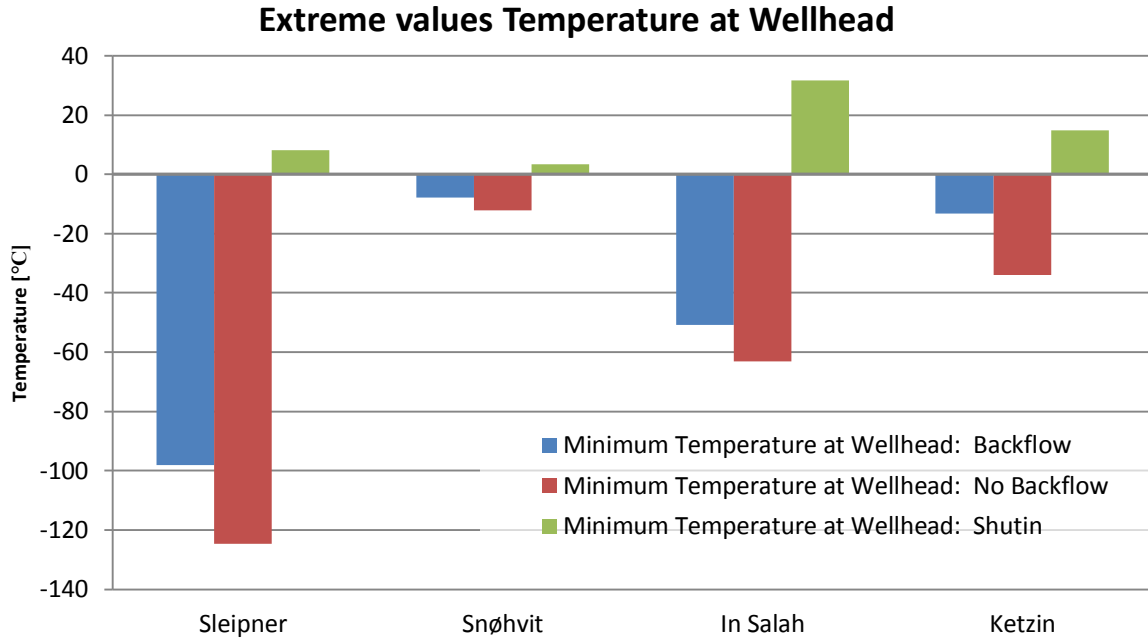


Figure 5-2 Extreme values Temperature at Wellhead All Cases

The discharge results all show relatively high estimates for the outflow. Measured in terms of the injection rate, only the Sleipner case with backflow and Snøhvit case without backflow have a discharge rate below 10 times the injection rate (approximately 3.5 and 6 respectively). For the Sleipner case without backflow on the other hand, the outflow was estimated to as much as 563 kg/s, and it was mentioned in section 4.1.4, that the blowout seemed to have the characteristics of a boiling liquid expanding vapor explosion. Regarding the maximum discharge rate, it should also be noted that the results is strongly dependent on the specified production coefficient, which in all the cases were assumed equal to the injection coefficient, but different for the respective wells.

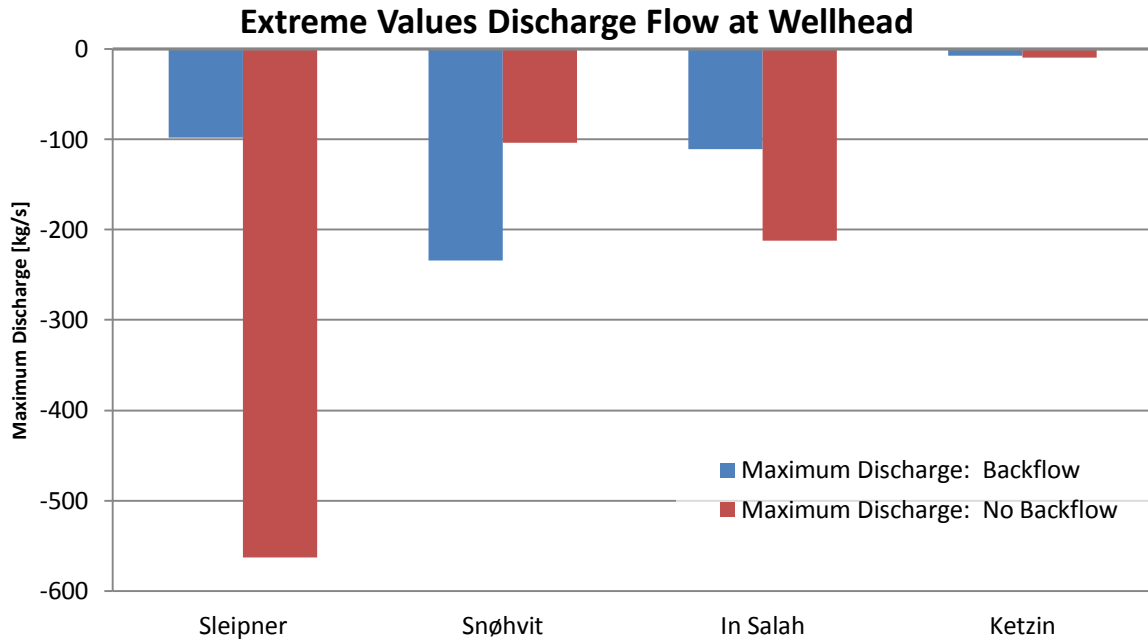


Figure 5-3 Extreme Values Mass Flow at Wellhead All Cases

The results from the history matching did close in on the wellhead pressure as intended. It did however also show some unexpected changes, particularly pronounced in the pressure plots. As the iteration cycle is determined to find the solution with the lowest deviation from the measured data, it does not necessarily have to be the most likely combination of parameters. It is therefore very important to be aware of what to expect, and how the parameters used to optimize the model, are expected to vary. It also showed a general tendency to a more rapid increase in both pressure and temperature for the simulations, compared to the measured data. This might indicate that the heat transfer is overestimated, or might be caused by the simplified reservoir description used in the model. Due to the elevated pressure throughout the well, it is not expected to be significantly influenced by numerical instabilities related to rapid changes in fluid properties. Changes in fluid properties related to impurities, might however affect the result. This is not encountered for in the simulations and might be one reason why the simulations showed a tendency to increase more rapidly in both pressure and temperature.

6 CONCLUSION

CONCLUSION

Four existing injection wells, Sleipner, Snøhvit, In Salah and Ketzin, were modeled in order to show how various operating and boundary conditions may change how the wells respond to different scenarios, and to identify the current capabilities and limitations of OLGA. For all the models, a steady state solution was obtained assuming normal operating conditions. Then, using this as the initial conditions, typical transient scenarios such as blowout and shut-in were simulated for all the wells. This should intentionally illustrate how dynamic simulations can be used to increase the general understanding of the behavior of CO₂ under various conditions. All simulations were performed using the dynamic multiphase flow simulator OLGA v7.2 and the single component module. Due to license issues, it was not possible to run all the simulations with the CO₂ VIP module as initially intended. This would likely have given a more stable results, as the governing equations have been rewritten to better handle pure components and fluids with narrow phase envelopes.

The simulations did to a large extent confirm the known limitations of the applied single component module in OLGA. Accordingly numerical instabilities were encountered in a varying extent near the critical point. The CO₂ VIP module, did on the other hand show promising results, and nearly eliminated the numerical instabilities related to operation in the critical region. Some fluctuations were still present within the two-phase region, but without operational data, it was not possible to validate the model or estimate the accuracy of the results.

One shut-in scenario and two blowout scenarios (with and without reservoir backflow) were simulated for both the Sleipner, Snøhvit, In Salah and Ketzin injection well. It was a general trend that all the simulations operating near the critical point did experience numerical instabilities. For the blowout simulations with reservoir backflow, the results were particularly unstable. This seemed to be caused by the elevated pressure which caused the conditions to remain in the region near the critical point for a large part of the simulation. The blowout simulations without reservoir backflow gave better results, but instabilities were still encountered for those simulations entering the critical region. Sleipner was the only well subject to numerical instabilities of significance during the shut-in. This seemed to be caused by the specified boundary conditions, which also here lead the solution to remain in the critical region for a large part of the simulation. Operation below the critical point seemingly gave rise to more unphysical results, and was experienced for both blowout scenarios, depending on whether the wellhead left the phase envelope before the triple point pressure was reached or not. This was also expected to some degree as pressures and temperatures below the triple point are outside the validity range of OLGA.

The initial and boundary conditions also proved to have a major impact on the results. Although the Snøhvit well was specified with a higher backpressure due to the subsea wellhead, the lower initial temperature did seem to give a more isenthalpic depressurization when compared to In Salah for instance. This in turn, seemed to be the reason why the discharge temperature did not decrease as much as in the In Salah case, as large parts of the depressurization was done in the liquid region, where the isotherms are more vertical. No temperatures below 0°C were experienced during either of the shut-ins. It should however be noted that a more instant shut-in procedure likely would have given a different results. All blowout simulations on the other hand did experience temperatures below 0°C. This could involve an

increased risk of hydrate and dry ice formation, but has not been considered by the simulations. The Ketzin well did not encounter any numerical issues of significance and can largely be explained by the initial state, well within the superheated region.

Operational data were made available by Statoil, and used to match the simulation results from the Snøhvit shut-in. After tuning the parameters, the simulation results got closer to the measured data, but also showed some unexpected changes, particularly pronounced in the pressure plots. However, as the iteration cycle is determined to find the solution with the lowest deviation from the measured data, it does not necessarily have to be the most likely combination of parameters. It is therefore very important to be aware of what to expect, and how the parameters used to optimize the model, are likely to vary. It also showed a general tendency to a more rapid increase in both pressure and temperature for the simulations, compared to the measured data. This might indicate that the heat transfer is overestimated, or might be caused by the simplified reservoir description used in the model. An expected deviance of 5-6 bar was calculated for the gauge, based on the compositional differences between the actual fluid and the pure CO₂ used in the simulations, and seemed to agree well with the results.

Despite the numerical instabilities that were encountered, the results did prove to have a high analytical value. It is however evident that more work is needed in order to validate the modules. Only then will it be possible to estimate the accuracy of the results. Furthermore, most industrial sized projects are likely to operate with some degrees of impurities. It is therefore a clear need to improve the ability to handle impurities. The CO₂ VIP module should be better suited for this, but is currently restricted to the equations of state available in PVTsim (fluid properties software). The reduced fluctuations are therefore mostly related to the handling of fluids with narrow phase envelopes, and do not address the challenge of establishing an equation of state for CO₂ with impurities. Nonetheless, the module did show promising results for the Sleipner shut-in with pure CO₂, and seems to be a big step in the right direction (this is solely based on the impression from the one simulation however). A coupled solution between the wellbore and reservoir is also needed to get a better prediction of the flow conditions, particularly during transient operations. The effect of impurities, water production from the reservoir, and hydrate and solid formation has not been considered by the simulations, but would likely affect the results significantly.

7 RECOMMENDATIONS

RECOMMENDATIONS

It is recommended that further work is based on the CO₂ VIP module, with a stronger focus on comparing the results with available experimental or operational data. The module should also be able to handle impurities better than the currently available single component module (with PT flash). It would therefore be highly interesting to run the same models with a typical composition related to CO₂ injection. If also optimized in RMO, a more correct composition would likely give better accordance at both the wellhead and gauge. This would however be limited to the equations of state available in PVTsim (software). Furthermore, it is recommended to investigate the coupling between the wellbore and the reservoir. This could be by applying a different relation for the flow between the wellbore and reservoir, or by modeling near well region of the reservoir in ROCX. The latter would likely give a better prediction of the flow conditions, especially during the transient scenarios.

8 REFERENCES

REFERENCES

- A. T. SINGHE, J. R. U., J. HENNINGES, G. PUSCH, AND L. GANZER 2013. Modeling of Temperature Effects in CO₂ Injection Wells. *Energy Procedia*, 1.
- ALNES, H. 2012. *RE: email*. Type to THU, E. S.
- BERND WIESE, M. N., MATTHIAS KLATT, MICHAEL KÜHN 2010. Sensitivities of injection rates for single well CO₂ injection into saline aquifers.
- BÍRÓ, K. 2009. BLOW OUT of NI-282/a at 0010 11.14. 1998. MOL Group.
- DIRECTORATE, N. P. 2012. CO₂ Storage ATLAS Norwegian North Sea.
- EIKEN, O., RINGROSE, P., HERMANRUD, C., NAZARIAN, B., TORP, T. A. & HØIER, L. 2011. Lessons learned from 14 years of CCS operations: Sleipner, In Salah and Snøhvit. *Energy Procedia*, 4, 5541-5548.
- ESPEN KROGH, R. N., ROAR HENNINGSEN 2012. Liquefied CO₂ injection modelling. *Energy Procedia* 23.
- GFZ, G. R. C. 2012. Underground Storage of CO₂ - The Ketzin Pilot Site.
- H. HANSEN, O. E. A. T. O. A. 2005. Tracing the path of Carbon Dioxide From a Gas/Condensate Reservoir, Through an Amine Plant and Back Into a Subsurface Aquifer - Case Study: The Sleipner Area, Norwegian North Sea.
- HANSEN, O. 20.06.2012 2012. *RE: email: RE: Modelling of the Snøhvit CO₂ injection well*. Type to THU, E.
- HENDRICKS, R. C., PELLER, I. C. & BARON, A. K. 1972. Joule-Thompson Inversion Curves and Related Coefficients for several simple fluids. NASA.
- HÅVARD ALNES, O. E., SCOTT NOONER, GLENN SASAGAWA, TORKJELL STENVOLD, MARK ZUMBERGE 2011. Results from Sleipner gravity monitoring: updated density and temperature distribution of the CO₂ plume *Energy Procedia* 4.
- HÅVELSRUD, M. 28.03.2012 2012. *RE: RE: CASE*.
- HÅVELSRUD, M. 23.04.2012 2012a. *RE: email*. Type to THU, E.
- HÅVELSRUD, M. 2012b. *Improved an verified models for flow of CO₂ in pipelines* [Online].
- HÅVELSRUD, M. 2012c. *RE: RE: CO₂-VIP*. Type to THU, E. S.
- HÅVELSRUD, M. 30.10.2012 2012d. *RE: (RequestID:24659) Determination of transition between two-phase and single phase in pipeline for single component CO₂*. Type to THU, E.
- IAIN WRIGHT, B., PHILIP RINGROSE, STATOILHYDRO, ALLAN MATHIESON, OLA EIKEN, STATOILHYDRO 2009. An overview of Active Large-Scale CO₂ Storage Projects. *SPE*.
- INSTITUTE, G. C. 2012. *Sleipner CO₂ Injection* [Online]. Available: <http://www.globalccsinstitute.com/projects/12401> [Accessed 28.11.2012].
- KJELL H. BENDIKSEN, D. M., RANDI MOE AND SVEN NULAND 1991. The Dynamic Two-Fluid Model OLGA: Theory and Application. 171-180.

- KOORNNEEF, J., SPRUIJT, M., MOLAG, M., RAMIREZ, A., TURKENBURG, W. & FAAIJ, A. 2010. Quantitative risk assessment of CO₂ transport by pipelines - A review of uncertainties and their impacts. *Journal of Hazardous Materials*, 177, 12-27.
- LAWRENCE J. PEKOT, P. P., YASMIN ADUSHITA, STEPHANIE SAUNIER, SCHLUMBERGER, ROHAN DE SILVA, NATIONAL GRID CARBON 2011a. Simulation of Two-Phase Flow in Carbon Dioxide Injection Wells.
- LAWRENCE J. PEKOT, S., PIERRE PETIT, YASMIN ADUSHITA, STEPHANIE SAUNIER, SCHLUMBERGER, ROHAN DE SILVA, NATIONAL GRID CARBON 2011b. Simulation of Two-Phase Flow in Carbon Dioxide Injection Wells. *SPE*.
- M. K. DOBSON, J. C. C., J. P. WATTELET, J. A. GAIBEL, M. PONCHNER,, P. J. KENNEY, R. L. S., T. C. VILLANEUVA, N. L. RHINES, K. A. SWEENEY, & D. G. ALLEN, A. T. T. H. 1994. Heat Transfer and Flow Regimes During Condensation in Horizontal Tubes. Available: <https://www.ideals.illinois.edu/handle/2142/10737>.
- MALDAL, T. & TAPPEL, I. M. 2004. CO₂ Underground storage for Snøhvit gas field development. *Energy*, 29, 1403-1411.
- MANTECON, J. C. 2007. The Virtual Well: Guidelines for the Application of Dynamic Simulation to Optimize Well Operations, Life Cycle Design and Production. *SPE*.
- MICHAEL ZETTLITZER, F. M., DARIA MOROZOVA, PETER LOKAY, HILKE WÜRDEMANN AND THE CO₂SINK GROUP 2010. Re-Establishment of the proper injectivity of the CO₂-injection well Ktzi 201 in Ketzin, Germany.
- MIT. 2012. *In Salah Fact Sheet: Carbon Dioxide Capture and Storage Project* [Online]. Available: http://sequestration.mit.edu/tools/projects/in_salah.html.
- MOHANARAJ, S. 31.10.2012 2012. *RE: (RequestID:24667) Source Void fraction*.
- NIST. 2011. *Thermophysical Properties of Fluid Systems* [Online].
- OECD/IEA 2011. KEY WORLD ENERGY STATISTICS. IEA.
- OLAV HANSEN, D. G., BAMSHAD NAZARIAN, BÅRD OSDAL, PHILIP & RINGROSE, J.-B. K., OLA EIKEN, HILDE HANSEN 2013. Snøhvit: The history of injecting and storing 1 Mt CO₂ in the fluvial Tubåen Fm. *Energy Procedia*, 1.
- OLAV HANSEN, O. E., SVEND ØSTMO, ROGER INGE JOHANSEN 2011. Monitoring CO₂ injection into a fluvial brine-filled sandstone formation at the Snøhvit field, Barents Sea. *SEG San Antonio 2011 Annual Meeting*.
- OOSTERKAMP, A. & RAMSEN, J. 2008. State of the art overview of CO₂ Pipeline transport with relevance to offshore pipelines. *Polytec*.
- PHILIP RINGROSE, B. N., LYKKE GEMMER AND ANDREW CAVANAGH 2011. Geological Controls on CO₂ injection and storage.
- R.C.BISSELL, D. W. V., M. ATBI, M. HAMDANI, M. OKWELEGBE, M.H. GOLDWATER 2011. A Full Field Simulation of the In Salah Gas Production and CO₂ Storage Project Using a Coupled Geo-mechanical and Thermal

Fluid Flow Simulator. *Energy Procedia* 4.

RØDUM, K. 2011. NG liquefaction. Presentation at Hammerfest LNG.

S. MARTENS, T. K., A. LIEBSCHER, S. LÜTH, F. MÖLLER, A. MYRTTINEN, B. NORDEN, C. SCHMIDT-HATTENBERGER, M. ZIMMER, M. KÜHN AND THE KETZIN GROUP 2011. Europe's longest-operating on-shore CO₂ storage site at Ketzin, Germany: a progress report after three years of injection. Springerlink.com.

SCHLUMBERGER. 2012. *ECLIPSE 2012 Reservoir Engineering Software* [Online]. <http://www.slb.com>. Available: <http://www.slb.com/services/software/reseng/eclipse.aspx> [Accessed 30.10.2012].

SPTGROUP 2012a. ROCX manual.

SPTGROUP 2012b. User manual OLGA 7.

STAFF, G. 25.04.2012 2012. *RE: email*. Type to THU, E. S.

SVEND TOLLAK MUNKEJORD, C. B., SIGMUND CLAUSEN, & MØLNVIK, G. D. K. A. M. J. 2013. Combining thermodynamic and fluid flow modelling

for CO₂ flow assurance. *Energy Procedia* 1.

TEP4185 2011. GAS PROCESSING PART – I - 2011 Lecture Note. NTNU.

THU, E. S. 2012. Comparison of simulation tools for transient CO₂ flow in pipes. NTNU.

UK, E. O. 2007. Equation of state prediction of carbon properties. DECC.

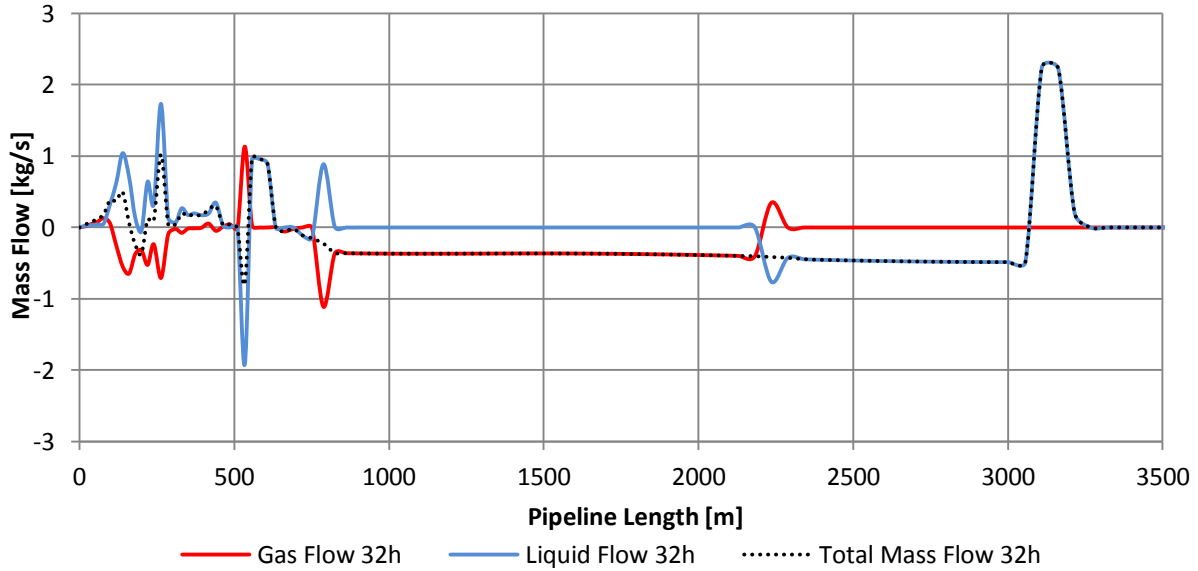
UNION 2007. Properties of Carbon Dioxide.

VAHEDI, S. & HINSLEY, J. 2011. Control Strategy development by dynamic modelling for CO₂ delivery network. *BHR Group 2011 Multiphase*, 15, 5-18.

A SLEIPNER FIGURES

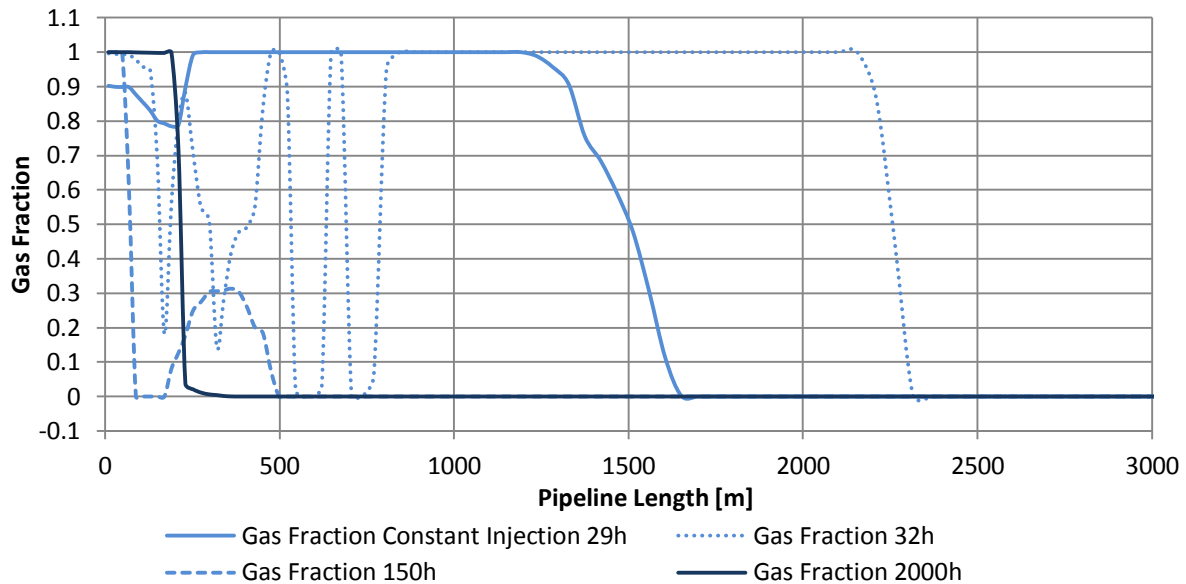
I. SHUT-IN SINGLE COMPONENT MODULE CO₂

Flow Profile Sleipner 32h



Appendix A-1 Flow Profile Plot Separate Phases Sleipner Shut-in at 32h

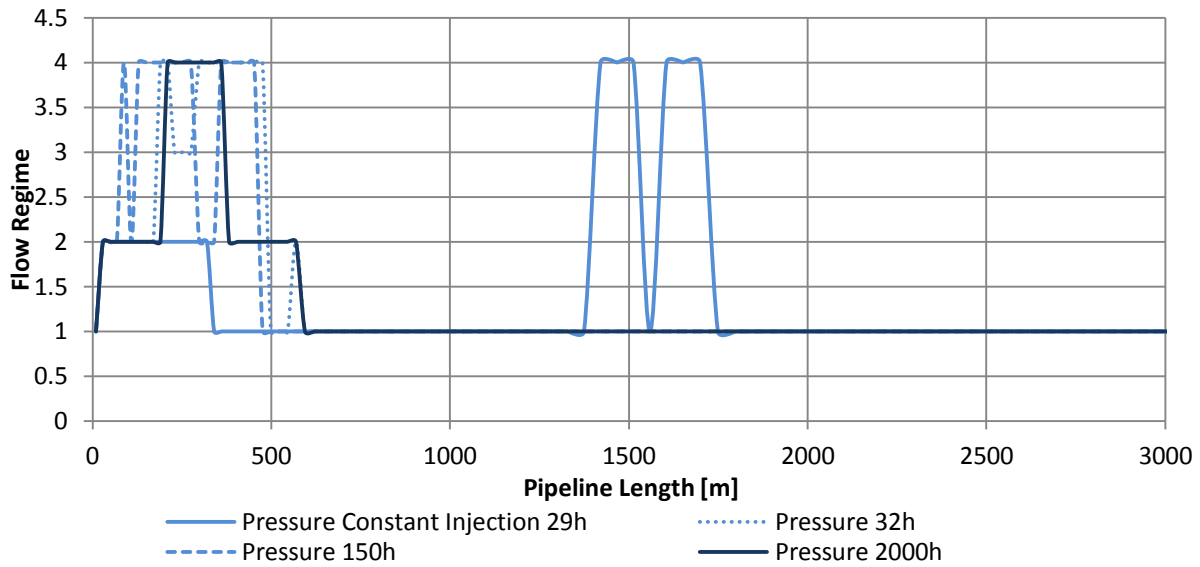
Gas Fraction Profile Sleipner



Appendix A-2 Gas Fraction Profile Plot Sleipner Shut-in at various times

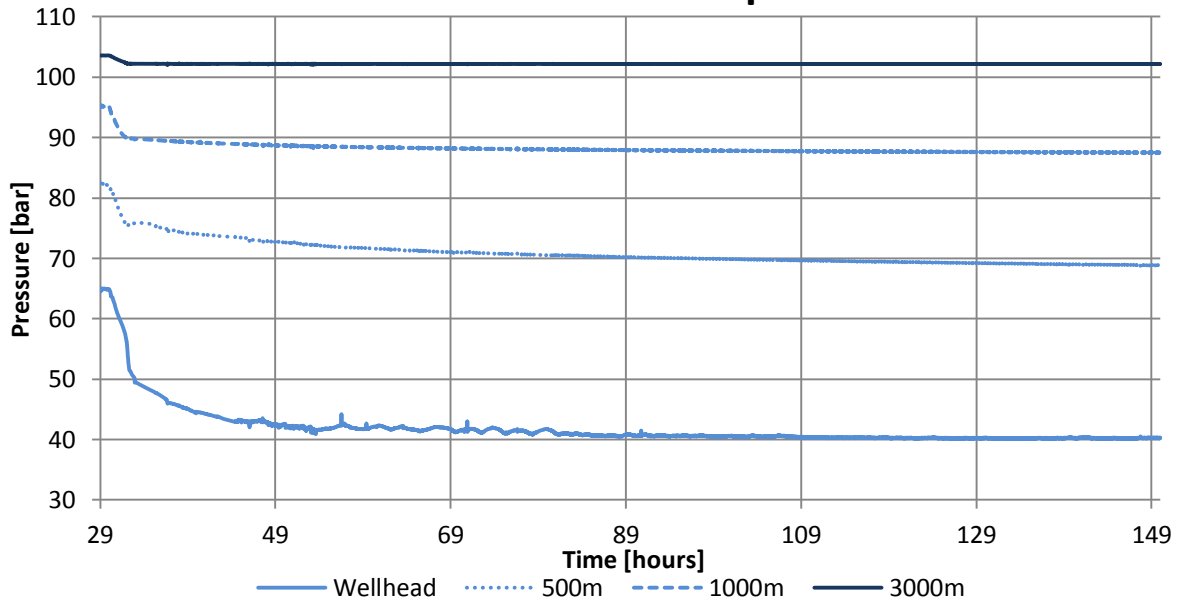
Flow Regime Profile Sleipner

Flow regime: 1=Stratified, 2=Annular, 3=Slug, 4=Bubble.



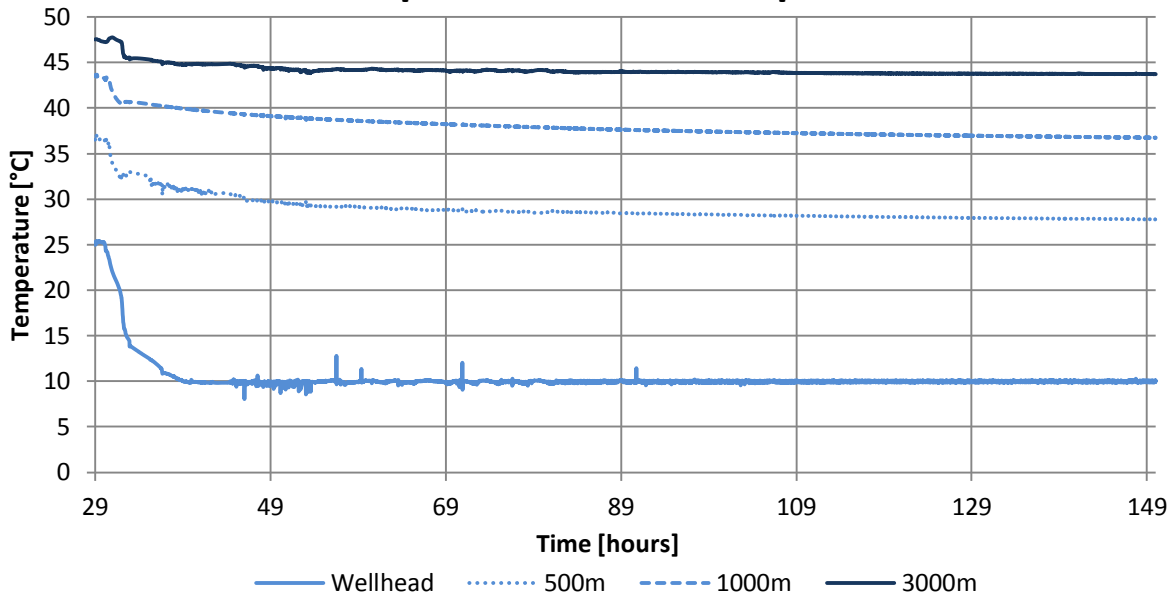
Appendix A-3 Flow Regime Sleipner Shut-in at Various Times

Pressure Trend Sleipner



Appendix A-4 Pressure Trend Sleipner Shut-in at Various Positions

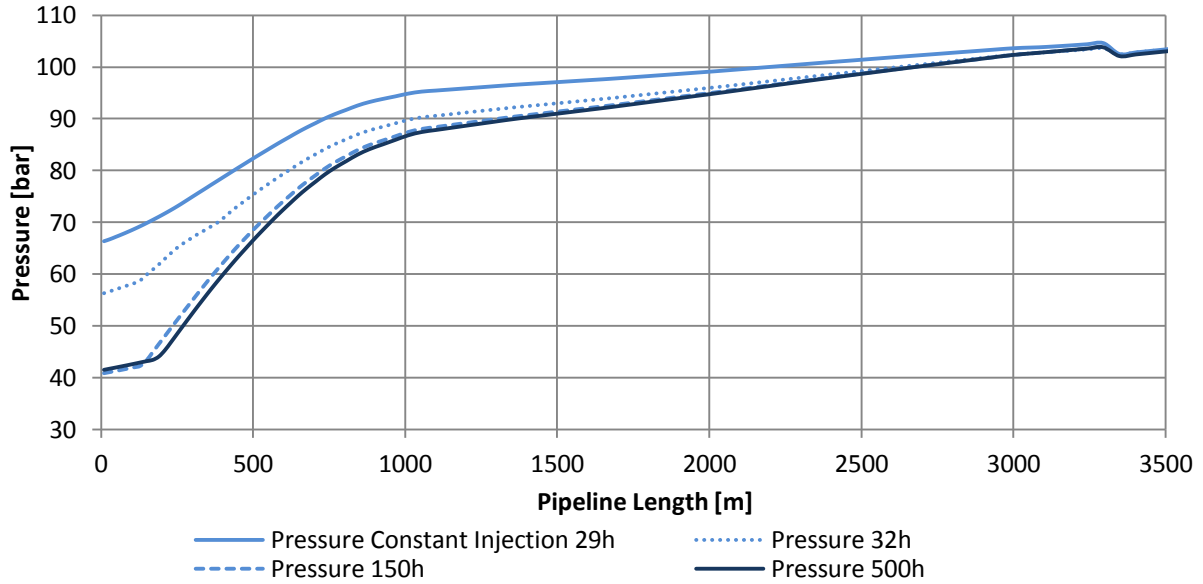
Temperature Trend Sleipner



Appendix A-5 Temperature Trend Sleipner Shut-in at Various Positions

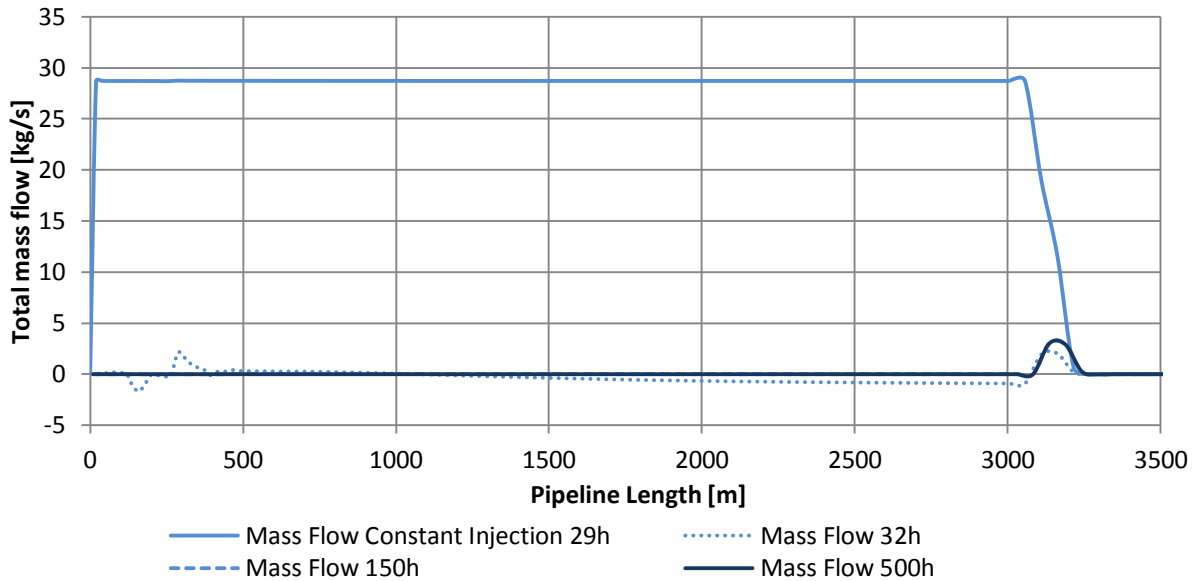
II. SHUT-IN CO₂ VIP MODULE

Pressure Profile Sleipner VIP



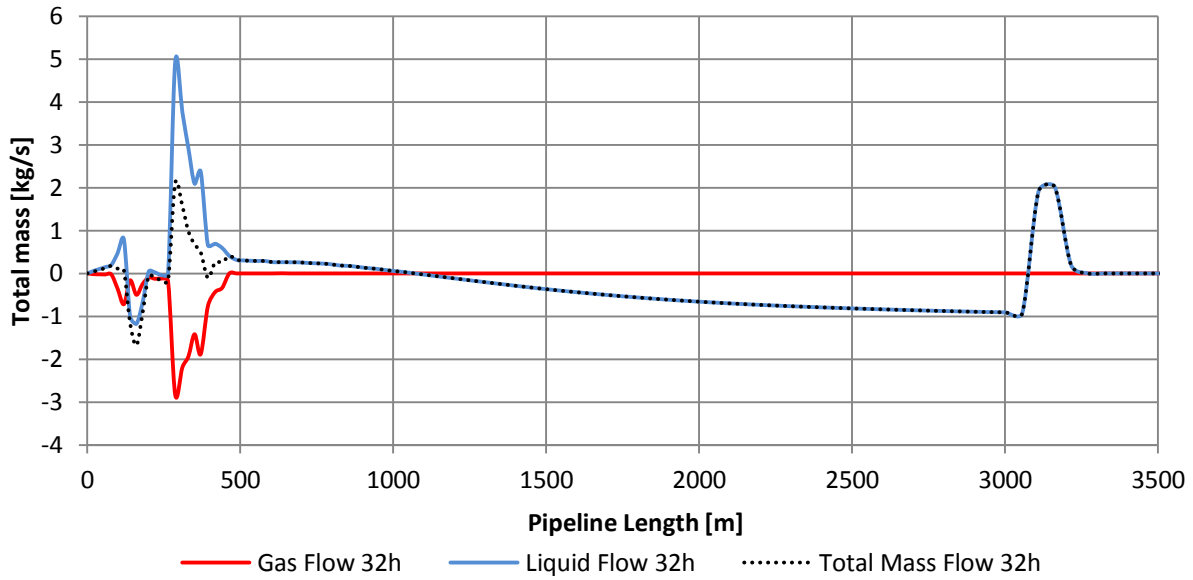
Appendix A-6 Pressure Profile Sleipner with CO₂ VIP module

Total Mass Flow Profile Sleipner VIP



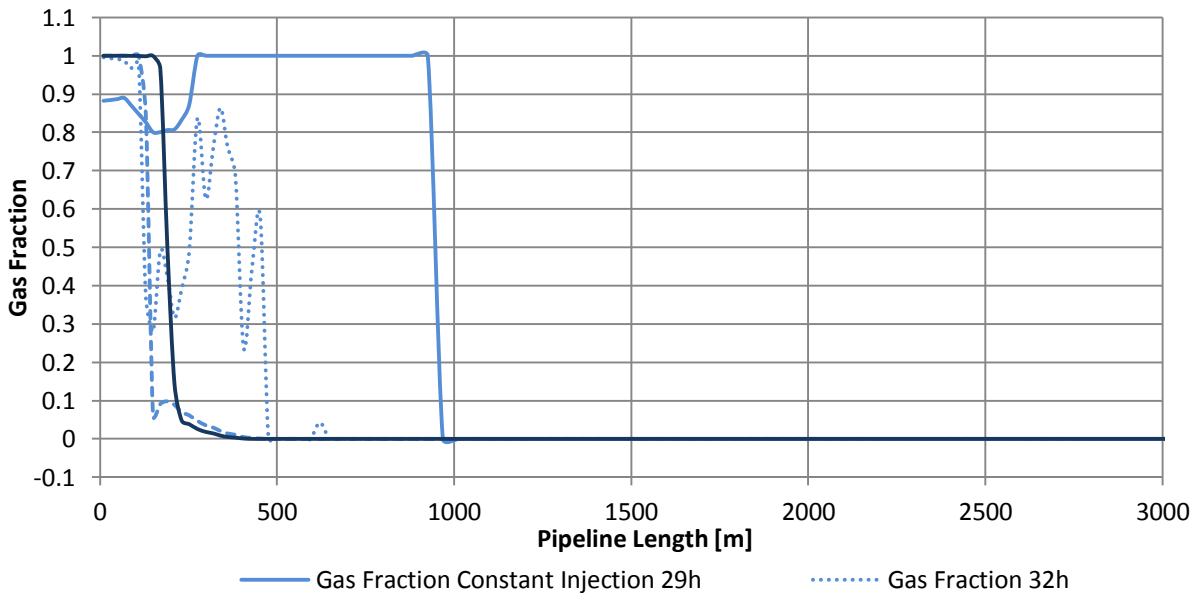
Appendix A-7 Total Mass Flow Profile Sleipner Shut-in CO₂ VIP

Flow Profile Sleipner VIP 32h



Appendix A-8 Flow Profile Sleipner Shut-in 32h CO2 VIP

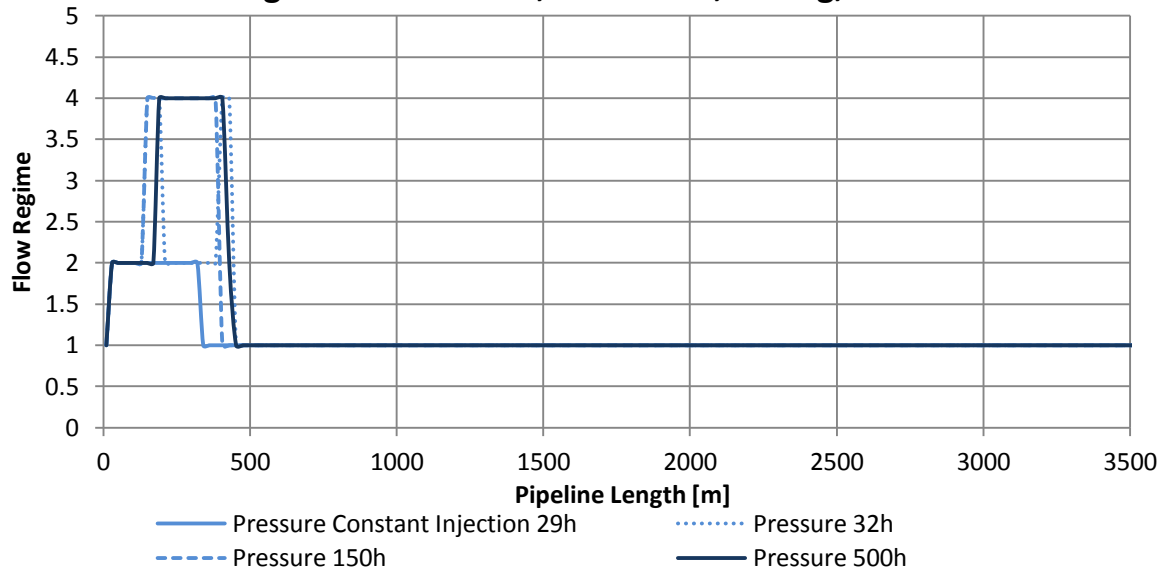
Gas Fraction Profile Sleipner VIP



Appendix A-9 Gas Fraction Profile CO2 VIP

Flow Regime Profile Sleipner VIP

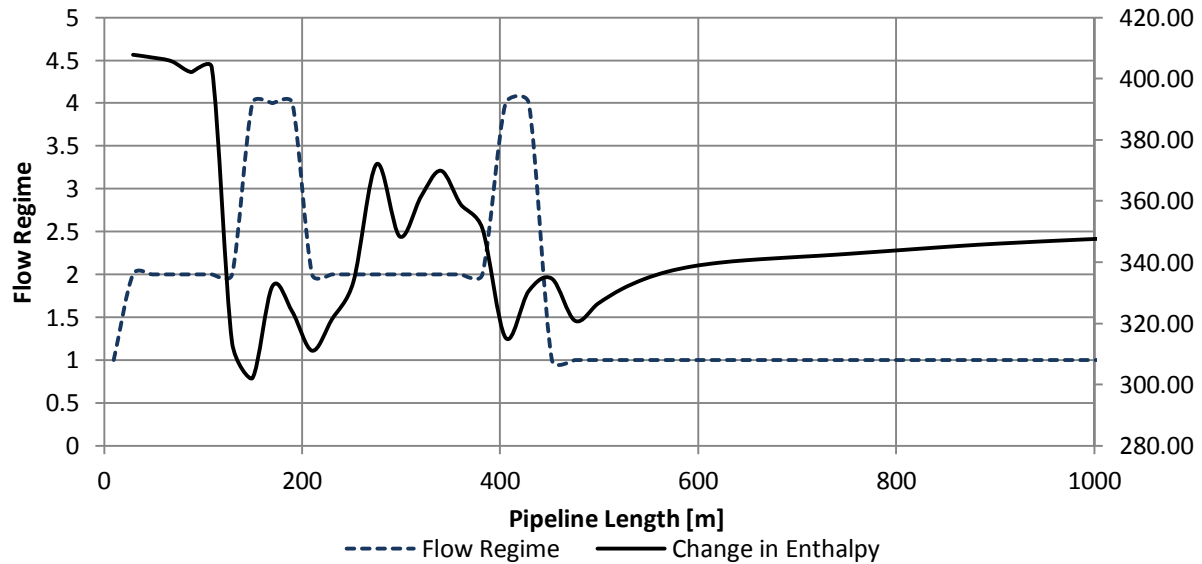
Flow regime: 1=Stratified, 2=Annular, 3=Slug, 4=Bubble.



Appendix A-10 Flow Regime Profile Sleipner Shut-in CO2 VIP

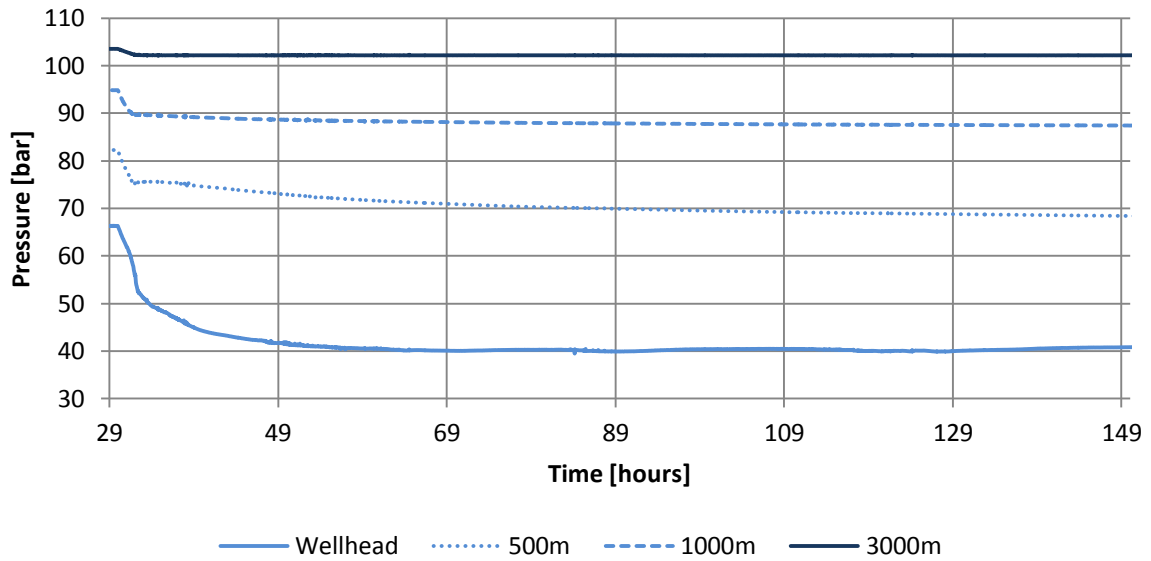
Flow Regime vs Change in Enthalpy at 32h

Flow regime: 1=Stratified, 2=Annular, 3=Slug, 4=Bubble.



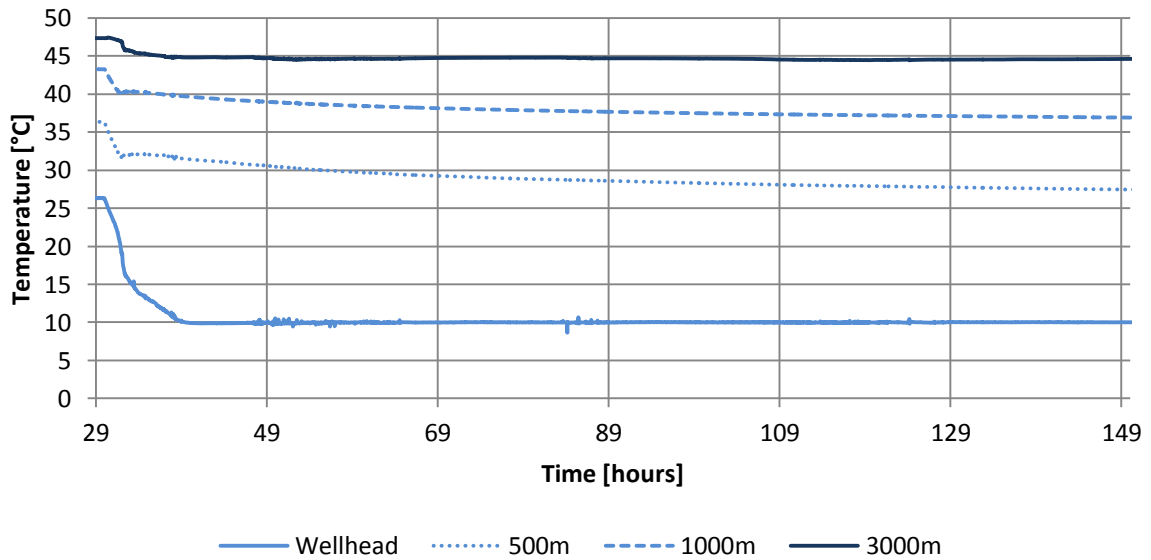
Appendix A-11 Flow Regime vs. Change in Enthalpy at 32h

Pressure Trend Sleipner VIP module



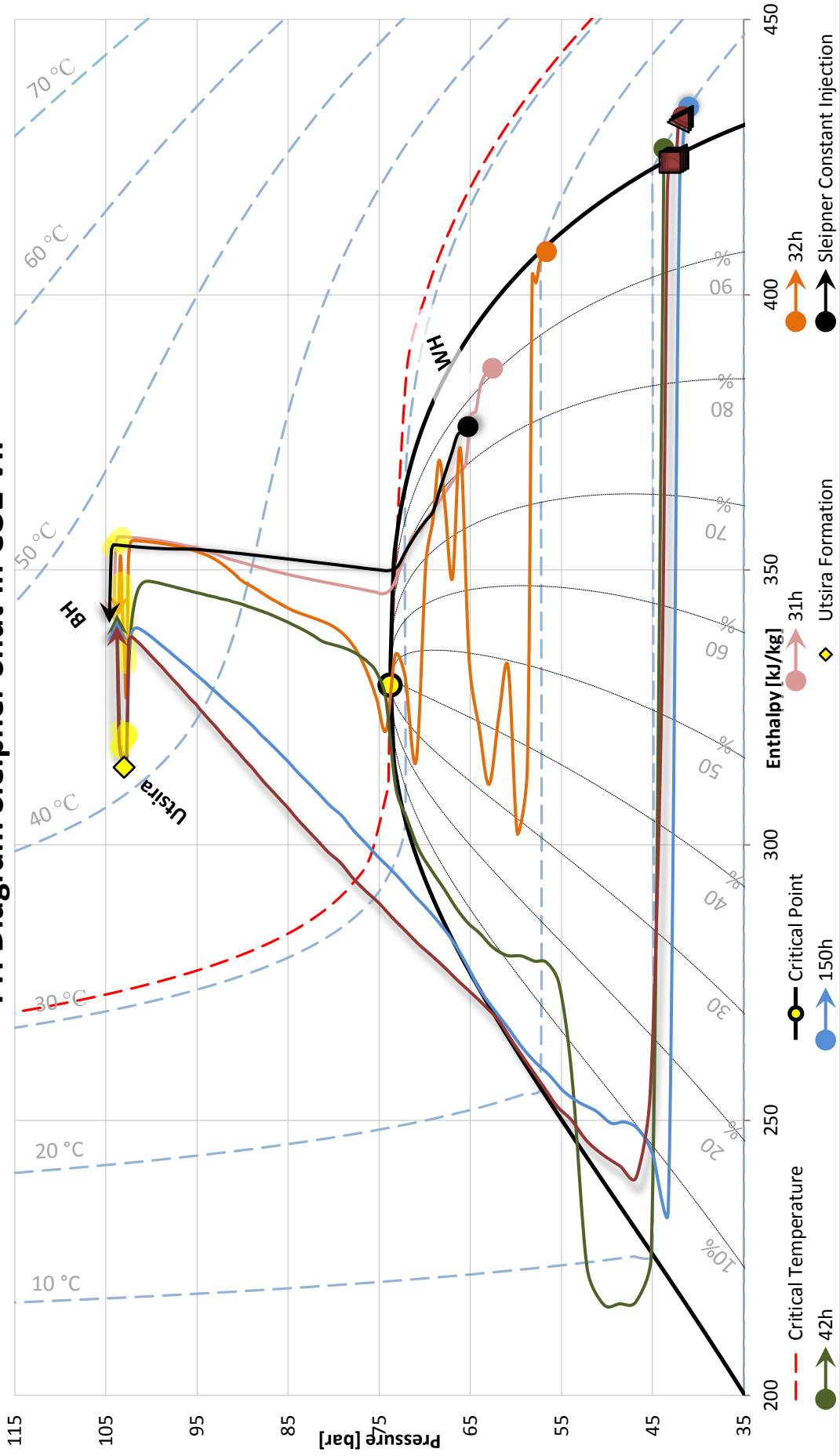
Appendix A-12 Pressure Trend Sleipner Shut-in CO2 VIP

Temperature Trend Sleipner VIP module



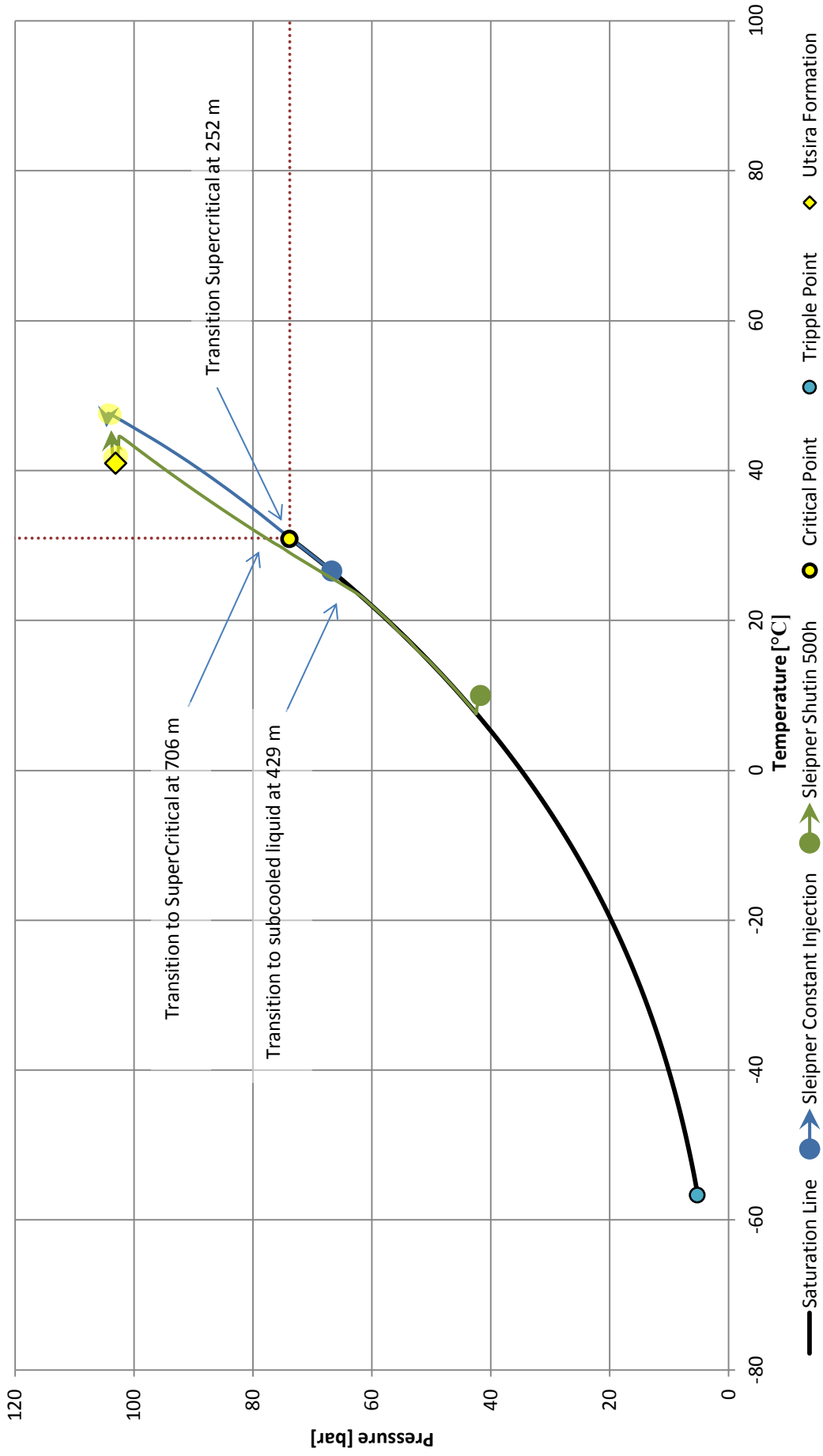
Appendix A-13 Temperature Trend Sleipner Shut-in CO2 VIP

PH Diagram Sleipner Shut-in CO2 VIP



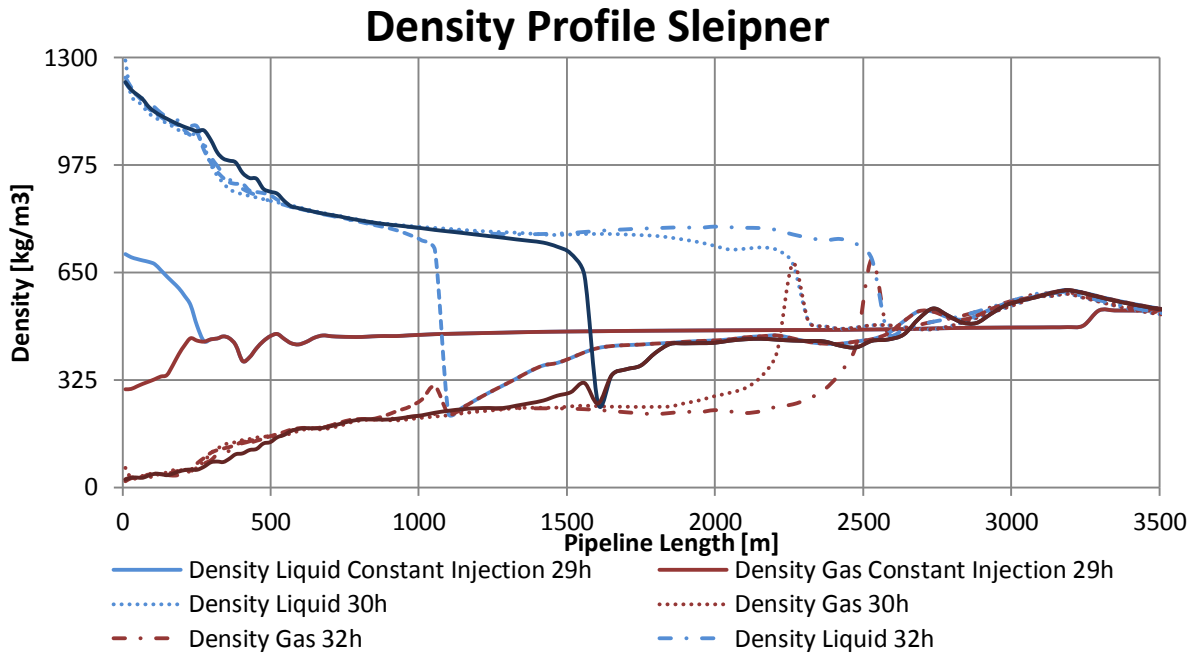
Appendix A-14 PH diagram Sleipner Shut-in CO2 VIP

PT Diagram Sleipner Shut-in CO2 VIP

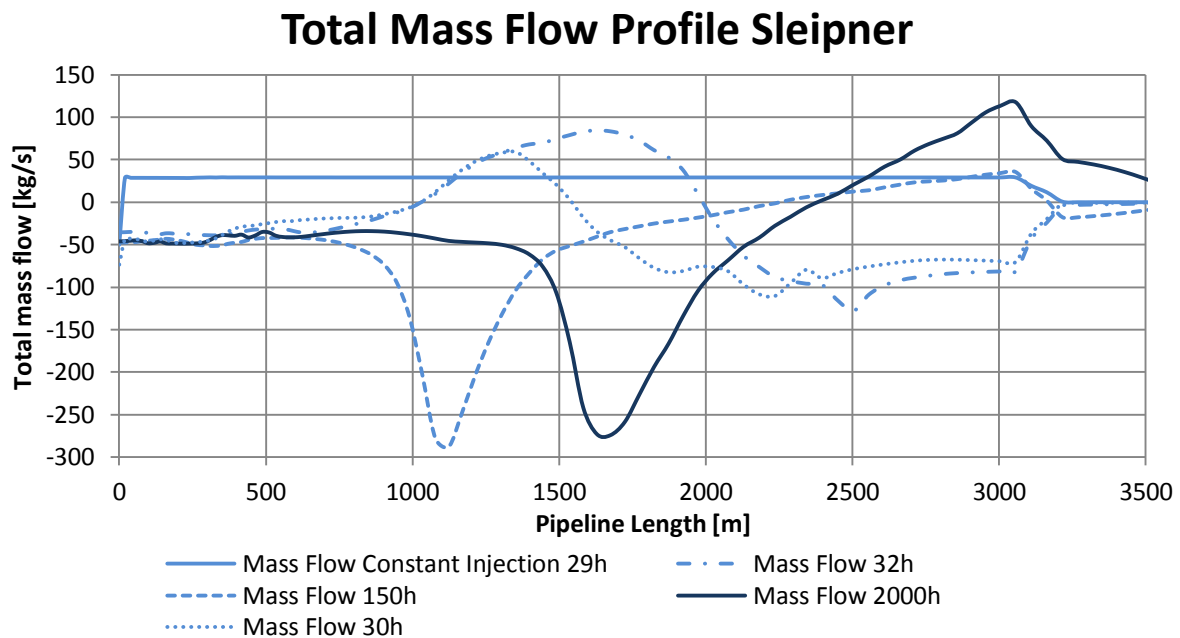


Appendix A-15 PT diagram Sleipner Shut-in CO2

III. BLOWOUT CO₂ WITH RESERVOIR BACKFLOW

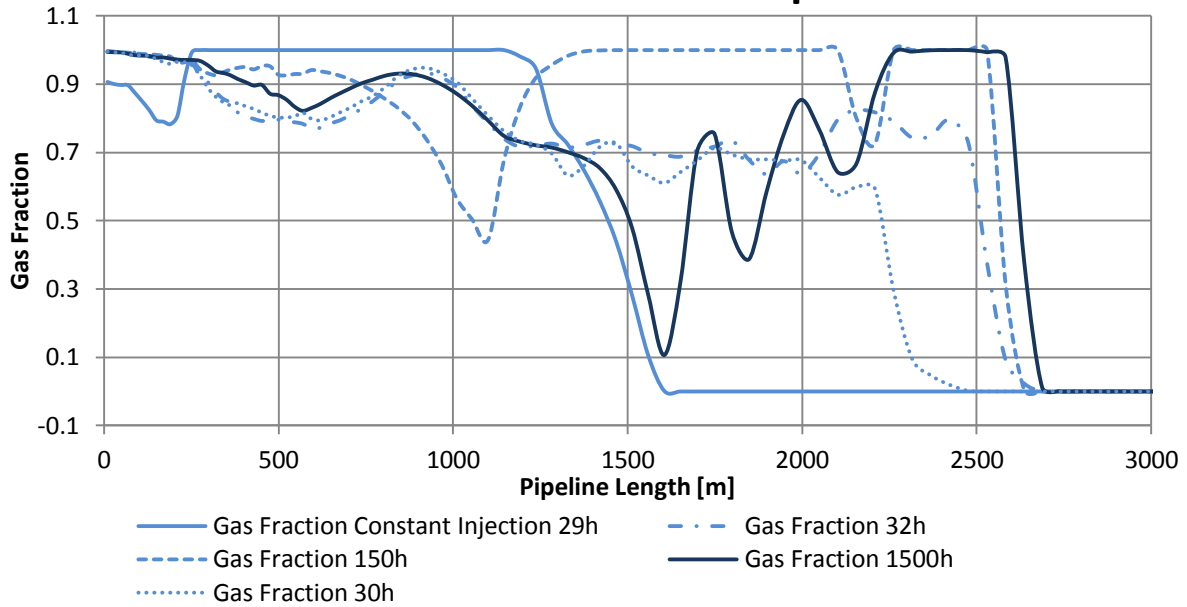


Appendix A-16 Density Profile Sleipner Blowout With Reservoir Backflow



Appendix A-17 Total Mass Flow Profile Sleipner Blowout With Reservoir Backflow

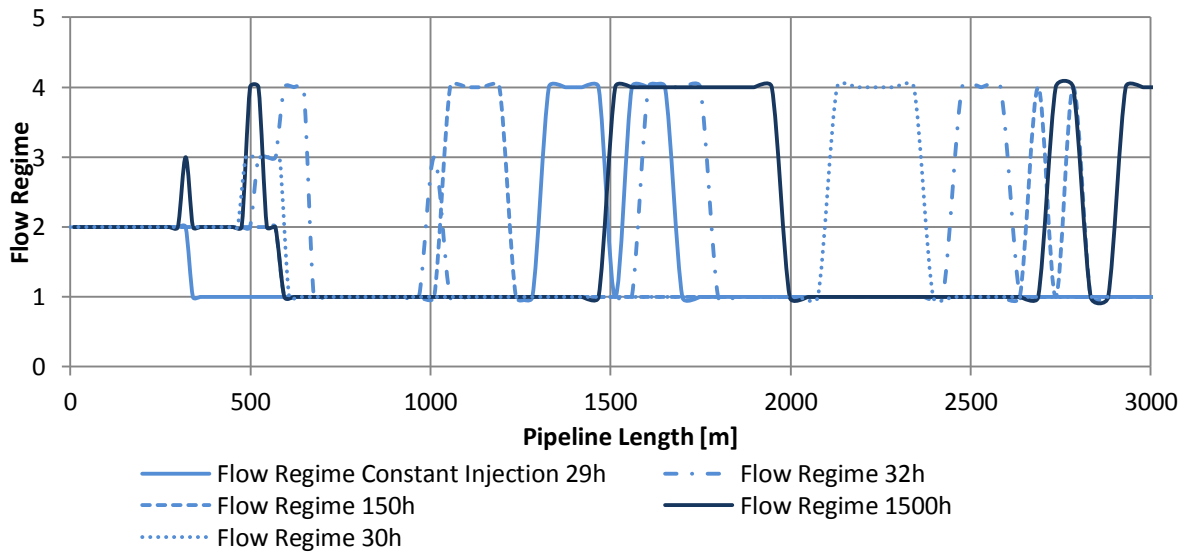
Gas Fraction Profile Sleipner



Appendix A-18 Gas Fraction Profile Sleipner Blowout With Reservoir Backflow

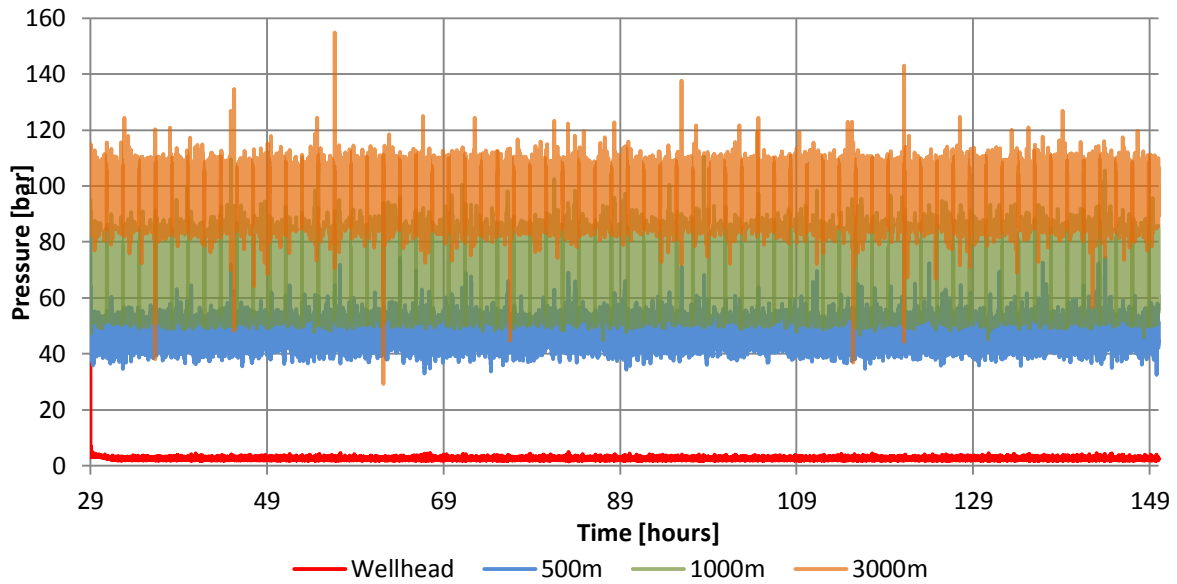
Flow Regime Profile Sleipner

Flow regime: 1=Stratified, 2=Annular, 3=Slug, 4=Bubble.



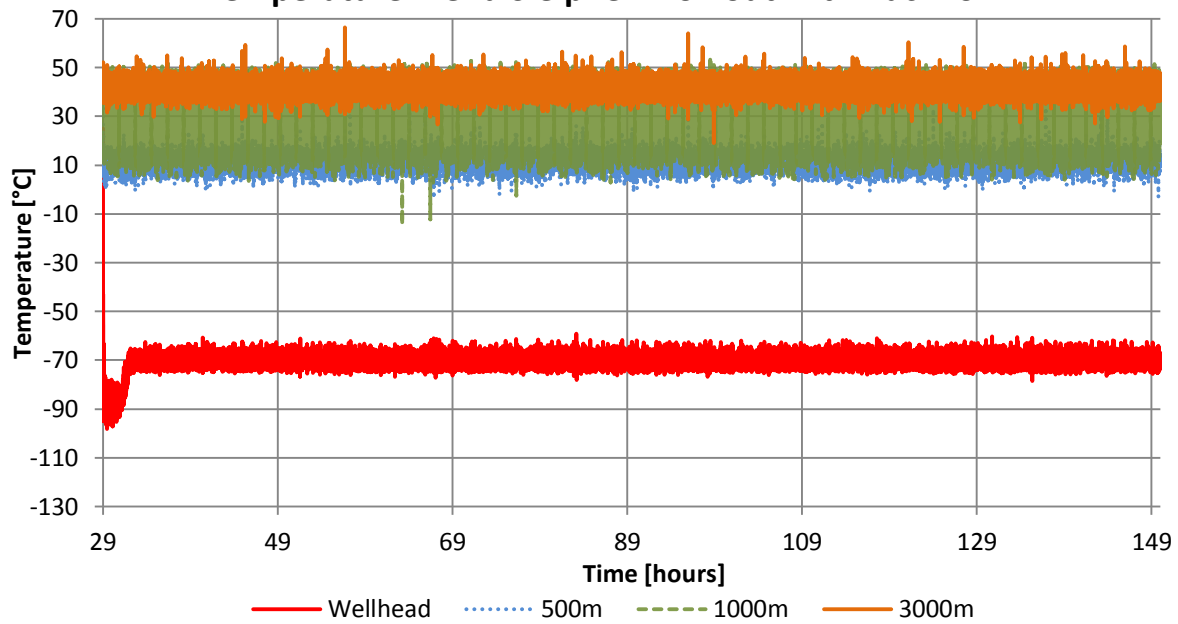
Appendix A-19 Flow Regime Profile Sleipner Blowout With Reservoir Backflow

Pressure Trend Sleipner Blowout with Backflow



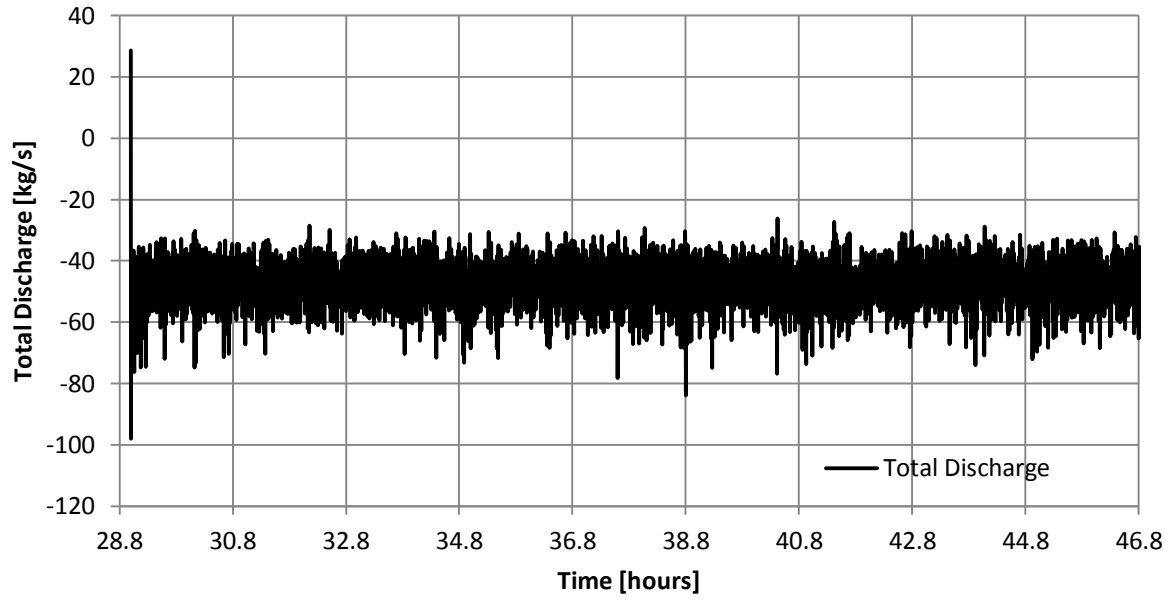
Appendix A-20 Pressure Trend Sleipner Blowout With Backflow

Temperature Trend Sleipner Blowout with Backflow



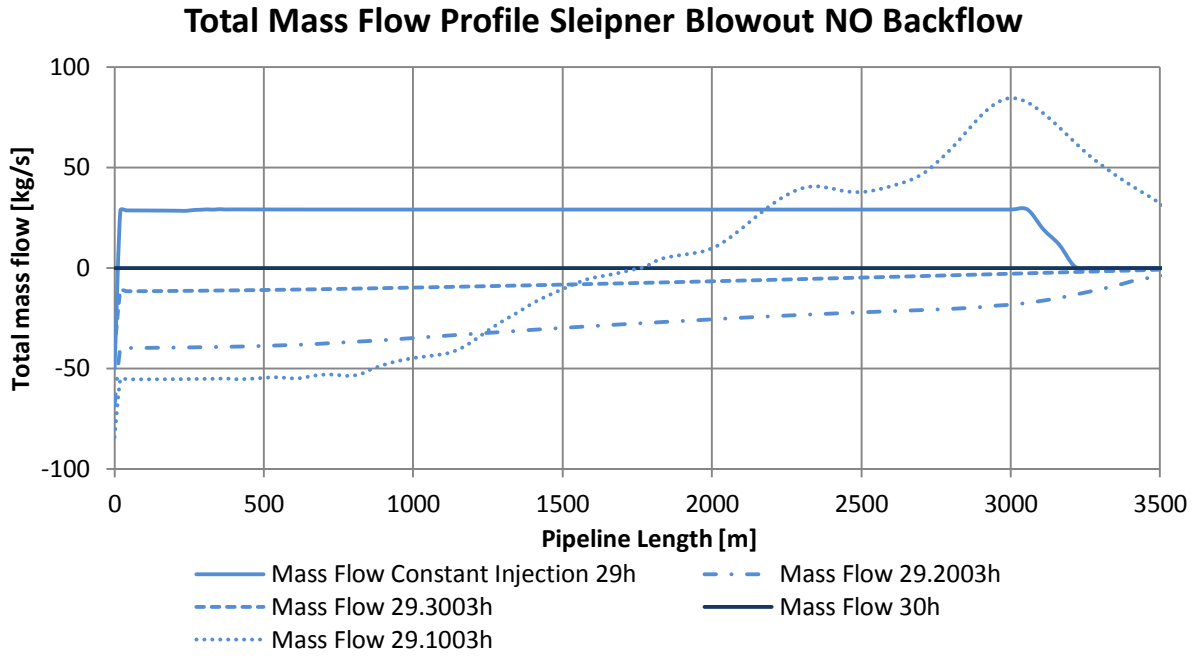
Appendix A-21 Temperature Trend Sleipner Blowout With Backflow

Total Mass Flow Trend at Wellhead Sleipner Blowout With Backflow

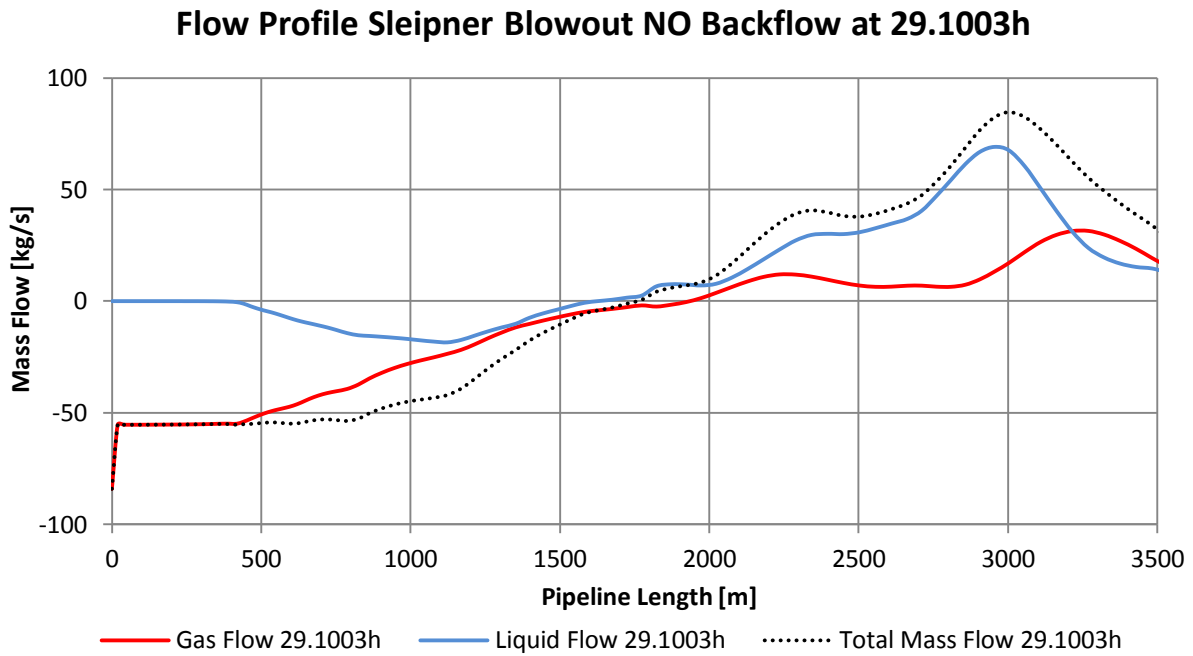


Appendix A-22 Total Mass Flow Trend at Wellhead Sleipner Blowout With Backflow

IV. BLOWOUT CO₂ WITHOUT RESERVOIR BACKFLOW

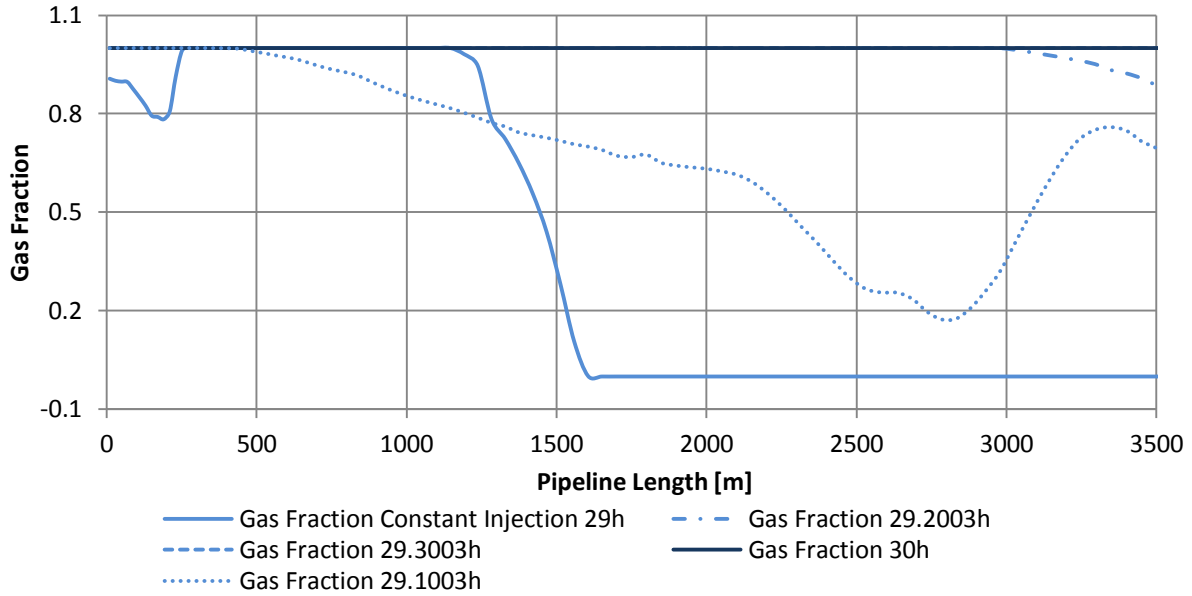


Appendix A-23 Total Mass Flow Profile Sleipner Blowout NO Backflow. Downwards flow is positive.



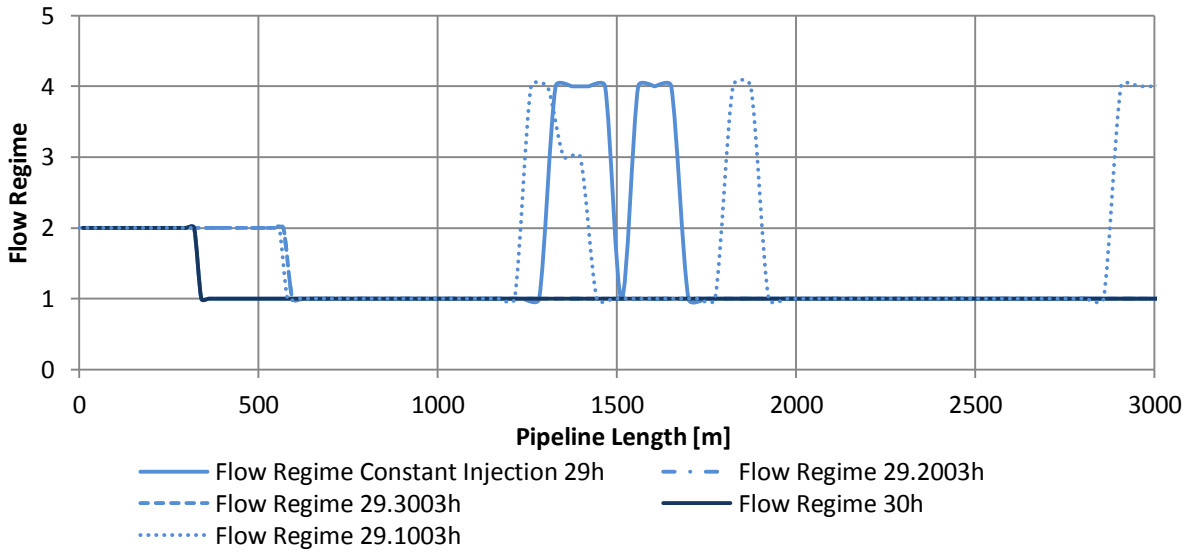
Appendix A-24 Flow Profile Sleipner Blowout NO Backflow. Downwards flow is positive.

Gas Fraction Profile Sleipner Blowout NO Backflow



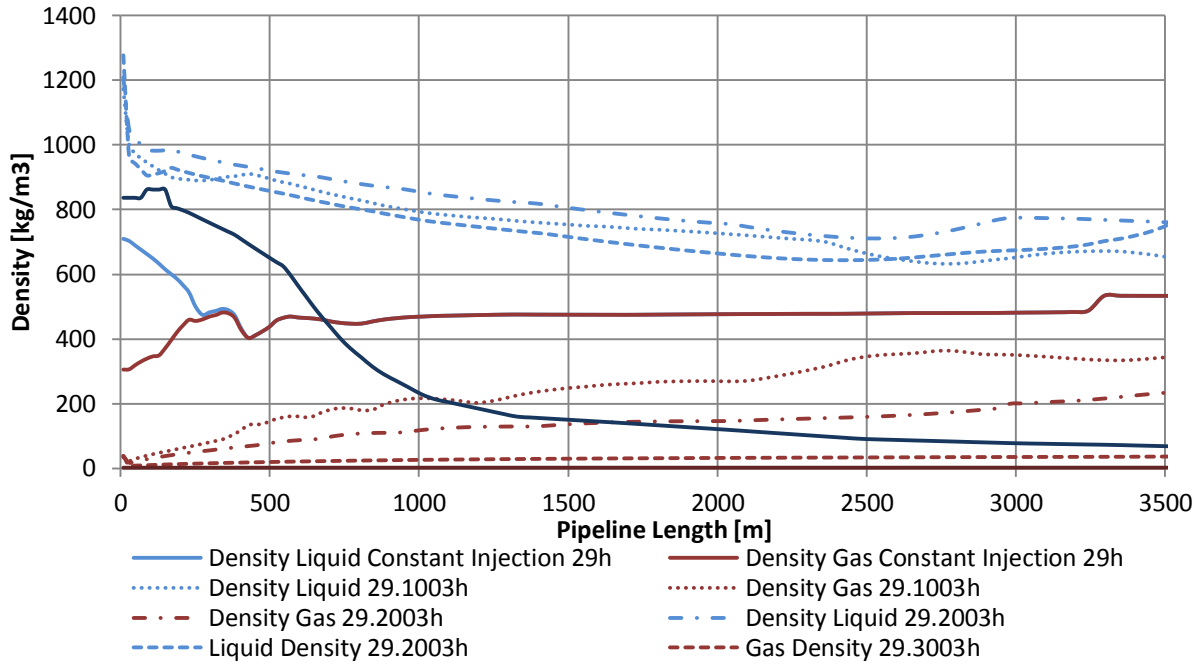
Appendix A-25 Gas Fraction Profile Sleipner Blowout NO Backflow

Flow Regime Profile Sleipner Blowout NO Backflow Flow regime: 1=Stratified, 2=Annular, 3=Slug, 4=Bubble.



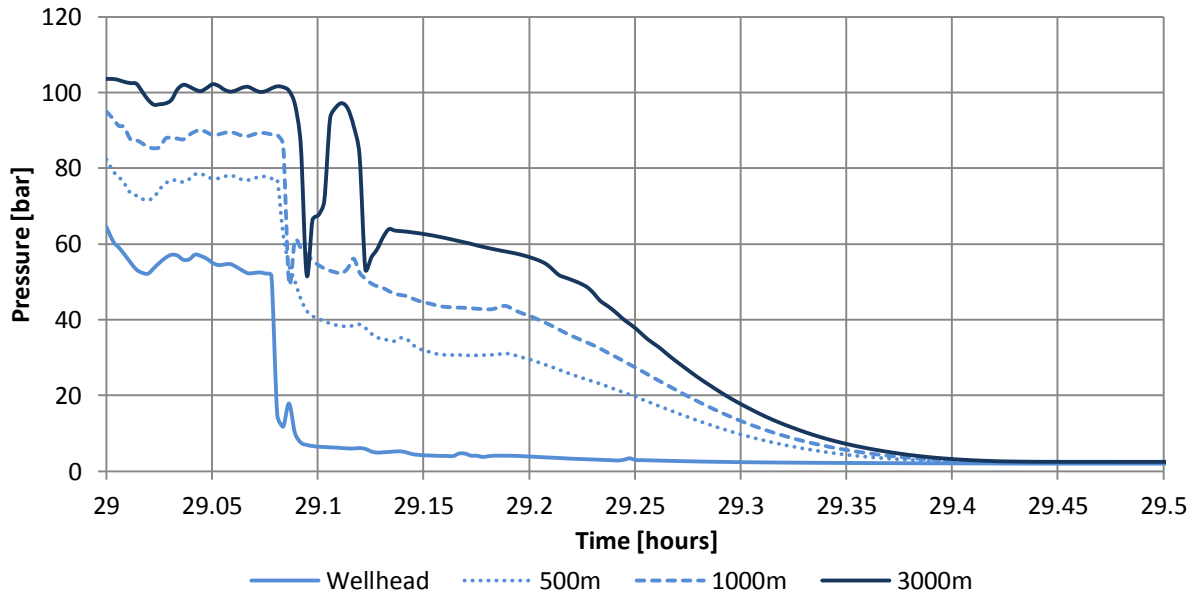
Appendix A-26 Flow Regime Profile Sleipner Blowout NO Backflow

Density Profile Sleipner Blowout NO Backflow



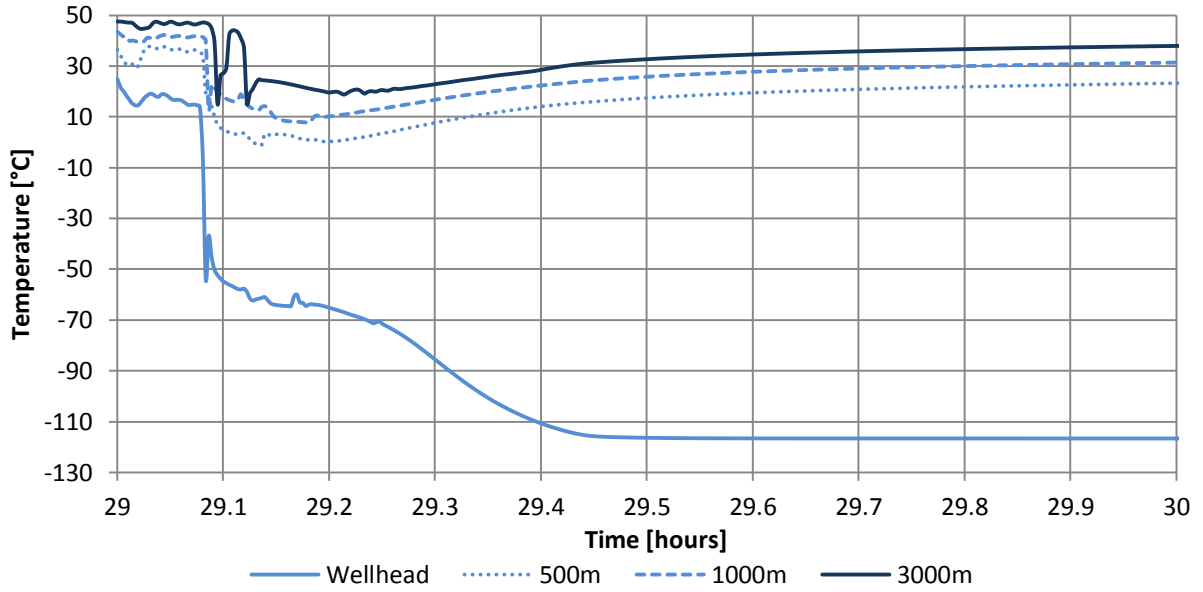
Appendix A-27 Density Profile Sleipner Blowout NO Backflow

Pressure Trend Sleipner Blowout NO Backflow



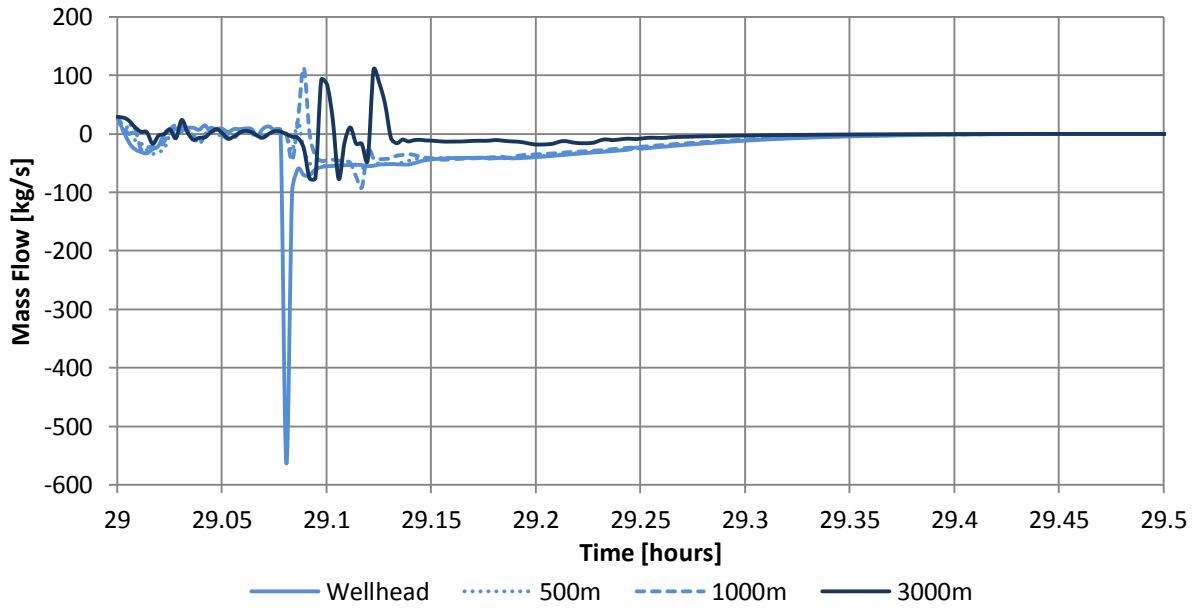
Appendix A-28 Pressure Trend Sleipner Blowout NO Backflow

Temperature Trend Sleipner Blowout NO Backflow



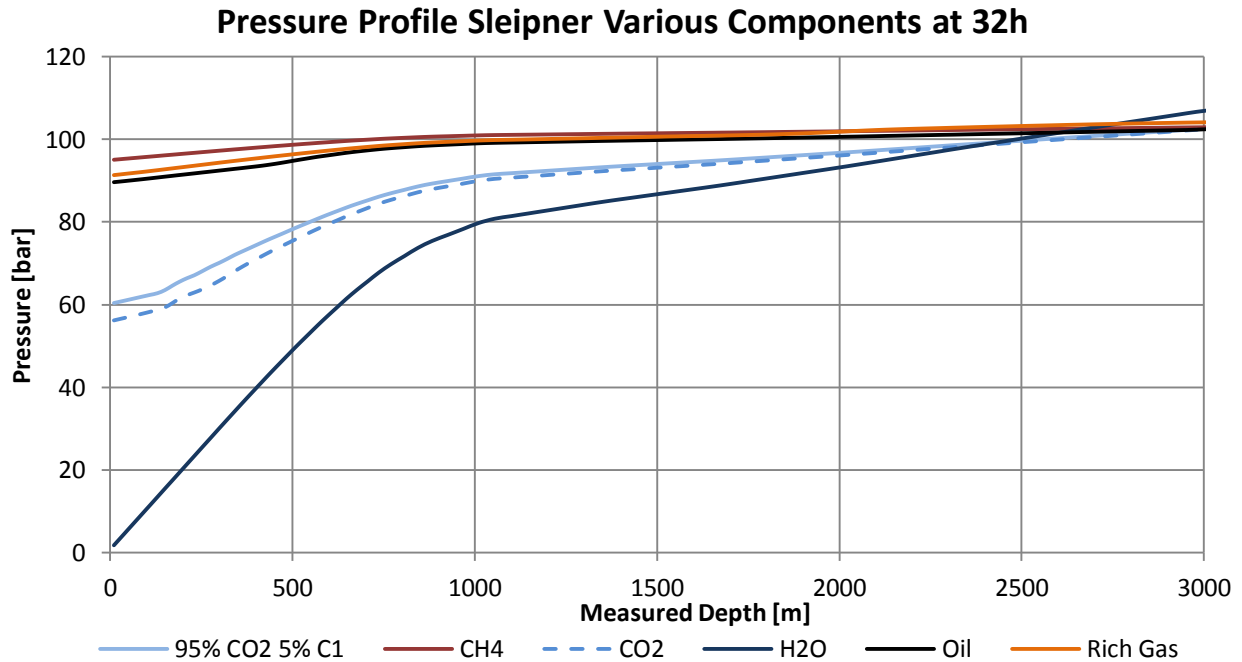
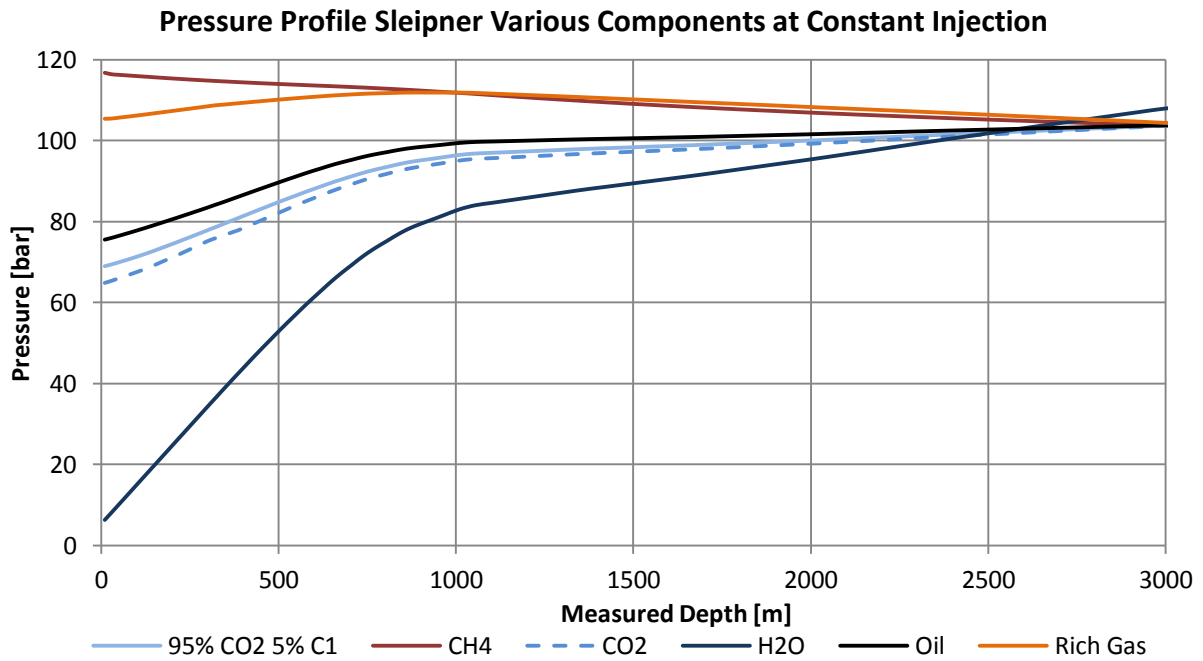
Appendix A-29 Temperature Trend Sleipner Blowout NO Backflow

Mass Flow Trend Sleipner Blowout NO Backflow

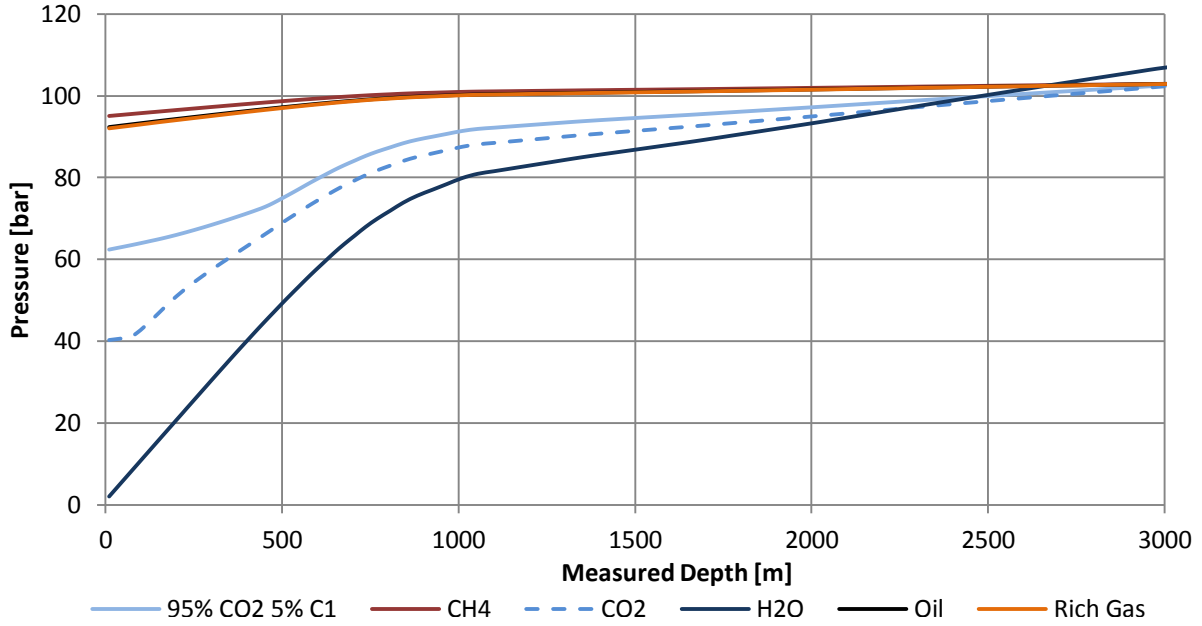


Appendix A-30 Mass Flow Trend Sleipner Blowout NO Backflow. Downwards flow is Positive.

V. SHUT-IN SLEIPNER WITH VARIOUS COMPONENTS

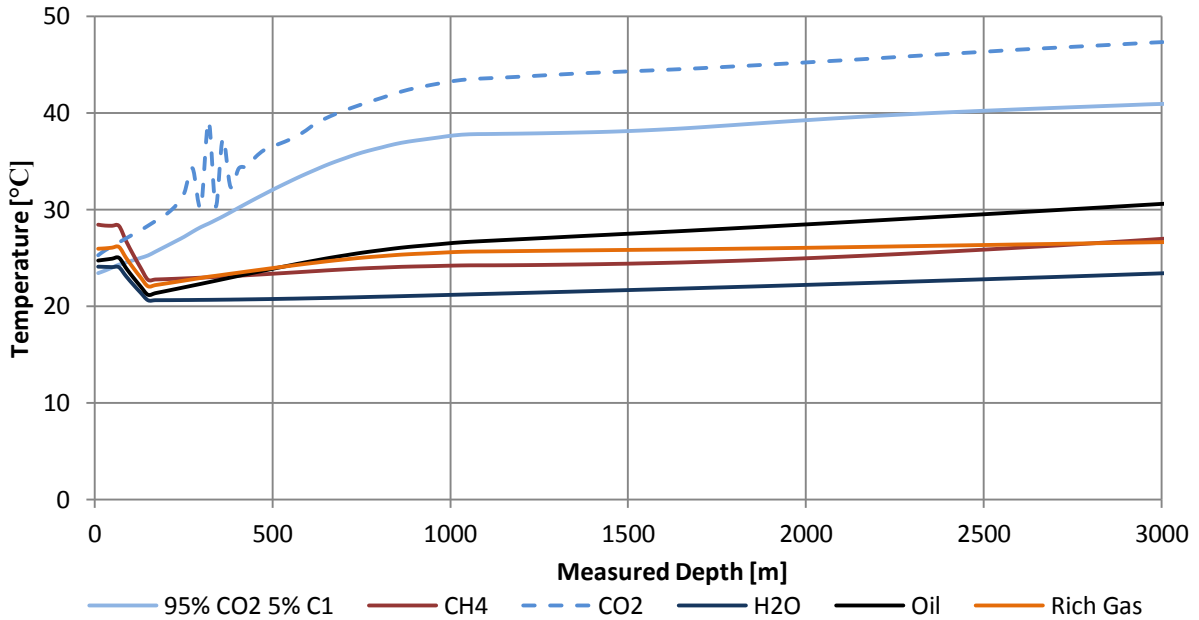


Pressure Profile Sleipner Various Components at 150h



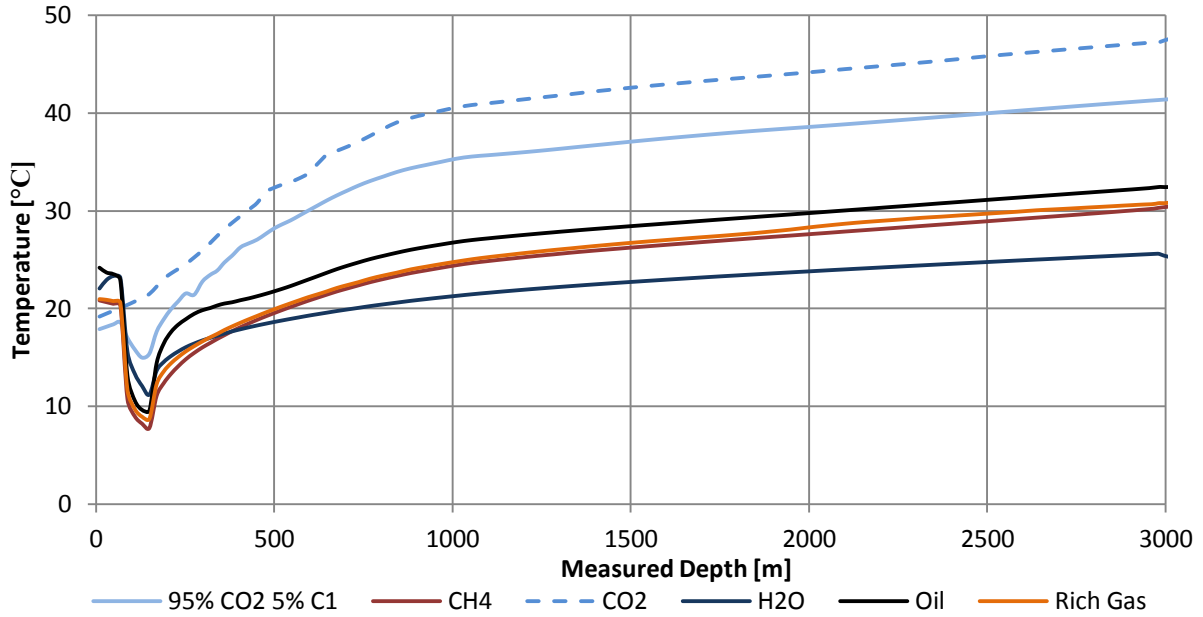
Appendix A-33 Pressure Profile Sleipner Various Components at 150h

Temperature Profile Sleipner Various Components at Constant Injection



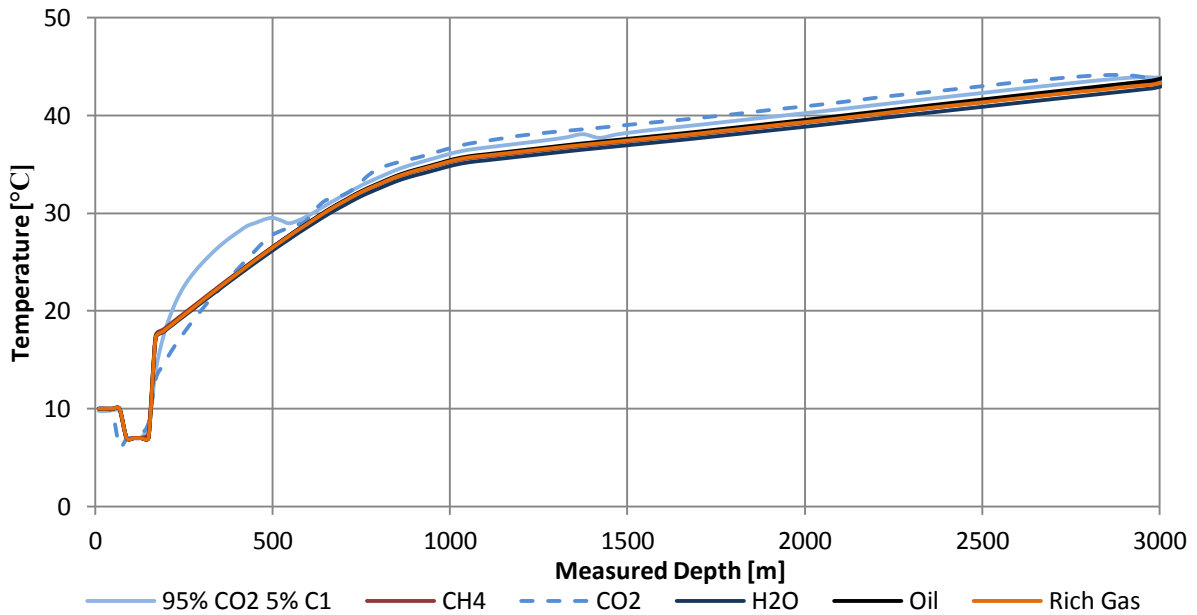
Appendix A-34 Temperature Profile Sleipner Various Components at Constant Injection

Temperature Profile Sleipner Various Components at 32h

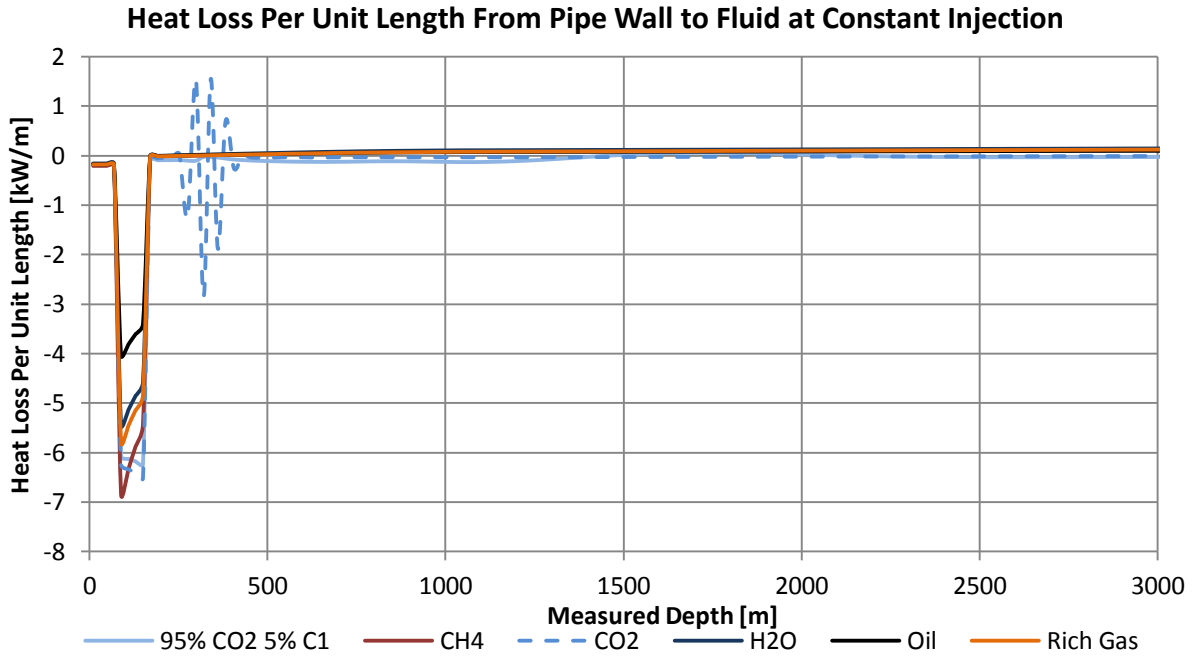


Appendix A-35 Temperature Profile Sleipner Various Components at 32h

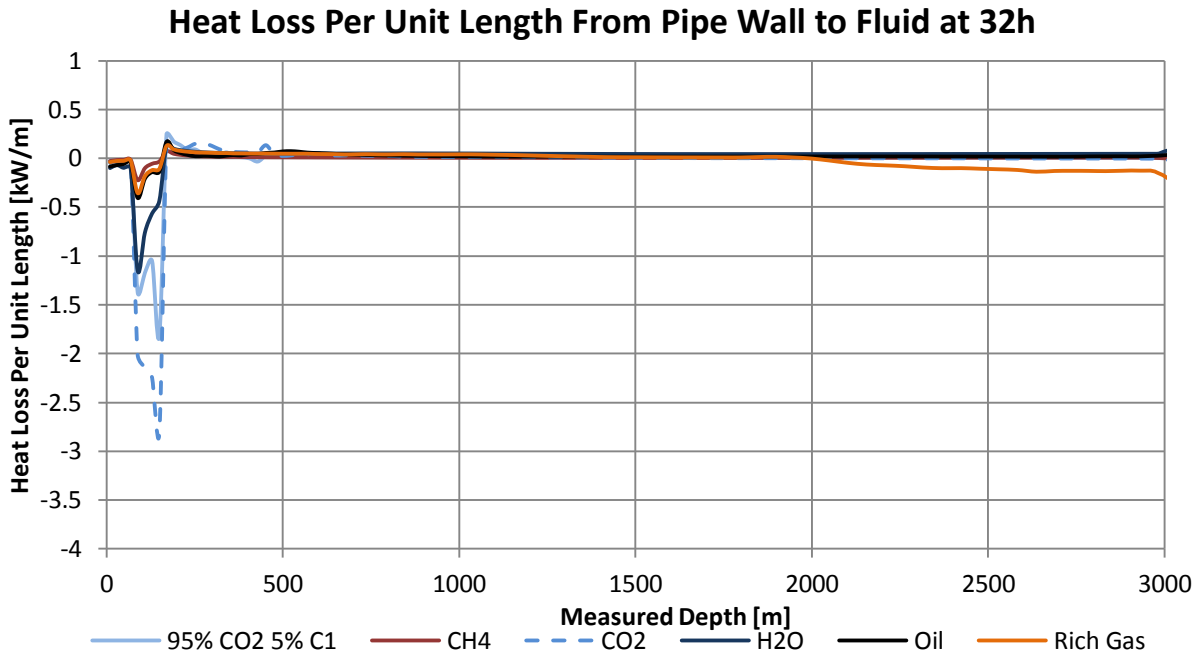
Temperature Profile Sleipner Various Components at 150h



Appendix A-36 Temperature Profile Sleipner Various Components at 150h

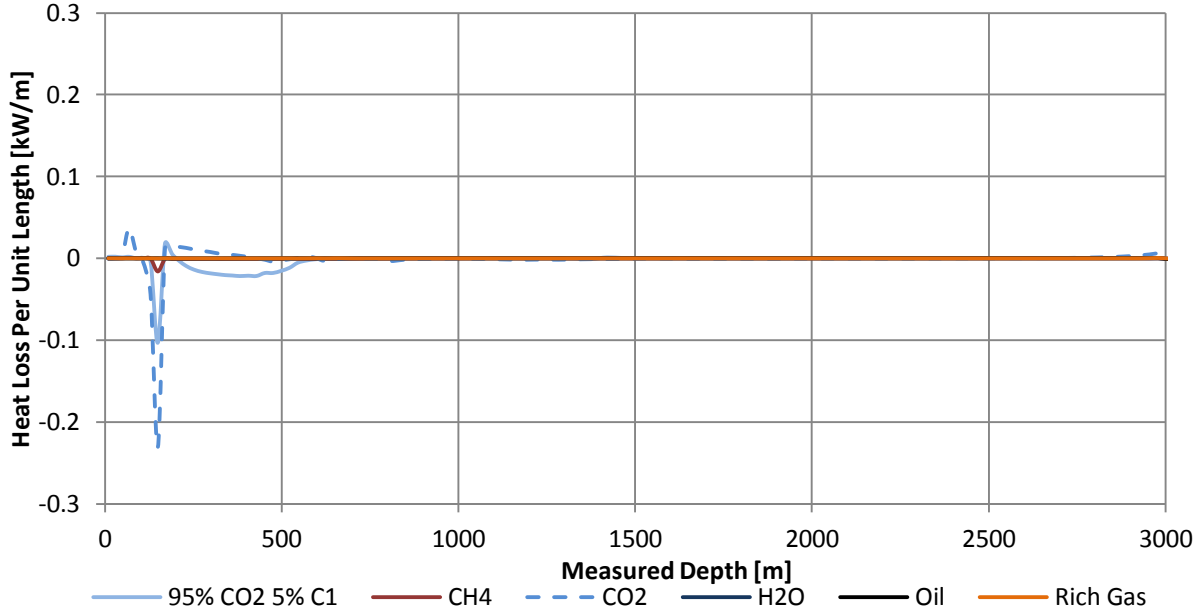


Appendix A-37 Heat Loss Per Unit Length From Pipe Wall to Fluid at Constant Injection



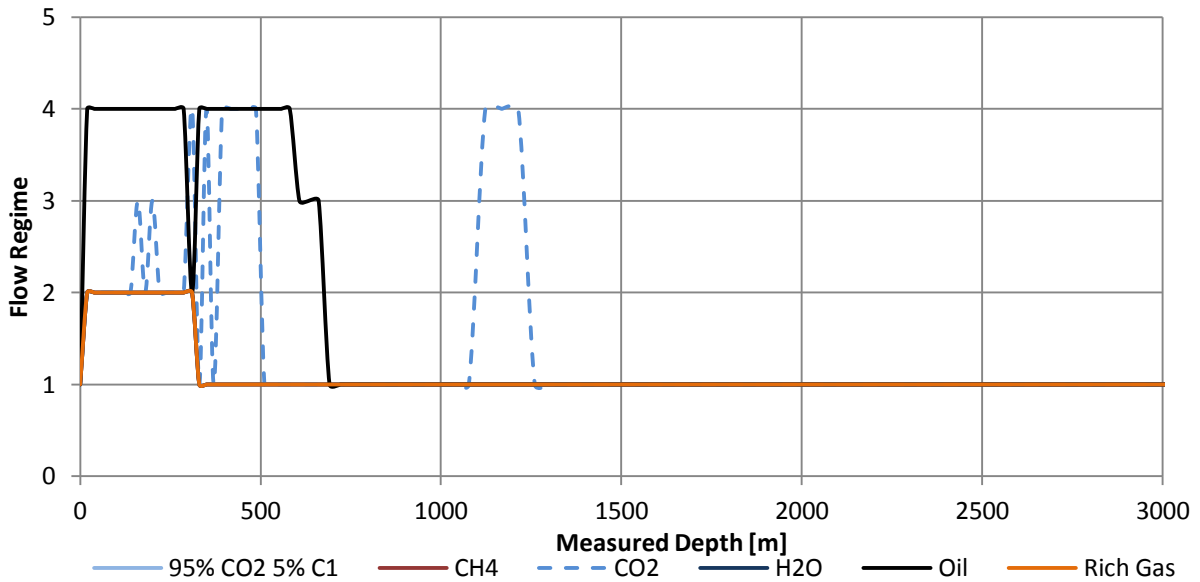
Appendix A-38 Heat Loss Per Unit Length From Pipe Wall to Fluid at 32h

Heat Loss Per Unit Length From Pipe Wall to Fluid at 150h



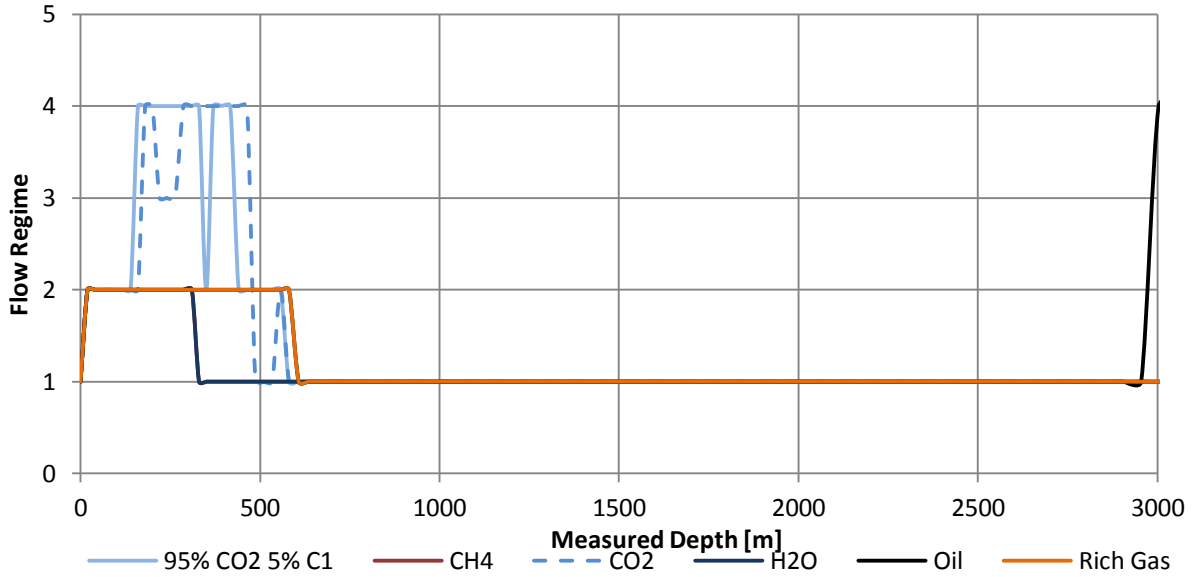
Appendix A-39 Heat Loss Per Unit Length From Pipe Wall to Fluid at 150h

Flow Regime Profile Sleipner Various Components at Constant Injection [1=Stratified, 2=Annular, 3=Slug, 4=Bubble]



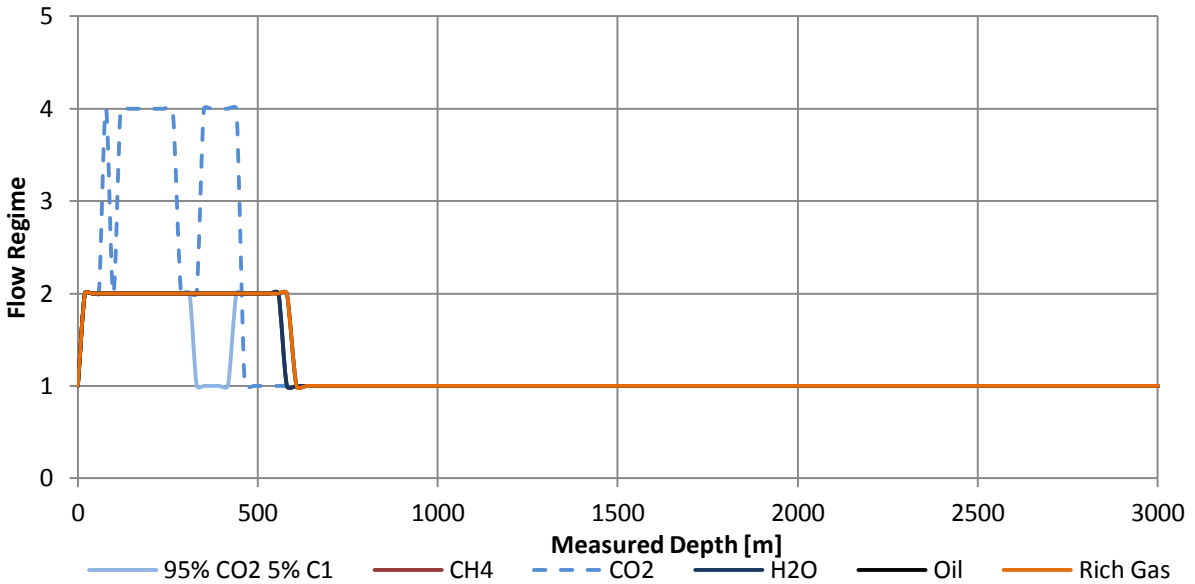
Appendix A-40 Flow Regime Profile Sleipner Various Components at Constant Injection

Flow Regime Profile Sleipner Various Components at 32h
 [1=Stratified, 2=Annular, 3=Slug, 4=Bubble]

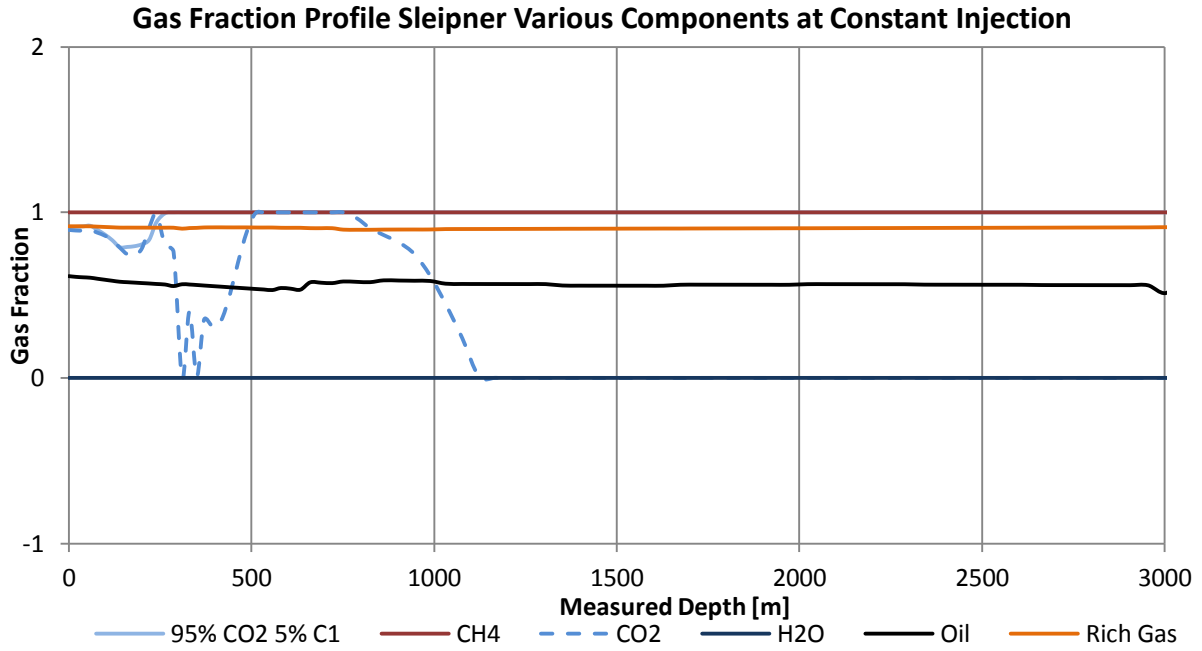


Appendix A-41 Flow Regime Profile Sleipner Various Components at 32h

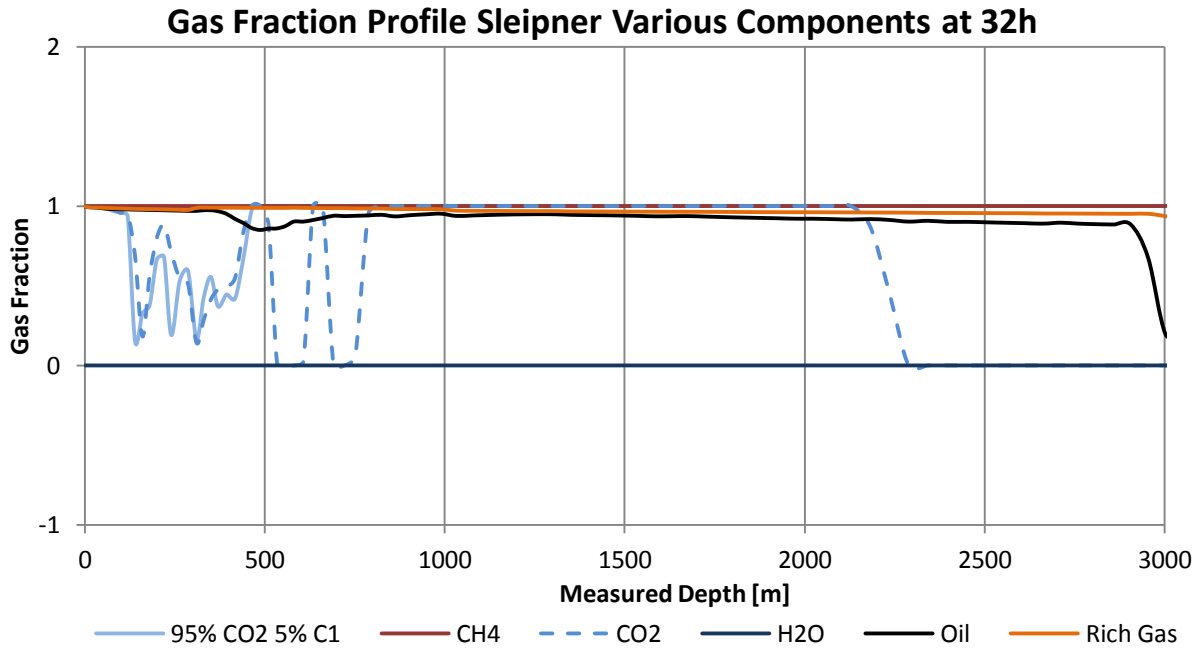
Flow Regime Profile Sleipner Various Components at 150h
 [1=Stratified, 2=Annular, 3=Slug, 4=Bubble]



Appendix A-42 Flow Regime Profile Sleipner Various Components at 150h

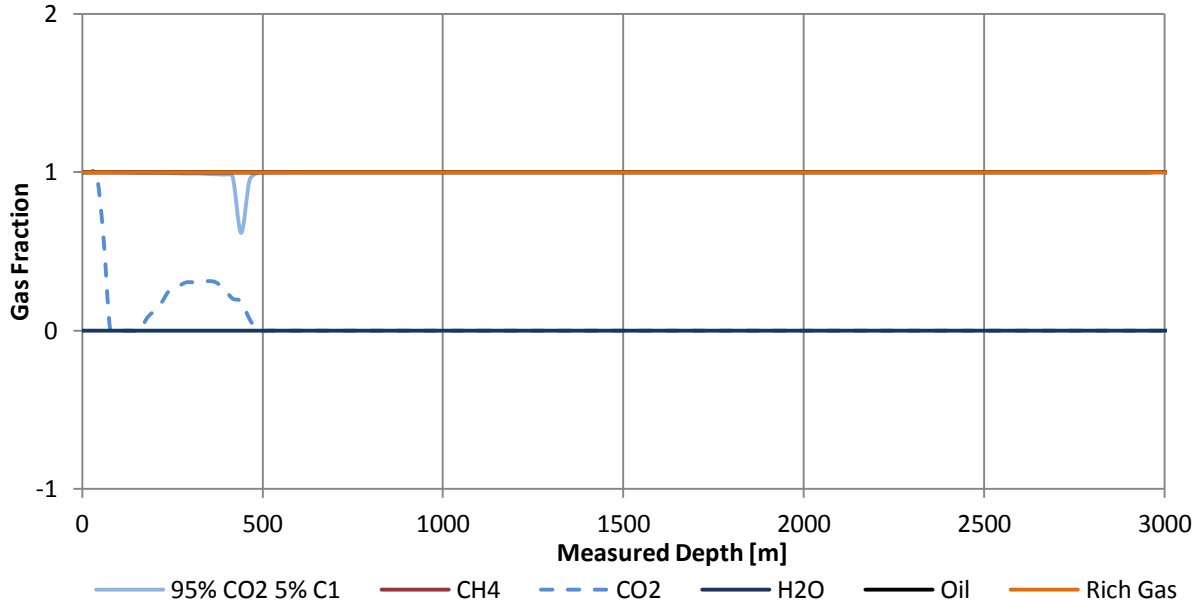


Appendix A-43 Gas Fraction Profile Sleipner Various Components at Constant Injection



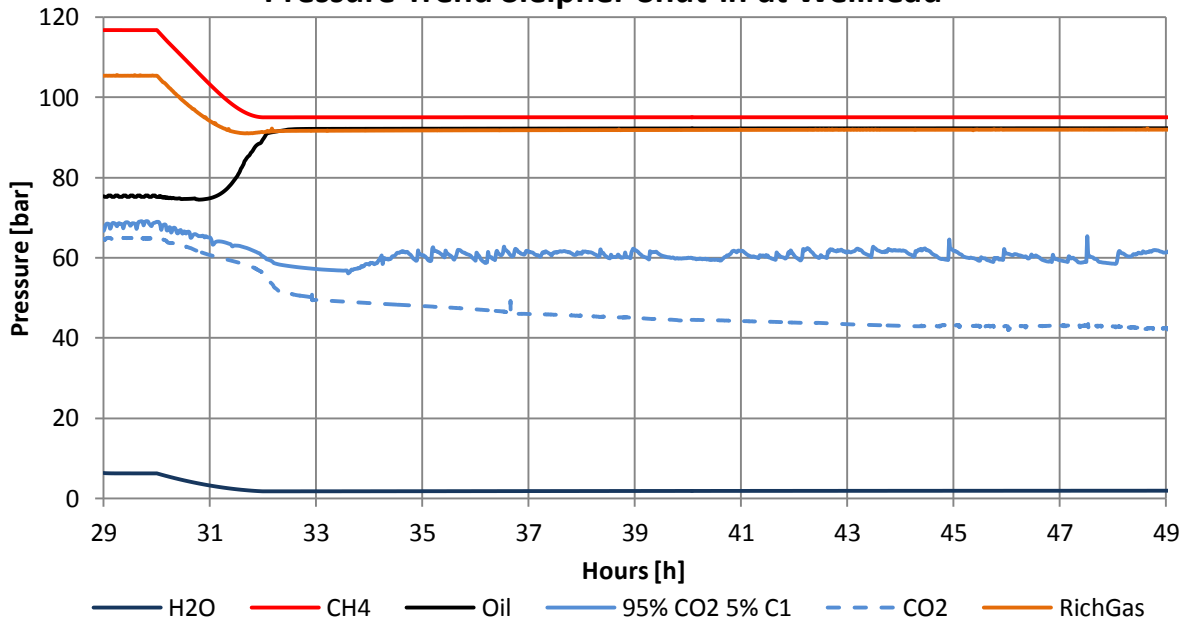
Appendix A-44 Gas Fraction Profile Sleipner Various Components at 32h

Gas Fraction Profile Sleipner Various Components at 150h



Appendix A-45 Gas Fraction Profile Sleipner Various Components at 150h

Pressure Trend Sleipner Shut-in at Wellhead



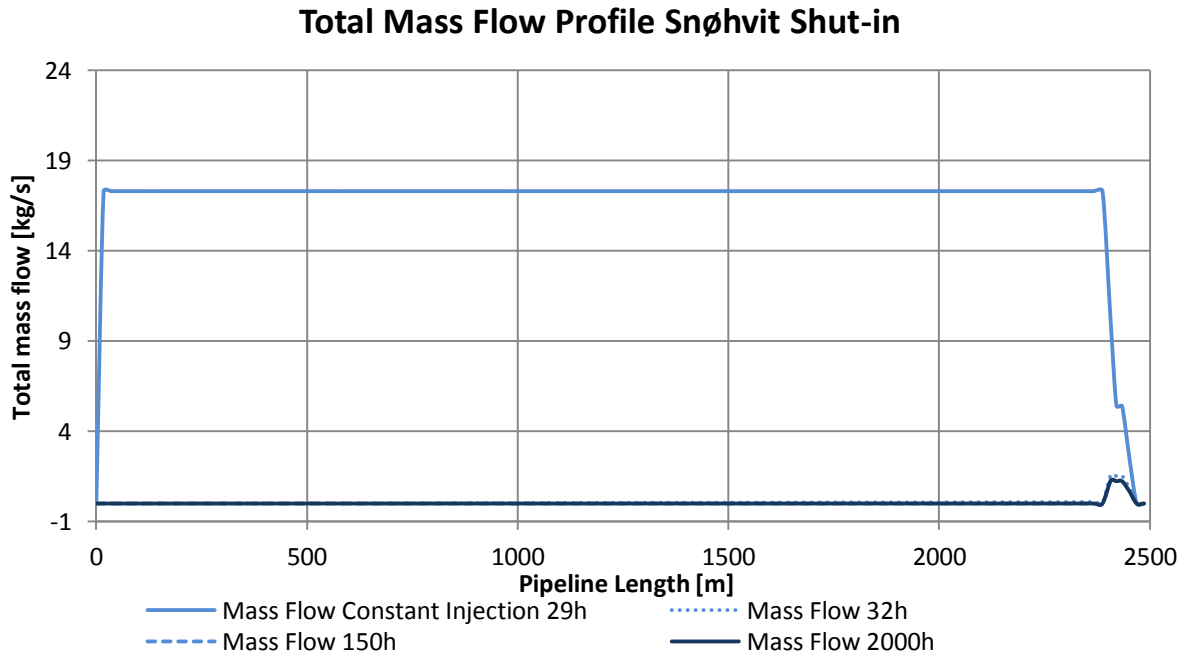
Appendix A-46 Pressure Trend Sleipner Shut-in at Wellhead

Component	Chemical formula	Wellstream
Water	H ₂ O	3.00
Nitrogen	N ₂	0.50
Carbon dioxide	CO ₂	3.00
Methane	CH ₄	75.00
Ethane	C ₂ H ₆	7.50
Propane	C ₃ H ₈	4.00
Butane	I-C ₄ H ₁₀	0.60
Normal butane	N-C ₄ H ₁₀	1.00
Pentane	I-C ₅ H ₁₂	0.30
Normal pentane	N-C ₅ H ₁₂	0.30
Hexane +	C ₆ +	4.80

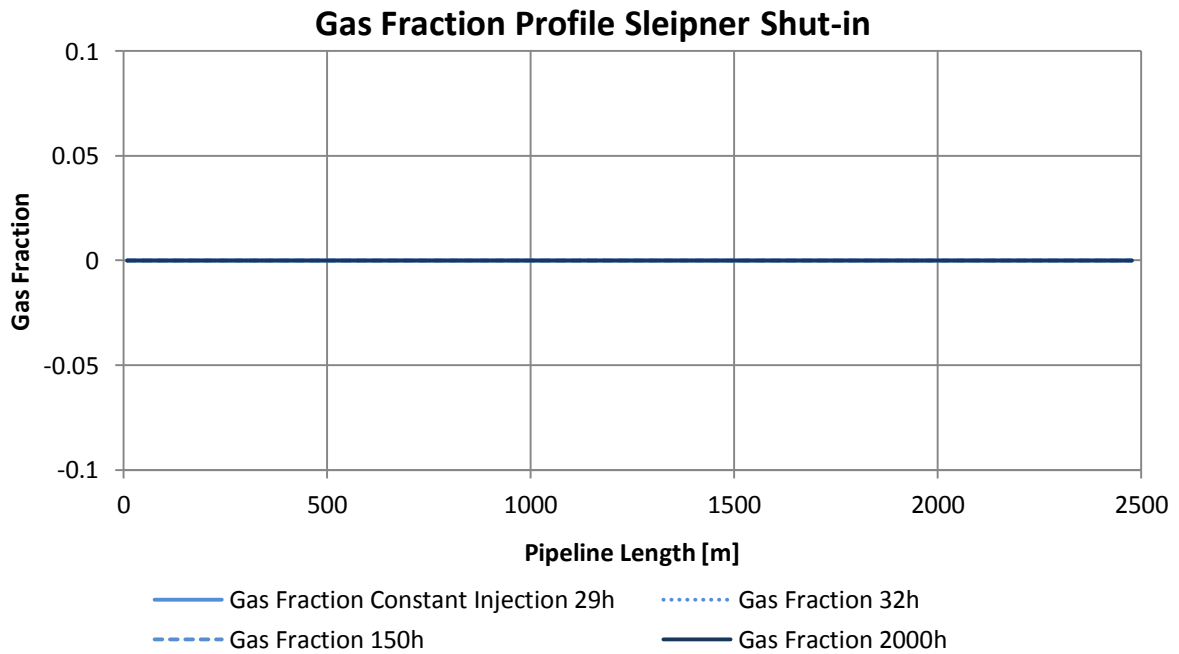
Appendix A-47 Rich Gas Composition (TEP4185, 2011)

B SNØHVIT FIGURES

I. SHUT-IN SINGLE COMPONENT MODULE CO₂

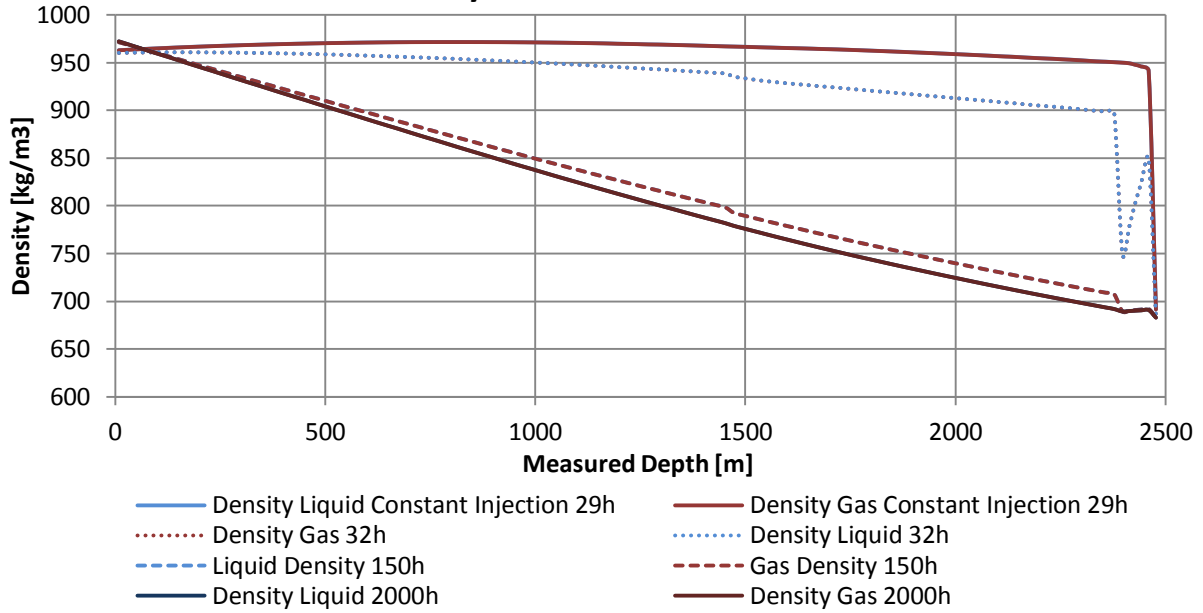


Appendix B-1 Total Mass Flow Profile Snøhvit Shut-in



Appendix B-2 Gas Fraction Profile Sleipner Shut-in

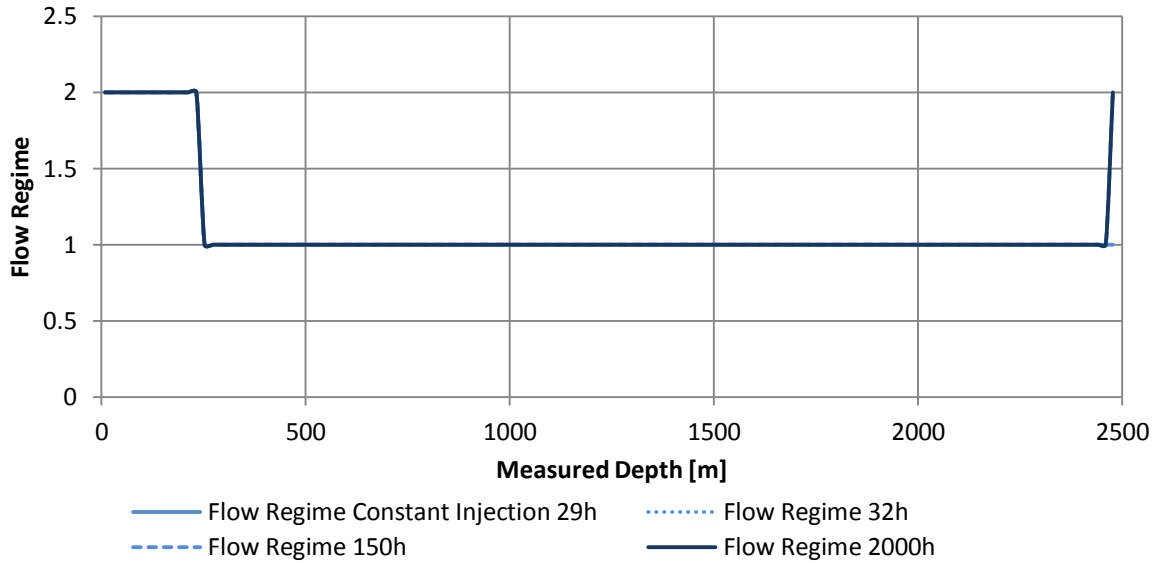
Density Profile Snøhvit Shut-in



Appendix B-3 Density Profile Snøhvit Shut-in

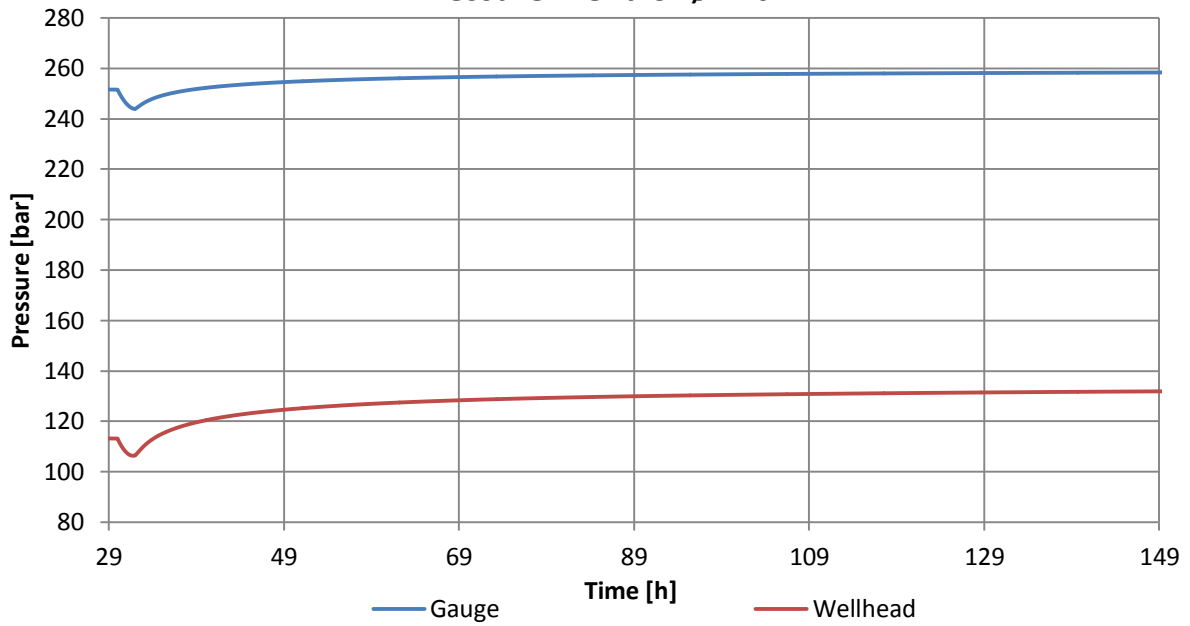
Flow Regime Profile Snøhvit

Flow regime: 1=Stratified, 2=Annular, 3=Slug, 4=Bubble.



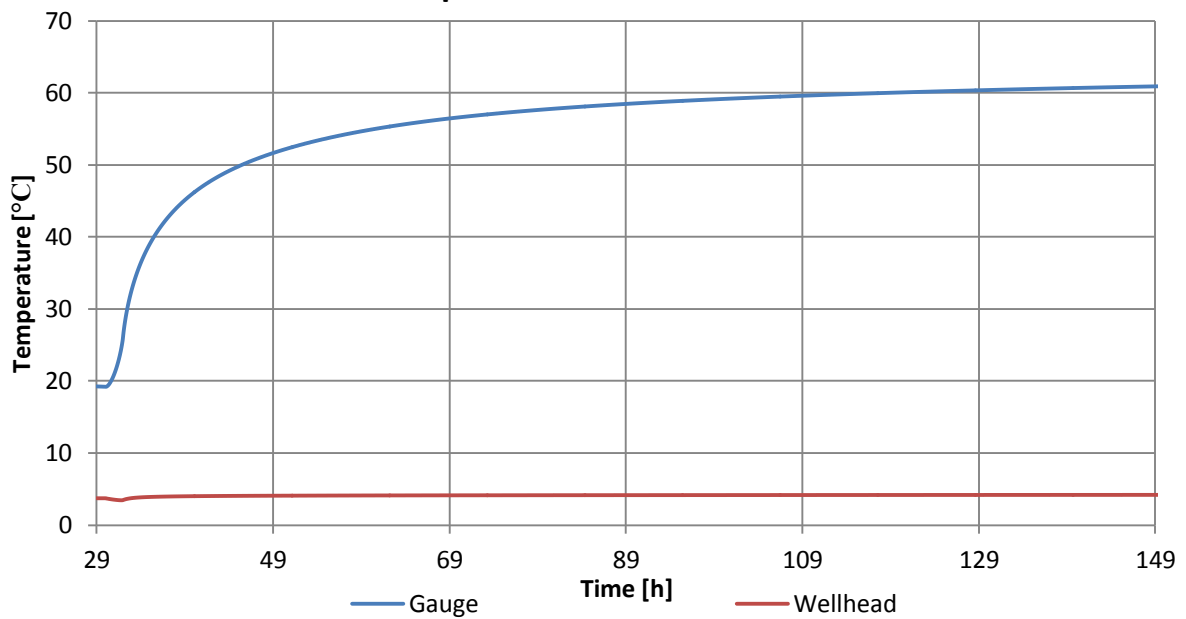
Appendix B-4 Flow Regime Profile Snøhvit Shut-in

Pressure Trend Snøhvit



Appendix B-5 Pressure Trend Snøhvit

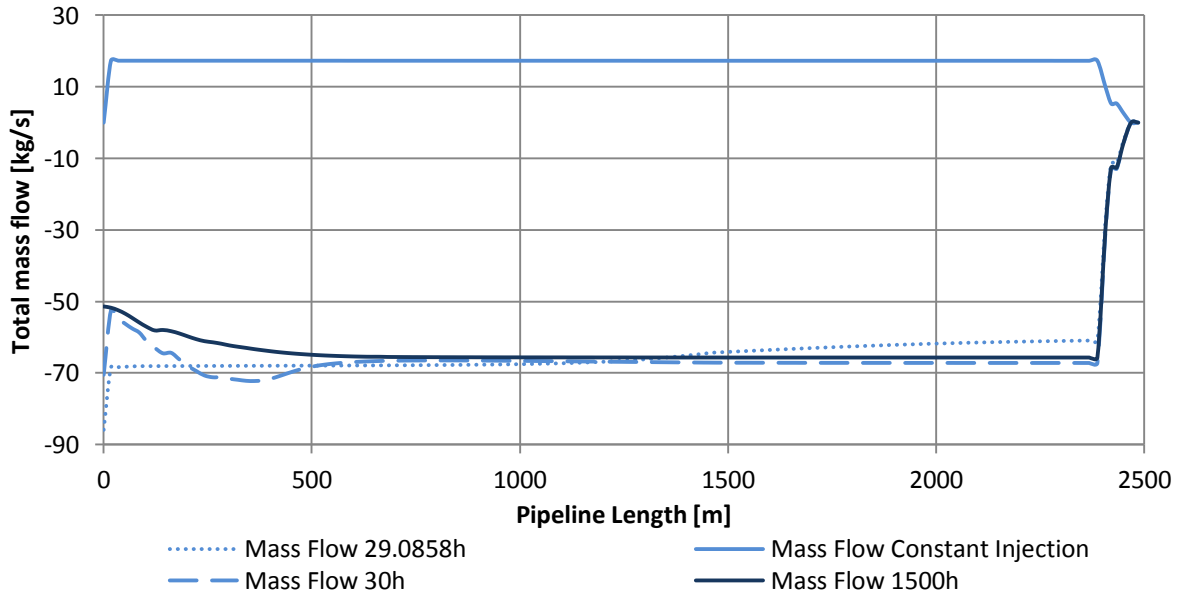
Temperature Trend Snøhvit



Appendix B-6 Temperature Trend Snøhvit

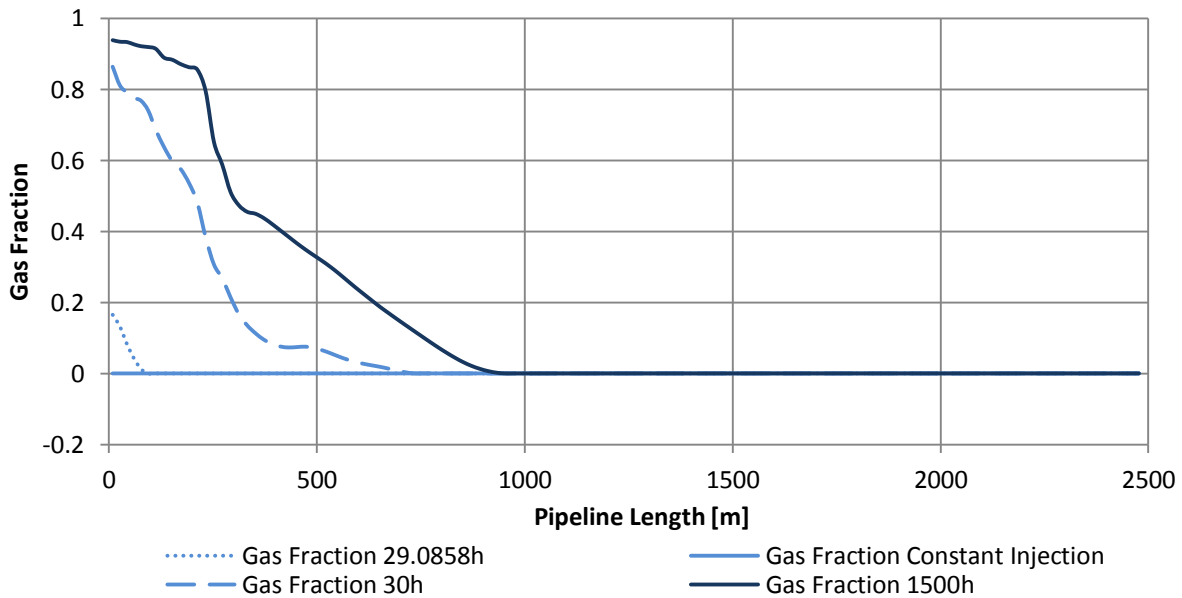
II. BLOWOUT CO₂ WITH RESERVOIR BACKFLOW

Total Mass Flow Profile Snøhvit Blowout With Backflow



Appendix B-7 Total Mass Flow Profile Snøhvit Blowout With Backflow

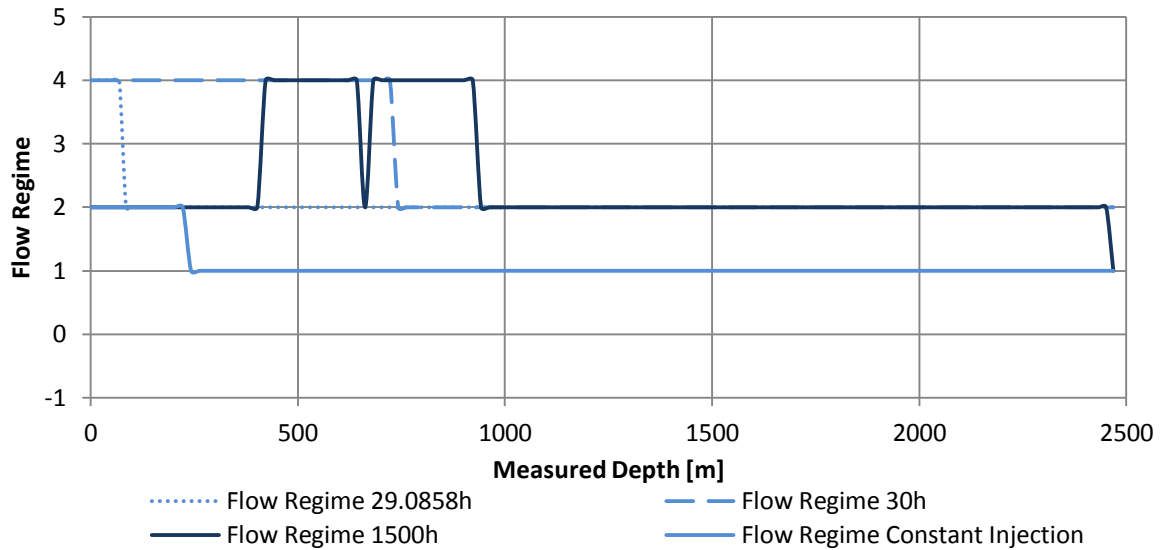
Gas Fraction Profile Sleipner Blowout With Backflow



Appendix B-8 Gas Fraction Profile Sleipner Blowout With Backflow

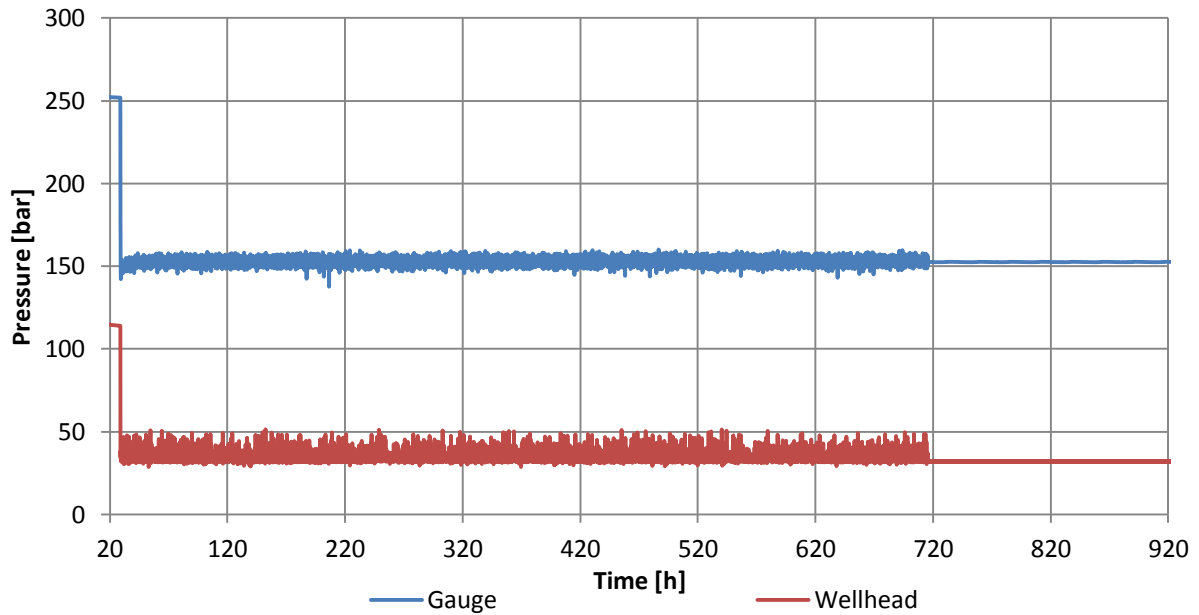
Flow Regime Profile Snøhvit Blowout With Backflow

Flow regime: 1=Stratified, 2=Annular, 3=Slug, 4=Bubble.

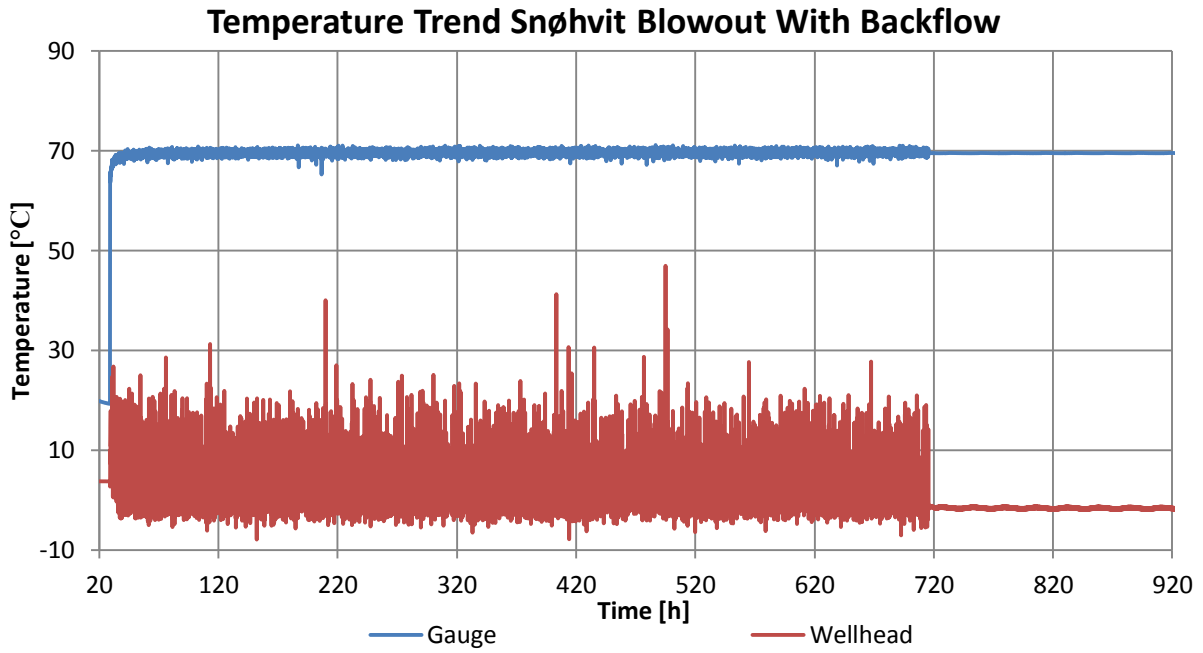


Appendix B-9 Flow Regime Profile Snøhvit Blowout With Backflow

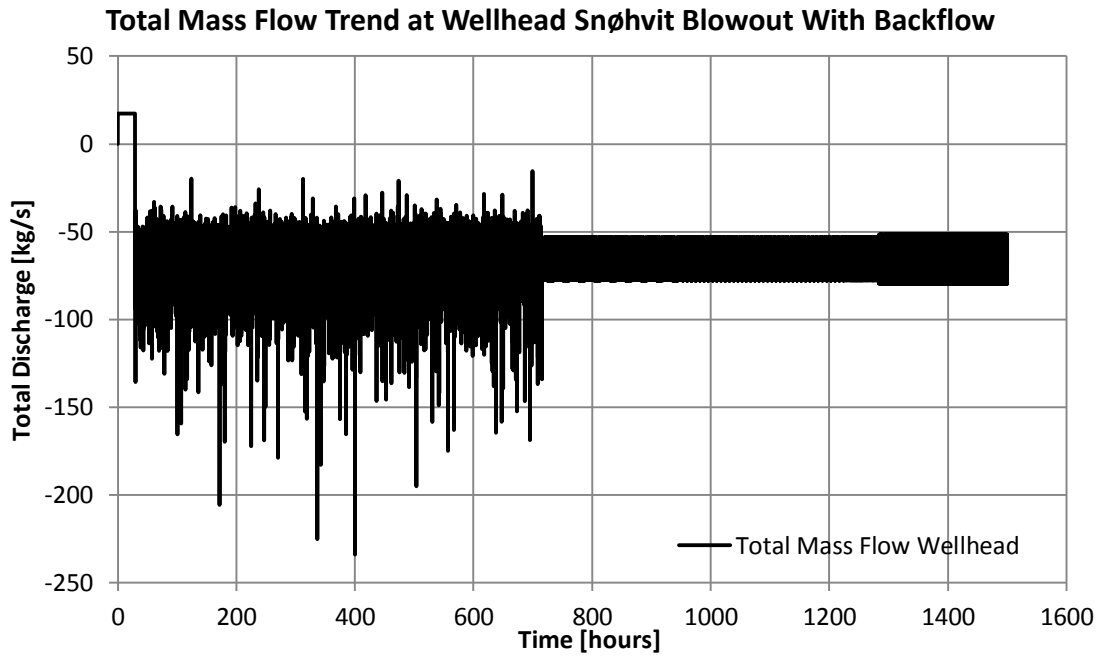
Pressure Trend Snøhvit Blowout With Backflow



Appendix B-10 Pressure Trend Snøhvit Blowout With Backflow

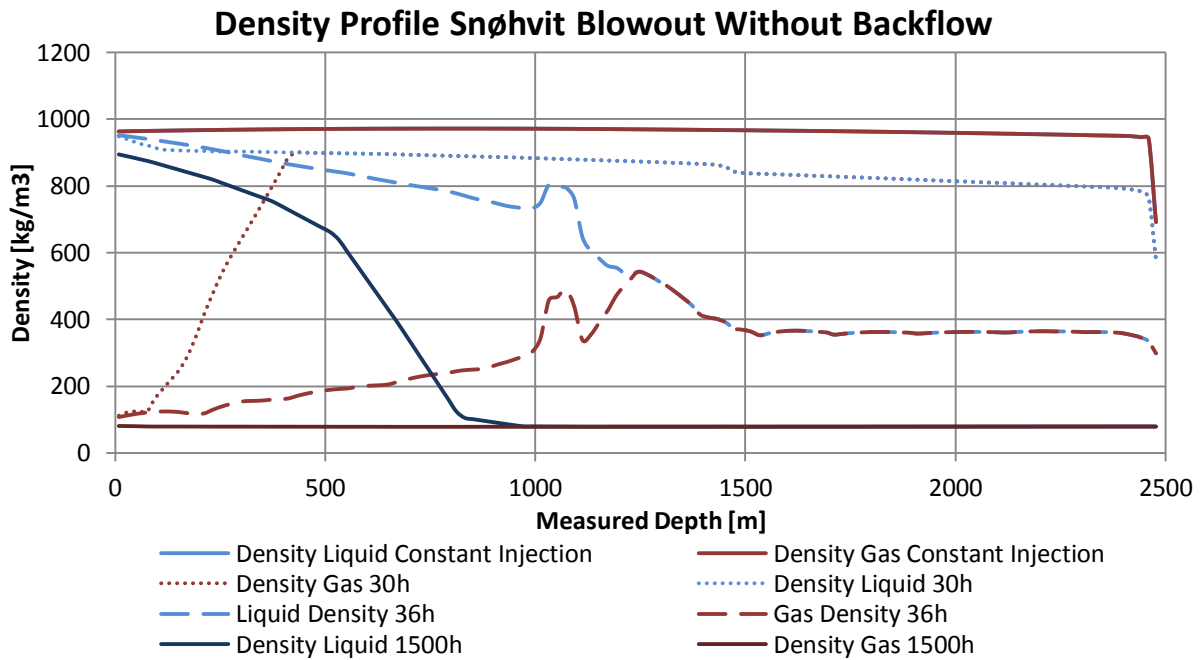


Appendix B-11 Temperature Trend Snøhvit Blowout With Backflow

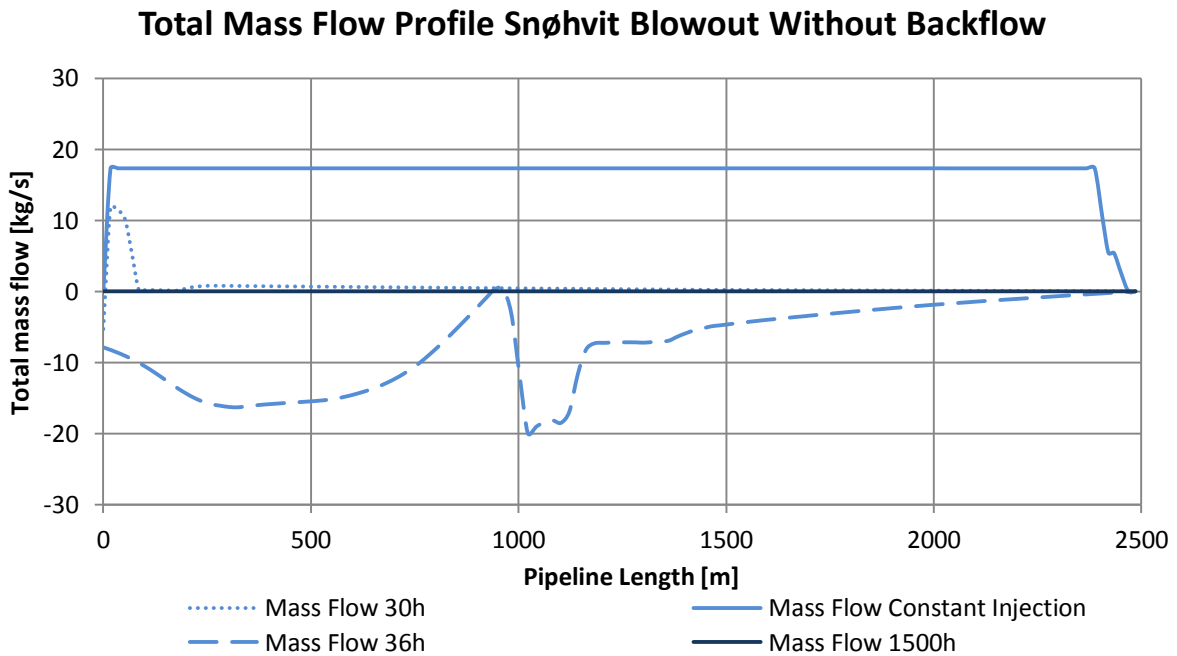


Appendix B-12 Total Mass Flow Trend at Wellhead Snøhvit Blowout With Backflow

III. BLOWOUT CO₂ WITHOUT RESERVOIR BACKFLOW

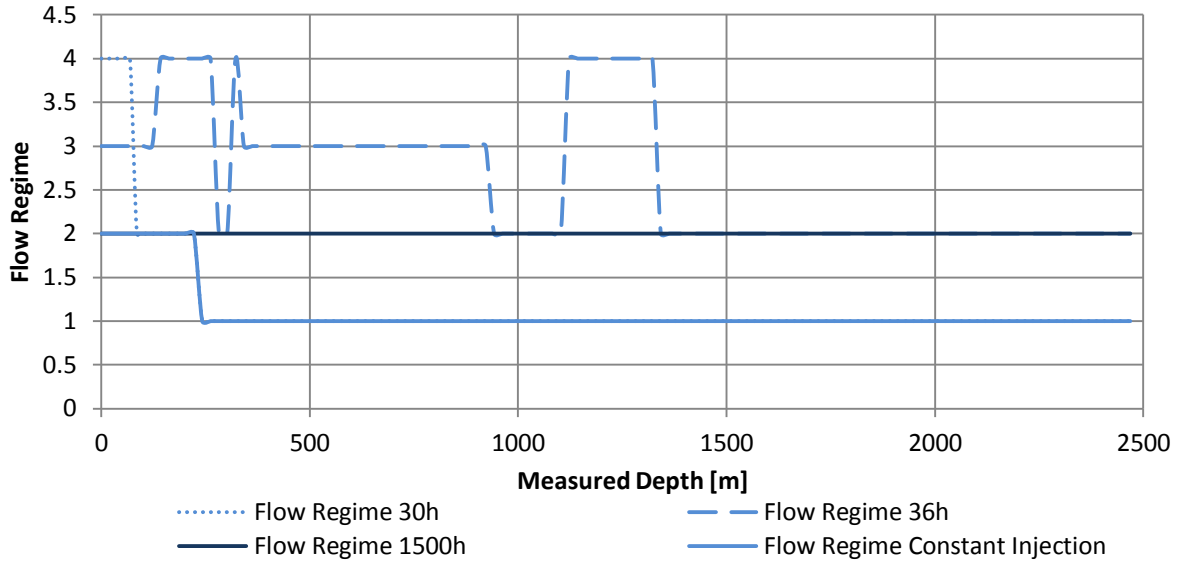


Appendix B-13 Density Profile Snøhvit Blowout Without Backflow



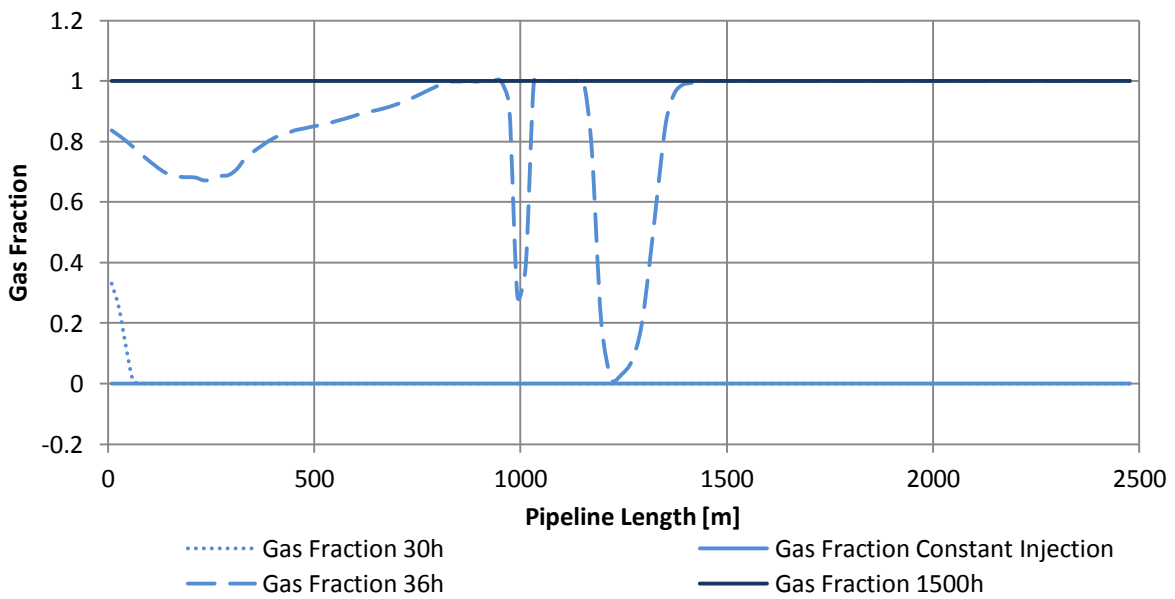
Appendix B-14 Total Mass Flow Profile Snøhvit Blowout Without Backflow

Flow Regime Profile Snøhvit Blowout Without Backflow
 Flow regime: 1=Stratified, 2=Annular, 3=Slug, 4=Bubble.



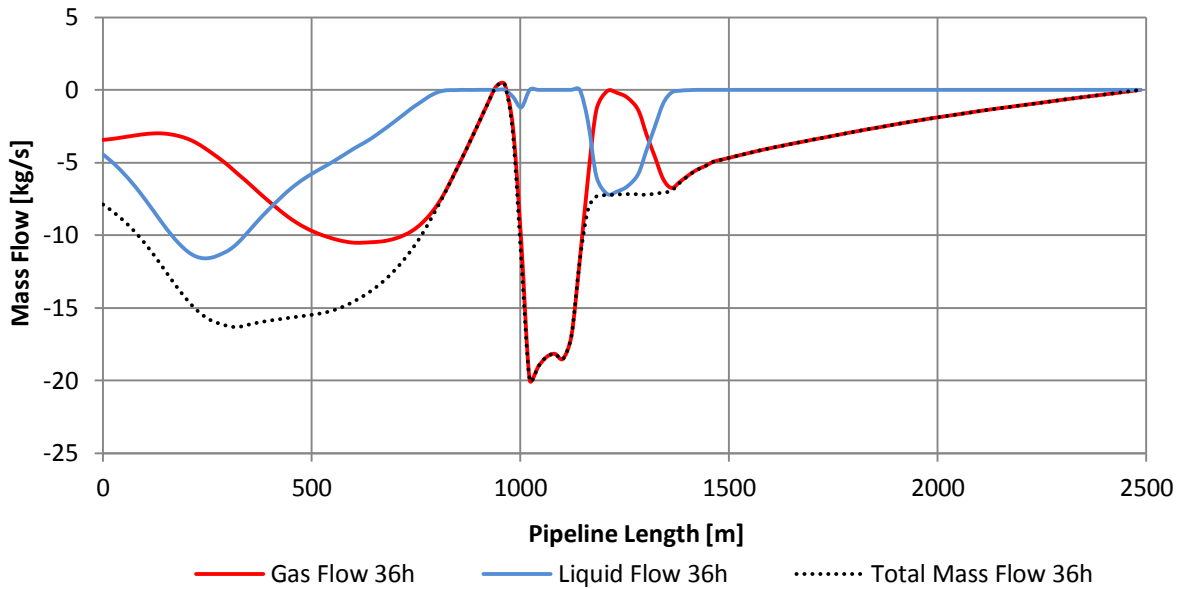
Appendix B-15 Flow Regime Profile Snøhvit Blowout Without Backflow

Gas Fraction Profile Sleipner Blowout Without Backflow



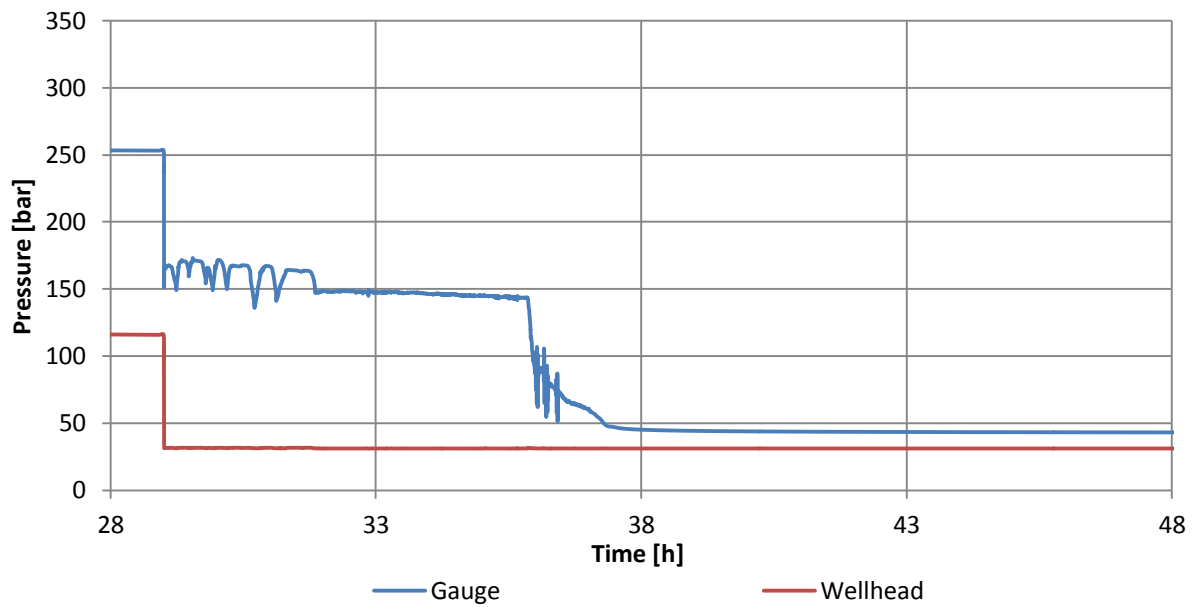
Appendix B-16 Gas Fraction Profile Sleipner Blowout Without Backflow

Flow Profile Snøhvit Blowout Without Backflow at 36h



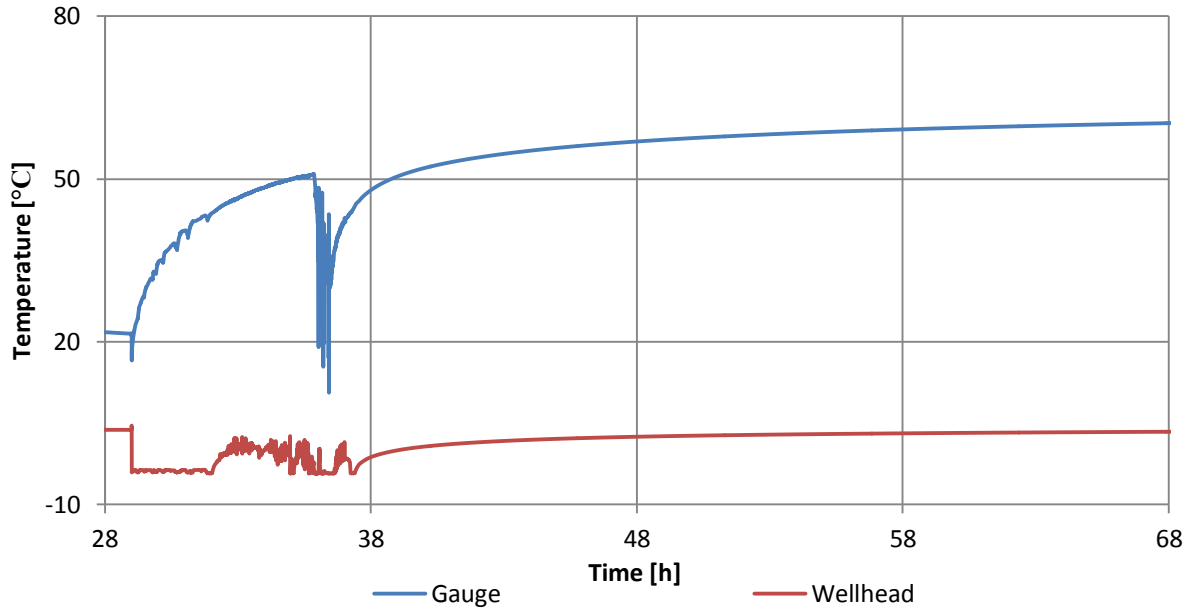
Appendix B-17 Flow Profile Snøhvit Blowout Without Backflow at 36h

Pressure Trend Snøhvit Blowout Witout Backflow at Wellhead



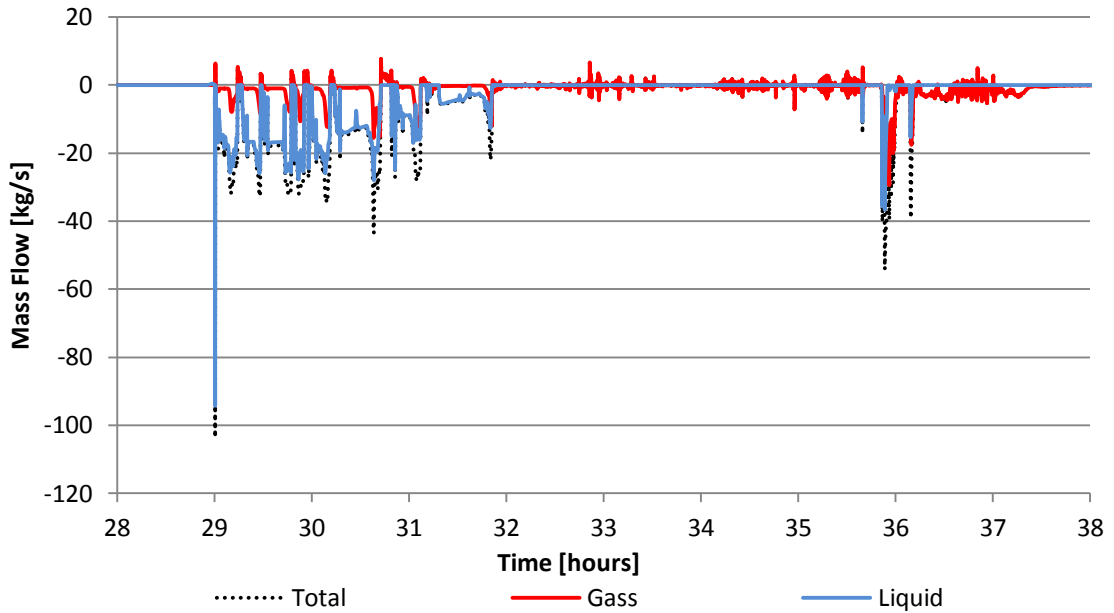
Appendix B-18 Pressure Trend Snøhvit Blowout Without Backflow at Wellhead

Temperature Trend Snøhvit Blowout Witout Backflow at Wellhead



Appendix B-19 Temperature Trend Snøhvit Blowout Without Backflow at Wellhead

Mass Flow Trend Snøhvit Blowout Witout Backflow at Wellhead

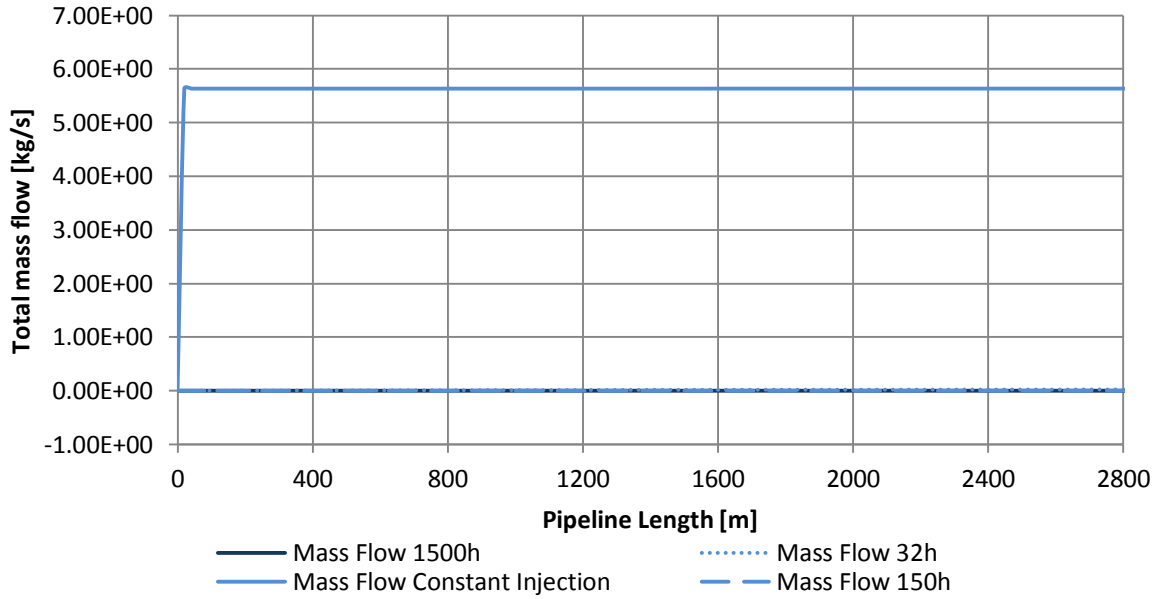


Appendix B-20 Mass Flow Trend Snøhvit Blowout Without Backflow at Wellhead

C IN SALAH FIGURES

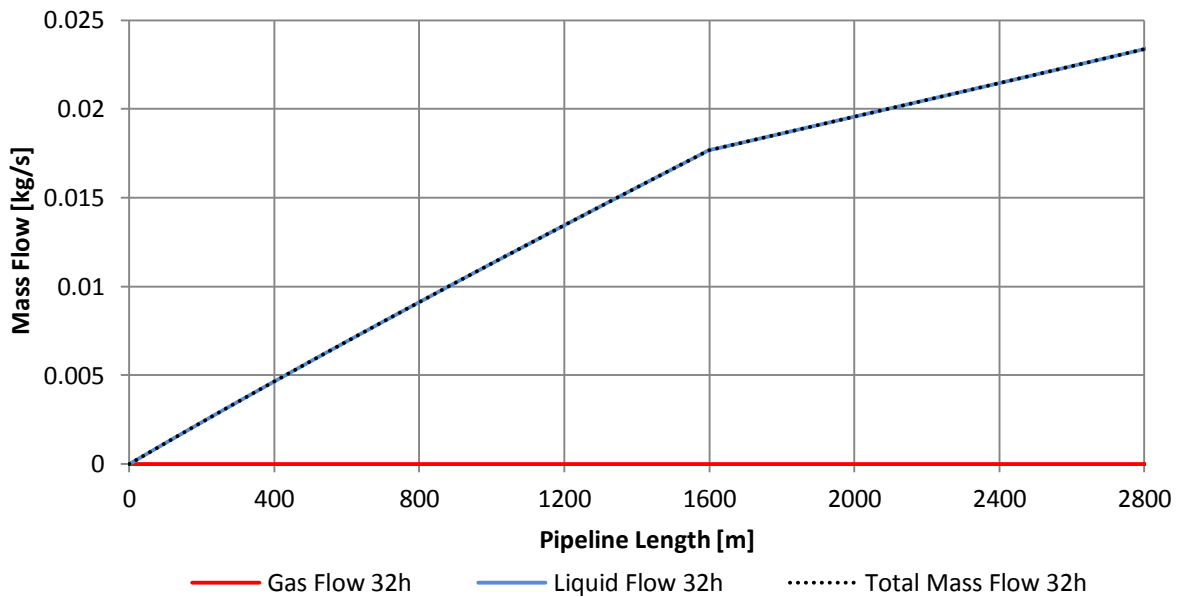
I. SHUT-IN SINGLE COMPONENT MODULE CO₂

Total Mass Flow Profile In Salah Shut-in



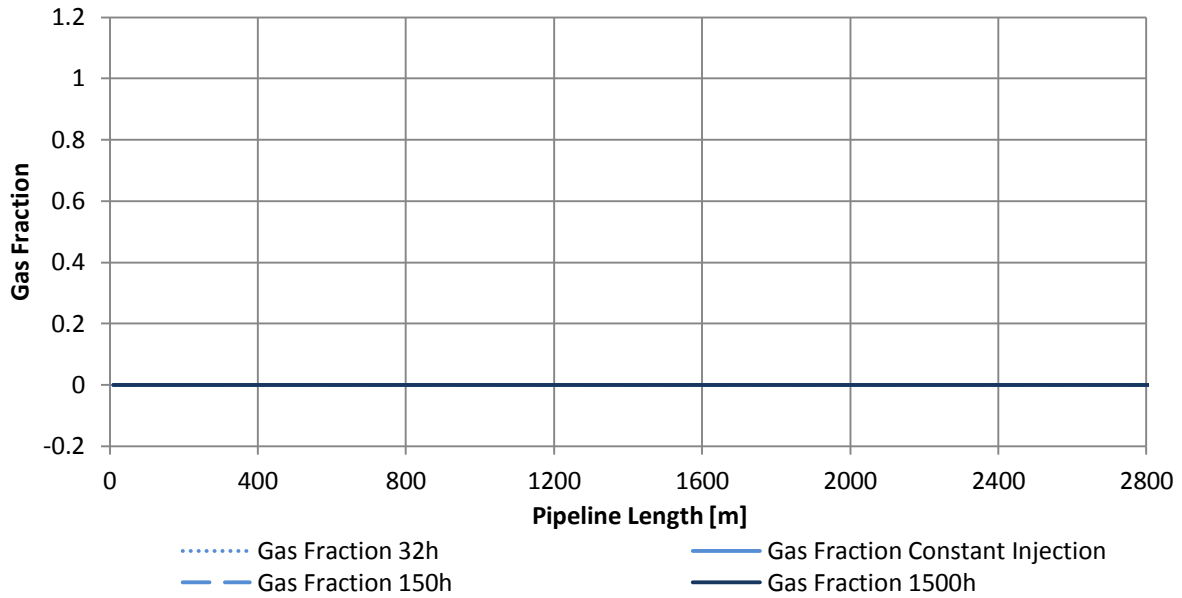
Appendix C-1 Total Mass Flow Profile In Salah Shut-in

Flow Profile In Salah Shut-in 32h



Appendix C-2 Flow Profile In Salah Shut-in 32h

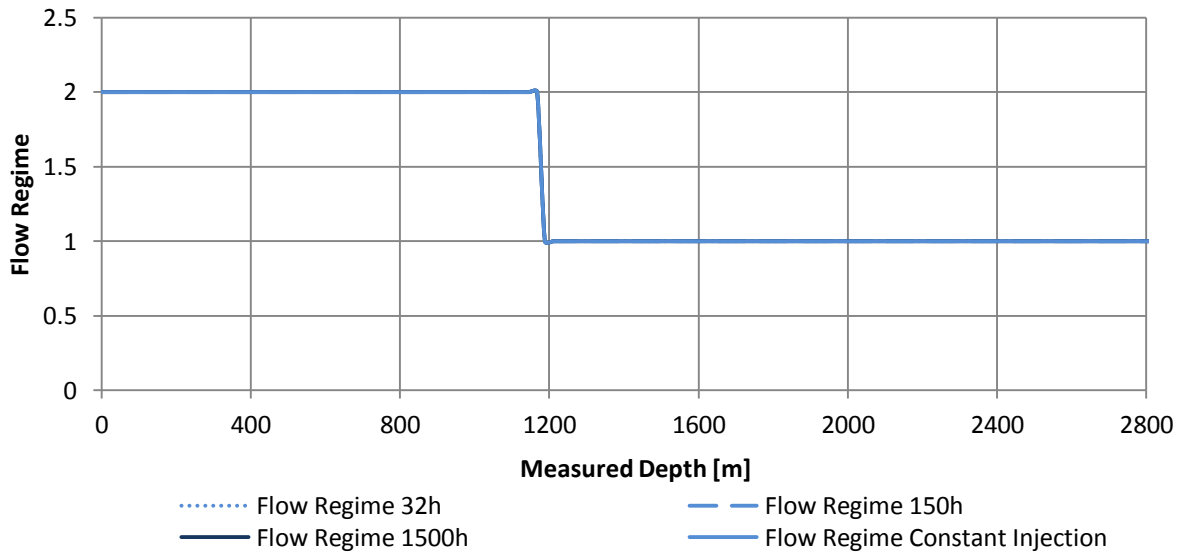
Gas Fraction Profile In Salah Shut-in



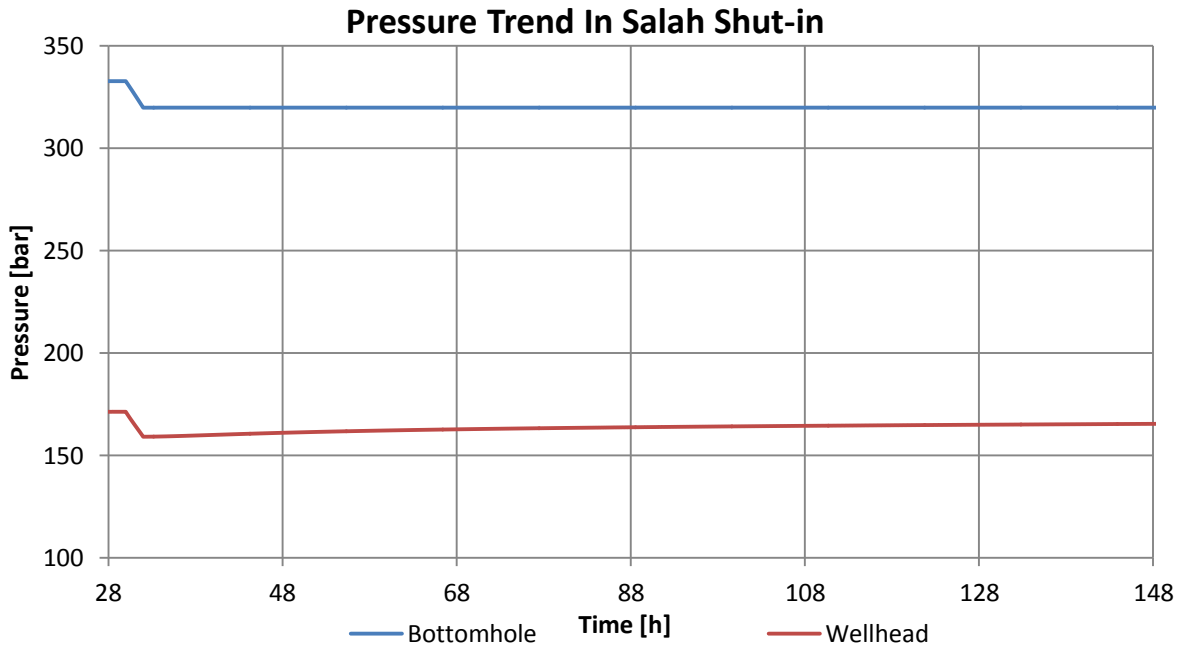
Appendix C-3 Gas Fraction Profile In Salah Shut-in

Flow Regime Profile In Salah Shut-in

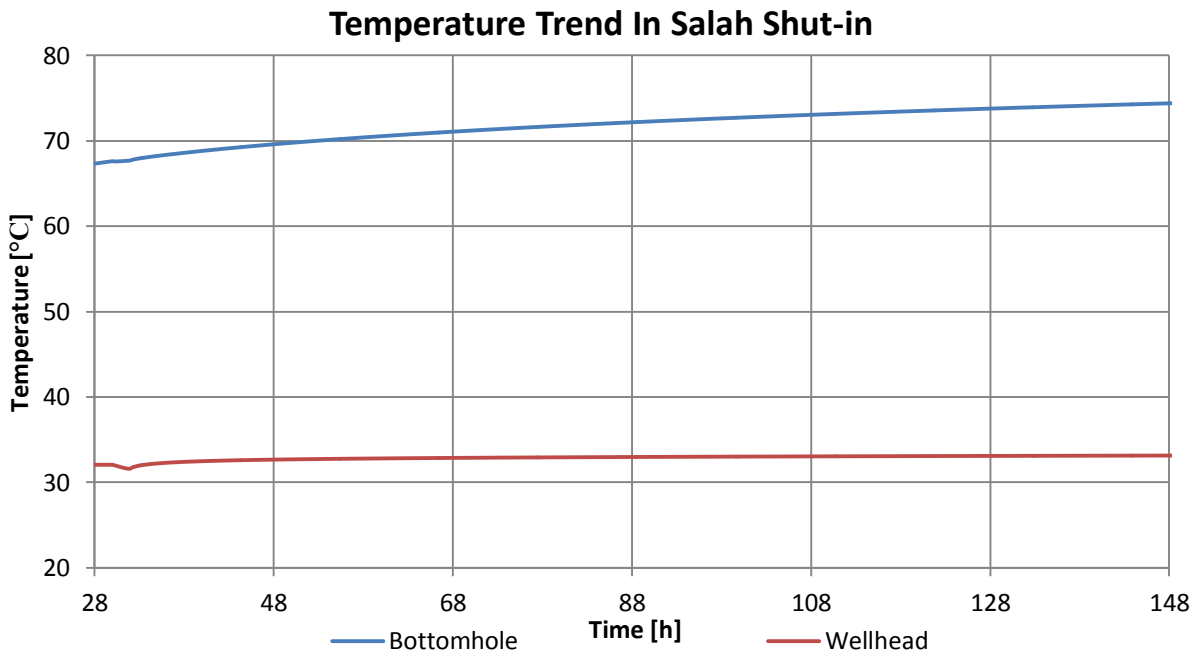
Flow regime: 1=Stratified, 2=Annular, 3=Slug, 4=Bubble.



Appendix C-4 Flow Regime Profile In Salah Shut-in

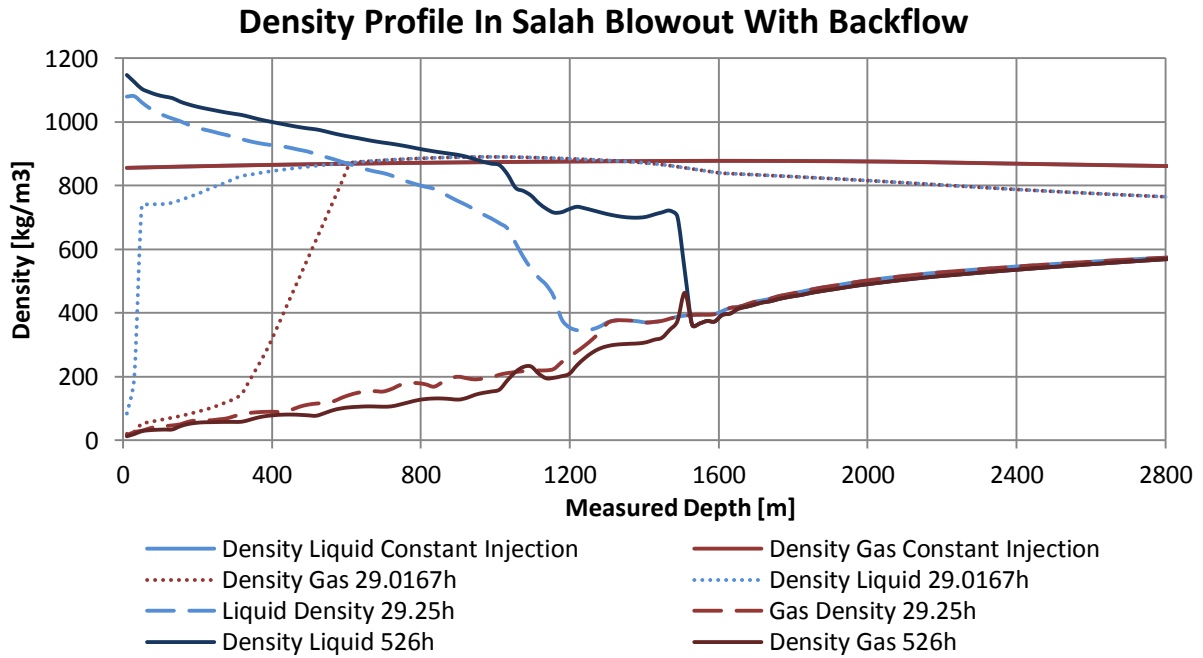


Appendix C-5 Pressure Trend In Salah Shut-in

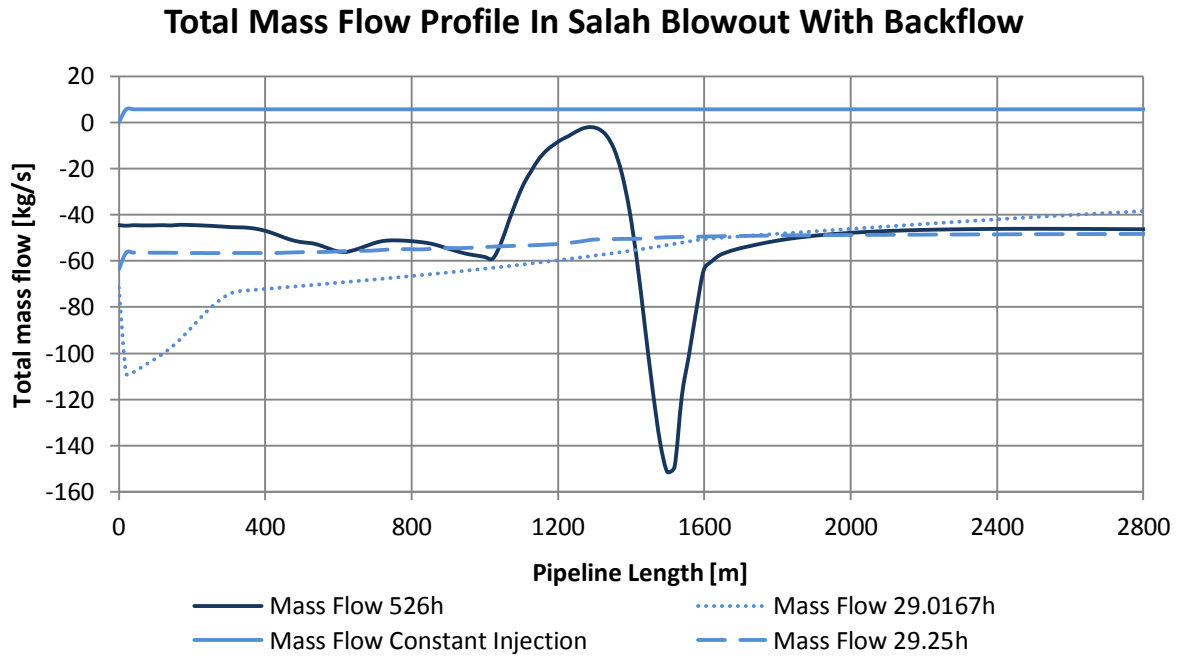


Appendix C-6 Temperature Trend In Salah Shut-in

II. BLOWOUT CO₂ WITH RESERVOIR BACKFLOW

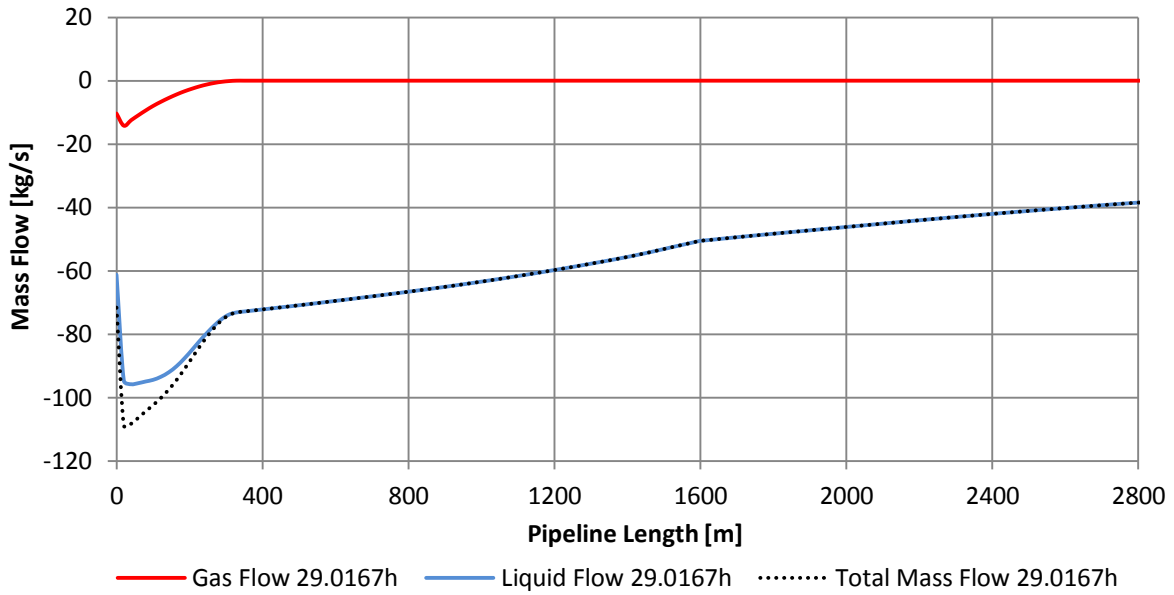


Appendix C-7 Density Profile In Salah Blowout With Backflow



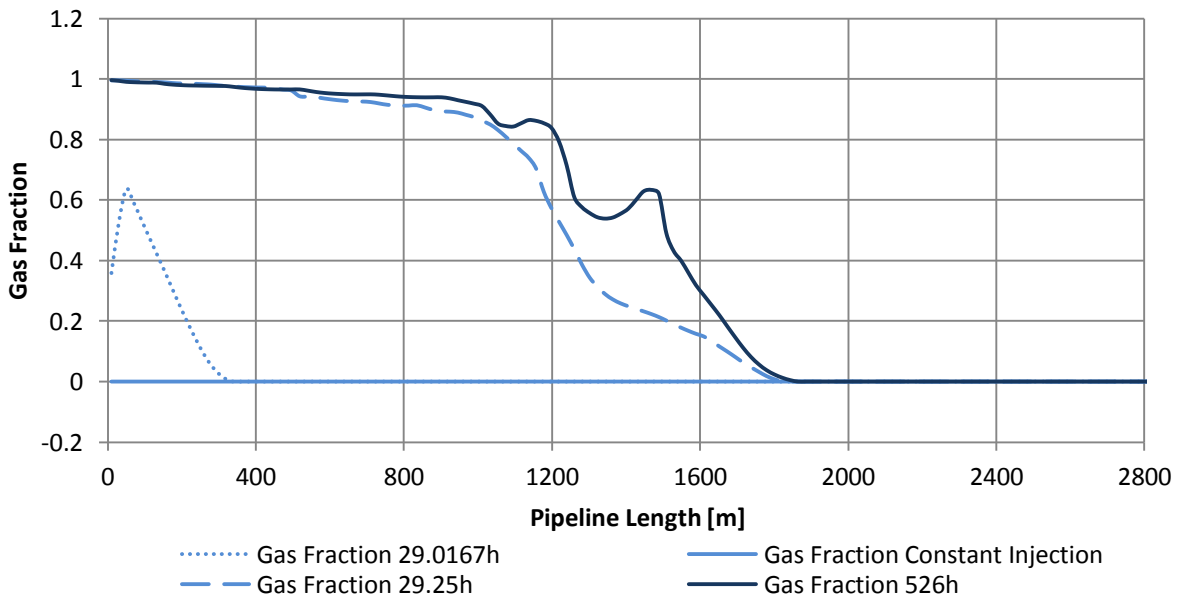
Appendix C-8 Total Mass Flow Profile In Salah Blowout With Backflow

Flow Profile In Salah Blowout With Backflow 29.0167h



Appendix C-9 Flow Profile In Salah Blowout With Backflow 29.0167h

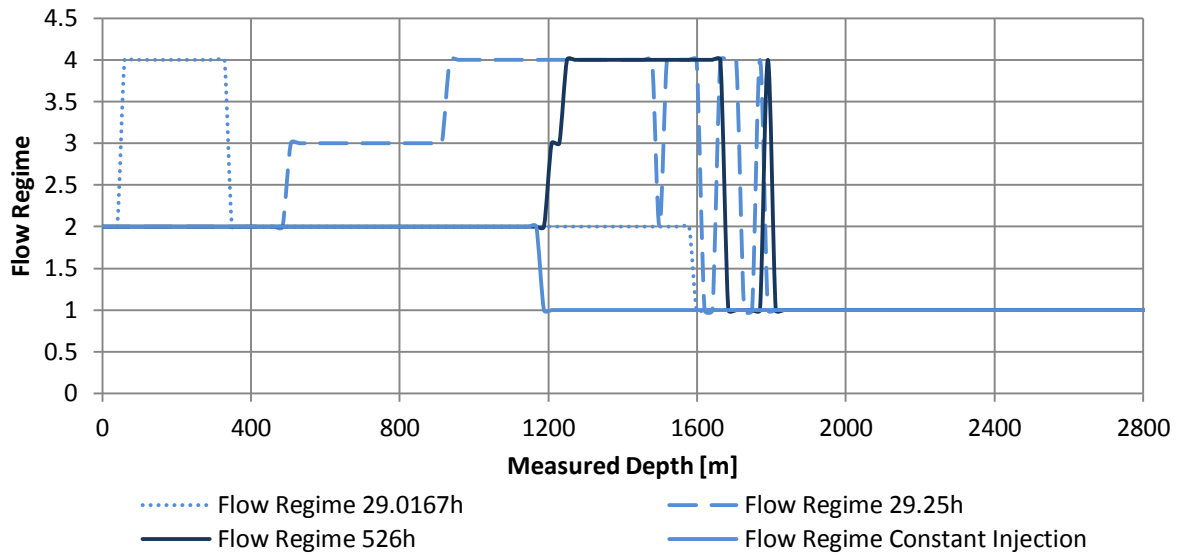
Gas Fraction Profile In Salah Blowout With Backflow



Appendix C-10 Gas Fraction Profile In Salah Blowout With Backflow

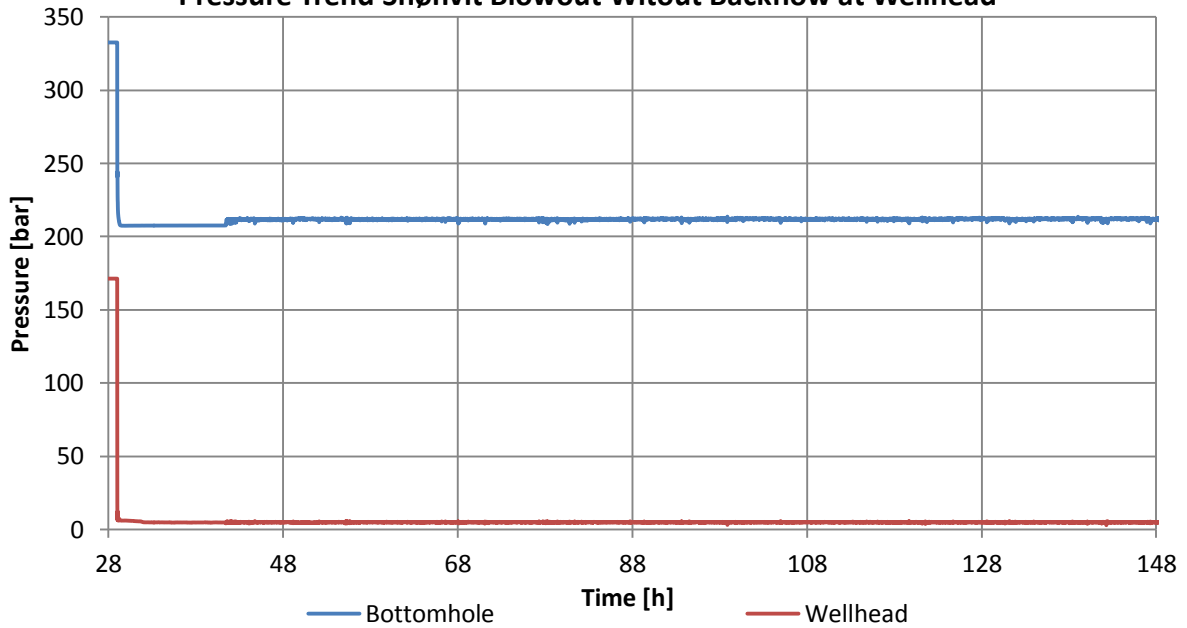
Flow Regime Profile In Salah Blowout With Backflow

Flow regime: 1=Stratified, 2=Annular, 3=Slug, 4=Bubble.

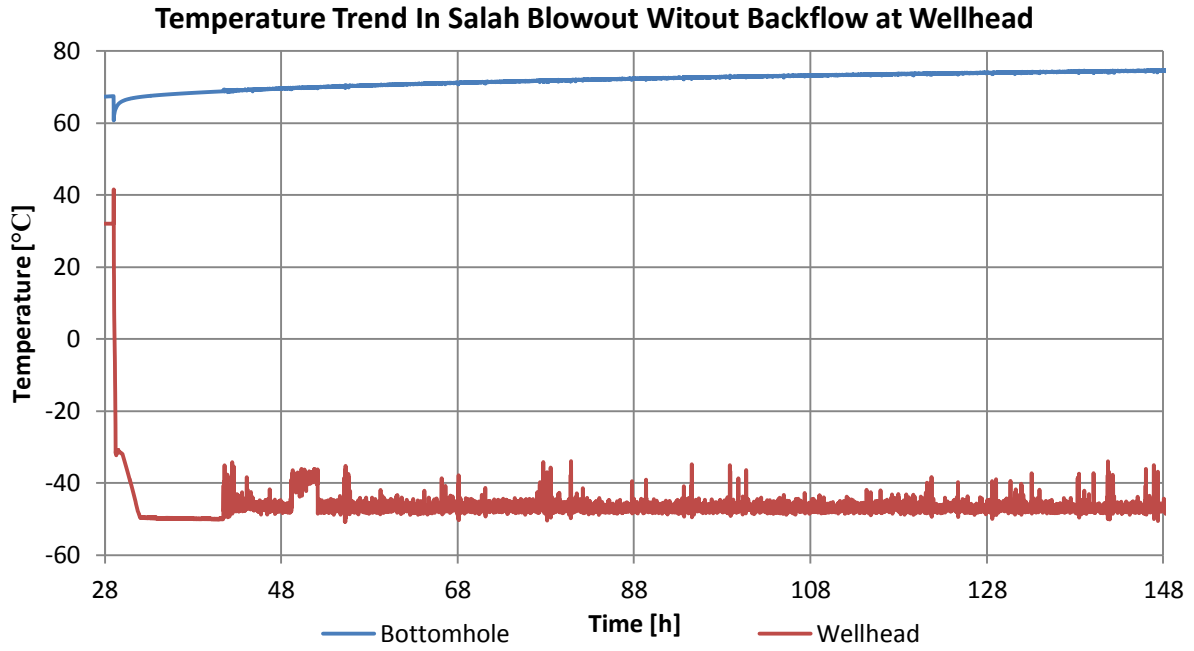


Appendix C-11 Flow Regime Profile In Salah Blowout With Backflow

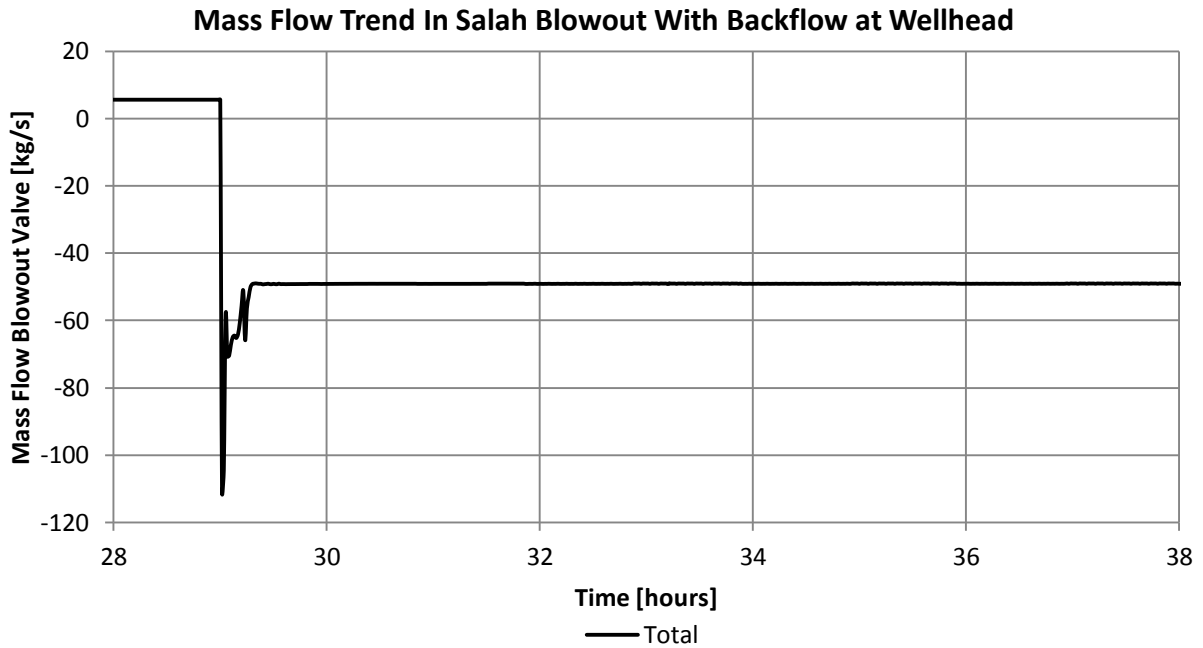
Pressure Trend Snøhvit Blowout Witout Backflow at Wellhead



Appendix C-12 Pressure Trend Snøhvit Blowout Without Backflow at Wellhead

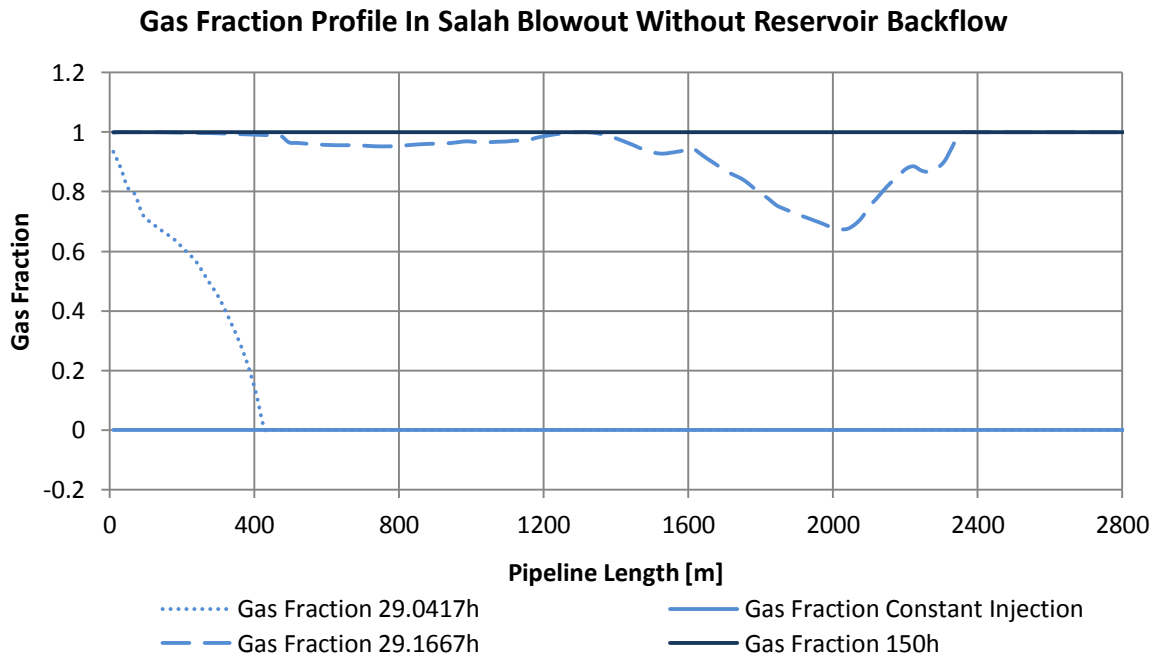
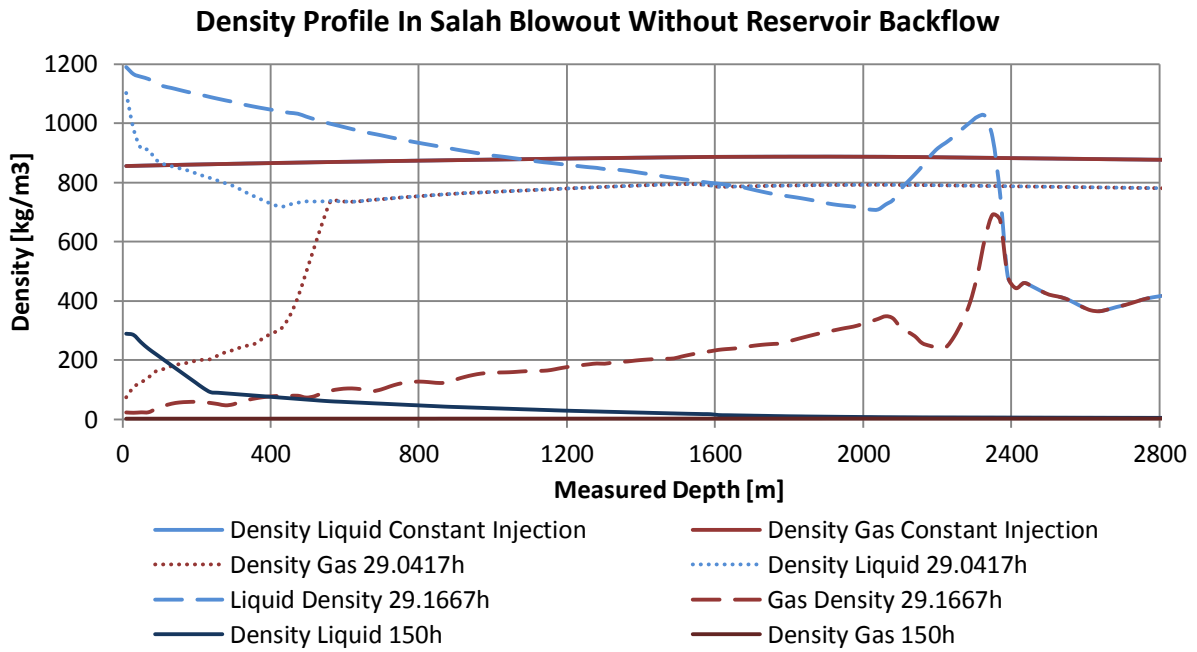


Appendix C-13 Temperature Trend In Salah Blowout Without Backflow at Wellhead

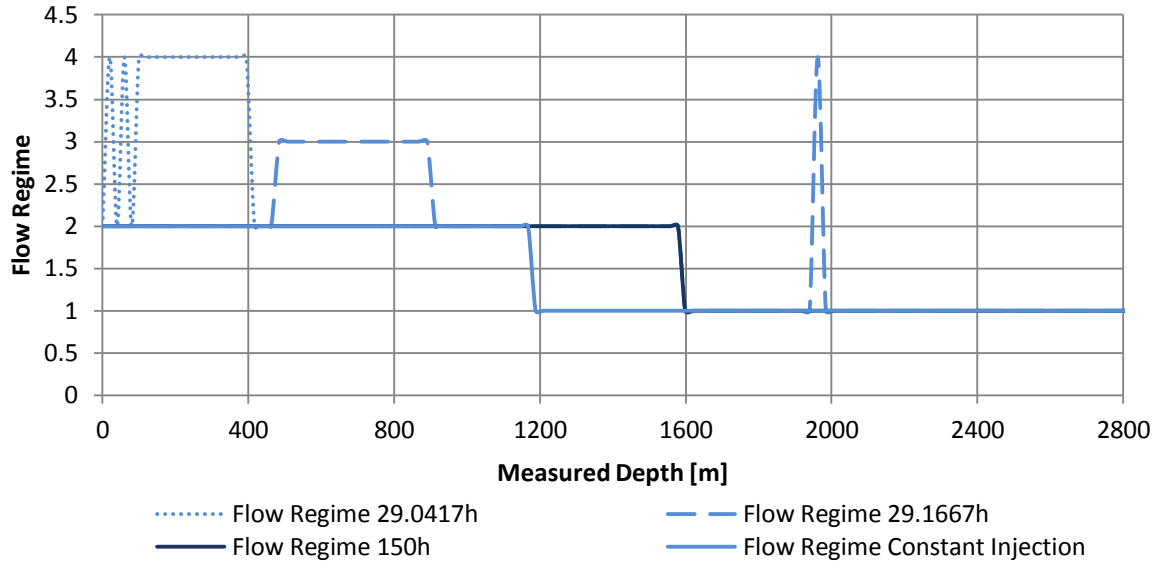


Appendix C-14 Mass Flow Trend In Salah Blowout With Backflow at Wellhead

III. BLOWOUT CO₂ WITHOUT RESERVOIR BACKFLOW

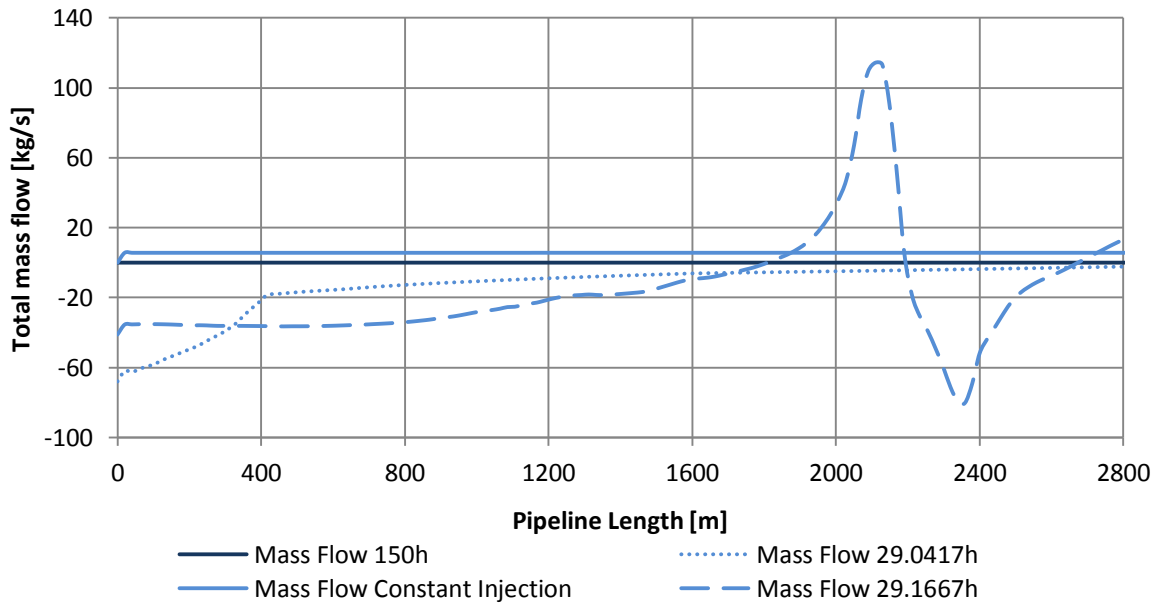


Flow Regime Profile In Salah Blowout Without Reservoir Backflow
Flow regime: 1=Stratified, 2=Annular, 3=Slug, 4=Bubble.



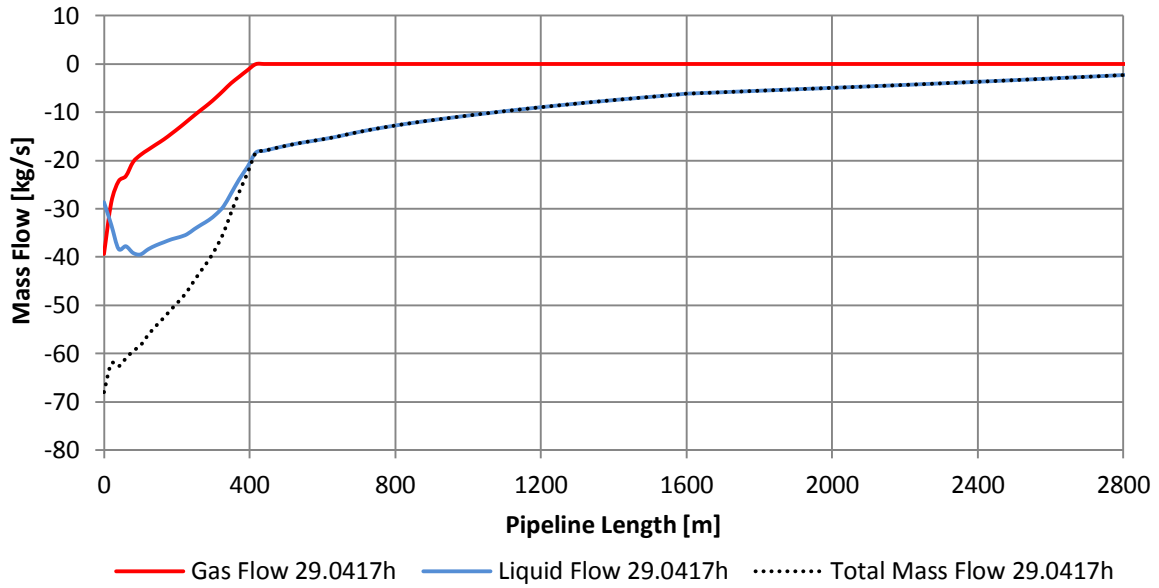
Appendix C-17 Flow Regime Profile In Salah Blowout Without Reservoir Backflow

Total Mass Flow Profile In Salah Blowout Without Reservoir Backflow



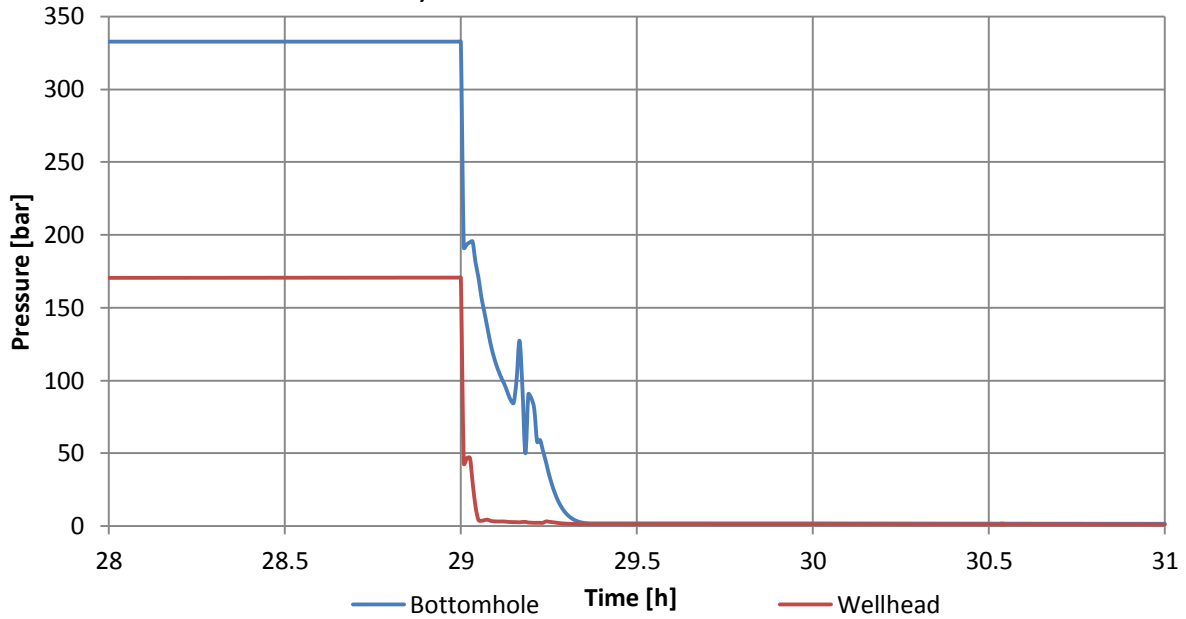
Appendix C-18 Total Mass Flow Profile In Salah Blowout Without Reservoir Backflow

Flow Profile In Salah Blowout Without Reservoir Backflow 29.0417h

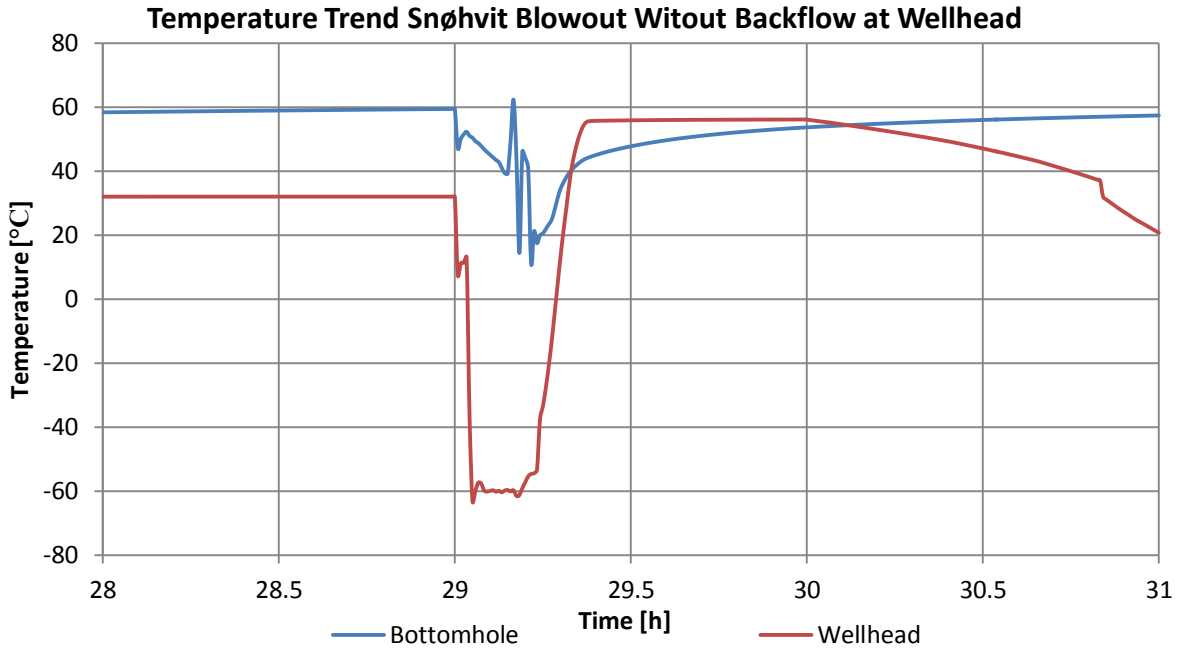


Appendix C-19 Flow Profile In Salah Blowout Without Reservoir Backflow 29.0417h

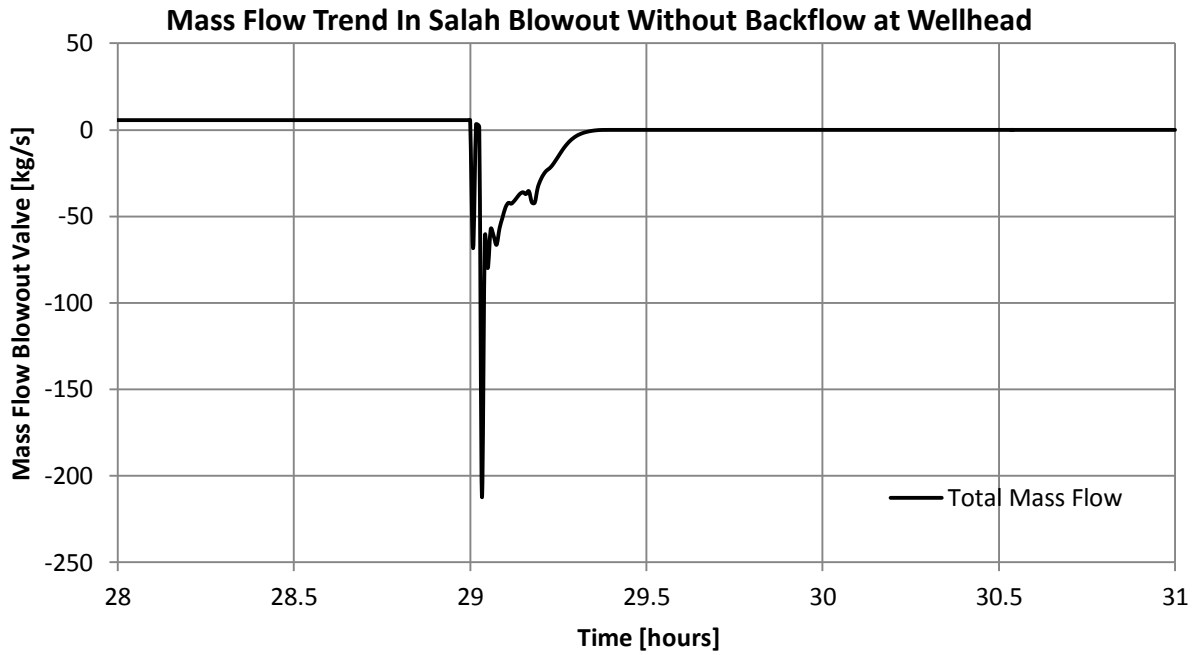
Pressure Trend Snøhvit Blowout Witout Backflow at Wellhead



Appendix C-20 Pressure Trend Snøhvit Blowout Without Backflow at Wellhead



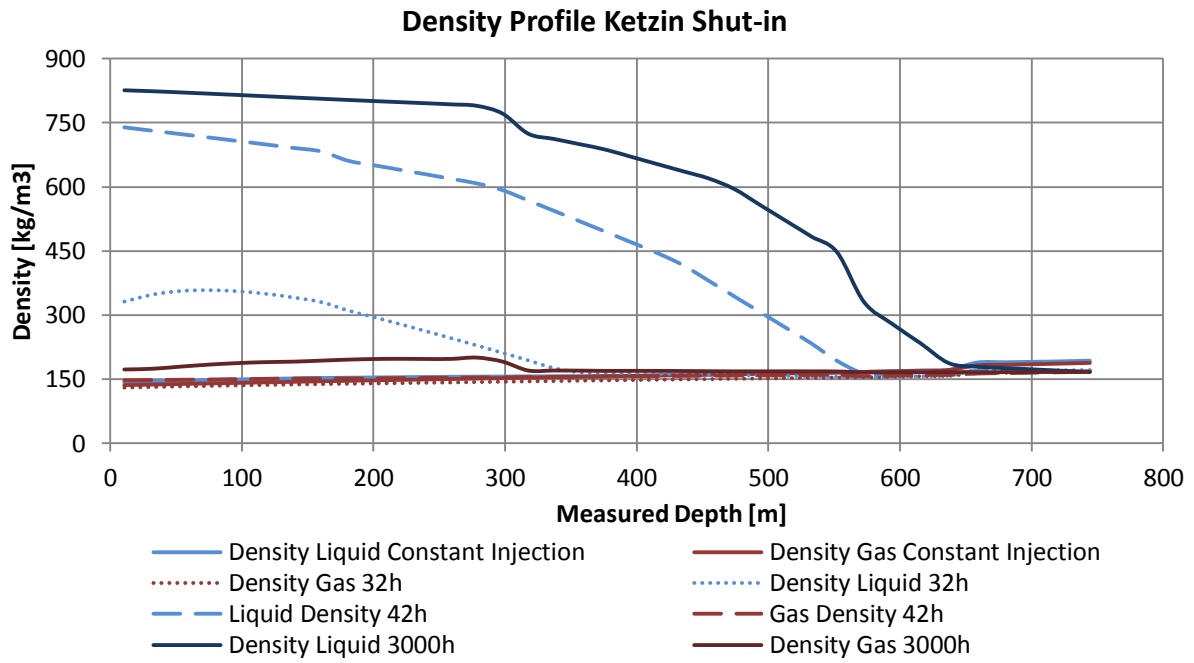
Appendix C-21 Temperature Trend Snøhvit Blowout Without Backflow at Wellhead



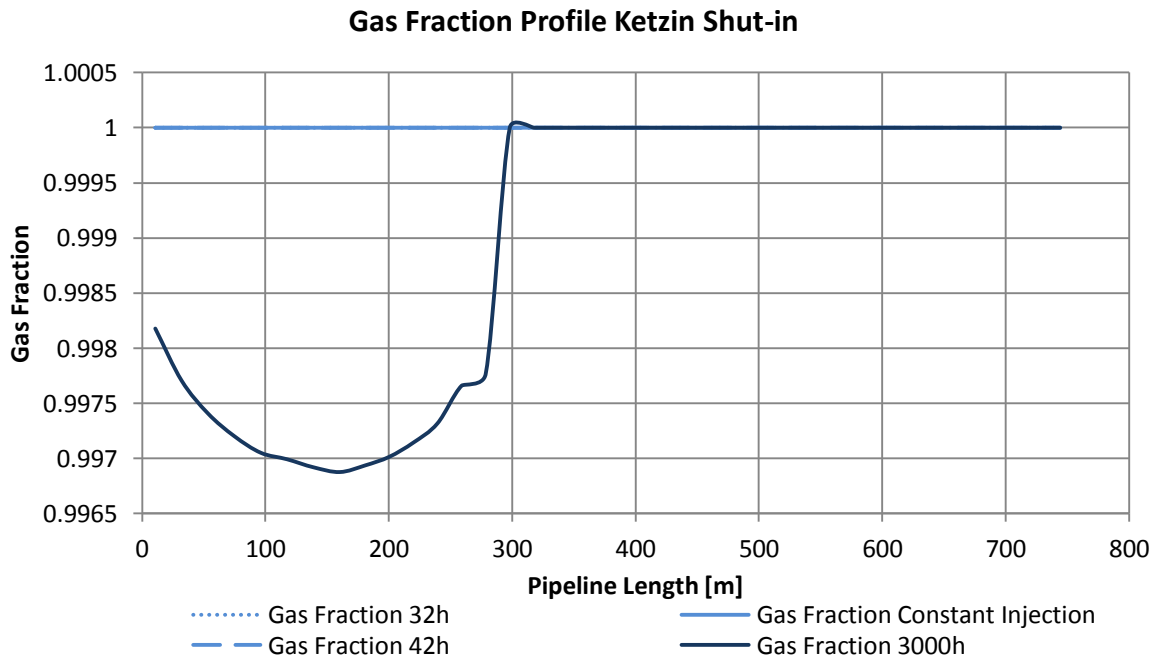
Appendix C-22 Mass Flow Trend In Salah Blowout With Backflow at Wellhead

D KETZIN FIGURES

I. SHUT-IN SINGLE COMPONENT MODULE CO₂

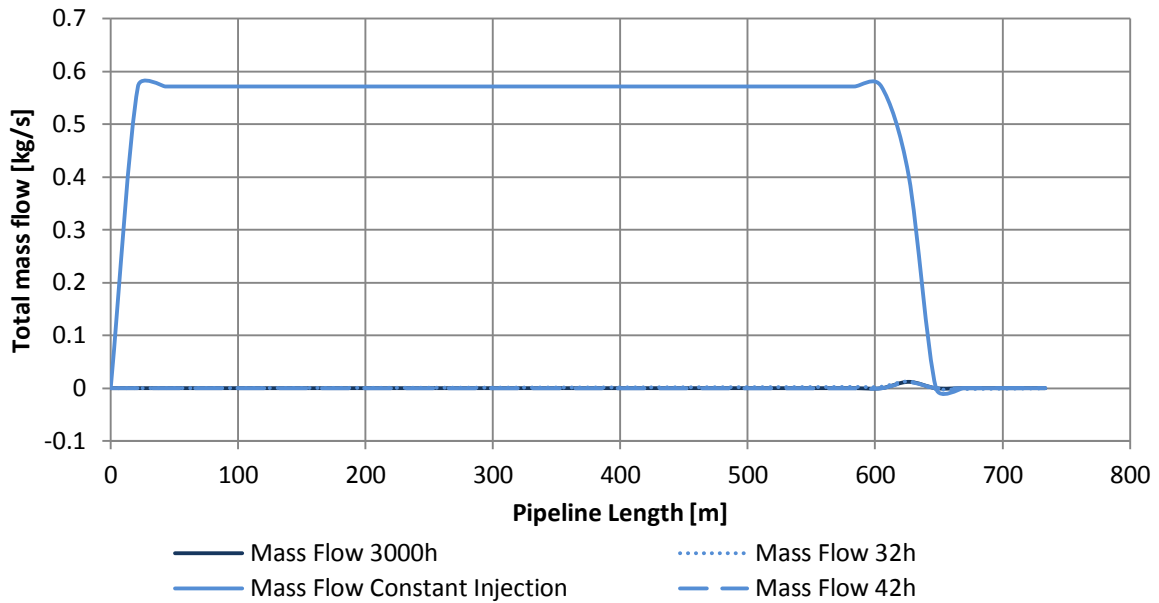


Appendix D-1 Density Profile Ketzin Shut-in



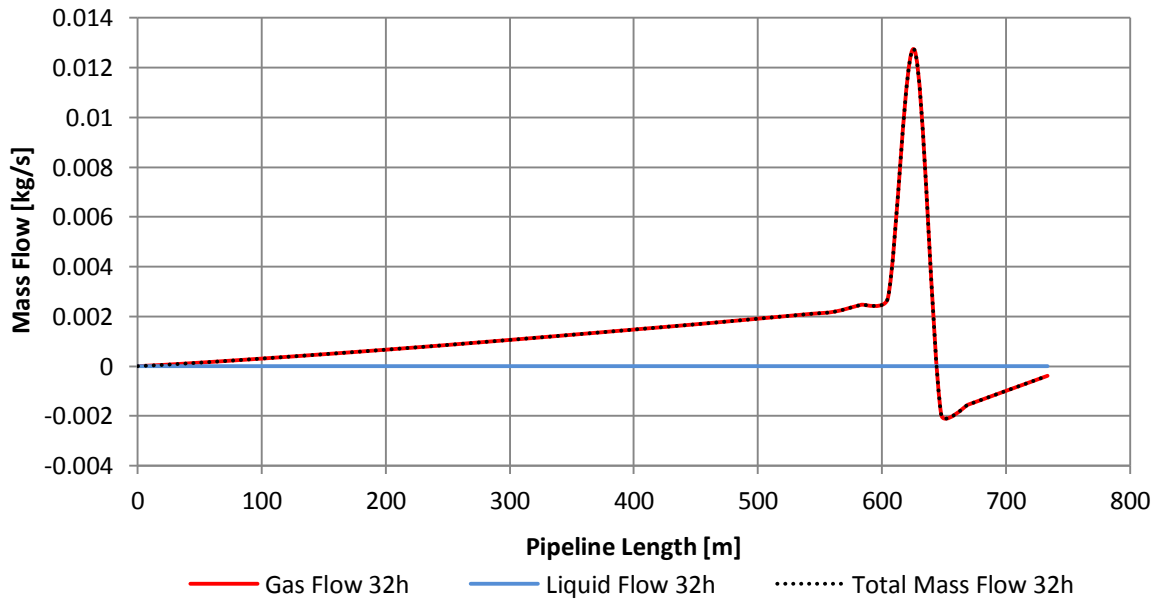
Appendix D-2 Gas Fraction Profile Ketzin Shut-in

Total Mass Flow Profile Ketzin Shut-in



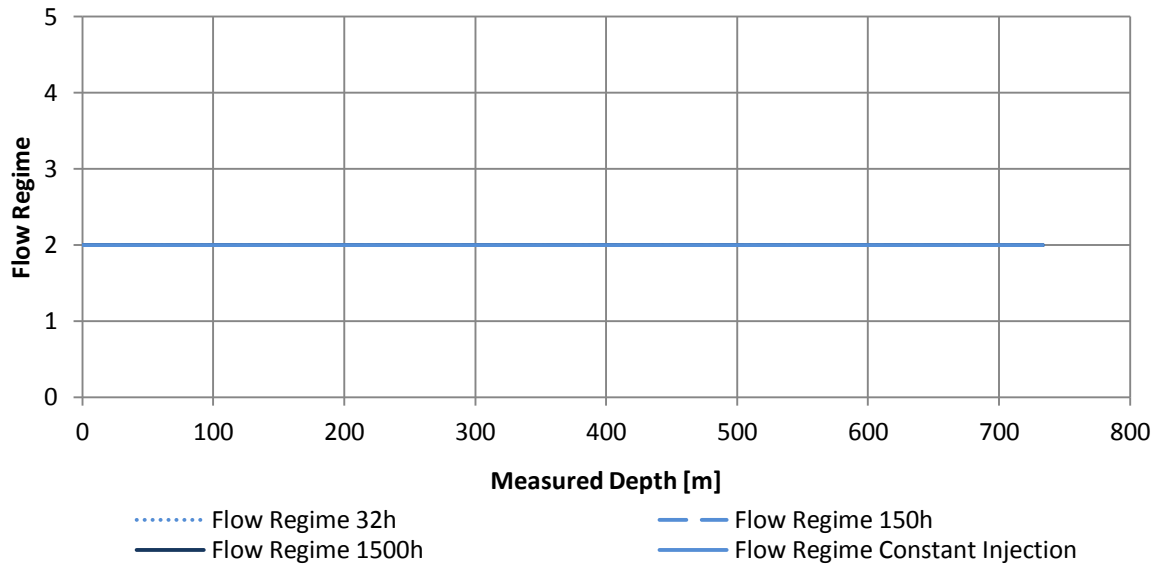
Appendix D-3 Total Mass Flow Profile Ketzin Shut-in

Flow Profile Ketzin Shut-in 32h



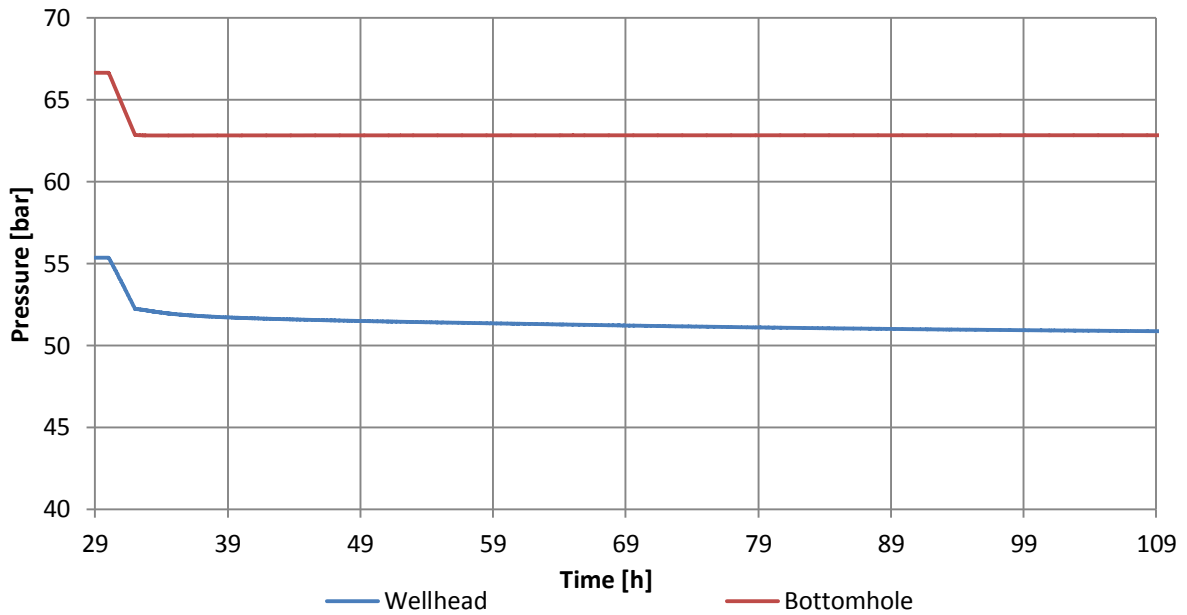
Appendix D-4 Flow Profile Ketzin Shut-in 32h

Flow Regime Profile Ketzin Shut-in
Flow regime: 1=Stratified, 2=Annular, 3=Slug, 4=Bubble.

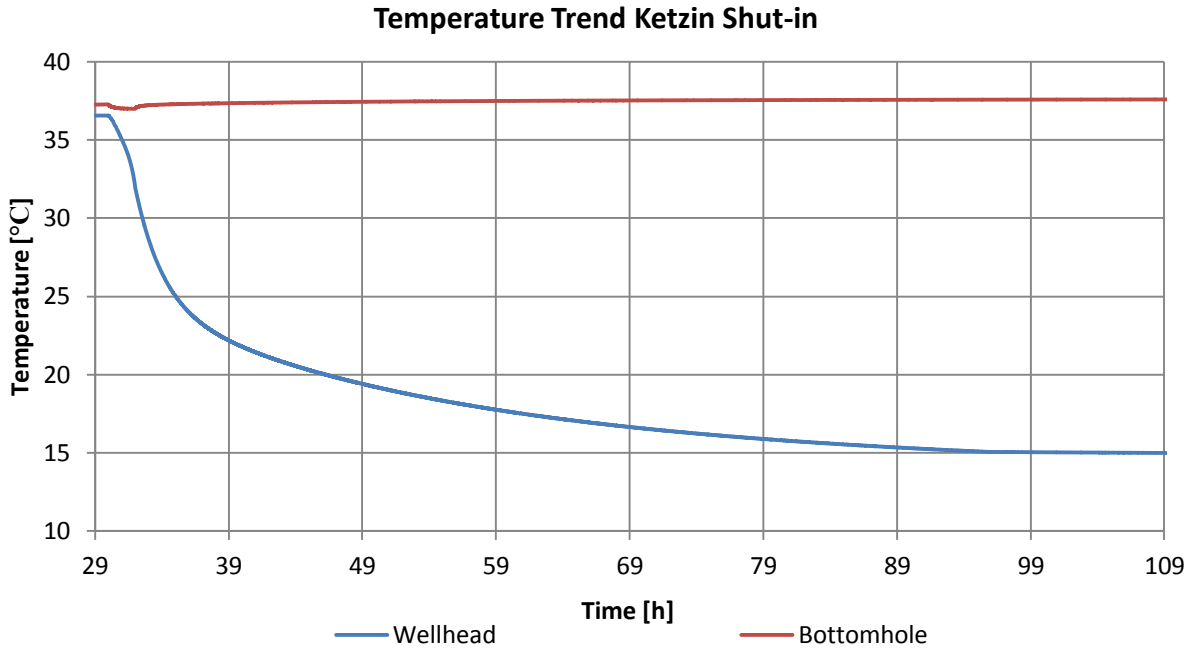


Appendix D-5 Flow Regime Profile Ketzin Shut-in

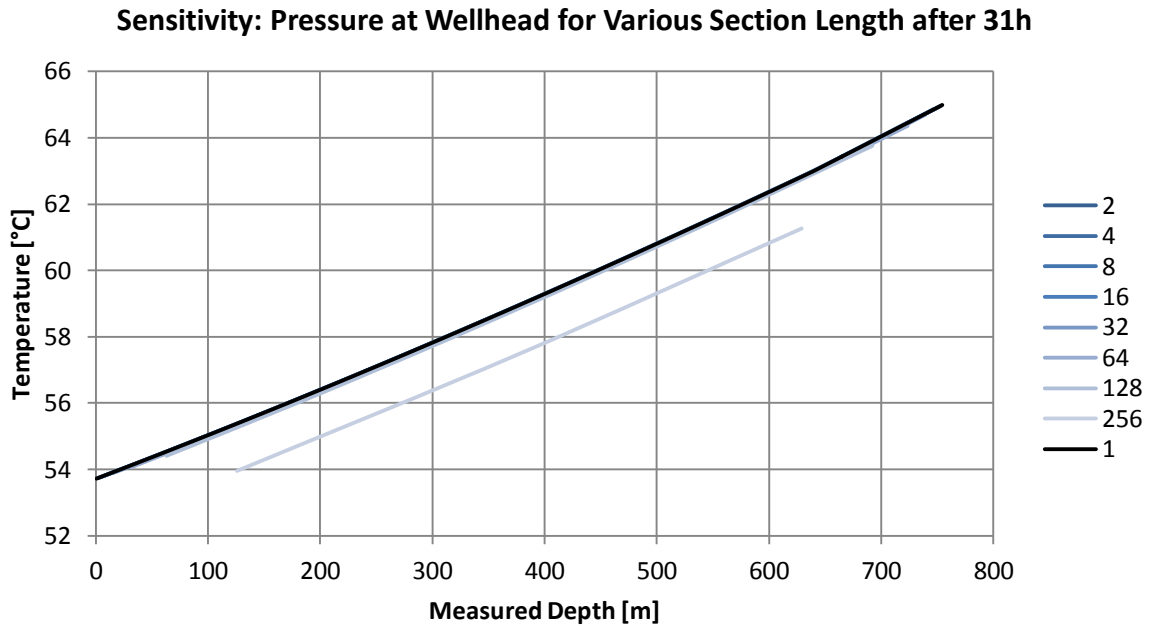
Pressure Trend Ketzin Shut-in



Appendix D-6 Pressure Trend Ketzin Shut-in

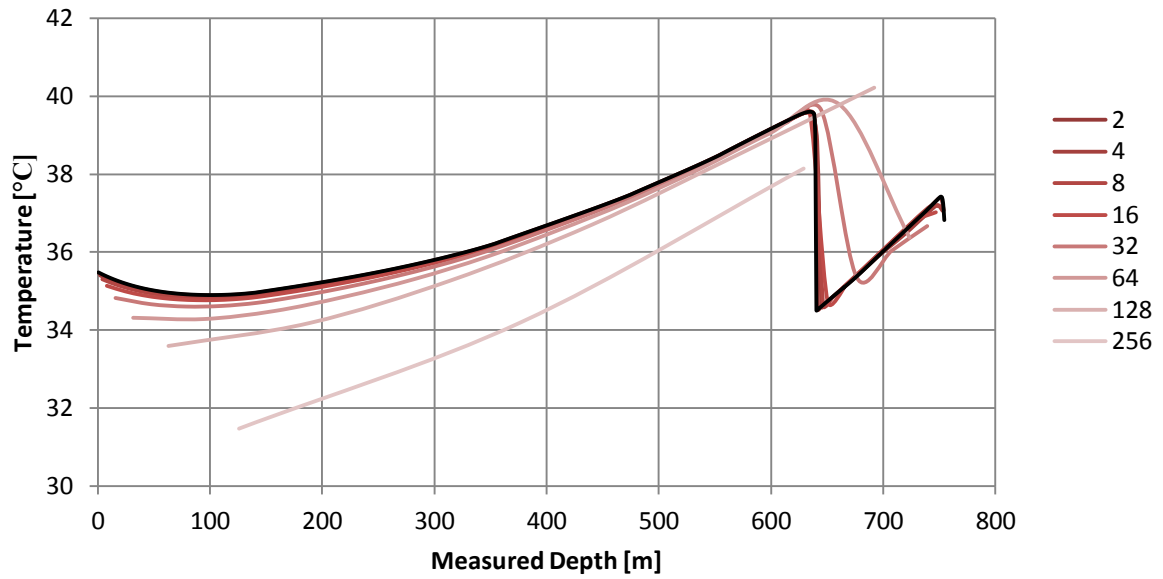


Appendix D-7 Temperature Trend Ketzin Shut-in



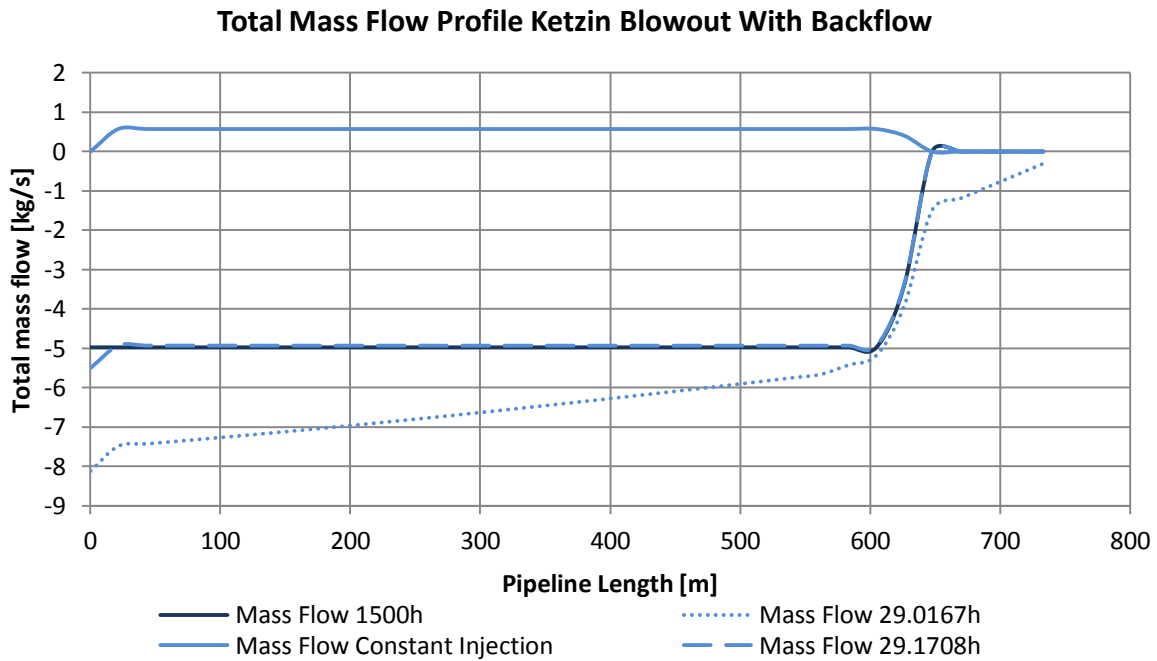
Appendix D-8 Sensitivity: Pressure at Wellhead for Various Section Lengths after 31h

Sensitivity: Temperature at Wellhead for Various Section Length after 31h

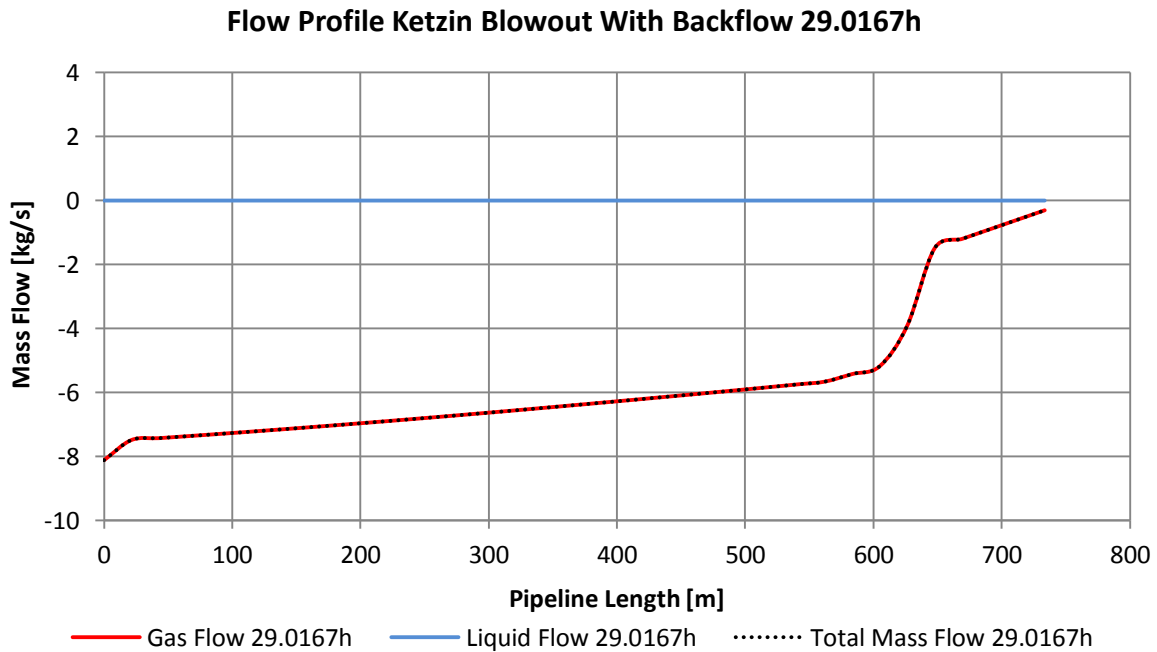


Appendix D-9 Sensitivity: Temperature at Wellhead for Various Section Length after 31h

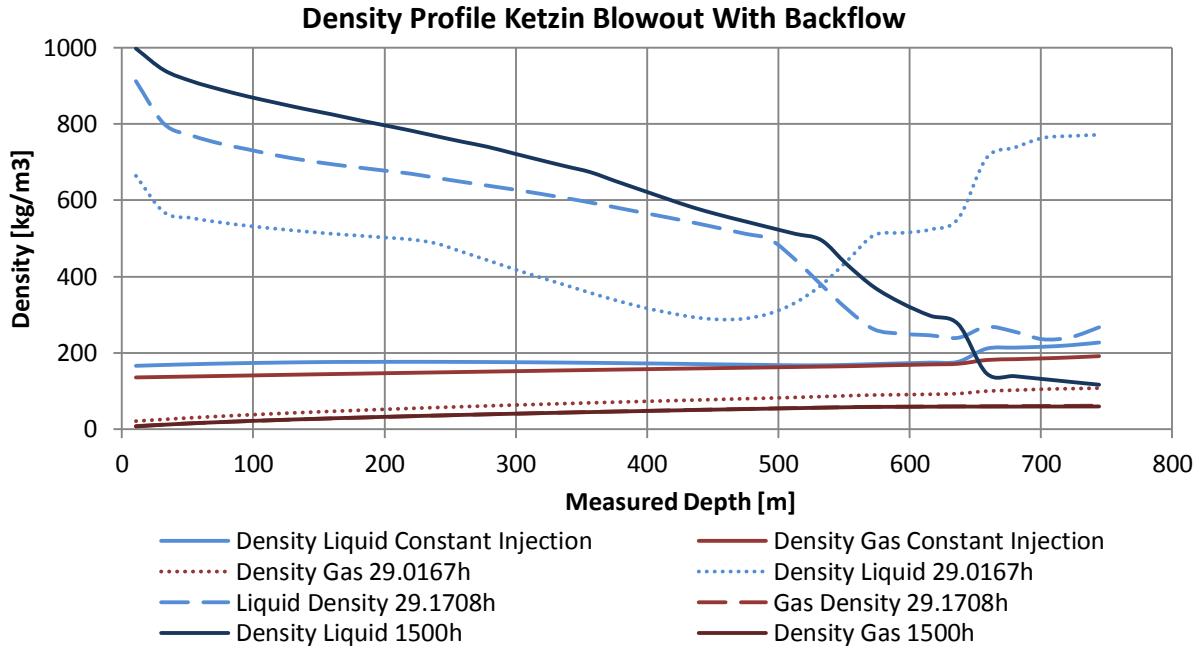
II. BLOWOUT CO₂ WITH RESERVOIR BACKFLOW



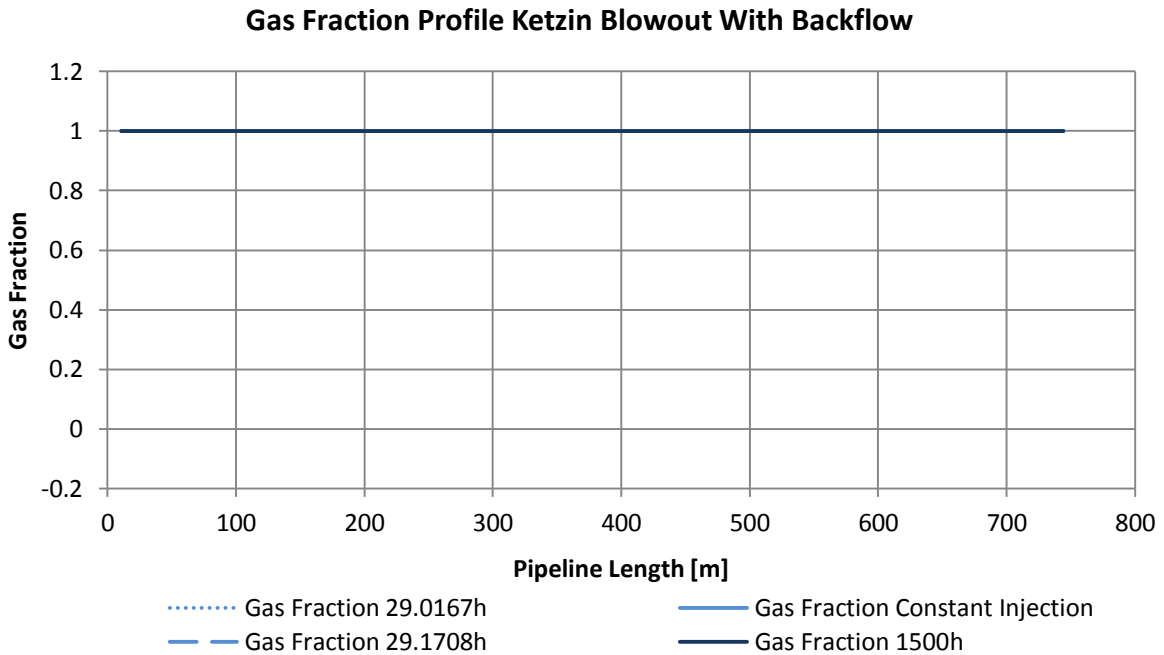
Appendix D-10 Total Mass Flow Profile Ketzin Blowout With Backflow



Appendix D-11 Flow Profile Ketzin Blowout With Backflow 29.0167h

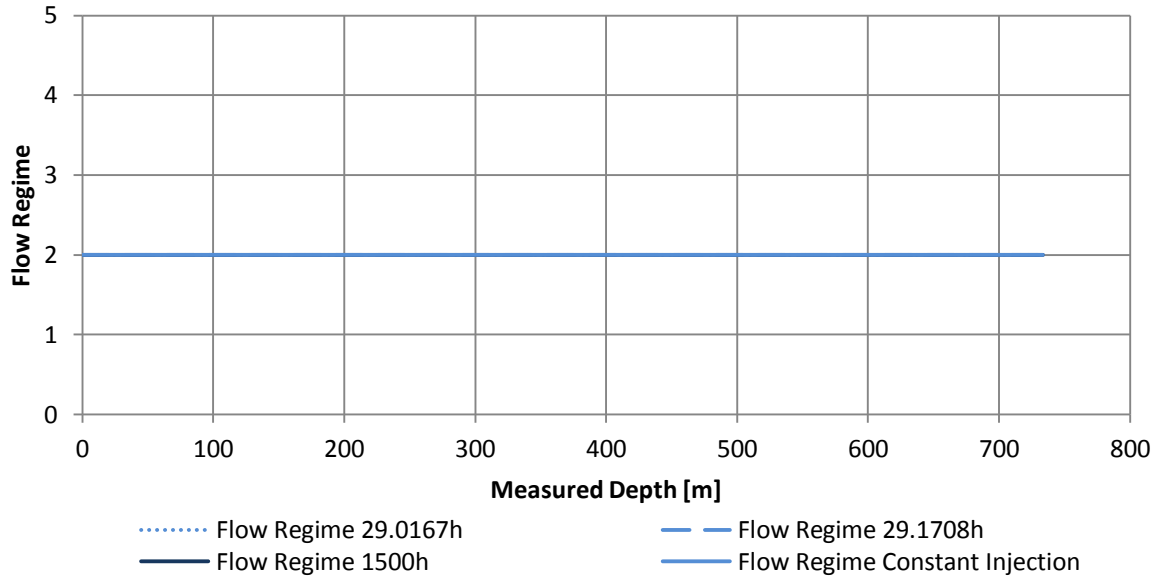


Appendix D-12 Density Profile Ketzin Blowout With Backflow



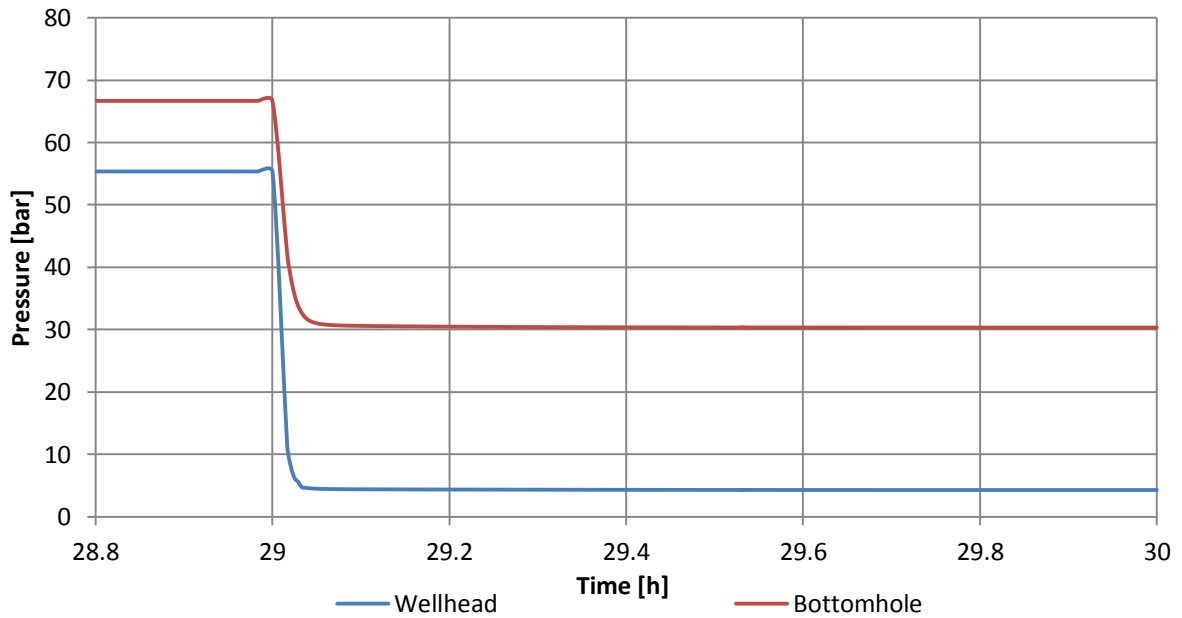
Appendix D-13 Gas Fraction Profile Ketzin Blowout With Backflow

Flow Regime Profile Ketzin Blowout With Backflow
 Flow regime: 1=Stratified, 2=Annular, 3=Slug, 4=Bubble.



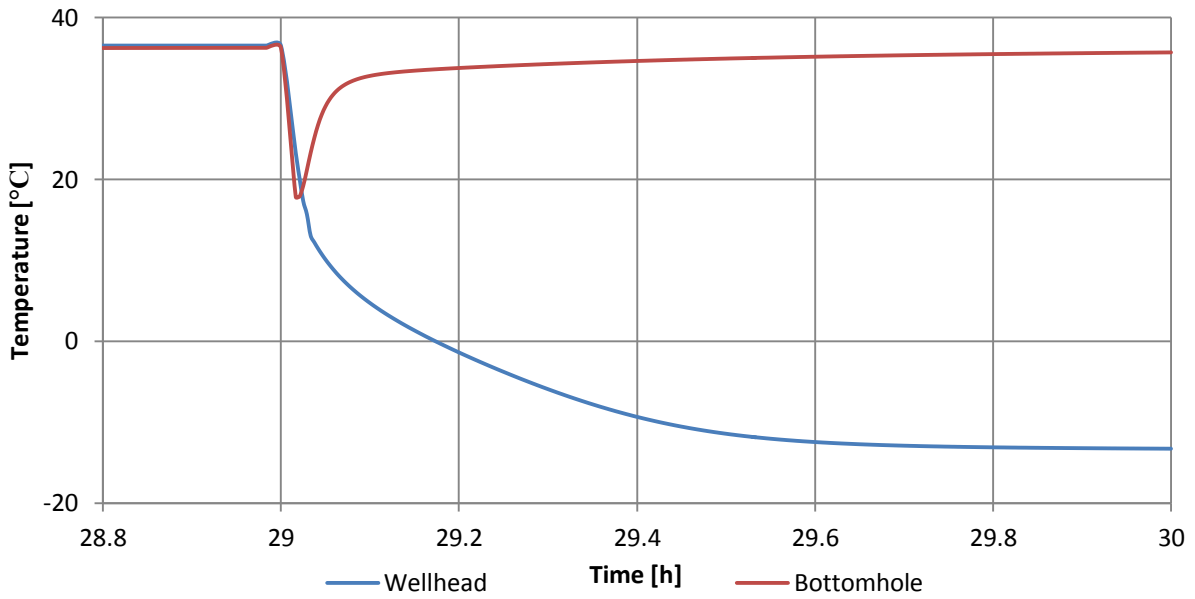
Appendix D-14 Flow Regime Profile Ketzin Blowout With Backflow

Pressure Trend Ketzin Blowout With Backflow



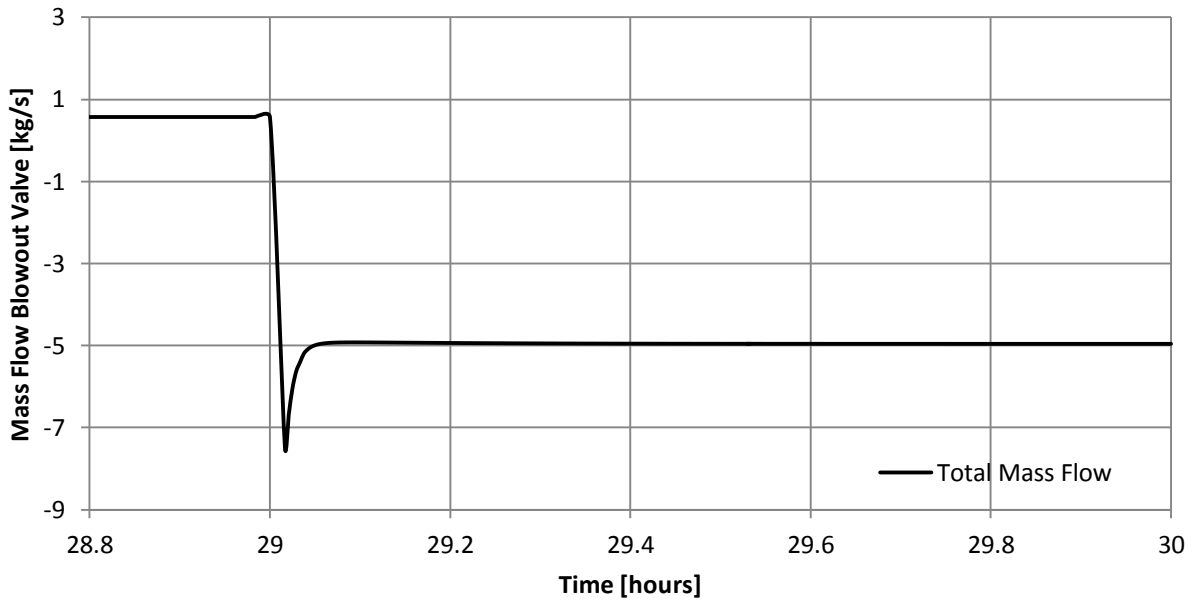
Appendix D-15 Pressure Trend Ketzin Blowout Without Backflow at Wellhead

Temperature Trend Ketzin Blowout With Backflow



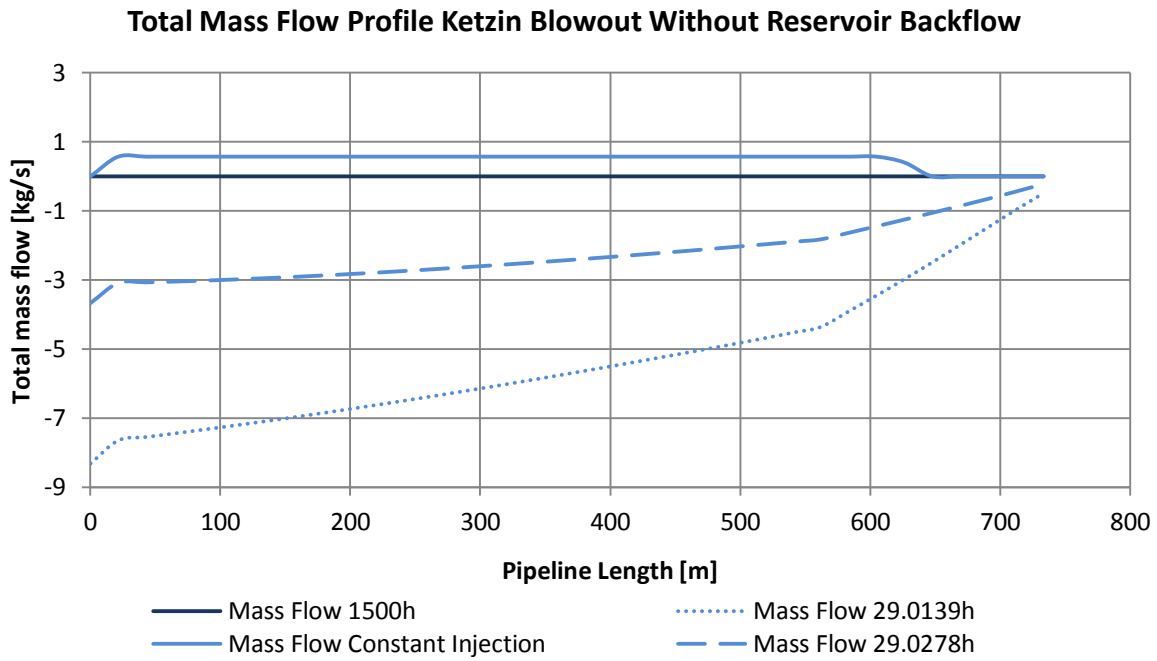
Appendix D-16 Temperature Trend Ketzin Blowout Without Backflow at Wellhead

Mass Flow Trend Ketzin Blowout With Backflow at Wellhead

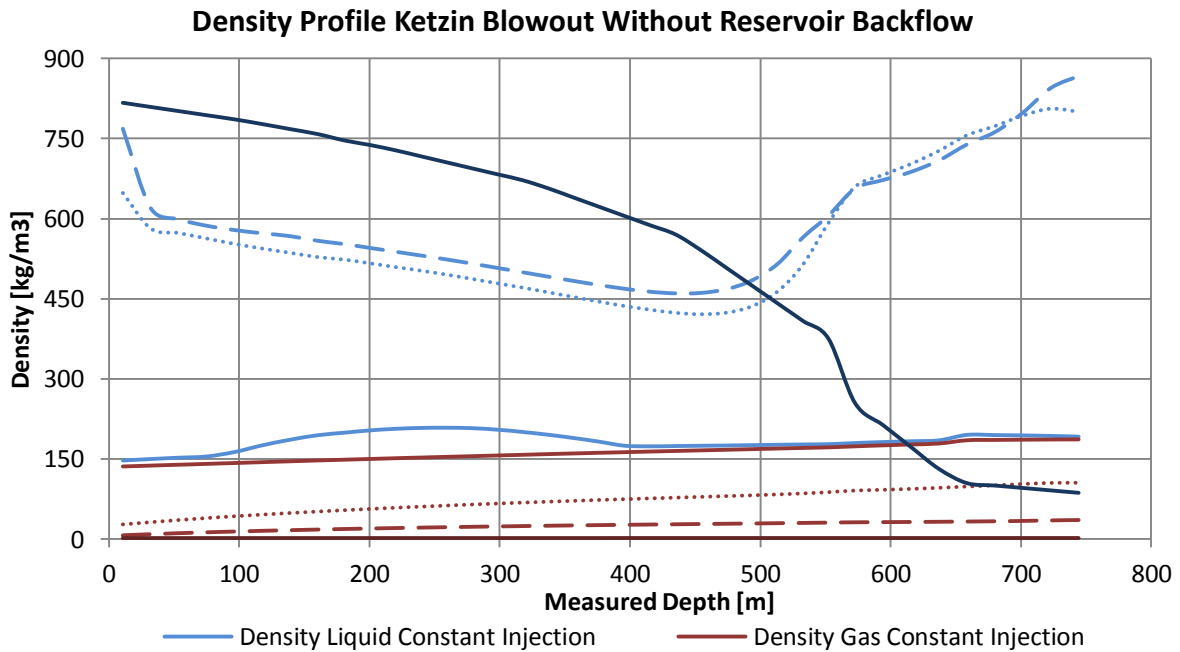


Appendix D-17 Mass Flow Trend Ketzin Blowout With Backflow at Wellhead

III. BLOWOUT CO₂ WITHOUT RESERVOIR BACKFLOW

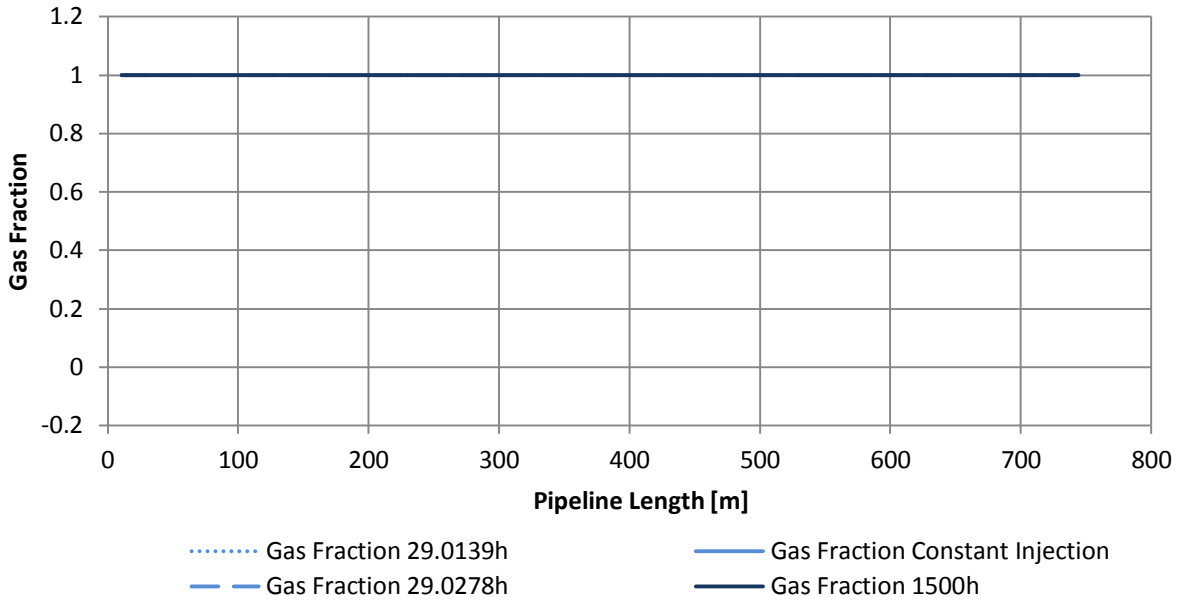


Appendix D-18 Total Mass Flow Profile Ketzin Blowout Without Reservoir Backflow



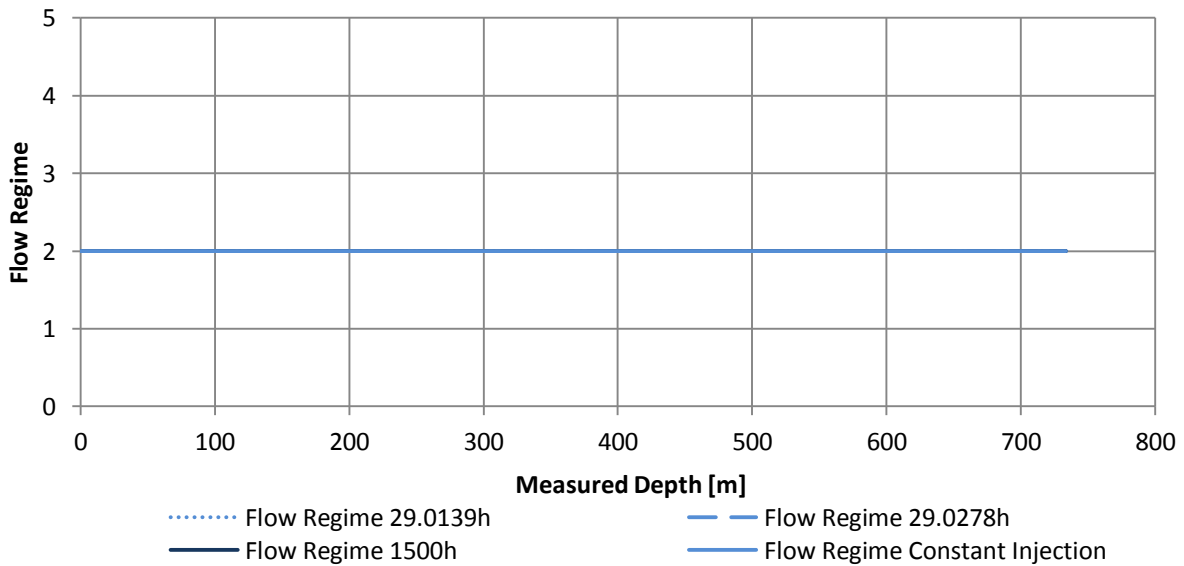
Appendix D-19 Density Profile Ketzin Blowout Without Reservoir Backflow

Gas Fraction Profile Ketzin Blowout Without Reservoir Backflow



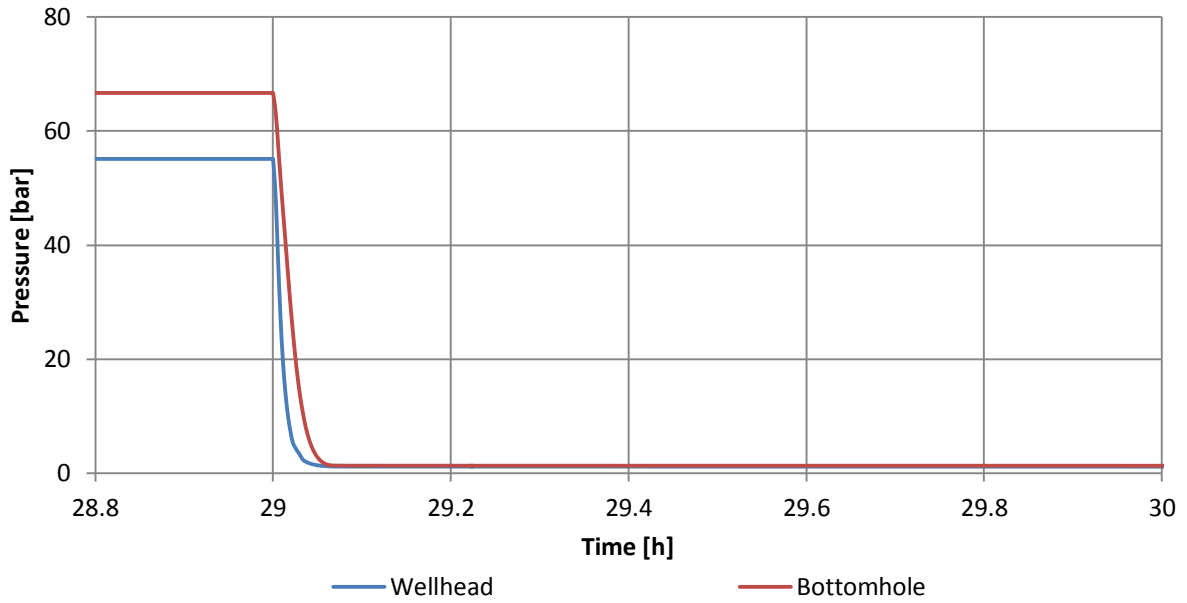
Appendix D-20 Gas Fraction Profile Ketzin Blowout Without Reservoir Backflow

Flow Regime Profile Ketzin Blowout Without Reservoir Backflow Flow regime: 1=Stratified, 2=Annular, 3=Slug, 4=Bubble.



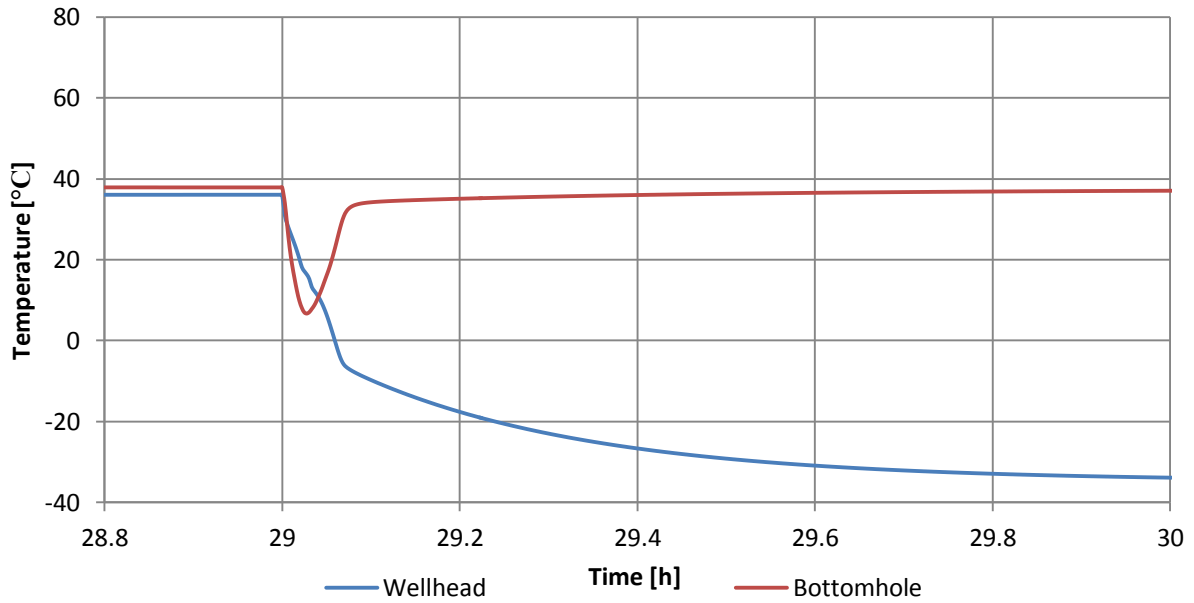
Appendix D-21 Flow Regime Profile Ketzin Blowout Without Reservoir Backflow

Pressure Trend Ketzin Blowout Without Backflow



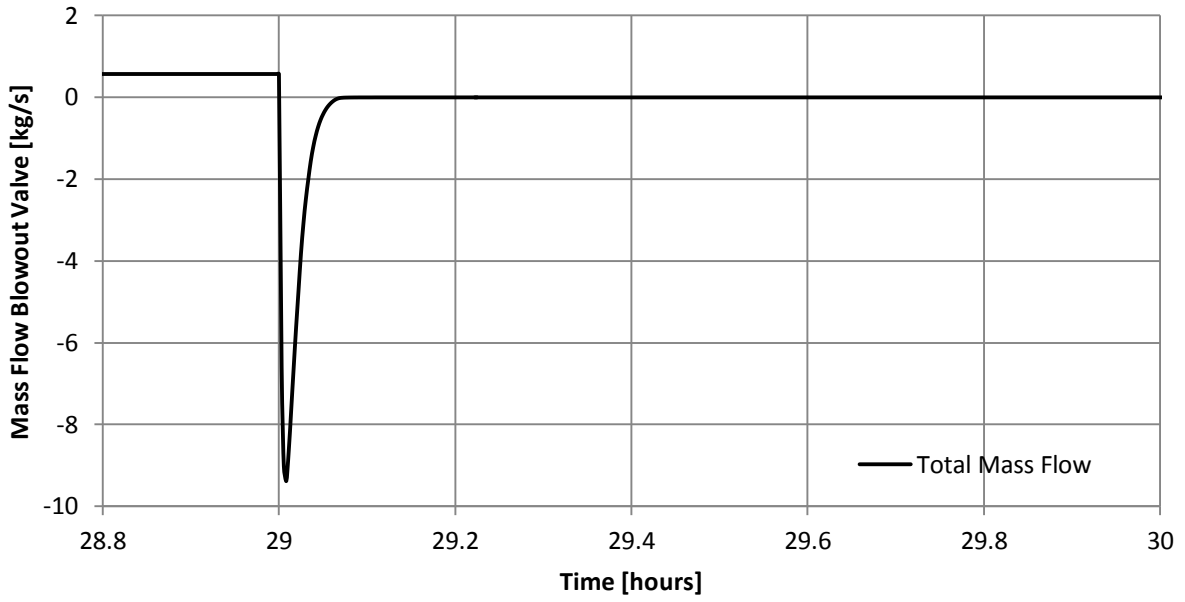
Appendix D-22 Pressure Trend Ketzin Blowout Without Backflow

Temperature Trend Ketzin Blowout Without Backflow



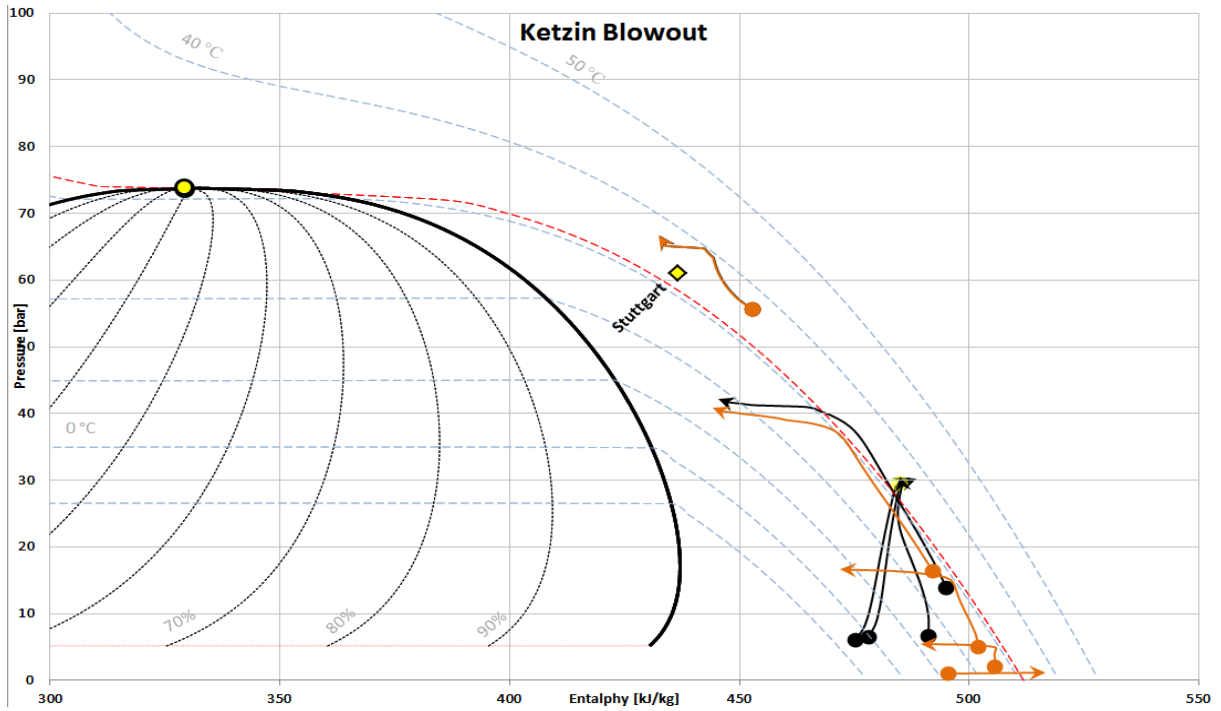
Appendix D-23 Temperature Trend Ketzin Blowout Without Backflow

Mass Flow Trend at Wellhead Ketzin Blowout Without Backflow

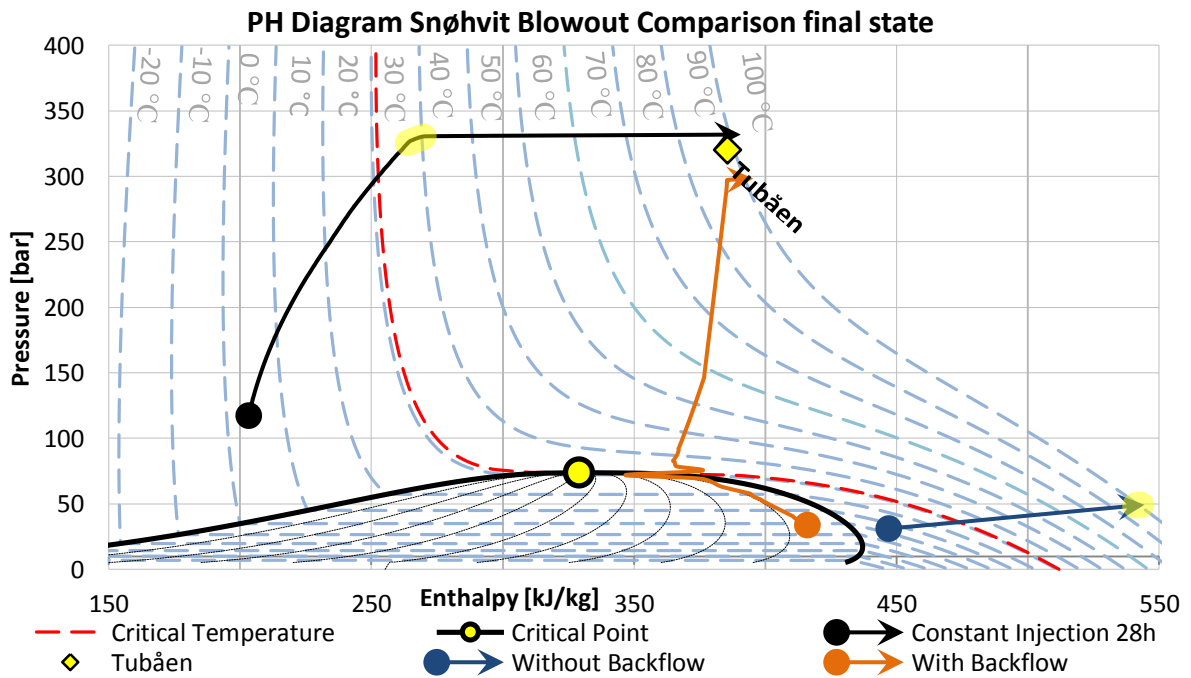


Appendix D-24 Mass Flow Trend at Wellhead Ketzin Blowout Without Backflow

E DISCUSSION

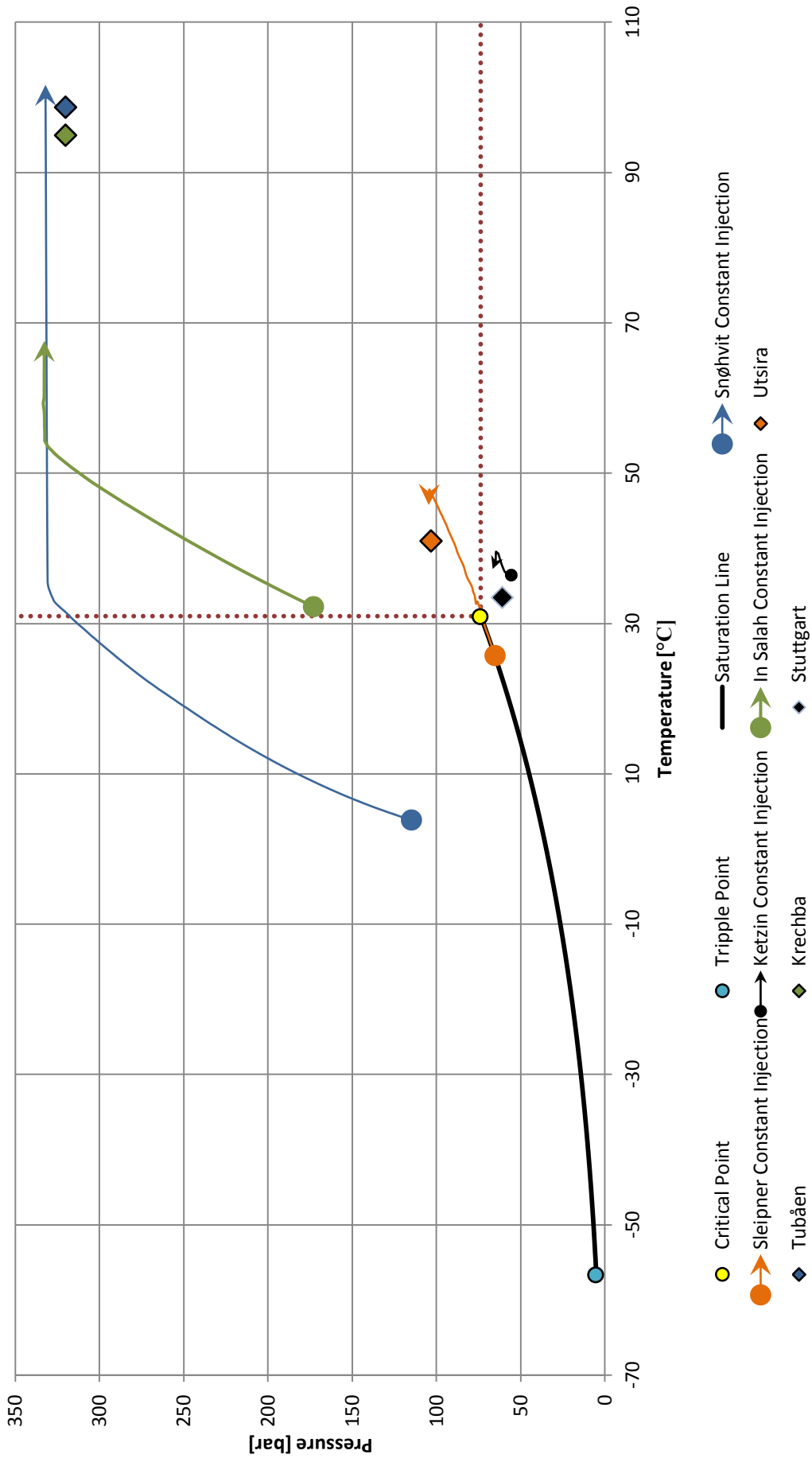


Appendix E-1 Blowout Comparison: Black is with and orange is without backflow



Appendix E-2 PH Diagram Snøhvit Blowout Comparison final state in simulation

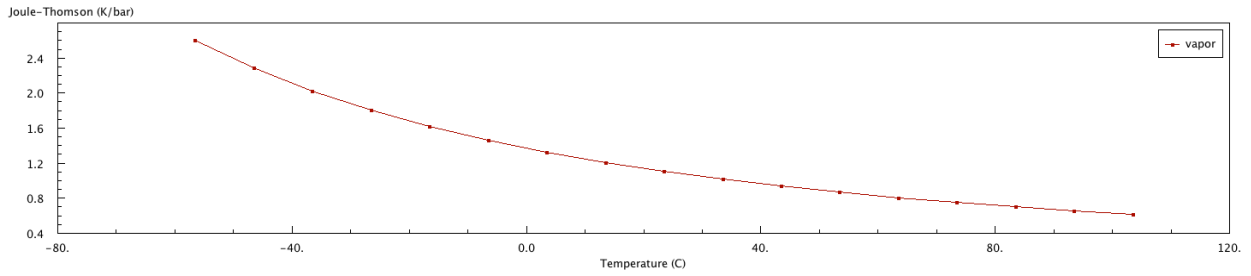
PT Diagram Constant Injection Snøhvit, Sleipner, Ketzin and In Salah



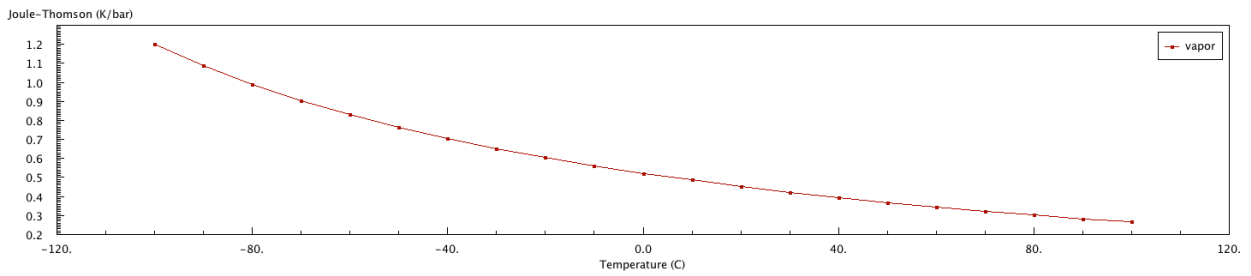
Appendix E-3 PT Diagram Constant Injection Snøhvit, Sleipner, Ketzin and In Salah

F THEORY

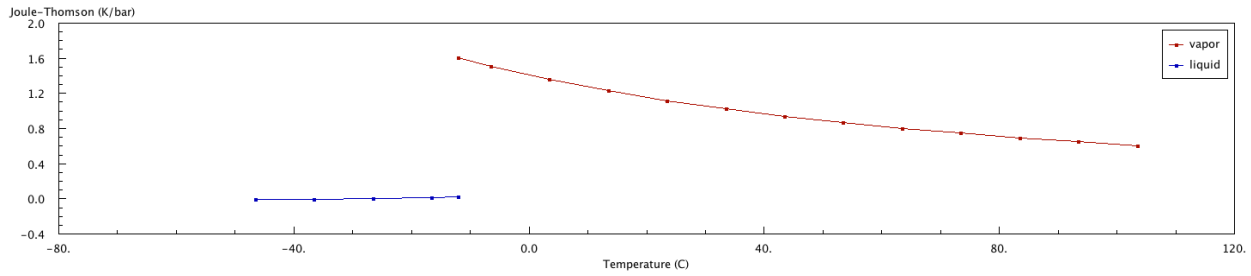
I. JOULE-THOMSON COEFFICIENT



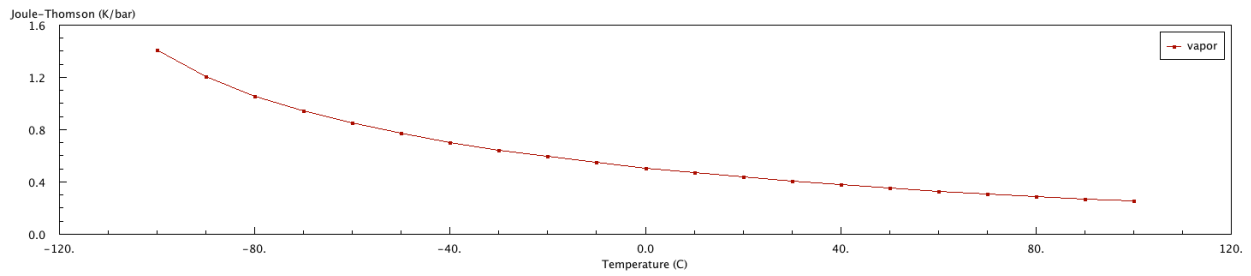
Appendix F-1 Joule-Thompson Coefficient CO₂ at 1 bar (NIST)



Appendix F-2 Joule-Thompson Coefficient CH₄ at 1 bar (NIST)

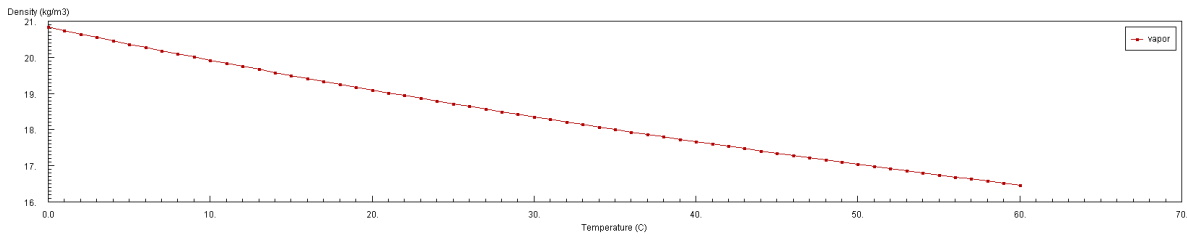


Appendix F-3 Joule-Thompson Coefficient CO₂ at 25 bar (NIST)

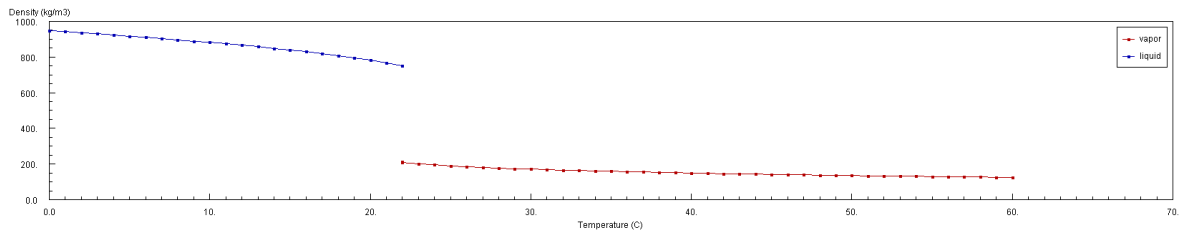


Appendix F-4 Joule-Thompson Coefficient CH₄ at 25 bar (NIST)

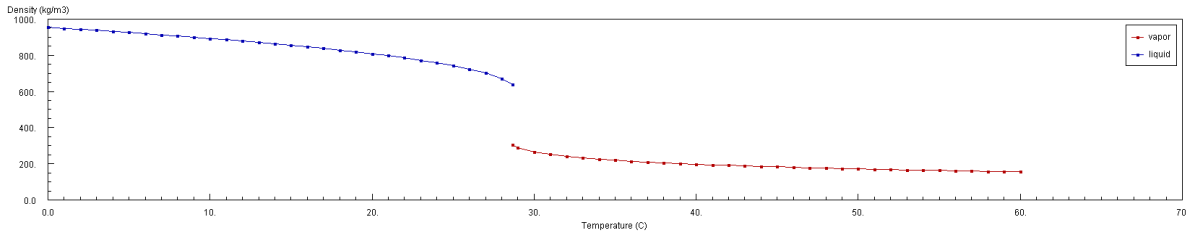
II. ISOBARIC CO₂ DENSITY



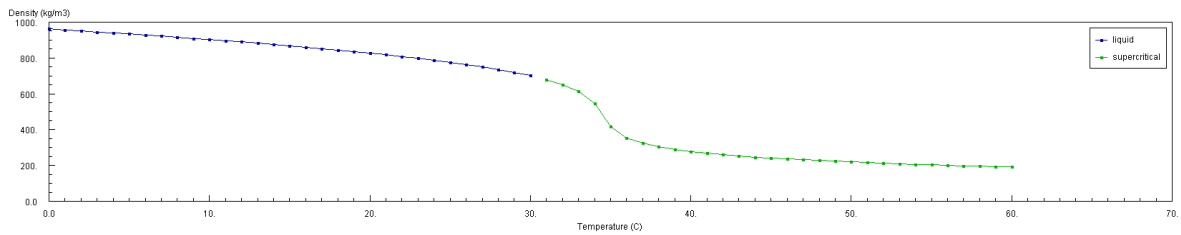
Appendix F-5 Isobaric CO₂ density at 10 bar (NIST)



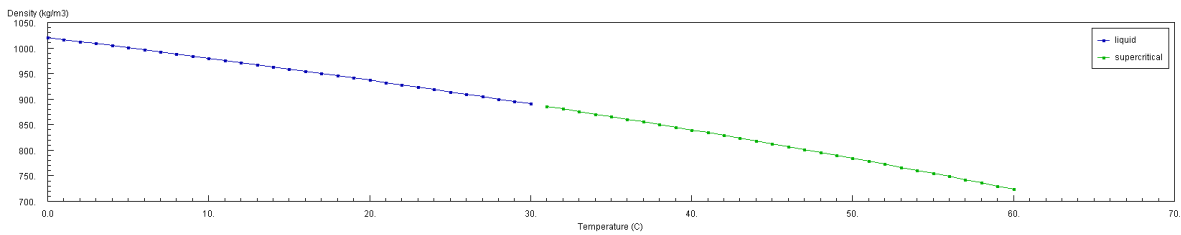
Appendix F-6 Isobaric CO₂ density at 60 bar (NIST)



Appendix F-7 Isobaric CO₂ density at 70 bar (NIST)



Appendix F-8 Isobaric CO₂ density at 80 bar (NIST)



Appendix F-9 Isobaric CO₂ density at 200 bar (NIST)

G MODEL SPECIFICATIONS

I. SLEIPNER

1. Introduction

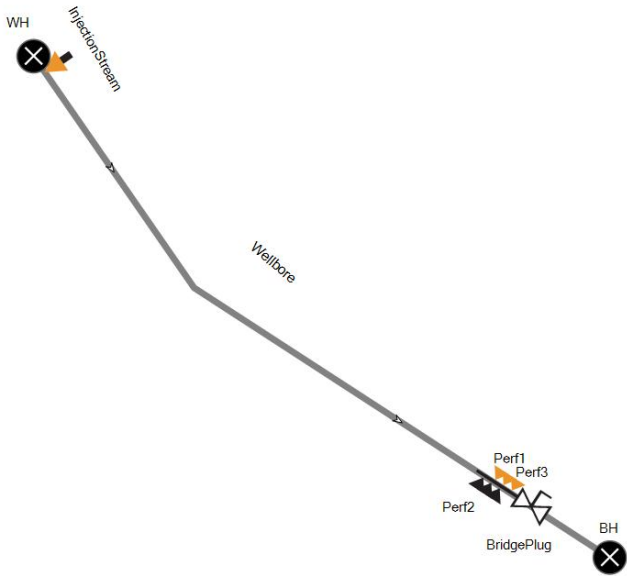
Project	Thesis
Case description	Shut-in Sleipner
Date	
Author	Eirik Thu
Restart File	../BaseCaseCO2/CO2.rsw

2. Simulation Options

Overall setting	Flow model	OLGA
	Mass eq scheme	1STORDER
	Compositional model	SINGLE
	Debug	ON
	Drilling	
	Phase	THREE
	Elastic walls	OFF
	Void in slug	SINTEF
	Steady state	OFF
	User defined plug-in	OFF
	Temp. calc.	WALL
	Wax deposition	
	Restart	ON
Integration	Simulation starttime	
	Simulation stoptime	150 h
	Minimum time step	1 s
	Maximum time step	5 s

3. System Layout - Graphics

OLGA



Layout filter On

4. System Layout - Table

4.1 Summary

4.1.1 Overall

No. of Branches	No. of Pipes	No. of Sections
1	22	94

4.1.2 Flows

Branches	No. of Pipes	No. of Sections	Min. Section Length	At	Max. Section Length	At
Wellbore	22	94	19.5004 M	PIPE-1	55.4782 M	PIPE-22

4.2 Layout

Pipe no.	Branch	Label	Diameter	Roughness	XEnd	YEND	Wall
1 - 1	Wellbore	PIPE-1	0.159 M	5E-05 M	0.478 M	-78 M	Riser
1 - 2	Wellbore	PIPE-2	0.159 M	5E-05 M	2.377 M	-160 M	Riser
1 - 3	Wellbore	PIPE-3	0.159 M	5E-05 M	5.513 M	-200 M	Tubing-7inch
1 - 4	Wellbore	PIPE-4	0.159 M	5E-05 M	7.1 M	-239.851 M	Tubing-7inch
1 - 5	Wellbore	PIPE-5	0.159 M	5E-05 M	12.85 M	-309.769 M	Tubing-7inch
1 - 6	Wellbore	PIPE-6	0.159 M	5E-05 M	23.65 M	-368.895 M	Tubing-7inch
1 - 7	Wellbore	PIPE-7	0.159 M	5E-05 M	43.34 M	-436.345 M	Tubing-7inch
1 - 8	Wellbore	PIPE-8	0.159 M	5E-05 M	70.35 M	-500.993 M	Tubing-7inch

1 - 9	Wellbore	PIPE-9	0.159 M	5E-05 M	103.66 M	-562.844 M	Tubing-7inch
1 - 10	Wellbore	PIPE-10	0.159 M	5E-05 M	149.37 M	-628.781 M	Tubing-7inch
1 - 11	Wellbore	PIPE-11	0.159 M	5E-05 M	213.11 M	-692.666 M	Tubing-7inch
1 - 12	Wellbore	PIPE-12	0.159 M	5E-05 M	305.72 M	-752.739 M	Tubing-7inch
1 - 13	Wellbore	PIPE-13	0.159 M	5E-05 M	465.08 M	-811.535 M	Tubing-7inch
1 - 14	Wellbore	PIPE-14	0.159 M	5E-05 M	781.8 M	-856.497 M	Tubing-7inch
1 - 15	Wellbore	PIPE-15	0.159 M	5E-05 M	1102.2 M	-896.715 M	Tubing-7inch
1 - 16	Wellbore	PIPE-16	0.159 M	5E-05 M	1446.89 M	-943.886 M	Tubing-7inch
1 - 17	Wellbore	PIPE-17	0.159 M	5E-05 M	1763.57 M	-990.016 M	Tubing-7inch
1 - 18	Wellbore	PIPE-18	0.159 M	5E-05 M	2081.34 M	-1034.68 M	Tubing-7inch
1 - 19	Wellbore	PIPE-19	0.159 M	5E-05 M	2418.17 M	-1080.95 M	Tubing-7inch
1 - 20	Wellbore	PIPE-20	0.159 M	5E-05 M	2736.04 M	-1107.43 M	Tubing-7inch
1 - 21	Wellbore	PIPE-21	0.159 M	5E-05 M	3053.6 M	-1145.44 M	Tubing-7inch
1 - 22	Wellbore	PIPE-22	0.102 M	5E-05 M	3163.01 M	-1163.9 M	Tubing-4.5inch

5. Insulation and Walls

5.1 Material

Label	Density	Conductivity	Heat Capacity
Formation	2500 kg/m ³	2 W/m-C	880 J/kg-C
Steel	7850 kg/m ³	50 W/m-C	500 J/kg-C
Stainless Steel	7850 kg/m ³	20 W/m-K	450 J/kg-C

5.2 Walls

Label	Material	Wall thickness	Elastic
Tubing-4.5inch	Stainless Steel	0.527 in	
	Formation	0.98425197 in	
	Formation	1.9685039 in	
	Formation	3.9370079 in	
	Formation	7.8740157 in	
	Formation	15.748031 in	
	Formation	31.496063 in	
	Formation	59.055118 in	
	Formation	118.11024 in	
Tubing-7inch	Stainless Steel	0.0206121 m	
	Formation	0.05 m	
	Formation	0.1 m	
	Formation	0.2 m	
	Formation	0.4 m	
	Formation	0.8 m	
	Formation	1.5 m	
	Formation	3 m	
Riser	Stainless Steel	20.6121 mm	

6. Boundary Conditions

6.1 Nodes

Label	Type	Pressure	Temperature	Mass flow
BH	CLOSED			
WH	CLOSED	65.096 bara	24.024 C	116987.5 kg/h

6.2 Heattransfer

Branch	Pipe	Interpolation	Houteroption.	Hambient	Tambient
Wellbore	PIPE-1	SECTIONWISE	AIR		10 C
Wellbore	PIPE-2	SECTIONWISE	WATER		7 C
Wellbore	3-22	VERTICAL	HGIVEN	9996.6 W/m ² -C	

6.3 Initial Conditions

Branch	Mass Flow
Wellbore	103354.35 kg/h

6.4 Sources

Label	Abs. Pos.	Branch	Pipe	Section	Massflow	Type	Time	Pressure	Temperature	GMF
InjectionStream		Wellbore	PIPE-1	1	(103354.35, 103354.35, 0) kg/h	MASS	(0, 30, 32) h	(65.096, 65.096, 65.096) bar	(24.024, 24.024, 24.024) C	(0.85, 0.85, 0.85) -

7. Equipment

7.1 Valves

Label	Branch	Abs. Pos.	Diameter	Opening	CD
BridgePlug	Wellbore	3320 m	0.159 m	0	0.84

7.2 Position

Label	Branch	Abs. Pos.	Pipe	Section
Perf11	Wellbore	3070.52 m		
Perf12	Wellbore	3108.52 m		
Perf21	Wellbore	3118.52 m		
Perf22	Wellbore	3168.52 m		
Perf31	Wellbore	3168.52 m		
Perf32	Wellbore	3218.52 m		
Perf41	Wellbore	3518.52 m		
Perf42	Wellbore	3541.52 m		
WH	Wellbore	PIPE-1	1	
Perf51	Wellbore	3558.52 m		
Perf52	Wellbore	3588.52 m		
BH	Wellbore	3721 m		
1000m	Wellbore	1000 m		
3500m	Wellbore	3500 m		
500m	Wellbore	500 m		
1500m	Wellbore	1500 m		
2000m	Wellbore	2000 m		
2500m	Wellbore	2500 m		
3000m	Wellbore	3000 m		

II. SNØHVIT

1. Introduction

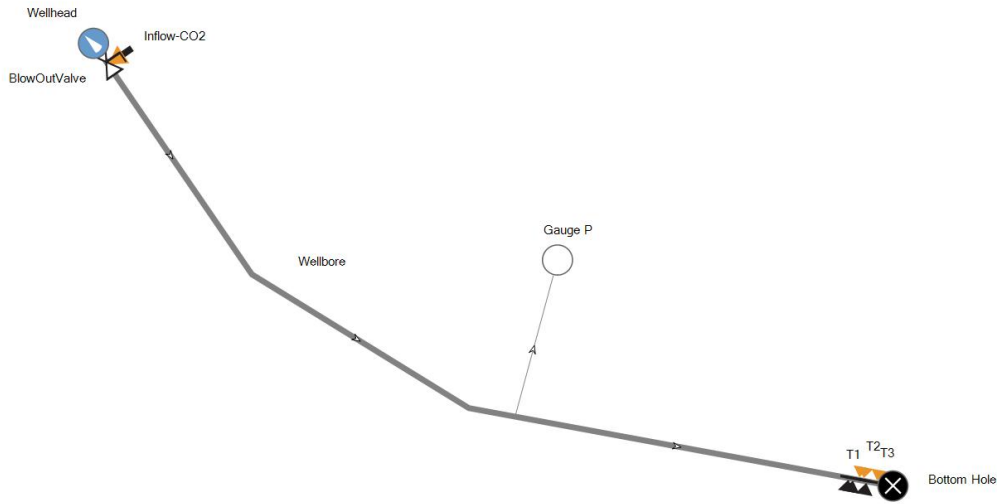
Project	Snohvit
Case description	Shut-in
Date	
Author	Eirik Thu
Restart File	/SnohvitBaseCase.rsw

2. Simulation Options

Overall setting	Flow model	OLGA
	Mass eq scheme	1STORDER
	Compositional model	SINGLE
	Debug	ON
	Drilling	
	Phase	THREE
	Elastic walls	OFF
	Void in slug	SINTEF
	Steady state	OFF
	User defined plug-in	OFF
	Temp. calc.	WALL
	Wax deposition	
	Restart	ON
Integration	Simulation starttime	
	Simulation stoptime	150 h
	Minimum time step	0.001
	Maximum time step	30 s

3. System Layout - Graphics

OLGF



Layout filter On

4. System Layout - Table

4.1 Summary

4.1.1 Overall

No. of Branches	No. of Pipes	No. of Sections
1	53	133

4.1.2 Flows

Branches	No. of Pipes	No. of Sections	Min. Section Length	At	Max. Section Length	At
Wellbore	53	133	12.1981019681073 M	PIPE-47	26.7209504136093 M	PIPE-50

4.2 Layout

Pipe no.	Branch	Label	Diameter	Roughness	XEnd	YEND	Wall
1-1	Wellbore	PIPE-1	0.155 M	5E-05 M	0.19 M	-390 M	Tubing-7inch
1-2	Wellbore	PIPE-2	0.155 M	5E-05 M	0.47 M	-440 M	Tubing-7inch
1-3	Wellbore	PIPE-3	0.155 M	5E-05 M	2.01 M	-499.98 M	Tubing-7inch
1-4	Wellbore	PIPE-4	0.155 M	5E-05 M	6.35 M	-559.83 M	Tubing-7inch
1-5	Wellbore	PIPE-5	0.155 M	5E-05 M	12.9 M	-619.49 M	Tubing-7inch
1-6	Wellbore	PIPE-6	0.155 M	5E-05 M	21.19 M	-678.93 M	Tubing-7inch
1-7	Wellbore	PIPE-7	0.155 M	5E-05 M	31.32 M	-738.09 M	Tubing-7inch
1-8	Wellbore	PIPE-8	0.155 M	5E-05 M	42.42 M	-797.07 M	Tubing-7inch
1-9	Wellbore	PIPE-9	0.155 M	5E-05 M	53.96 M	-855.95 M	Tubing-7inch
1-10	Wellbore	PIPE-10	0.155 M	5E-05 M	64.9 M	-914.93 M	Tubing-7inch
1-11	Wellbore	PIPE-11	0.155 M	5E-05 M	75.32 M	-974.01 M	Tubing-7inch
1-12	Wellbore	PIPE-12	0.155 M	5E-05 M	85.08 M	-1033.2 M	Tubing-7inch
1-13	Wellbore	PIPE-13	0.155 M	5E-05 M	94.13 M	-1092.51 M	Tubing-7inch
1-14	Wellbore	PIPE-14	0.155 M	5E-05 M	103.53 M	-1151.78 M	Tubing-7inch
1-15	Wellbore	PIPE-15	0.155 M	5E-05 M	113.89 M	-1210.92 M	Tubing-7inch
1-16	Wellbore	PIPE-16	0.155 M	5E-05 M	124.3 M	-1269.98 M	Tubing-7inch

1-17	Wellbore	PIPE-17	0.155 M	5E-05 M	135.28 M	-1328.97 M	Tubing-7inch
1-18	Wellbore	PIPE-18	0.155 M	5E-05 M	146.53 M	-1387.91 M	Tubing-7inch
1-19	Wellbore	PIPE-19	0.155 M	5E-05 M	157.92 M	-1446.82 M	Tubing-7inch
1-20	Wellbore	PIPE-20	0.155 M	5E-05 M	169.69 M	-1505.67 M	Tubing-7inch
1-21	Wellbore	PIPE-21	0.155 M	5E-05 M	180.3 M	-1554.55 M	Tubing-7inch
1-22	Wellbore	PIPE-22	0.155 M	5E-05 M	190.87 M	-1603.4 M	Tubing-7inch
1-23	Wellbore	PIPE-23	0.155 M	5E-05 M	201.8 M	-1662.35 M	Tubing-7inch
1-24	Wellbore	PIPE-24	0.155 M	5E-05 M	211.46 M	-1721.57 M	Tubing-7inch
1-25	Wellbore	PIPE-25	0.155 M	5E-05 M	221.33 M	-1780.76 M	Tubing-7inch
1-26	Wellbore	PIPE-26	0.099 M	5E-05 M	232.49 M	-1839.73 M	Tubing-4.5inch
1-27	Wellbore	PIPE-27	0.099 M	5E-05 M	242.83 M	-1888.68 M	Tubing-4.5inch
1-28	Wellbore	PIPE-28	0.099 M	5E-05 M	255.38 M	-1937.14 M	Tubing-4.5inch
1-29	Wellbore	PIPE-29	0.099 M	5E-05 M	267.35 M	-1975.36 M	Tubing-4.5inch
1-30	Wellbore	PIPE-30	0.099 M	5E-05 M	280.26 M	-2013.24 M	Tubing-4.5inch
1-31	Wellbore	PIPE-31	0.099 M	5E-05 M	290.78 M	-2041.4 M	Tubing-4.5inch
1-32	Wellbore	PIPE-32	0.099 M	5E-05 M	302.18 M	-2069.21 M	Tubing-4.5inch
1-33	Wellbore	PIPE-33	0.099 M	5E-05 M	314.82 M	-2096.52 M	Tubing-4.5inch
1-34	Wellbore	PIPE-34	0.099 M	5E-05 M	327.9 M	-2123.51 M	Tubing-4.5inch
1-35	Wellbore	PIPE-35	0.099 M	5E-05 M	340.82 M	-2150.58 M	Tubing-4.5inch
1-36	Wellbore	PIPE-36	0.099 M	5E-05 M	353.72 M	-2177.67 M	Tubing-4.5inch
1-37	Wellbore	PIPE-37	0.099 M	5E-05 M	367.09 M	-2204.57 M	Tubing-4.5inch
1-38	Wellbore	PIPE-38	0.099 M	5E-05 M	380.56 M	-2231.37 M	Tubing-4.5inch
1-39	Wellbore	PIPE-39	0.099 M	5E-05 M	393.94 M	-2258.21 M	Tubing-4.5inch
1-40	Wellbore	PIPE-40	0.099 M	5E-05 M	407.13 M	-2285.14 M	Tubing-4.5inch
1-41	Wellbore	PIPE-41	0.099 M	5E-05 M	420.14 M	-2312.16 M	Tubing-4.5inch
1-42	Wellbore	PIPE-42	0.099 M	5E-05 M	433.24 M	-2339.16 M	Tubing-4.5inch
1-43	Wellbore	PIPE-43	0.099 M	5E-05 M	446.69 M	-2366.01 M	Tubing-4.5inch
1-44	Wellbore	PIPE-44	0.099 M	5E-05 M	462.08 M	-2397.42 M	Tubing-4.5inch
1-45	Wellbore	PIPE-45	0.099 M	5E-05 M	475.05 M	-2423.83 M	Tubing-4.5inch
1-46	Wellbore	PIPE-46	0.099 M	5E-05 M	501.01 M	-2474.69 M	Tubing-4.5inch
1-47	Wellbore	PIPE-47	0.099 M	5E-05 M	513.38 M	-2498.81 M	Tubing-4.5inch
1-48	Wellbore	PIPE-48	0.099 M	5E-05 M	526.8 M	-2524.9 M	Tubing-4.5inch
1-49	Wellbore	PIPE-49	0.099 M	5E-05 M	540.69 M	-2551.83 M	Tubing-4.5inch
1-50	Wellbore	PIPE-50	0.099 M	5E-05 M	562.11 M	-2594.38 M	Tubing-4.5inch
1-51	Wellbore	PIPE-51	0.099 M	5E-05 M	587.84 M	-2646.89 M	Tubing-4.5inch
1-52	Wellbore	PIPE-52	0.099 M	5E-05 M	599.18 M	-2671.21 M	Tubing-4.5inch
1-53	Wellbore	PIPE-53	0.099 M	5E-05 M	620.22 M	-2718.75 M	Tubing-4.5inch

5. Insulation and Walls

5.1 Material

Label	Density	Conductivity	Heat Capacity
Formation	2500 kg/m3	2 W/m-C	880 J/kg-C
Steel	7850 kg/m3	50 W/m-C	500 J/kg-C
Stainless Steel	7850 kg/m3	20 W/m-K	450 J/kg-C

5.2 Walls

Label	Material	Wall thickness	Elastic
Tubing-4.5inch	Stainless Steel	0.0133858 m	
	Formation	0.025 m	
	Formation	0.05 m	
	Formation	0.1 m	
	Formation	0.2 m	
	Formation	0.4 m	
	Formation	0.8 m	
	Formation	1.5 m	
	Formation	3 m	
	Formation	6 m	
Tubing-7inch	Stainless Steel	0.0206121 m	
	Formation	0.05 m	
	Formation	0.1 m	
	Formation	0.2 m	
	Formation	0.4 m	
	Formation	0.8 m	
	Formation	1.5 m	
	Formation	3 m	
	Formation	6 m	

6. Boundary Conditions

6.1 Nodes

Label	Type	Pressure	Temperature	GMF
Wellhead	PRESSURE	31.013 bar	4 C	-1
Bottom Hole	CLOSED	348.1 bar	5 C	

6.2 Heattransfer

Branch	Pipe	Interpolation	Houteroption.	Hambient	Tambient
Wellbore	ALL	VERTICAL	HGIVEN	9996.6 W/m2-C	4 C

6.3 Initial Conditions

Branch
Wellbore

6.4 Sources

Label	Abs. Pos.	Branch	Pipe	Section	Massflow	Type	Time	Pressure	Temperature	GMF
Inflow-CO2		Wellbore	PIPE-1	1	(17.307, 17.307, 0) kg/s	MASS	(0, 30, 32) h	(113.324, 113.324, 106.944) bar	(3.722, 3.722, 3.408) C	(-1, -1, -1)

7. Equipment

7.1 Valves

Label	Branch	Pipe	Section	Diameter	Opening	CD
BlowOutValve	Wellbore	PIPE-1	1	0.155 m	0	1-

7.2 Position

Label	Branch	Abs. Pos.	Pipe	Section
P-WH	Wellbore	PIPE-1	1	
P-BH	Wellbore	PIPE-53	3	
Gauge	Wellbore	1483.6 m		
T22	Wellbore	2420.6 m		
T31	Wellbore	2445.6 m		
T32	Wellbore	2455.6 m		
T11	Wellbore	2397.6 m		
T12	Wellbore	2404.6 m		
T21	Wellbore	2409.6 m		

III. IN SALAH

1. Introduction

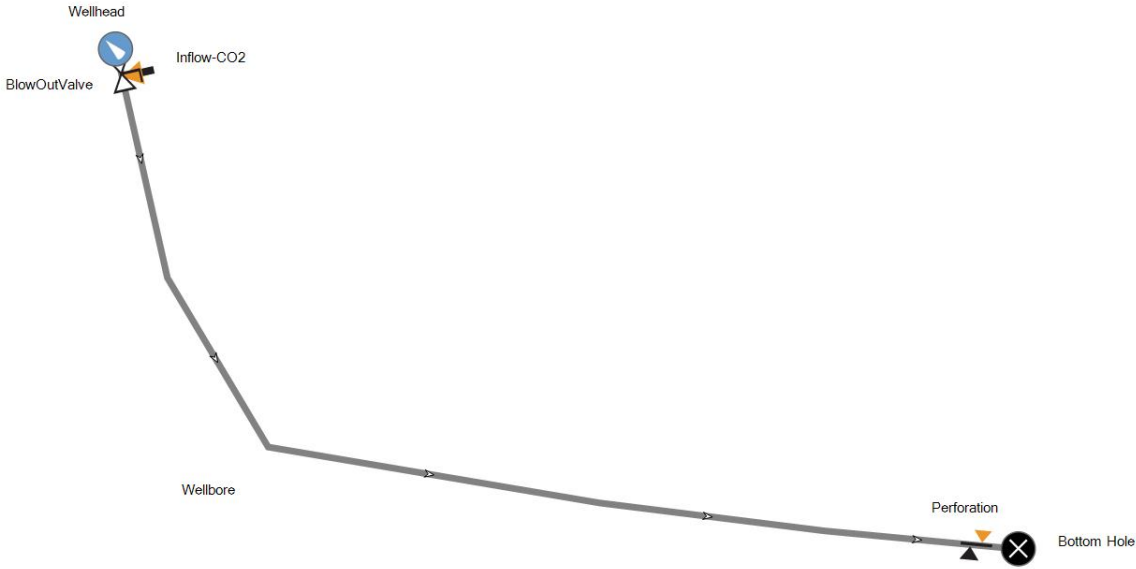
Project	In Salah
Case description	Shut-in
Date	
Author	Eirik Thu

2. Simulation Options

Overall setting	Flow model	OLGA
	Mass eq scheme	1STORDER
	Compositional model	SINGLE
	Debug	ON
	Drilling	
	Phase	THREE
	Elastic walls	OFF
	Void in slug	SINTEF
	Steady state	OFF
	User defined plug-in	OFF
	Temp. calc.	WALL
	Wax deposition	
	Restart	OFF
	Integration	Simulation starttime
	Simulation stoptime	150 h
	Minimum time step	0.001
	Maximum time step	30 s

3. System Layout - Graphics

OLGA



Layout filter On

4. System Layout - Table

4.1 Summary

4.1.1 Overall

No. of Branches	No. of Pipes	No. of Sections
1	29	159

4.1.2 Flows

Branches	No. of Pipes	No. of Sections	Min. Section Length	At	Max. Section Length	At
Wellbore	29	159	19.628591 M	PIPE-18	22.857859 M	PIPE-7

4.2 Layout

Pipe no.	Branch	Label	Diameter	Roughness	XEnd	YEND	Wall
1 - 1	Wellbore	PIPE-1	0.155 M	5E-05 M	0.403 M	-100 M	Tubing-7inch
1 - 2	Wellbore	PIPE-2	0.155 M	5E-05 M	1.28 M	-207.56 M	Tubing-7inch

1 - 3	Wellbore	PIPE-3	0.155 M	5E-05 M	1.92 M	-348.87 M	Tubing-7Inch
1 - 4	Wellbore	PIPE-4	0.155 M	5E-05 M	2.49 M	-462.39 M	Tubing-7Inch
1 - 5	Wellbore	PIPE-5	0.155 M	5E-05 M	3.35 M	-574.11 M	Tubing-7Inch
1 - 6	Wellbore	PIPE-6	0.155 M	5E-05 M	5.47 M	-686.99 M	Tubing-7Inch
1 - 7	Wellbore	PIPE-7	0.155 M	5E-05 M	7.57 M	-801.26 M	Tubing-7Inch
1 - 8	Wellbore	PIPE-8	0.155 M	5E-05 M	9.2 M	-913.09 M	Tubing-7Inch
1 - 9	Wellbore	PIPE-9	0.155 M	5E-05 M	10.75 M	-1065.13 M	Tubing-7Inch
1 - 10	Wellbore	PIPE-10	0.155 M	5E-05 M	12.34 M	-1167.3 M	Tubing-7Inch
1 - 11	Wellbore	PIPE-11	0.155 M	5E-05 M	22.79 M	-1270.06 M	Tubing-7Inch
1 - 12	Wellbore	PIPE-12	0.155 M	5E-05 M	42.04 M	-1371.96 M	Tubing-7Inch
1 - 13	Wellbore	PIPE-13	0.155 M	5E-05 M	70.2 M	-1472.58 M	Tubing-7Inch
1 - 14	Wellbore	PIPE-14	0.155 M	5E-05 M	117.37 M	-1582.73 M	Tubing-7Inch
1 - 15	Wellbore	PIPE-15	0.099 M	5E-05 M	225.84 M	-1714.36 M	Tubing-4.5Inch
1 - 16	Wellbore	PIPE-16	0.099 M	5E-05 M	336.83 M	-1812.97 M	Tubing-4.5Inch
1 - 17	Wellbore	PIPE-17	0.099 M	5E-05 M	454.81 M	-1874.88 M	Tubing-4.5Inch
1 - 18	Wellbore	PIPE-18	0.099 M	5E-05 M	569.93 M	-1899.73 M	Tubing-4.5Inch
1 - 19	Wellbore	PIPE-19	0.099 M	5E-05 M	679.39 M	-1900.5 M	Tubing-4.5Inch
1 - 20	Wellbore	PIPE-20	0.099 M	5E-05 M	801.52 M	-1901.25 M	Tubing-4.5Inch
1 - 21	Wellbore	PIPE-21	0.099 M	5E-05 M	914.49 M	-1903.29 M	Tubing-4.5Inch
1 - 22	Wellbore	PIPE-22	0.099 M	5E-05 M	1027.49 M	-1904.03 M	Tubing-4.5Inch
1 - 23	Wellbore	PIPE-23	0.099 M	5E-05 M	1140.73 M	-1905.43 M	Tubing-4.5Inch
1 - 24	Wellbore	PIPE-24	0.099 M	5E-05 M	1247.16 M	-1906.26 M	Tubing-4.5Inch
1 - 25	Wellbore	PIPE-25	0.099 M	5E-05 M	1361.22 M	-1908.82 M	Tubing-4.5Inch
1 - 26	Wellbore	PIPE-26	0.099 M	5E-05 M	1475.18 M	-1913.69 M	Tubing-4.5Inch
1 - 27	Wellbore	PIPE-27	0.099 M	5E-05 M	1583.7 M	-1916.8 M	Tubing-4.5Inch
1 - 28	Wellbore	PIPE-28	0.099 M	5E-05 M	1702.61 M	-1913.43 M	Tubing-4.5Inch
1 - 29	Wellbore	PIPE-29	0.102 M	5E-05 M	1803.99 M	-1908.41 M	Tubing-4.5Inch

5. Insulation and Walls

5.1 Material

Label	Density	Conductivity	Heat Capacity
Formation	2500 kg/m ³	2 W/m-C	880 J/kg-C
Steel	7850 kg/m ³	50 W/m-C	500 J/kg-C
Stainless Steel	7850 kg/m ³	20 W/m-K	450 J/kg-C

5.2 Walls

Label	Material	Wall thickness	Elastic
Tubing-4.5Inch	Stainless Steel	0.0133858 m	
	Formation	0.025 m	
	Formation	0.05 m	
	Formation	0.1 m	
	Formation	0.2 m	
	Formation	0.4 m	
	Formation	0.8 m	
	Formation	1.5 m	
	Formation	3 m	
	Formation	6 m	
Tubing-7Inch	Stainless Steel	0.0206121 m	
	Formation	0.05 m	
	Formation	0.1 m	
	Formation	0.2 m	
	Formation	0.4 m	
	Formation	0.8 m	
	Formation	1.5 m	
	Formation	3 m	
	Formation	6 m	

6. Boundary Conditions

6.1 Nodes

Label	Type	Pressure	Temperature	GMF
Wellhead	PRESSURE	1 atm	10 C	-1
Bottom Hole	CLOSED	348.1 bar	5 C	

6.2 Heattransfer

Branch	Pipe	Interpolation	Houteroption.	Hambient	Tambient
Wellbore	ALL	VERTICAL	HGIVEN	9996.6 W/m ² -C	4 C

6.3 Initial Conditions

Branch	Pipe	Mass Flow
Wellbore	ALL	5.633 kg/s

6.4 Sources

Label	Abs. Pos.	Branch	Pipe	Section	Massflow	Type	Time	Pressure	Temperature	GMF
Inflow-CO2		Wellbore	PIPE-1	1	(5.633, 5.633, 0) kg/s	MASS	(0, 30, 32) h	(170.427, 170.427, 170.427) bar	(32, 32, 32) C	(-1, -1, -1) -

7. Equipment

7.1 Valves

Label	Branch	Pipe	Section	Diameter	Opening	CD
BlowOutValve	Wellbore	PIPE-1	1	0.155 m	0	1 -

7.2 Position

Label	Branch	Abs. Pos.	Pipe	Section
P-WH	Wellbore	PIPE-1	1	
P-BH	Wellbore	PIPE-29	5	
T22	Wellbore	3355 m		
T31	Wellbore	2445.6 m		
T32	Wellbore	2455.6 m		
T11	Wellbore	2397.6 m		
T12	Wellbore	2404.6 m		
T21	Wellbore	3300 m		

IV. KETZIN

1. Introduction

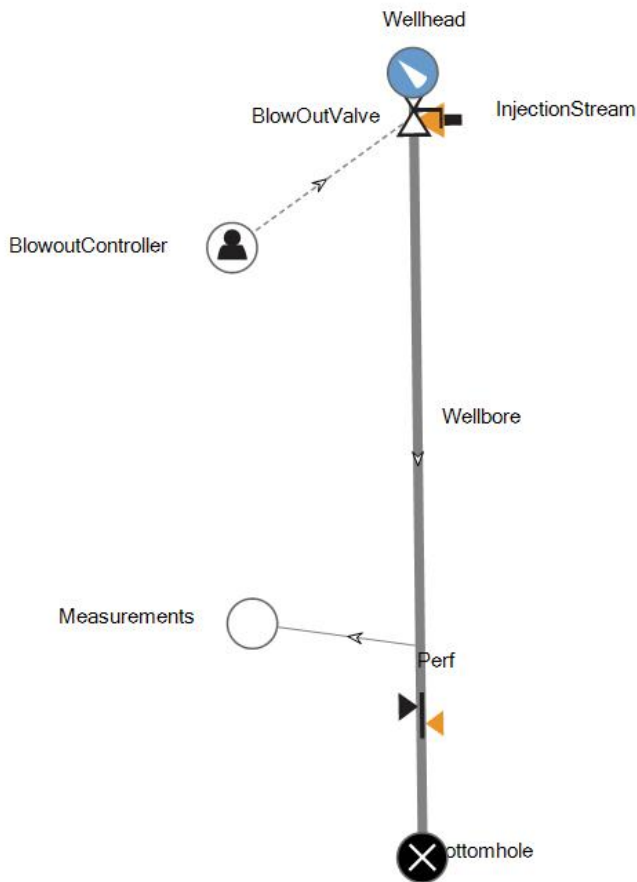
Project	Ketzin
Case description	Shut-in
Date	
Author	Eirik Thu
Restart File	../BaseCaseCO2/CO2.rsw

2. Simulation Options

Overall setting	Flow model	OLGA
	Mass eq scheme	1STORDER
	Compositional model	SINGLE
	Debug	ON
	Drilling	
	Phase	THREE
	Elastic walls	OFF
	Void in slug	SINTEF
	Steady state	OFF
	User defined plug-in	OFF
	Temp. calc.	WALL
	Wax deposition	
	Restart	ON
Integration	Simulation starttime	
	Simulation stoptime	150 h
	Minimum time step	0.001
	Maximum time step	5 s

3. System Layout - Graphics

OLGA*



Layout filter On

4. System Layout - Table

4.1 Summary

4.1.1 Overall

No. of Branches	No. of Pipes	No. of Sections
1	3	37

4.1.2 Flows

Branches	No. of Pipes	No. of Sections	Min. Section Length	At	Max. Section Length	At
Wellbore	3	37	19.55 M	PIPE-2	21.4444444444445 M	PIPE-3

4.2 Layout

Pipe no.	Branch	Label	Diameter	Roughness	XEnd	YEND	Wall
1 - 1	Wellbore	PIPE-1	0.076 M	5E-05 M	0 M	-171 M	K1
1 - 2	Wellbore	PIPE-2	0.076 M	5E-05 M	0 M	-562 M	K2
1 - 3	Wellbore	PIPE-3	0.12 M	5E-05 M	0 M	-755 M	K3

5. Insulation and Walls

5. 1 Material

Label	Density	Conductivity	Heat Capacity
Formation	2380 kg/m3	3 W/m-C	900 J/kg-C
Steel	7850 kg/m3	50 W/m-C	500 J/kg-C
Stainless Steel	7850 kg/m3	20 W/m-K	450 J/kg-C
KTubing	7850 kg/m3	45 W/m-C	450 J/kg-C
KCasing	7850 kg/m3	45 W/m-C	500 J/kg-C
Concrete	3000 kg/m3	1.4 W/m-K	880 J/kg-C
Annulus	800 kg/m3	0.26 W/m-C	2544 J/kg-C
Formation2	2200 kg/m3	2.5 W/m-C	880 J/kg-C
Formation3	2200 kg/m3	1.75 W/m-C	880 J/kg-C

5. 2 Walls

Label	Material	Wall thickness	Elastic
K1	KTubing	0.014 m	
	Annulus	0.14 m	
	KCasing	0.02 m	
	Concrete	0.06 m	
	Formation	0.025 m	
	Formation	0.05 m	
	Formation	0.1 m	
	Formation	0.2 m	
	Formation	0.4 m	
	Formation	0.8 m	
	Formation	1.5 m	
	Formation	3 m	
	Formation	6 m	
K2	KTubing	0.014 m	
	Annulus	0.14 m	
	KCasing	0.02 m	
	Concrete	0.06 m	
	Formation2	0.025 m	
	Formation2	0.05 m	
	Formation2	0.1 m	
	Formation2	0.2 m	
	Formation2	0.4 m	
	Formation2	0.8 m	
	Formation2	1.5 m	
	Formation2	3 m	
	Formation2	3 m	

	Formation2	6 m		
K3	KTubing	0.01 m		
	Annulus	0.001 m		
	KCasing	0.009 m		
	Concrete	0.08 m		
	Formation3	0.025 m		
	Formation3	0.05 m		
	Formation3	0.1 m		
	Formation3	0.2 m		
	Formation3	0.4 m		
	Formation3	0.8 m		
	Formation3	1.5 m		
	Formation3	3 m		
	Formation3	6 m		

6. Boundary Conditions

6.1 Nodes

Label	Type	Pressure	Temperature	Mass flow	GMF
Bottomhole	CLOSED				
Wellhead	PRESSURE	1 atm	10 C	116987.5 kg/h	-1

6.2 Heattransfer

Branch	Pipe	Interpolation	Houteroption.	Hambient
Wellbore	ALL	VERTICAL	HGIVEN	10000 W/m2-C

6.3 Initial Conditions

Branch	Mass Flow
Wellbore	2057.943 kg/h

6.4 Sources

Label	Abs. Pos.	Branch	Pipe	Section	Massflow	Type	Time	Pressure	Temperature	GMF
InjectionStream		Wellbore	PIPE-1	1	(2057.9, 2057.9, 0) kg/h	MASS	(0, 30, 32) h	(55.37, 55.37, 55.37) bar	(37.09, 37.09, 37.09) C	(-1, -1, -1) -

7. Equipment

7.1 Valves

Label	Branch	Pipe	Section	Diameter	Opening	CD
BlowOutValve	Wellbore	PIPE-1	1	0.076 m	1	1 -

7.2 Position

Label	Branch	Abs. Pos.	Pipe	Section
WH	Wellbore	PIPE-1	1	
BH	Wellbore	PIPE-3	9	
100m	Wellbore	100 m		
200m	Wellbore	200 m		
300m	Wellbore	300 m		
400m	Wellbore	400 m		
500m	Wellbore	500 m		
600m	Wellbore	600 m		
700m	Wellbore	700 m		
p1	Wellbore	620 m		
p2	Wellbore	640 m		
549m	Wellbore	549 m		
Measurment	Wellbore	549 m		

